Adıyaman University
Journal of Science

June 2021

Volume: 11 Issue: 1

An international peer reviewed journal of science

PHYSIC
SCIENCE
BIOLOGY
MATHEMATICS
CHEMISTRY

ADYU J SCI

ISSN 2147-1630
e-ISSN 2146-586X

An open access, peer reviewed, international journal of science. Biannual (June & December). ISSN 2147-1630 | e-ISSN 2146-586X. Publisher: Adıyaman University.

Publication language: English (with Turkish title and abstract)

Issue published date: 30.06.2021

Privilege owner: On Behalf of Rectorate of Adıyaman University, Prof. Dr. Mehmet TURGUT (Rector)

Web site: EN: https://dergipark.org.tr/en/pub/adyujsci
TR: https://dergipark.org.tr/tr/pub/adyujsci

Table of Contents (İçindekiler)

Volume (Cilt): 11 Number (Sayı): 1
June (Haziran) 2021

BIOLOGY

CHEMISTRY

MATHEMATICS

Adıyaman University Journal of Science
https://dergipark.org.tr/en/pub/adyujsci
DergiPark AKADEMİK
ISSN 2147-1630
e-ISSN 2146-586X

Investigation of the Role of *cyaA/crp* Genes of *Escherichia coli* in Metal Stress

Gülçin ÇETİN KILIÇASLAN[1,*], Özge KAYGUSUZ[2], Önder İDİL[3], Cihan DARCAN[1]

[1]*Bilecik Şeyh Edebali University, Department of Molecular Biology and Genetic Faculty of Arts and Sciences, Bilecik, Turkey*
gulcin.cetin@bilecik.edu.tr, ORCID: 0000-0002-9625-224X
cihan.darcan@bilecik.edu.tr, ORCID: 0000-0003-0205-3774
[2]*Bilecik Şeyh Edebali University, Biotechnology Application and Research Center, Bilecik, Turkey*
ozge.kaygusuz@bilecik.edu.tr, ORCID: 0000-0002-3652-4266
[3]*Amasya University, Department of Basic Education, Faculty of Education, Amasya, Turkey*
onidil@gmail.com, ORCID: 0000-0003-1744-4006

Received: 02.12.2020 **Accepted:** 05.03.2021 **Published:** 30.06.2021

Abstract

Adenosine 3′, 5′-monophosphate (cAMP) is an important signaling molecule. CRP, the receptor protein of cAMP, acts as the 'main' regulator for transcription factors. The CRP-cAMP complex directly controls at least 500 promoters in *Escherichia coli*. In this study, the roles of *cyaA* and *crp* genes in *E. coli* BW25113 strain under metal stress were investigated. The minimal inhibition concentration (MIC) and minimal cidal concentration (MCC) of 5 different metals (Zn, Ni, Co, Cd and Cu) on *Escherichia coli* BW25113 wild type, *cyaA* and *crp* mutant cells were determined. In addition, the effect of these metals on the survival of *E. coli cyaA/crp* mutants was determined by growth and drop plate method. According to *E. coli* BW25113 wild type, *cyaA* mutant strain was observed sensitivity in all metals except copper, whereas resistance was observed in *crp* mutant strain only to zinc metal. The roles of the *cyaA* and *crp* genes in metal stress were confirmed by completing the genes on the plasmid. As a result, the roles of *cyaA* and *crp* genes in metal resistance were revealed in this study.

Keywords: *cyaA*; *crp;* Metal stress; *Escherichia coli.*

* Corresponding Author DOI: 10.37094/adyujsci.834522

Metal Stresinde *Escherichia coli'nin cyaA/crp* Genlerinin Rolünün Araştırılması

Öz

Adenosin 3 ′, 5′-monofosfat (cAMP), önemli bir sinyal molekülüdür. cAMP'nin reseptör proteini olan CRP, transkripsiyon faktörleri için 'ana' düzenleyici olarak görev almaktadır. *Escherichia coli*'de CRP-cAMP kompleksi, en az 500 promotor'u doğrudan kontrol etmektedir. Bu çalışmada *E. coli* BW25113 suşunda *cyaA* ve *crp* genlerinin metal stresi altındaki rolleri araştırılmıştır. *Escherichia coli* BW25113 yabanıl tip, *cyaA* ve *crp* mutant hücrelerinin 5 farklı metale (Zn, Ni, Co, Cd ve Cu) karşı minimal inhibisyon konsantrasyonu (MİK) ve minimal sidal konsantrasyonu (MSK) belirlenmiştir. Ayrıca bu metal stresinin *E. coli cyaA/crp* mutantlarının yaşamı üzerine etkisi büyüme ve petri damlatma yöntemi ile belirlenmiştir. Çalışmada *E. coli* BW25113 yabanıl tipe göre, bakır hariç tüm metallerde *cyaA* mutant suşunda duyarlılık gözlenirken, sadece çinko metalinde *crp* mutant suşunda dirençlilik gözlenmiştir. *cyaA* ve *crp* genlerinin metal stresindeki rolleri, genlerin plazmit üzerinde tamamlanması yapılarak doğrulanmıştır. Sonuç olarak; bu çalışmada *cyaA* ve *crp* genlerinin metal direncindeki rolleri ortaya konulmuştur.

Anahtar Kelimeler: *cyaA*; *crp*; Metal stresi; *Escherichia coli.*

1. Introduction

Metals are very important as they serve as structural or catalytic components of living organisms [1, 2]. Many important biological processes in living organisms, including respiration, photosynthesis, and nitrogen fixation are dependent on metal ion co-factors [3]. However, metals function as redox centers of metalloproteins, such as cytochromes and iron sulfur proteins, which play a vital role in electron transport [4]. Since transition metals are often in the oxidized state, they also play a role as electron carriers [5].

The metal concentration in the environment is gradually increasing due to various reasons such as the progress of the industry in the world, the incorrect discharge of waste products, and direct throw to water and land areas. With this increase, heavy metals such as copper, cadmium, lead, zinc, nickel, mercury, and chromium accumulated in nature have become one of the most important environmental problems affecting life on land and water [6-8]. Despite their essential roles in cellular reactions, metals exhibit toxicity when their concentrations exceed a certain level [9]. Excess metal ions catalyze unwanted reactions and biomolecular damage. It also leads to improper metal binding to random regions of metalloproteins or other proteins, resulting in

inactivation or inappropriate allosteric effects [10-12]. Metals cannot be synthesized and metabolized inside the cell. Since metals can be beneficial as well as toxic, the proper arrangement of metals in the cell is extremely important for bacteria [3, 13].

Bacteria have complex metal homeostasis mechanisms to maintain the delicate balance between the amount of metal required and toxicity [14]. These mechanisms are regulated by metal-sensitive transcription factors (metal sensor proteins and metalloregulators) that detect the level of bioavailability of a particular metal type in the cell and then regulate the transcription of genes associated with that metal [3, 15-17]. When the extracellular concentration of a particular metal increases in bacteria, the first "checkpoint" is to limit metal entry to ensure metal homeostasis and prevent cellular damage. It regulates this by reducing the expression of genes that allow metal entry [3]. For example, one of the regulators induced by copper in *E. coli* is the outer membrane protein ComC (YcfR). In the presence of high copper, the increase of *comC* expression in the cell prevents copper from being taken into the periplasmic space from the external environment [18]. Chelating or precipitation of soluble metal ions in the extracellular environment is another way to limit metal entry [19]. Also, another way to protect bacteria from metals is to reduce the toxicity of metals by using detoxification means. For example, Cue regulon in *E. coli* is responsible for copper detoxification. CueR, the main regulator of this system, is responsible for cytoplasmic Cu detection. CueO, a multiple copper oxidase enzyme regulated by CueR, oxidizes Cu^{+} to divalent Cu^{2+}, which cannot pass through the inner membrane. Thus, it helps protect periplasmic proteins [20, 21]. In addition, bacteria resist metals by increasing the excretion with many pulse-type pumps such as P1b type ATPase, resistance nodulation-division (RND) carrier, cation diffusion facilitators (Cation Diffusion Facilitato (CDF)), ABC carriers [22]. For example, in *E. coli*, Zn^{+2} and Cu^{+} are transported from the cytoplasm to the periplasm by P1b-type ATPases, which are ZntA and CopA proteins, respectively [23]. While RND complexes share a common structure in Gram negative bacteria, they are diverse for different metals. For example, in *Pseudomonas putida*, CzcCBA system provides resistance against Zn^{2+}, Cd^{2+} and Pb^{2+} [24], while in *Caulobacter crescentus*, CzrCBA and NczCBA systems are involved in Cd, Zn, Ni and Co transport, respectively [25]. CDF are mostly flow pumps that remove bivalent metal ions such as Zn^{2+}, Co^{2+}, Cd^{2+}, Ni^{2+} and Fe^{2+} from cells [26, 27]. In *E. coli,* the ZitB and YiiP antiporter pumps Zn^{2+} against H^{+} [28, 29]. However, nonspecific multidrug flow pumps have also been shown to mediate the removal of a wide variety of compounds and molecules, including metals [30].

In *E. coli*, the *cyaA* and *crp* genes encode adenylate cyclase and cAMP receptor protein, respectively [31]. Adenosine 3′, 5′-monophosphate (cAMP) is an important signaling molecule

found in many organisms. CRP, the receptor protein of cAMP, is known mostly to play a general regulatory role in carbon catabolism in *E. coli*. That is, in the absence of easily metabolized carbon sources such as glucose, the adenylate cyclase enzyme is activated by producing cyclic AMP (cAMP) from ATP. cAMP binds and activates CRP, which in most cases activates operons participating in the use of alternative carbon sources such as lactose and maltose [32]. In *E. coli*, CRP has a major role in global gene expression, with its effect on more than 380 promoters and 70 transcription factors [33]. For example, it contributes to the multiple roles of cAMP in processes such as the regulation of virulence phenotypes in pathogenic bacteria [34-36]. Bacterial cAMP systems also have key roles in cellular homeostasis, phototaxis, protein secretion, regulation of virulence, and biofilm formation [37]. Although cAMP and CRP play various roles in many known mechanisms, there are not many studies on their roles in metal resistance.

The CAMP signaling pathway is a highly conserved regulatory mechanism that plays an important role in a variety of essential cellular processes. Therefore, considering that *cyaA-crp* genes may have a role in metal stress, the importance of *cyaA-crp* genes in *E. coli* under metal stress was investigated in this study.

2. Materials and Methods

2.1. *E. coli* Strains used in the study

Wild type *E. coli* BW25113 and mutant strains (JW3378 and JW5702) used in this study were obtained from the Japanese National Genetics Center (Keio collection-Japan National Genetic Center), and are shown in Table 1. Stocks were prepared in Luria-Bertani (LB-Merck) broth medium containing 20% glycerol (Merck) and stored at –80°C (Panasonic) for future studies. The strains in the freezer were inoculated on the LB agar medium. Before being used in the study, antibiotic resistance properties were tested by colony PCR method.

Table 1: Wild type *E.coli* and mutant strains used in this study

Stock number of Strains	Genotype	Resource
BW25113	Wild type	Keio Collection
JW3378	BW25113 *cyaA::km*	Keio Collection
JW5702	BW25113 *crp::km*	Keio Collection
b3806	*cyaA*	Mobile plasmid pNT3 (Keio collection)
b3357	*crp*	Mobile plasmid pNT3 (Keio collection)
CD102	BW25113 *pnt3::cyaA*	This study
CD103	BW25113 *pnt3::crp*	This study

2.2. Plasmid isolation

In order to verify the role of the gene we studied, plasmids carrying the *E. coli* BW25113 *cyaA* and *crp* gene regions were first obtained. From the mobile plasmids bearing the *cyaA* and *crp* gene regions given in Table 1, a single colony was cultivated separately in 5 ml LB broth and incubated overnight at 37°C and 160 rpm in a shaking incubator. Plasmid isolation from bacterial cultures obtained after incubation was performed using Purelink Quick Mini Prep plasmid isolation kit (InvitroGen) and procedure. A part of the isolated plasmid was used for quantitation and the obtained plasmids were stored at –20°C. The amount of plasmid was determined non-quantitatively by running it in 0.8% agarose gel and comparing it with GeneRuler brand DNA Ladder mix (Thermo) marker.

2.3. Transformation

To obtain complementary cells of *E. coli* BW25113 mutant strains, *E. coli* BW25113 mutants (BW25113 *cyaA::km* and BW25113 *crp::km*) were inoculated separately in 2 ml of LB containing kanamycin at a final concentration of 25 µg/ml. The cultivated cultures were grown in a shaking incubator at 37ºC for 18 hours at 160 rpm and used as pre-culture for transformation. Mobile plasmids carrying the gene regions we studied were transferred to the relevant *E. coli* BW25113 mutant strains by transformation [38]. The next day, 100 µl of 2 M Mg^{2+}, a final concentration of 25 µg/ml, and 50 µl of kanamycin antibiotic and pre-culture are added to sterilized 9.9 ml Hanahan's broth (SOB medium) until the cells reach OD_{600} 0.3. It was incubated at 37ºC and 160 rpm with shaking. After incubation, each tube was divided into 2 centrifuge tubes and cooled in ice for 5 min and centrifuged at 12000 rpm for 5 min at 4ºC. One ml of 0.1 M cold $CaCl_2$ was added to the pellets and suspended. Then the tubes were kept on ice for 10 min and centrifuged again at 12000 rpm for 5 min at 4ºC. The supernatant was discarded and resuspended by adding 200 µl of 0.1 M cold $CaCl_2$ per tube and kept on ice for 30 min. The obtained 200 µl competent cell was added to 10-100 ng of 2 different concentrations of isolated plasmid and kept on ice for 45 min. Then the cell suspensions were heat shocked at 42ºC for 2 min and then on ice for 2 min. 0.8 ml of SOB medium (SOC medium) enriched with 20 mM magnesium (Merck) and 3% glucose (Merck) was added onto the cell suspension and left for 60 min incubation at 37°C. After the incubation, the cells were centrifuged at 5000 rpm for 1 min at 4ºC. Later, 100 µl SOC medium was added to the pellet and resuspended. It was spread on LB agar containing ampicillin antibiotic in a final concentration of 100 µg/ml and left for 18 h incubation. The complementary cells were confirmed by colony PCR.

2.4. Colony PCR

Colony PCR method was used to confirm the mutants and complementary cells to be used in the study. For this, the mutants obtained were suspended in 20 µl distilled water, and 1 µl was used as a mold for PCR. 7.5 µl of the reaction mixture in Table 2 was distributed on the mold, and the colony PCR was made according to the reaction conditions in Table 3. The primers used for the validation of each gene are shown in Table 4. The band sizes of the products obtained from the PCR reaction were verified with GeneRuler brand DNA Ladder mix (Thermo) by running in 1% agarose gel.

Table 2: Colony PCR reaction mixture

10x ThermaPol Reaction Buffer (Biolab)	1.0 µl
10 mM dNTP Mix	0.2 µl
10 µM forward primer (İnvitrogen)	0.5 µl
10 µM reverse primer (İnvitrogen)	0.5 µl
2 mM Mg^{+2} containing $MgCl_2$ (Biolab)	0.6 µl
0.25U Taq DNA Polymerase (Biolab)	0.05 µl
dH_2O	6.15 µl
Bacterial suspension	1 µl
Total	10 µl

Table 3: Colony PCR reaction conditions

94 ºC	3 min	1 cycle
94 ºC	1 min	30 cycle
58 ºC	1 min	
72 ºC	1 min 30 sec	
72 ºC	10 min	1 cycle

Table 4: Primers used in colony PCR reaction

Universal K1 reverse primer	5’ CAGTCATAGCCGAATAGCCT3’
BW25113::*cya* forward primer	5’ TGTTACCGTTGATTGTGGCG 3’
BW25113::*crp* forward primer	5’ GAGAAAGCTTATAACAGAGG 3’
Universal pNT3 SP6 forward primer	5’ ATTTAGGTGACACTATAG 3’
Universal pNT3 21M13 reverse primer	5’ CAGGAAACAGCTATGACC 3’

2.5. Determination of minimum inhibition concentrations (MIC) and minimum cidal concentrations (MCC) of metals

The 0.2 M stock solutions of $CuSO_4$, $NiCl_2$, $CdSO_4$, $CoCI_2$ and $ZnSO_4$ metals used in the study were prepared by dissolving in water and sterilized by filtration. MIC and MCCs of metals

were determined in round bottom 96-well microplates according to the CLSI method [39]. Each of the wild type and mutant strains was incubated in 5 ml nutrient broth medium at 37°C for 18 h with shaking. After the incubation, the absorbance of bacteria was adjusted to 0.1 at 600 nm wavelength. Then 400 µl from stock bacteria culture was prepared in 60 ml. From this culture, the 180 µl culture was added to the 96-well microplate in the first well and 100 µl in the other wells. 20 µl of the metals was added to 180 µl wells, and serial dilution was made in 12 wells. Plates were incubated at 37°C for 18 h and MIC values were determined. In addition, in order to determine the cidal effects of metals, 10 µl of culture was taken from each well where no growth was observed, and it was dropped into a medium containing nutrient agar. Then the plates were incubated at 37°C for 18 h, and their MCC values were determined. The experiments were repeated at least 3 times.

2.6. The effect of metal stress on the survival of *Escherichia coli cya*/*crp* mutants

2.6.1. Growth experiments

Each of the pure cultures obtained from *E. coli* BW25113 wild type, *cyaA::km* and *crp ::km* mutants were inoculated in 5 ml nutrient broth medium and incubated at 37°C in a shaking incubator for 18 h. After the incubation, the absorbance of the bacterial cultures was adjusted as 1.0. In order to the starting numbers to be equal (approximately OD_{600} 0.005), 75 µl of the pre-cultures adjusted to 1.0 was added to the media containing 15 ml of nutrient broth, and growth experiments were started. In metal growth experiments, ¾ of the wild-type MIC value from metal stocks was added to the growth medium. The prepared samples were left to incubate for 8 h in an agitated oven at 37°C and 160 rpm. Growth graphs were obtained by taking samples from the bacteria every 2 h and measuring their absorbance in OD_{600} in a spectrophotometer. The experiments were repeated at least independently 3 times.

2.6.2. Drop plate experiments

Plate dropping experiments were performed to see the effect of solid media on growth of metal-free and metal-based growth experiments. Also, the the number of bacteria on effect of metals was observed here. Firstly, the amount of metals used was determined in 3 different concentrations by taking into account the MIC value of wild type *E. coli* BW25113. Petri dishes containing metal at concentrations of 0.06, 0.07 and 0.08 mM for cadmium, 0.8, 0.9 and 1.0 mM for copper, 0.4, 0.45 and 0.5 mM for cobalt, 0.7, 0.8 and 0.9 mM for nickel and 0.27, 0.28 and 0.29 mM for zinc were prepared.

For plate dropping experiments, a single bacterial colony was taken from *E. coli* BW25113, *cyaA::km* and *crp::km* mutants and incubated in 15 ml NB at 37°C in a 160 rpm shaking incubator for 18 h. After incubation, the bacteria cultures were adjusted to an absorbance of OD_{600} 1.0. 1 ml of the adjusted samples was centrifuged and washed twice with Ringer's (Merck) solution. 100 µl of the obtained bacterial suspension was taken, and the final cell count was adjusted between 10^1 and 10^7 cfu/ml by diluting a series of 1/10 with Ringer's solution. Later, those with cell numbers between 10^3 and 10^7 cfu/ml from these tubes were dropped to metal-free (control) and metal-containing Nutrient Agar media as 10 µl and incubated at 37°C for 18 h. After the incubation, bacterial colonies formed in the plate were photographed with SYNGENE G: Box Chemi XRQ device. The experiments were repeated at least 3 times.

2.7. Complementation tests

At the end of the studies, complementation tests were carried out to verify the genes found to have roles according to the significance test performed with IBM SPSS 21. In these tests, the relevant gene region, which is mutant in the main chromosome, was added to the mutant strains by adding on pNT3 plasmid and *E. coli* BW25113 pnt3::*cyaA* and *E. coli* BW25113 pnt3::*crp* cells were obtained. In order to induce the pNT3 plasmid in the completed cells, IPTG (isopropyl β-D-1-thiogalactopyranoside) (Sigma) was added to the media used in the experiments at a final concentration of 1 mM. The experiments were repeated at least 3 times.

3. Results

3.1. Obtaining complementary cells

Confirmation of cells obtained as a result of transforming *cyaA* and *crp* genes into cells with mutants in the main chromosome by means of pNT3 plasmid was performed by colony PCR method. The agarose gel image of the colony PCR products made using the traditional SP6-21M13 primer of the pNT3 vector is shown in Fig. 1. According to the PCR results, samples 1, 2, and 3 are *E. coli* pnt3::*cyaA* cells with a size of 2611 bp, while samples 4, 5, and 6 are positive for *E. coli* pnt3 :: *crp* cells with a size of 697 bp. Among these cells, number 2 for *E. coli* pnt3::*cyaA* and number 6 for *E. coli* pnt3::*crp* were used in validation studies.

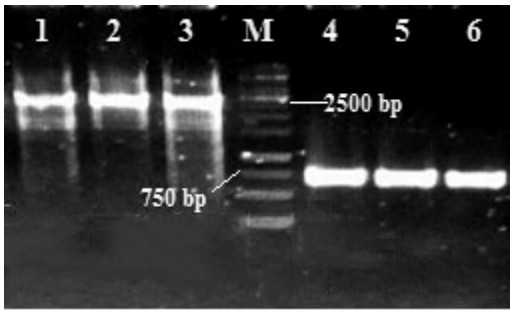

Figure 1: The colony PCR results of *E. coli* pnt3::*cyaA* and pnt3::*crp* complement strains obtained as a result of transformation. M: 1 kb DNA Ladder, 1-3. *E. coli* pnt3::*cyaA* 4-6. *E.coli* pnt3::*crp*

3.2. Minimum inhibition concentration (MIC) and minimum cidal concentration (MCC) values

Minimal inhibition concentration (MIC) and minimum cidal concentration (MCC) values of metals belonging to *E. coli* wild type and mutant strains are shown in Table 5. According to the determined results, the MIC values of *E. coli* wild type are 468 µg/ml for copper (Cu) and 30 µg/ml for cobalt (Co), and they are the same as for mutant strains. While MIC values of Ni metal did not differ between wild type and mutant strains, when MIC values of Cd metal were compared, MIC values of mutant bacteria (145 µg/ml) were two times higher than wild type MIC values (72 µg/ml). When the MIC values of Zn metal were compared, it was determined that it was 180 µg/ml in wild type *E. coli*, 135 µg/ml in *cyaA::km* and 360 µg/ml in *crp::km.* According to these results, it is seen that the *crp* mutant is sensitive while the *cyaA* mutant is resistant compared to the wild type *E. coli*. It was observed that the determined MCC results were higher than the MIC values, and the metals had growth inhibitory properties at MIC values.

Table 5: Minimum inhibition concentration (MIC) and minimum cidal concentration (MCC) values of wild-type BW25113 and *cyaA/crp* mutant strains used in the study

Metal	**MIC (µg/ml)**			**MCC (µg/ml)**		
	Wild-tip BW25113	BW25113 *cya::km*^{r}	BW25113 *crp:: km*^{r}	Wild-tip BW25113	BW25113 *cya:: km*^{r}	BW25113 *crp:: km*^{r}
$CuSO_4$	468	468	468	625	625	625
$NiCI_2$	493	329	493	986	493	986
$CdSO_4$	72	145	145	96	193	193
$CoCI_2$	30	30	30	30	60	60
$ZnSO_4$	180	135	360	720	540	1078

3.3. Growth experiments

E. coli wild type, mutant and complement bacteria were observed to grow for 8 h at 160 rpm in nutrient broth medium that does not contain metal and contains metal at the rate of the

wild type MIC value and growth graphs are given in Figs. 2-7. It was shown in Fig. 2 that the growth of *E. coli* wild type and mutant cells in medium without metal is very similar with each other and approximately OD_{600} is between 1.4-1.6.

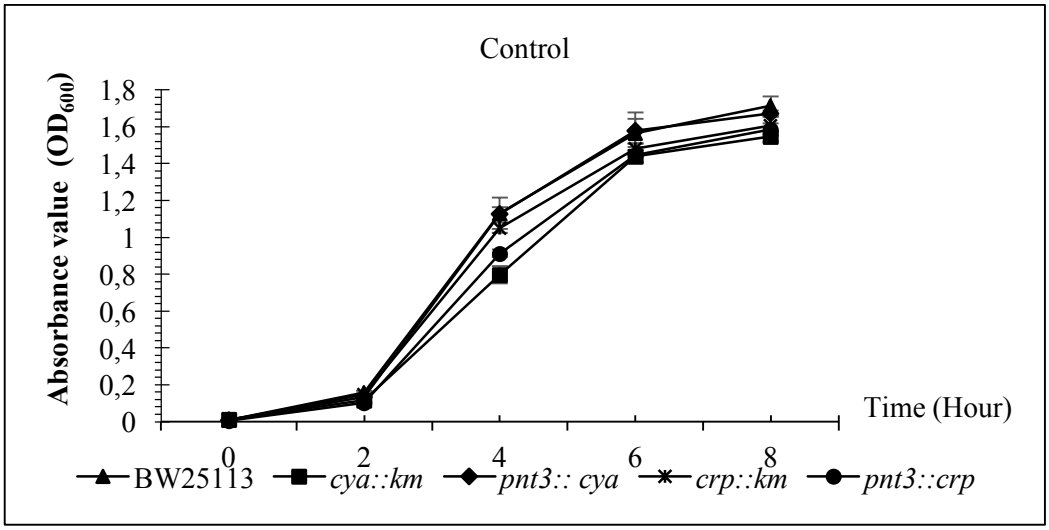

Figure 2: Growth of *E. coli* BW25113, *cyaA::km*^{r}, pnt3: *cyaA*, *crp::km*^{r} and pnt3 :: *crp* strains in metal-free medium. (*) ($p < 0.05$)

When the growth graphs in copper containing medium are examined in Fig. 3, it is seen that there was no a difference between wild type and mutant cells, and it grows up to OD_{600} 1.0. It was seen at the growth graphs obtained in the medium containing nickel metal that the wild type and the *crp::km* mutant grew close to each other, grew up to 0.5, while the *cyaA::km* mutant was more affected by nickel metal, and can grow up to 0.1. Therefore, it has been determined that the *cyaA* gene has an important role in growth in the presence of Ni (Fig. 4).

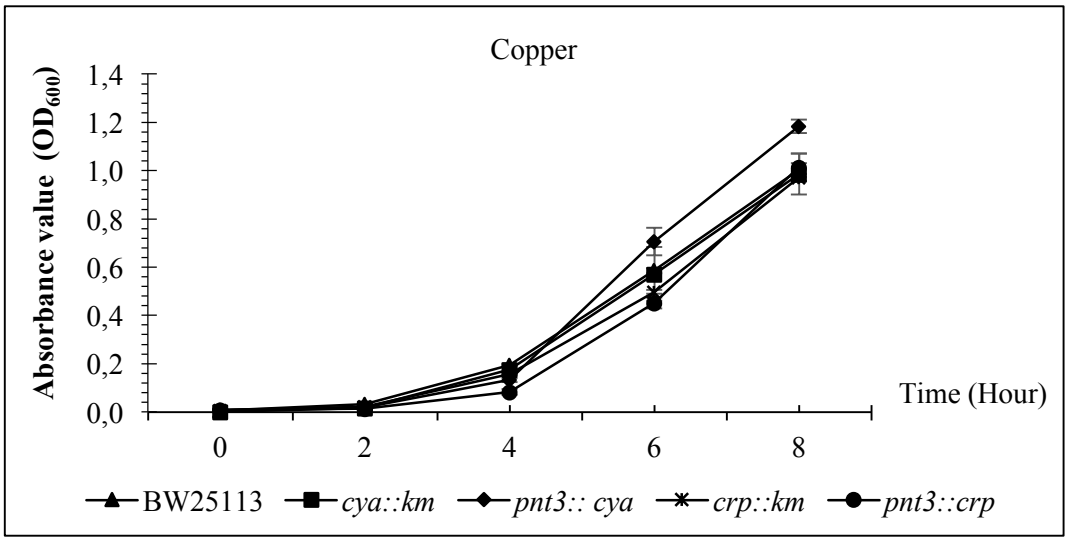

Figure 3: Growth of *E. coli* BW25113, *cyaA::km*^{r}, pnt3:: *cyaA*, *crp::km*^{r} and pnt3 :: *crp* strains in the presence of copper (Cu) metal. (*) ($p < 0.05$)

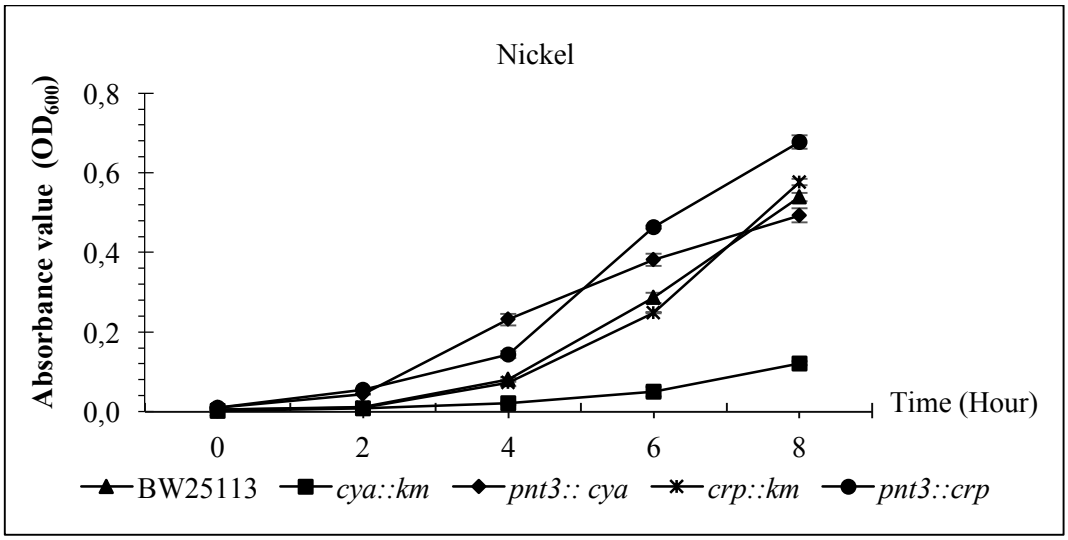

Figure 4: Growth of *E. coli* BW25113, *cyaA*::km^r, pnt3::*cyaA,* crp::km^r and pnt3::*crp* strains in the presence of Nickel (Ni) metal. (*) ($p < 0.05$)

When we look at the growth profiles in the medium containing cadmium metal, as seen in Fig. 5, the *crp::km* mutant grew up to 1.0 and partially affected as same as the wild type, which grows up to OD_{600} 1.2, while the *cyaA::km* mutant is highly affected by the cadmium metal. It has grown up to 0.7. The positive role of the *cya* gene in the presence of Cd was confirmed by complement tests.

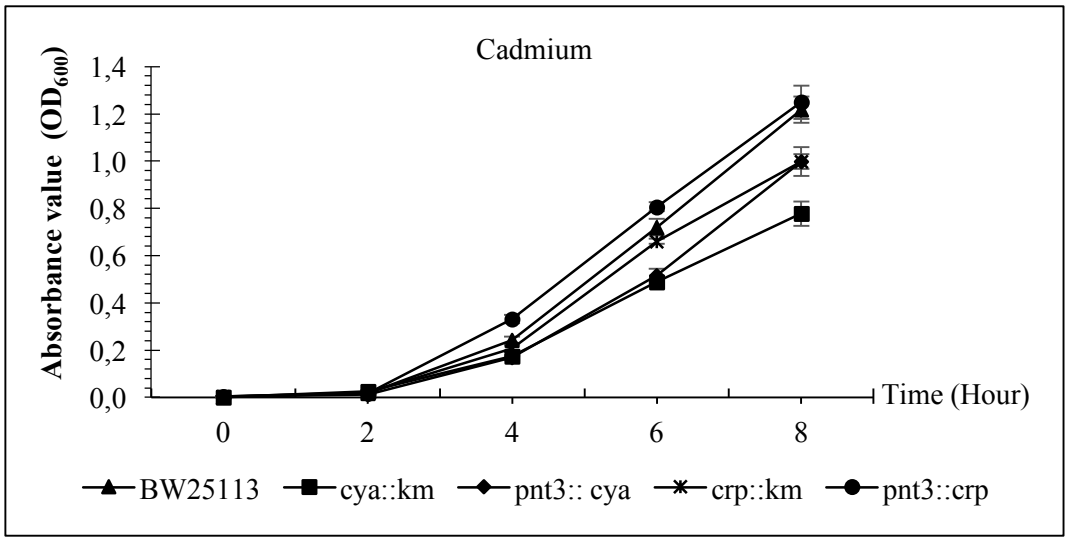

Figure 5: Growth of *E. coli* BW25113, *cyaA::km*^{r}, pnt3: *cyaA, crp::km*^{r} and pnt3*::crp* strains in the presence of cadmium (Cd) metal. (*) ($p < 0.05$)

As seen in Fig. 6, wild type and *crp::km* mutant grew close to each other (OD_{600} 0.6), while the *cyaA::km* mutant grew up to OD_{600} 0.3, and it was more sensitive to metal. Since the presence of the *cyaA* gene product induced in complement cells enables the cell to grow better, the role of this gene in the presence of Co has been confirmed.

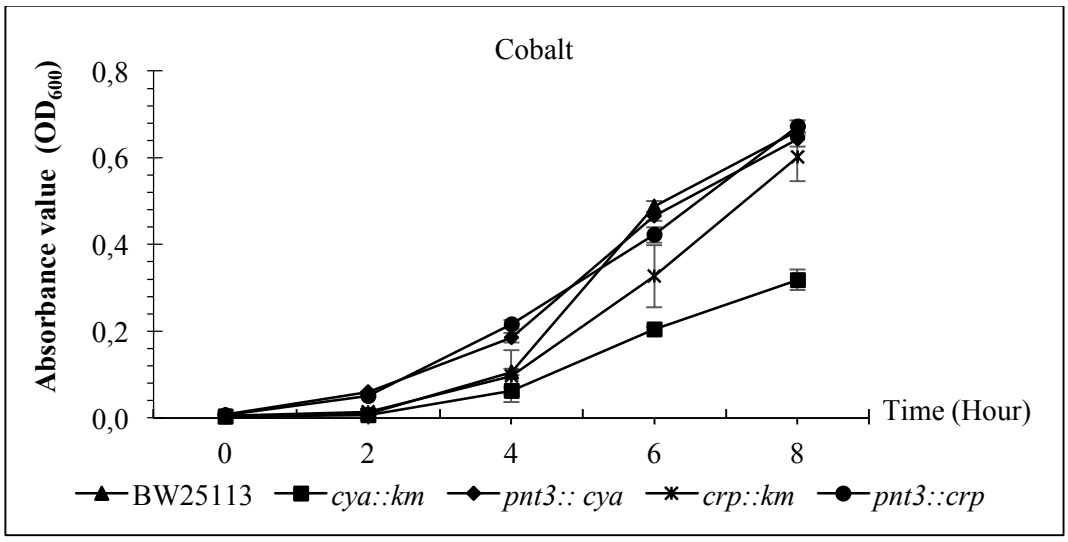

Figure 6: Growth of *E. coli* BW25113*, cyaA::km*^{r}, pnt3: *cyaA, crp::km*^{r} and pnt3*::crp* strains in the presence of cobalt metal. (*) ($p < 0.05$)

When the growth profiles of the wild-type and mutant strains in the zinc metal-containing medium in Fig. 7 were seen, it was observed that the *crp::km* mutant can grow up to 1.4 while the *cyaA::km* mutant can grow up to 0.8 compared to the wild-type growing up to OD_{600} 1.2. It has

been observed that the mutant is more affected by the metal and can grow to OD_{600} 0.8 (Fig. 7). It has been determined that cell growth is restored by the *cyaA* gene induced in complemented cells.

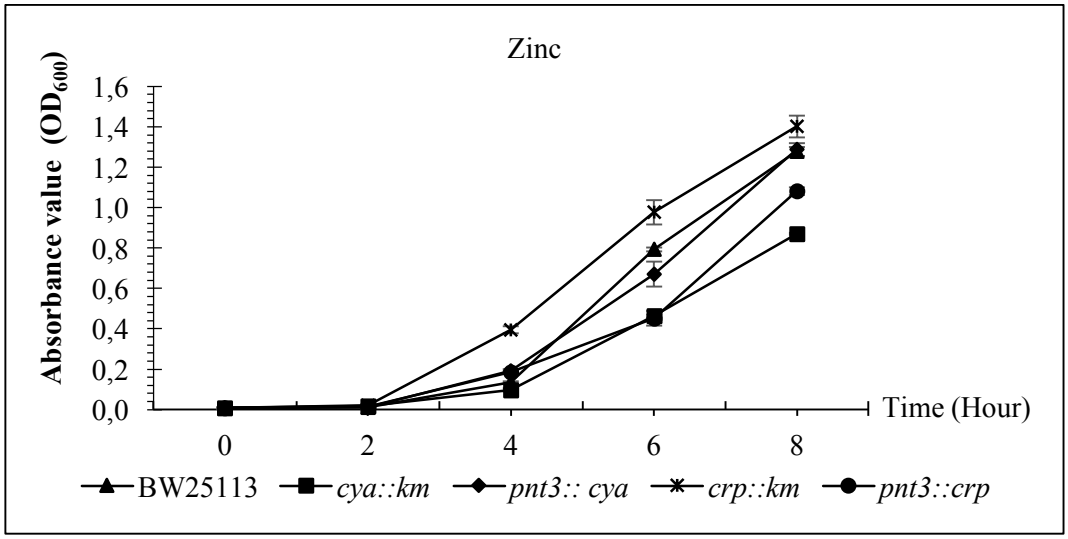

Figure 7: Growth test results of *E. coli* BW25113, *cyaA::km*^{r}, pnt3::*cyaA, crp::km*^{r} and pnt3::*crp* strains in the presence of zinc metal, (*) ($p < 0.05$)

3.4. Drop plate experiments

The effect of metal on different cell numbers was determined by plate dropping experiments of *E. coli* BW25113, *cyaA::km*^{r}, pnt3 :: *cyaA, crp ::km*^{r} and pnt3 *::crp* strains. As seen in Fig. 8A, there is no difference between the growth of wild type BW25113 and mutant cells in a metal-free plate dish. However, in plate dishes containing 1.0 mM copper, the highest concentration studied, the mutants show similar growth as the wild type (Fig. 8B). This result also supports the results in growth experiments.

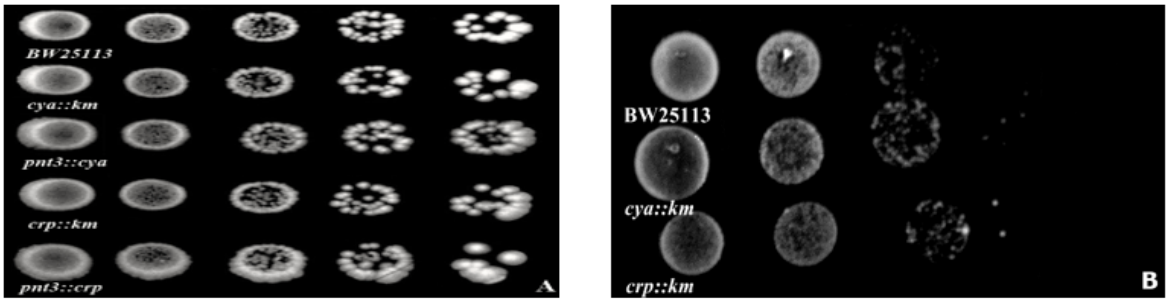

Figure 8: Plate dropping test results of *E. coli* BW25113, *cyaA::*km^r, pnt3: : *cyaA*, *crp::km*^{r} ve pnt3::*crp* strains. A: Metal free NA, B: NA with 1.0 mM Cu

It was seen in Fig. 9A that *crp::km*^{r} cells developed similar to *E. coli* BW25113 according to the dropping experiments performed on 0.7, 0.8 and 0.9 mM nickel-containing plate. However, it was seen in Figure 9B that *cyaA::km*^{r} cells were more affected and as a result of the expression of the complementary cell and the product of the *cyaA* gene on the plasmid again behaved like a wild type. As a result, when the *cyaA* gene is made mutant, the survival rate of the bacteria decreases in the presence of Ni, and it is seen that sensitivity occurs.

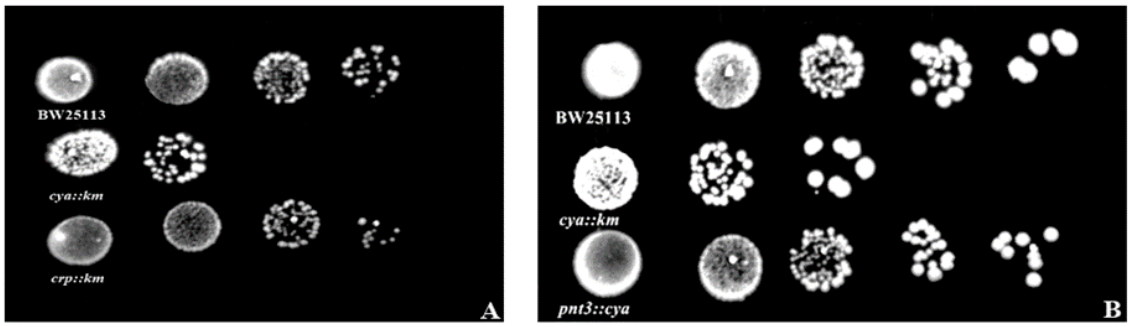

Figure 9: Plate dropping test results of *E. coli* BW25113, *cyaA::*km^r, pnt3::*cyaA*, *crp::km*^{r} ve pnt3::*crp* strains. A: NA containing 0.9 mM Ni, B: NA containing 0.8 mM Ni

According to the results of dropping on plate dishes containing 0.07 mM cadmium metal, the effect of the metal on *crp::km*^{r} cells was similar to *E. coli* BW25113, while its effect on *cyaA::km*^{r} cells was higher in Fig. 10A. Therefore, it has been determined that knockout of the *cyaA* gene causes sensitivity in the life of *E. coli* in the presence of Cd. This sensitivity indicates that *cyaA* as a role to live in the presence of Cd. The effect of the metal on the *cyaA::km*^{r} cells was again seen to resemble the wild type upon gene completion (Fig. 10B).

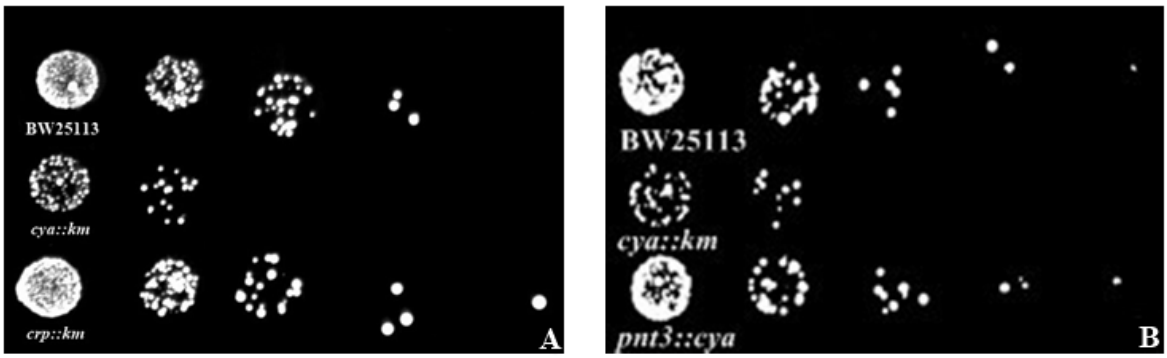

Figure 10: Plate dropping test results of *E. coli* BW25113, *cyaA::*km^r, pnt3::*cyaA*, *crp::km*^{r} ve pnt3::*crp* strains. A: NA with 0.07 mM Cd, B: NA with 0.07 mM Cd

According to the results of plate dropping with cobalt metal, *cyaA*::*km*^{r} strains were the most sensitive, while *crp*::km^{r} cells were affected similarly to the wild type (Fig. 11A). It was determined that the *cyaA* gene product is necessary for life in the presence of Co, and the cell's sensitivity increases when it is not. By using pnt3::*cyaA* complementary cell in the complement tests, it was determined that the effect of the metal against the cell was reduced and similar to the wild type (Fig. 11B).

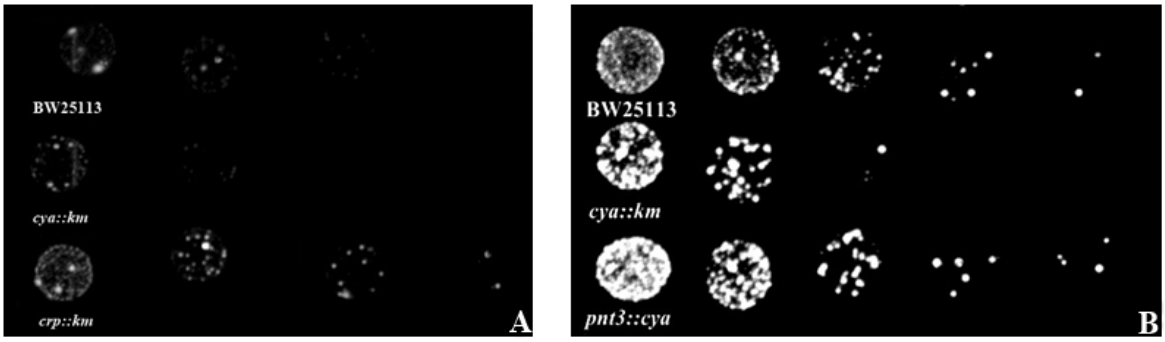

Figure 11: Plate dropping test results of *E. coli* BW25113, *cyaA*::km^{r}, pnt3: : *cyaA*, *crp*::*km*^{r} ve pnt3::*crp* strains. A: NA containing 0.50 mM Co, B: NA containing 0.40 mM Co

According to the results of plate dropping containing 0.27, 0.28 and 0.29 mM zinc, *cyaA*::*km*^{r} strains were the most sensitive to metal while *crp*::*km*^{r} cells were the most resistant (Fig. 12A-C). Performing these results with the completed cells was confirmed by affecting the cells as wild type again.

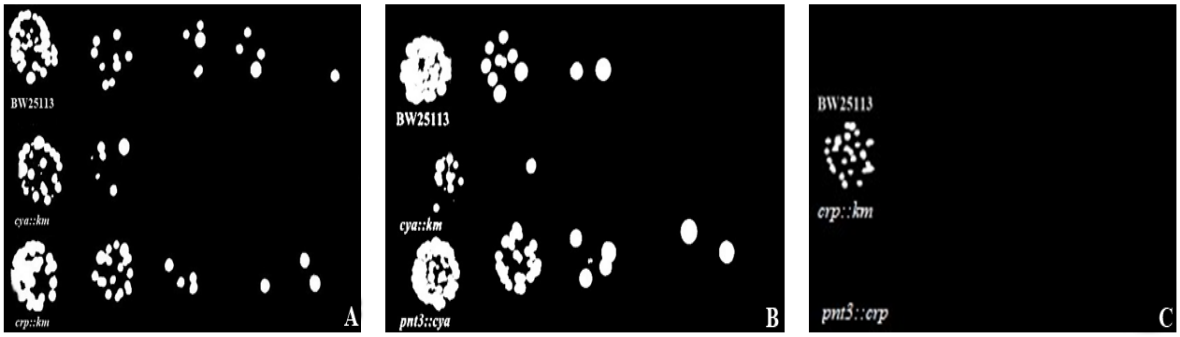

Figure 12: Plate dropping test results of *E. coli* BW25113, *cyaA*::km^{r}, pnt3: : *cyaA*, *crp*::*km*^{r} ve pnt3::*crp* strains A: NA with 0.27 mM Zn, B: NA with 0.28 mM Zn, C: NA with 0.29 mM Zn

4. Discussion

Metals are essential trace nutrients for the growth of living organisms. However, metals are toxic at high concentrations. For this reason, maintaining the metal balance in the cell is very

important for life. Bacteria possess complex metal homeostasis mechanisms to maintain the delicate balance between this metal starvation and toxicity [41]. Determining the genes involved in these complex regulatory systems and the functions of these genes is very important in terms of both bacterial life and fight against bacteria.

In this study, according to the MIC results of the copper, nickel, and cobalt metals, no significant difference was observed in the *cyaA* and *crp* mutants when compared with the wild type, while the MIC results of cadmium showed that the mutants were twice resistant according to the wild type. When MIC results of zinc metal were compared, it was determined that *cyaA* mutants were susceptible, while *crp* mutants were resistant according to wild type. The MCC results also support the MIC results of copper, cobalt, zinc, and cadmium metal. However, it was observed that the *cyaA* mutant, which did not show a significant difference in MIC results of nickel metal, was more sensitive than wild type in MCC results. This sensitivity was evident in growth experiments in the presence of nickel.

In our study, according to the results of plate dropping and growth experiments obtained with copper metal, cell life is not affected by deletion of *cyaA* and *crp* genes. According to these results, it can be thought that the *cyaA* and *crp* genes in *E. coli* do not have a role in protecting the copper metal balance in the cell. However, it is known that *E. coli* has many regulator systems in charge of ensuring the use of copper under changing environmental conditions and to protect it from its toxicity [14]. In *E. coli*, Cue and Cus, two important systems responsible for detoxification of excess copper, adjust the intracellular copper level according to cellular demand [18-42]. The CopA protein induced by CueR, which detects copper in the cell, enables the transfer of copper in the cytoplasm to the periplasm, while the CusCFBA pump induced by the CusR/S system, which detects the copper in the periplasm, ensures that the copper is expelled to the outside environment [18, 21, 43]. Our study shows that *cyaA* and *crp* genes do not play a role in maintaining copper metal balance, since they do not affect the life of mutant cells under copper stress.

In the results of cobalt, zinc, nickel, and cadmium petri dripping and growth experiments performed in our study, it was observed that *cyaA* mutant cells were more sensitive than wild type. cAMP is an intracellular messenger molecule synthesized from ATP by the adenylate cyclase enzyme CyaA, and its concentration in the cell changes due to various reasons [44]. Changes in intracellular cAMP concentration are known to be detected by the transcription factor CRP, and the resulting CRP-cAMP complex directly controls at least 500 promoters in *E. coli* [45]. Therefore, according to the results obtained in our study, it was determined that *cyaA* mutant cells exposed to nickel, cobalt, zinc, and cadmium metal stress were more affected than wild type.

In the literature, it has been reported that cAMP is degraded by enzymes stimulated by the increase in the amount of Ca^{2+}, Fe^{2+} or Co^{2+} in the cell, and thus the amount of cAMP in the environment decreases [46]. In our study, it can be stated that the deletion of the *cyaA* gene, which acts as the 'main' regulator for transcription factors, is sensitive to the inhibition of cAMP production from ATP and in the presence of Ni^{2+}, Cd^{2+} and Zn^{2+} metals in the cell, because it cannot show a regulatory role on the genes required for resistance. In this case, it can be stated that *cyaA* mutants control genes associated with Ni, Cd, and Zn resistance, and their regulation of these genes should be studied.

Another situation obtained in our study was that although there was no difference between the wild type and *crp* mutant cells in the presence of cobalt, copper, nickel, and cadmium metals, it was determined that mutant cells were more resistant under zinc stress. Sun, H., et al. (2011), sequencing of *crp* genes were performed in Fe^{3+} resistant *E. coli* K-12 MG1655 bacteria, and it was determined that two mutations occurred on the gene. In addition, in the study, it was determined that different metals caused mutations on different genes and as a result, resistant strains were obtained [47]. Because Zn^{2+} forms more stable complexes than other basic metal ions, zinc toxicity is thought to be due to improper binding of metalloproteins to metals. Therefore, intracellular concentrations must be tightly regulated [48, 49]. The presence of Zn^{2+} in bacteria is detected by various transcription factors sensitive to zinc inside the cell [50, 51]. Among these transcription factors, Zur [52-55] and AdcR [56-58] to increase zinc uptake; *zntR*, *smtB*, *ziaR*, and *czrA* genes [59-62] are included to increase the excretion and intracellular secretion of zinc. It is also known to play a role in many global regulatory mechanisms such as RpoS, which are found to be involved in metal stress [63-66]. In the study, it is thought that the *crp* gene mutant cells in the presence of zinc metal are more resistant than the wild type, either because they prevent excess zinc passage into the cell as a result of affecting the genes associated with zinc uptake, or it may be due to the excretion of excess zinc in the cell by affecting the genes that play a role in zinc excretion mechanisms.

5. Conclusion

In this study, it has been found that there is a relationship between *cyaA*-*crp* genes and resistance or sensitivity to Ni, Cd, Co, Cu, and Zn metals. It has been determined that adenylate cyclase has an important role in life against metals since it is sensitive to metals except Cu, especially in the absence of adenylate cyclase, the product of *cyaA gene*. In this case, the roles of genes such as *zntR, cueO, cueR,* and *nikR,* which are directly involved in the intracellular regulation of metals in *E. coli*, should be investigated in future studies.

Acknowledgement

We would like to thank Bilecik Şeyh Edebali University for supporting our study with the BAP project number 2016-02.BŞEÜ.04-02.

References

[1] Waldron, K.J., Robinson, N.J., *How do bacterial cells ensure that metalloproteins get the correct metal?,* Nature Reviews Microbiology, 7, 25-35, 2009.

[2] Porcheron, G., Garénaux, A., Proulx, J., Sabri, M., Dozois, C.M., *Iron, copper, zinc, and manganese transport and regulation in pathogenic Enterobacteria: correlations between strains, site of infection and the relative importance of the different metal transport systems for virulence,* Frontiers in Cellular and Infection Microbiology, 3, 90, 2013.

[3] Chandrangsu, P., Rensing, C., Helmann, J.D., *Metal homeostasis and resistance in bacteria,* Nature Reviews Microbiology,15, 338-350, 2017.

[4] Gray, H.B., Ellis Jr., W.R. *Electron transfer* In Bioinorganic Chemistry. (Bertini, I., Gray, H.B., Lippard, S.J. &Valentine, J.S., eds.), University Science Books, Mill Valley, California., pp. 315-363, 1994.

[5] Shaivastave, A., Singh V., Jadon, S., Bhadauria, S., *Heavy Metal Tolerance of Three Different Bacteria Isolated from Industrial Effluent,* International Journal of Pharmaceutical Research and Bio-Science, 2, 137-47, 2013.

[6] Hohl, H., Varma, A., *Soil: The Living Matrix*, *Soil Heavy Metals*, 1-18, 2010.

[7] Sherameti I, Varma A., *Heavy metal contamination of soils: monitoring and remediation*. Springer, New York 2015.

[8] Dixit R., Wasiullah, Malaviya, D., Pandiyan, K., Singh U.B., Sahu A., Shukla R., Singh B.P., Rai J.P., Sharma P.K., Lade H., Paul, D., *Bioremediation of Heavy Metals from Soil and Aquatic Environment: An Overview of Principles and Criteria of Fundamental Processes*, Sustainability, 7(2), 2189-2212, 2015.

[9] Kılınç, K.N., Dönmez, G., *Mikroorganizmalarda Ağır Metal Stresine Yanıtın Proteom Analizi ile Araştırılması,* Elektronik Mikrobiyoloji Dergisi TR, 06, 27-33, 2008.

[10] Lemire, J.A., Harrison, J.J., Turner, R.J., *Antimicrobial activity of metals: mechanisms, molecular targets and applications,* Nature Reviews Microbiology, 11, 371-384. 2013.

[11] Palmer, L.D., Skaar, E.P., *Transition metals and virulence in bacteria*, Annual Review of Genetics, 50, 67-91, 2016.

[12] Macomber, L., Hausinger, R.P., *Mechanisms of nickel toxicity in microorganisms*, Metallomics, 3, 1153-1162, 2011.

[13] Baksh K.A., Zamble, D.B. *Allosteric control of metal-responsive transcriptional regulators in bacteria*, Journal of Biological Chemistry, 295(6), 1673-1684, 2019.

[14] Bruins, R.M., Kapil, S., Oehme W.F., *Microbial Resistance to Metals in the Environment*, Ecotoxicology and Environmental Safety, 45, 198-207. 2000.

[15] Capdevila, D.A., Edmonds, K.A., Giedroc, D.P. *Metallochaperones and metalloregulation in bacteria*, Essays Biochemistry. 61, 177-200, 2017.

[16] Foster, A.W., Osman, D., Robinson, N.J., *Metal preferences and metalation*, Journal of Biological Chemistry. 289, 28095–28103, 2014.

[17] O'Halloran, T.V. *Transition metals in control of gene expression*, Science, 261, 715-725, 1993.

[18] Mermod, M., Magnani, D., Solioz, M., Stoyanov, J.V. *The copper- inducible ComR (YcfQ) repressor regulates expression of ComC (YcfR), which affects copper permeability of the outer membrane of Escherichia coli*, BioMetals, 25, 33-43. 2012.

[19] Harrison, J.J., Turner, R.J., Ceri, H., *Persister cells, the biofilm matrix and tolerance to metal cations in biofilm and planktonic Pseudomonas aeruginosa*, Environmental Microbiology 7 (7), 981-994, 2005.

[20] Grass, G., Rensing, C., *Genes involved in copper homeostasis in Escherichia coli,* Journal of Bacteriology, 183, 2145-2147, 2001.

[21] Rensing, C., Grass, G., *Escherichia coli mechanisms of copper homeostasis in a changing environment*, FEMS Microbiology Reviews, 27, 197-213. 2003.

[22] Rensing, C., Mitra, B., Rosen, B.P., *The zntA gene of Escherichia coli encodes a Zn(II)-translocating P-type ATPase*, Proceedings of the National Academy of Sciences USA, 94, 14326-14331, 1997. 22

[23] Lee, C., Kuo, Y.L., *The evolution of diffusion barriers in copper metallization*, The Journal of The Minerals, 59, 44-49, 2008.

[25] Valencia, E.Y., Braz, V.S., Guzzo, C., Marques M.V., *Two RND proteins involved in heavy metal efflux in Caulobacter crescentus belong to separate clusters within proteobacteria*, BMC Microbiology, 13:79, 1471-2180, 2013.

[25] Higuchi, M., Ozaki, H., Matsui, M., Sonoike, K., *A T-DNA insertion mutant of AtHMA1 gene encoding a Cu transporting ATPase in Arabidopsis thaliana has a defect in the water–water cycle of photosynthesis*, Journal of Photochemistry and Photobiology B: Biology, 94 (3), 205-213, 2009.

[26] Nies, D.H., *Efflux-mediated heavy metal resistance in prokaryotes*, FEMS Microbiology Reviews, 27, 313-339, 2003.

[27] Chao, Y., Fu, D., *Kinetic Study of the Antiport Mechanism of an Escherichia coli Zinc Transporter*, *ZitB*, Journal of Biological Chemistry, 279(13), 12043-12050, 2004.

[28] Wei, Y., Fu, D., *Selective metal binding to a membraneembedded aspartate in the Escherichia coli metal transporter YiiP (FieF)*, Journal of Biological Chemistry, 280, 33716-33724, 2005.

[29] Blanco, P., Hernando-Amado, S., Reales-Calderon, J., Corona, F., Lira, F., Alcalde-Rico, M., vd., *Bacterial multidrug efflux pumps: much more than antibiotic resistance determinants,* Microorganisms, 4 (1), 14, 2016.

[30] Sakamoto,Y., Furukawa, S., Ogihara, H., Yamasaki, M., *Fosmidomycin Resistance in Adenylate Cyclase Deficient (cya) Mutants of Escherichia coli,* Bioscience, Biotechnology, and Biochemistry, 67(9), 2030-2033, 2003.

[31] Botsford, L. J., *Cyclic AMP in Prokaryotes*, Microbiological Rewievs, 56(1), 100-122. 1992.

[32] Nosho, K., Fukushima, H., Asai, T., Masahiro Nishio, M., Takamaru, R., Kobayashi-Kirschvink, K.J., Ogawa,T., Hidaka, M., Masaki, H., *cAMP-CRP acts as a key regulator for the viable but non-culturable state in Escherichia coli,* Microbiology, 164, 410-419, 2018.

[33] Shimada, T., Fujita, N., Yamamoto, K., Ishihama, A., *Novel roles of cAMP receptor protein (CRP) in regulation of transport and metabolism of carbon sources.* PLoS One, 6:e20081. 2011.

[34] Xue, J., Tan, B., Yang, S., Luo, M., Xia, H., Zhang, X., Zhou, X., Yang, X., Yang, R., Li, Y. et al., *Influence of cAMP receptor protein (CRP) on bacterial virulence and transcriptional regulation of allS by CRP in Klebsiella pneumoniae*, Gene, 593, 28-33, 2016.

[35] El Mouali, Y., Gaviria-Cantin, T., Sa´ nchez-Romero, M.A., Gibert M., Westermann A.J., Vogel, J., Balsalobre, C., *CRP-cAMP mediates silencing of Salmonella virulence at the post-transcriptional level,* PLoS Genetics, 14:e1007401. 2018.

[36] Manneh-Roussel, J., Haycocks, J.R.J., Magan, A., Perez-Soto, N., Voelz, K., Camilli, A., Krachler, A.M., Grainger, D.C., *cAMP receptor protein controls vibrio cholerae gene expression in response to host colonization,* mBio., 9, 2018.

[37] McDonough, K.A., Rodriguez, A., *The myriad roles of cyclic AMP in microbial pathogens: from signal to sword,* Nature Reviews Microbiology, 10, 27-38, 2011.

[38] Miller, D., *The Generic Strategy Trap*, Journal of Business Strategy, 13(1), 37-41, 1992.

[39] Wiegand, I., Hilpert, K., Hancock, R.E., *Agar and broth dilution methods to determine the minimal inhibitory concentration (MIC) of antimicrobial substances, Nature Protocols*., 3(2), 163-75, 2008.

[40] Hoben, H.J., Somasegaran, P., *Comparison of the pour, spread, and drop plate methods for enumeration of Rhizobium spp. in inoculants made from presterilized peat*, Applied and Environmental Microbiology, 44, 1246-1247, 1982.

[41] Li, C., Li, Y., Ding, C., *The Role of Copper Homeostasis at the Host-Pathogen Axis: From Bacteria to Fungi*, International Journal of Molecular Sciences., 20(1), 175, 2019.

[42] Solioz, M., *Copper homeostasis in gram-negative bacteria, In: Copper and Bacteria: Evolution, Homeostasis and Toxicity.* Cham: Springer International Publishing, 49-80, 2018.

[43] Rademacher, C., Masepohl, B., *Copper-responsive gene regulation in bacteria*, Microbiology, 158(10), 2451-2464, 2012.

[44] Mouali, Y.E., Gaviria-Cantin, T., MarõÂa Antonia SaÂnchez-Romero, M.A., Gibert, M., Westermann, A.J., Jörg Vogel, J., Balsalobre, C., *CRP-cAMP mediates silencing of Salmonella virulence at the post-transcriptional level,* PLoS Genetics, 14(6), 2018.

[45] Amin, N., Peterkofsky A., *A Dual Mechanism for Regulating cAMP Levels in Escherichia coli*, Journal of Biological Chemistry., 270, 11803-11805, 1995.

[46] Iwasa Y., Yonemitsu, K., Miyamoto, *A calcium-dependent cyclic nucleotide phosphodiesterase from Escherichia coli,* FEBS Letters., 124, 207-209, 1981.

[47] Sun, H., Lu, X., Gao, P., *The exploration of the antibacterial mechanism of* Fe^{3+} *against bacteria.* Brazilian Journal of Microbiology 42(1), 410-414, 2011.

[48] Irving, H.M.N.H., Williams, R.J.P., *The stability of transition-metal complexes,* Journal of the Chemical Society, 3192-3210, 1953.

[49] Shin, J.H., Helmann, J.D., *Molecular logic of the Zur-regulated zinc deprivation response in Bacillus subtilis, Nature Communications*. 7, 9, 2016.

[50] Waldron, K.J., Robinson, N.J., *How do bacterial cells ensure that metalloproteins get the correct metal?*, Nature Reviews Microbiology, 7, 25-35, 2009.

[51] Outten, C.E., O'Halloran, T.V., *Femtomolar sensitivity of metalloregulatory proteins controlling zinc homeostasis*, Science 292, 2488-2492, 2001.

[52] Patzer, S.I., Hantke, K., *The ZnuABC high-affinity zinc uptake system and its regulator Zur in Escherichia coli*, Molecular Microbiology. 28, 1199-1210, 1998.

[53] Lucarelli, D., Vasil, M.L., Meyer-Klaucke, W., Pohl, E., *The metal-dependent regulators FurA and FurB from Mycobacterium tuberculosis,* International Journal of Molecular Sciences. 9, 1548-1560, 2008.

[54] Shin, J.H., Oh, S.Y., Kim, S.J., Roe, J.H., *The zinc-responsive regulator Zur controls a zinc uptake system and some ribosomal proteins in Streptomyces coelicolor A3(2),* Journal of Bacteriology. 189, 4070-4077, 2007.

[55] Gilston, B.A., Wang, S.N., Marcus, M.D., Canalizo-Hernandez, M.A., Swindell, E.P., Xue, Y. et al., *Structural and mechanistic basis of zinc regulation across the E. coli Zur regulon,* PLOS Biology. 12, 16, 2014.

[56] Zhu, R.F., Song, Y.Q., Liu, H.P., Yang, Y.F., Wang, S.L., Yi, C.Q. et al. *Allosteric histidine switch for regulation of intracellular zinc(II) fluctuation*, Proceedings of the National Academy of Sciences. U.S.A. 114, 13661-13666, 2017.

[57] Guerra, A.J., Dann, C.E., Giedroc, D.P. *Crystal structure of the zinc-dependent MarR family transcriptional regulator AdcR in the Zn(II)-bound state,* Journal of the American Chemical Society. 133, 19614-19617, 2011.

[58] Sanson, M., Makthal, N., Flores, A.R., Olsen, R.J., Musser, J.M., Kumaraswami, M. *Adhesin competence repressor (AdcR) from Streptococcus pyogenes controls adaptive responses to zinc limitation and contributes to virulence*, Nucleic Acids Research. 43, 418-432, 2015.

[59] Morby, A.P., Turner, J.S., Huckle, J.W., Robinson, N.J., *SmtB is a metal-dependent repressor of the cyanobacterial metallothionein gene smtA—identification of a Zn inhibited DNA-protein complex,* Nucleic Acids Research. 21, 921-925, 1993.

[60] Kondrat, F.D.L., Kowald, G.R., Scarff, C.A., Scrivens, J.H., Blindauer, C.A. *Resolution of a paradox by native mass spectrometry: facile occupation of all four metal binding sites in the dimeric zinc sensor SmtB*, Chemical Communications, 49, 813-815, 2013.

[61] Thelwell, C., Robinson, N.J., Turner-Cavet, J.S., *An SmtB-like repressor from Synechocystis PCC 6803 regulates a zinc exporter,* Proceedings of the National Academy of Sciences , U.S.A. 95, 10728-10733, 1998.

[62] Arunkumar, A.I., Campanello, G.C., Giedroc, D.P. *Solution structure of a paradigm ArsR family zinc sensor in the DNA-bound state,* Proceedings of the National Academy of Sciences, U.S.A. 106, 18177-18182, 2009.

[63] Darcan, C., Kaygusuz, Ö., Aydın, E., *Investigation of the role of RpoS in Escherichia coli againts Metals*, Anadolu University Journal of Science and Technology C- Life Sciences and Biotechnology, 7(2), 105-121, 2018.

[64] Dong, T., Kirchhof, G.M., Schellhorn, H.E., *RpoS regulation of gene expression during exponential growth of Escherichia coli K12*, Molecular Genetics and Genomics, 279, 267-277, 2008.

[65] Macomber, L., Rensing, C., Imlay, J.A., *Intracellular copper does not catalyze the formation of oxidative DNA damage in Escherichia coli,* Journal of Bacteriology 189, 1616-1626, 2007.

[66] Troxell, B., Ye, M., Yang, Y., Carrasco, S.E., Lou, Y., Yanga, X.F., *Manganese and Zinc Regulate Virulence Determinants in Borrelia burgdorferi,* Infection and Immunity, 81(8), 2743-2752, 2013.

Adıyaman University Journal of Science
https://dergipark.org.tr/en/pub/adyujsci
DergiPark AKADEMİK
ISSN 2147-1630
e-ISSN 2146-586X

Parameter Estimation on Geometric Distribution of Order k with Different Reward Laws

Fatih ŞAHİN[1], Coşkun KUŞ[2], İsmail KINACI[3], Kadir KARAKAYA[4,*], Yunus AKDOĞAN[5]

[1]*Selçuk University, Science Faculty, Department of Statistics, Konya, Turkey*
fatihsahin0644@gmail.com, ORCID: 0000-0002-2012-0021
[2]*Selçuk University, Science Faculty, Department of Statistics, Konya, Turkey*
coskun@selcuk.edu.tr, ORCID: 0000-0002-7176-0176
[3]*Selçuk University, Science Faculty, Department of Actuarial Science, Konya, Turkey*
ikinaci@selcuk.edu.tr, ORCID: 0000-0002-0992-4133
[4]*Selçuk University, Science Faculty, Department of Statistics, Konya, Turkey*
kkarakaya@selcuk.edu.tr, ORCID: 0000-0002-0781-3587
[5]*Selçuk University, Science Faculty, Department of Statistics, Konya, Turkey*
yakdogan@selcuk.edu.tr, ORCID: 0000-0003-3520-7493

Received: 02.02.2021 **Accepted:** 13.04.2021 **Published:** 30.06.2021

Abstract

Let $\xi_1, \xi_2, \ldots$ be a sequence of independent trials with two possible outcomes, "0" and "1" where "1" represents the success of Type-I, and "0" denotes the success of Type-II. For nonnegative integers k_r and k_l using a reward scheme, we obtained the distribution of the number of trials (W) until the sum of consecutive rewards of Type-I is equal to or exceeds the level k_r, or the sum of consecutive rewards of Type-II is equal to or exceeds the level k_l. The geometric distributed rewards are studied by Eryılmaz et al. in [1]. In this study, the survival function of W is obtained for binary sequence with Bernoulli and exponential rewards as well as geometric rewards. A simulation study is performed to compare the theoretical and simulated probabilities. Proportion estimates are also discussed for distribution of W with geometric rewards.

* Corresponding Author
DOI: 10.37094/adyujsci.873193

Keywords: Geometric distribution of order k; Bernoulli reward; Exponential reward; Estimation.

Farklı Ödül Kuralları ile Ödüllü *k* Ardıl Geometrik Dağılımın Parametre Tahmini

Öz

$\xi_1, \xi_2, \ldots$ "0" ve "1" olmak üzere iki olası sonuca sahip bağımsız denemelerin bir dizisi olsun, burada "1", I. tip başarıyı ve "0", II. tip başarıyı temsil etmektedir. Ödül şemasında kullanan negatif olmayan k_r ve k_l tamsayıları için, ardışık I. tip başarılardan elde edilen toplam ödüllerin k_r yi veya ardışık II. tip başarılardan elde edilen ödüllerin toplamı k_l'yi aşana kadar yapılan deneme sayısının (W) dağılımı elde edilmiştir. Geometrik dağılımlı ödüller Eryılmaz ve arkadaşları [1] tarafından çalışılmıştır. Bu çalışmada, W'nun yaşam fonksiyonu geometrik ödülün yanı sıra Bernoulli ve üstel ödüller için de elde edilmiştir. Teorik ve simüle edilmiş olasılıkları karşılaştırmak için bir simülasyon çalışması yapılmıştır. Ayrıca W'nun oran tahmini, ödüllerin geometrik olduğu durum için tartışılmıştır.

Anahtar Kelimeler: Ödüllü k ardıl geometrik dağılım; Bernoulli ödül; Üstel ödül; Tahmin.

1. Introduction

The geometric distribution is a well-known discrete distribution in the probability theory. Therefore, distribution with many generalized geometric sub-models are constructed. Some generalization of the geometric distribution can be found in [1-4].

In this paper, the survival function of the waiting time introduced by Eryılmaz et al. [1] is presented in a different way. Eryılmaz et al. [1] use the phase type distribution with matrix notations to obtaining waiting time distribution. However, we use the longest run's distribution without matrix calculation (it is introduced by Demir and Eryılmaz [5]) to get the distribution of W. It is only a different way and it is not main contribution. The main contribution of the paper is to provide the different kinds of rewards such as exponential and binomial and to discuss the estimation for the parameters of the distribution of waiting time W. In Section 2, the survival function of W is presented for binary sequence in a different way with Bernoulli and exponential rewards besides geometric one. A simulation study is also performed to control the true probabilities. In Section 3, point estimation is discussed by the proportion method. In section 4, a numerical example is given. Some concluding remarks are provided in Section 5.

2. Distribution of Waiting Time *W* with Different Rewards

In this section, we present the distribution of waiting time proposed by Eryılmaz et al. [1] under independent binary trials with different rewards. It is noticed that survival probabilities of [1] is obtained in a different way.

Let $\{\xi_n,\ n\geq 1\}$ be a sequence of independent trials that can take values 0 and 1. Let "1" and "0" indicate the Type-I and Type-II success, Y and Z denote the random earned rewards associated with the Type-I and Type-II success, respectively. Furthermore, $P\{Y>0\}=1$ and $P\{Z>0\}=1$. Throughout the paper, we suppose that $Y_1,Y_2,...$ and $Z_1,Z_2,\ldots$ are independent (also independent with trials) random rewards with cumulative distribution functions $F(x)=P\{Y_i\leq x\}$ and $G(x)=P\{Z_i\leq x\}$, $i=1,2,\ldots$, respectively. Mallor and Santos [6] proposed a scheme for giving rewards $\{Y_i,\ i\geq 1\}$ and $\{Z_i,\ i\geq 1\}$. The random variable $Y_i(Z_i)$ is associated with Type-I (Type-II) success when it occupies the *i*th place in a run of successes of Type-I (Type-II).

Let us consider the sequence of binary trials

101011001001011.

According to [6] the reward scheme, reward sequence is as following:

$$y_1,z_1,y_1,z_1,y_1,y_2,z_1,z_2,y_1,z_1,z_2,y_1,z_1,y_1,y_2$$

where $y(z)$, is a realization of $Y(Z)$. This scheme is also used by [1].

Eryılmaz et al. [1] consider the trinary independent sequence and obtained the distribution of the number of trials W until either the sum of consecutive rewards of Type-I is equal to or exceeds the level k_r, or the sum of consecutive rewards of Type-II is equal to or exceeds the level k_l.

We give the following two lemmas in order to obtain another representation for the distribution of W. The following lemma is a consequence of Theorem 2 in [1].

Lemma 1. Let $\{\xi_n,\ n\geq 1\}$ arbitrarily dependent binary trials and $L_n^{(1)}$ and $L_n^{(2)}$ denote the number of longest runs for Type-I and Type-II success. Then survival function of W is given by

$$P\{W>n\}=\sum_{m_1=0}^{n}\sum_{m_2=0}^{n}P\left\{\sum_{i=1}^{m_1}Y_i<k_r,\sum_{i=1}^{m_2}Z_i<k_l\right\}P\left\{L_n^{(1)}=m_1,L_n^{(2)}=m_2\right\}$$

$$=\sum_{m_1=0}^{n}\sum_{m_2=0}^{n}\left\{1-P\left(\sum_{i=1}^{m_1}Y_i\geq k_r\right)\right\}\left\{1-P\left(\sum_{i=1}^{m_2}Z_i\geq k_l\right)\right\}$$

$$\times\left[P\left\{L_n^{(1)}<m_1,L_n^{(2)}<m_2\right\}-P\left\{L_n^{(1)}<m_1+1,L_n^{(2)}<m_2\right\}\right.$$

$$\left.-P\left\{L_n^{(1)}<m_1,L_n^{(2)}<m_2+2\right\}+P\left\{L_n^{(1)}<m_1+1,L_n^{(2)}<m_2+1\right\}\right].$$

Lemma 2. [5] Let $\{\xi_n,\, n\geq 1\}$ independent binary trials with $P(\xi_1=1)=p$ and $P(\xi_1=0)=1-p$. In addition, $L_n^{(1)}$ and $L_n^{(2)}$ denote the number of longest runs for Type-I and Type-II success. Then

$$P\left\{L_n^{(1)}<k_1,L_n^{(2)}<k_2\right\}=\sum_{r_1}\sum_{r_2}\sum_{n_1}N(r_1,k_1,n_1)N(r_2,k_2,n-n_1)b(r_1,r_2,n_1,n),$$

where

$$N(a,b,c)=\sum_{j=0}^{a}(-1)^j\binom{a}{j}\binom{c-j(b-1)-1}{a-1} \tag{1}$$

and

$$b(r_1,r_2,n_1,n)=\begin{cases}2p^{n_1}(1-p)^{(n-n_1)}, & r_1=r_2\\ p^{n_1}(1-p)^{(n-n_1)}, & r_2=r_1+1 \text{ veya } r_1=r_2+1\\ 0, & \text{otherwise}\end{cases} \tag{2}$$

The following theorem is another form of the Theorem 2 of [1].

Theorem 1. Let $\{\xi_n,\, n\geq 1\}$ independent binary trials and $\{\xi_n,\, n\geq 1\}$ independent from rewards $\{Y_i,\, i\geq 1\}$ and $\{Z_i,\, i\geq 1\}$. Then survival function of W is given by

$$
\begin{aligned}
P\{W>n\} = \sum_{m_1=0}^{n}\sum_{m_2=0}^{n}\left\{1-P\left(\sum_{i=1}^{m_1}Y_i \geq k_r\right)\right\}\left\{1-P\left(\sum_{i=1}^{m_2}Z_i \geq k_l\right)\right\} \\
\times\Bigg\{\sum_{r_1=1}^{\left[\frac{n}{2}+1\right]}\sum_{r_2=1}^{\left[\frac{n}{2}+1\right]}\sum_{n_1=0}^{n}N\left(r_1,m_1,n_1\right)N\left(r_2,m_2,n-n_1\right)b\left(r_1,r_2,n_1,n\right) \\
-\sum_{r_1=1}^{\left[\frac{n}{2}+1\right]}\sum_{r_2=1}^{\left[\frac{n}{2}+1\right]}\sum_{n_1=0}^{n}N\left(r_1,m_1+1,n_1\right)N\left(r_2,m_2,n-n_1\right)b\left(r_1,r_2,n_1,n\right) \\
-\sum_{r_1=1}^{\left[\frac{n}{2}+1\right]}\sum_{r_2=1}^{\left[\frac{n}{2}+1\right]}\sum_{n_1=0}^{n}N\left(r_1,m_1,n_1\right)N\left(r_2,m_2+2,n-n_1\right)b\left(r_1,r_2,n_1,n\right) \\
\sum_{r_1=1}^{\left[\frac{n}{2}+1\right]}\sum_{r_2=1}^{\left[\frac{n}{2}+1\right]}\sum_{n_1=0}^{n}N\left(r_1,m_1+1,n_1\right)N\left(r_2,m_2+1,n-n_1\right)b\left(r_1,r_2,n_1,n\right)\Bigg\},
\end{aligned}
\tag{3}
$$

where $N\left(a,b,c\right)$ and $b\left(r_1,r_2,n_1,n\right)$ are defined as in Eqn. (1) and Eqn. (2), respectively.

Proof. Proof follows from using Lemma 2 in Lemma 1.

Let gives some numerical computation for the survival function of W with the geometric rewards. $Y_1,Y_2,\ldots$ iid random variables with probability mass function (pmf)

$$P\{Y_i=y\}=p_r(1-p_r)^{y-1},\ y=1,2,\ldots \tag{4}$$

and $Z_1,Z_2,\ldots$ iid random variables with

$$P\{Z_i=z\}=p_l(1-p_l)^{z-1},\ \ z=1,2,\ldots \tag{5}$$

for $i=1,2,\ldots.$ In this case for $k_r>n>0$, Eryılmaz et al. [1] gives

$$P\left\{\sum_{i=1}^{n}Y_i \geq k_r\right\}=1-\sum_{y=n}^{k_r-1}\binom{y-1}{n-1}p_r^n\left(1-p_r\right)^{y-n}, \tag{6}$$

and for $k_l>n>0$

$$P\left\{\sum_{i=1}^{n}Z_i \geq k_l\right\}=1-\sum_{z=n}^{k_l-1}\binom{z-1}{n-1}p_l^n\left(1-p_l\right)^{z-n}. \tag{7}$$

We consider two different kinds of rewards as well as geometric ones.

Let us consider $Y_1, Y_2, \ldots$ are iid Bernoulli random variables with pmf $f_{Y_i}(y) = P(Y_i = y) = {p_r}^{y}(1-p_r)^{1-y}$, $y = 0,1$ and $Z_1, Z_2, \ldots$ denote the iid random variables with pmf $f_{Z_i}(z) = P(Z_i = z) = {p_l}^{z}(1-p_l)^{1-z}$, $z = 0,1$. For $k_r > n > 0$,

$$P\left\{\sum_{i=1}^{n} Y_i \geq k_r\right\} = \sum_{j=k_r}^{n} \binom{n}{j} {p_r}^{j}(1-p_r)^{n-j} = \frac{\binom{n}{k_r}(1-p_r)^{(n-k_r)}\, hypergeom\left(\left[1,-n+k_r\right],\left[k_r+1\right],\frac{p_r}{-1+p_r}\right)\left({p_r}^{k_r} - {p_r}^{(k_r+1)}\right)}{1-p_r} \tag{8}$$

and $k_l > n > 0$

$$P\left\{\sum_{i=1}^{n} Z_i \geq k_l\right\} = \sum_{j=k_l}^{n} \binom{n}{j} {p_l}^{j}(1-p_l)^{n-j} = \frac{\binom{n}{k_l}(1-p_l)^{(n-k_l)}\, hypergeom\left(\left[1,-n+k_l\right],\left[k_l+1\right],\frac{p_l}{-1+p_l}\right)\left({p_l}^{k_l} - {p_l}^{(k_l+1)}\right)}{1-p_l}, \tag{9}$$

where hypergeom is a hypergeometric function, which is a particular case represented by the hypergeometric series.

Let us consider $Y_1, Y_2, \ldots$ are iid random variables with pdf $f_{Y_i}(y) = \frac{1}{\beta_r}\exp\left(-\frac{y}{\beta_r}\right)$, $y > 0$ and $Z_1, Z_2, \ldots$ are iid random variables with pdf $f_{Z_i}(z) = \frac{1}{\beta_l}\exp\left(-\frac{z}{\beta_l}\right)$, $z > 0$. For $k_r > n > 0$

$$P\left\{\sum_{i=1}^{n} Y_i \geq k_r\right\} = \int_{k_r}^{\infty} \frac{1}{\Gamma(n){\beta_r}^{n}} y^{n-1}\exp\left(-\frac{y}{\beta_r}\right)dx = \exp\left(-\frac{k_r}{\beta_r}\right)\sum_{j=0}^{n-1}\frac{\left(\frac{k_r}{\beta_r}\right)^{j}}{j!} \tag{10}$$

and for $k_l > n > 0$

$$P\left\{\sum_{i=1}^{n} Z_i \geq k_l\right\} = \int_{k_l}^{\infty} \frac{1}{\Gamma(n){\beta_l}^{n}} y^{n-1}\exp\left(-\frac{y}{\beta_l}\right)dx = \exp\left(-\frac{k_l}{\beta_l}\right)\sum_{j=0}^{n-1}\frac{\left(\frac{k_l}{\beta_l}\right)^{j}}{j!}. \tag{11}$$

Table 1: $P(W > n)$ for $p = 0.3$, $p_l = 0.6$, $p_r = 0.4$ when the rewards from geometric distribution

k_l	k_r	n	$P(W = n)$	Simulated values	$P(W > n)$
5	3	1	0.1259	0.1252	0.8741
		2	0.1956	0.1945	0.6785
		3	0.2105	0.2086	0.4680
		4	0.1637	0.1654	0.3043
		5	0.0836	0.0801	0.2208
		6	0.0510	0.0550	0.1698
		7	0.0355	0.0352	0.1343
		8	0.0301	0.0302	0.1042
		9	0.0214	0.0222	0.0828
		10	0.0168	0.0170	0.0660
5	4	1	0.0827	0.0832	0.9173
		2	0.1626	0.1619	0.7547
		3	0.1972	0.1961	0.5576
		4	0.1656	0.1730	0.3919
		5	0.0938	0.0917	0.2981
		6	0.0629	0.0627	0.2352
		7	0.0450	0.0425	0.1903
		8	0.0385	0.0378	0.1517
		9	0.0282	0.0302	0.1235
		10	0.0226	0.0226	0.1009
5	5	1	0.0568	0.0579	0.9432
		2	0.1376	0.1430	0.8056
		3	0.1852	0.1832	0.6204
		4	0.1642	0.1669	0.4563
		5	0.0988	0.0973	0.3575
		6	0.0700	0.0668	0.2875
		7	0.0511	0.0487	0.2364
		8	0.0442	0.0404	0.1922
		9	0.0331	0.0327	0.1591
		10	0.0269	0.0283	0.1322
5	6	1	0.0412	0.0382	0.9588
		2	0.1195	0.1227	0.8393
		3	0.1751	0.1693	0.6642
		4	0.1612	0.1628	0.5030
		5	0.1008	0.0984	0.4023
		6	0.0741	0.0787	0.3282
		7	0.0550	0.0576	0.2732
		8	0.0480	0.0514	0.2252
		9	0.0365	0.0360	0.1887
		10	0.0300	0.0283	0.1586

Table 2: $P(W > n)$ for $p = 0.3$, $k_l = 5$, $k_r = 3$ when the rewards from geometric distribution

p_l	p_r	n	$P(W = n)$	Simulated values	$P(W > n)$
0.6	0.3	1	0.1649	0.1650	0.8351
		2	0.2161	0.2103	0.6190
		3	0.2175	0.2142	0.4015
		4	0.1583	0.1586	0.2431
		5	0.0732	0.0777	0.1700
		6	0.0404	0.0389	0.1295
		7	0.0279	0.0287	0.1016
		8	0.0236	0.0263	0.0780
		9	0.0166	0.0167	0.0614
		10	0.0130	0.0129	0.0484
0.6	0.5	1	0.0929	0.0915	0.9071
		2	0.1755	0.1713	0.7316
		3	0.2035	0.2079	0.5281
		4	0.1673	0.1690	0.3608
		5	0.0922	0.0907	0.2686
		6	0.0600	0.0620	0.2086
		7	0.0422	0.0445	0.1664
		8	0.0359	0.0357	0.1305
		9	0.0258	0.0256	0.1046
		10	0.0205	0.0204	0.0842
0.6	0.7	1	0.0449	0.0492	0.9551
		2	0.1364	0.1342	0.8187
		3	0.1897	0.1926	0.6290
		4	0.1694	0.1609	0.4596
		5	0.1040	0.1017	0.3556
		6	0.0737	0.0751	0.2819
		7	0.0530	0.0551	0.2289
		8	0.0455	0.0471	0.1834
		9	0.0337	0.0358	0.1497
		10	0.0270	0.0264	0.1227
0.6	0.9	1	0.0209	0.0204	0.9791
		2	0.0988	0.1011	0.8802
		3	0.1763	0.1741	0.7039
		4	0.1646	0.1673	0.5394
		5	0.1085	0.1118	0.4308
		6	0.0815	0.0785	0.3494
		7	0.0604	0.0607	0.2890
		8	0.0523	0.0517	0.2367
		9	0.0401	0.0368	0.1966
		10	0.0327	0.0346	0.1639

Table 3: $P(W > n)$ for $p = 0.9$, $p_l = 0.6$, $p_r = 0.4$ when the rewards from geometric distribution

k_l	k_r	n	$P(W = n)$	Simulated values	$P(W > n)$
5	3	1	0.3266	0.3215	0.6734
		2	0.4234	0.4267	0.2501
		3	0.1587	0.1598	0.0913
		4	0.0493	0.0474	0.0420
		5	0.0178	0.0205	0.0241
		6	0.0150	0.0140	0.0091
		7	0.0038	0.0045	0.0053
		8	0.0026	0.0032	0.0028
		9	0.0015	0.0015	0.0013
		10	0.0006	0.0005	0.0007
5	4	1	0.1970	0.1962	0.8030
		2	0.3722	0.3635	0.4308
		3	0.2478	0.2532	0.1830
		4	0.0970	0.1004	0.0860
		5	0.0304	0.0317	0.0556
		6	0.0277	0.0278	0.0279
		7	0.0100	0.0099	0.0179
		8	0.0082	0.0083	0.0096
		9	0.0038	0.0040	0.0058
		10	0.0021	0.0014	0.0037
5	5	1	0.1192	0.1215	0.8808
		2	0.2948	0.2907	0.5860
		3	0.2828	0.2958	0.3031
		4	0.1536	0.1487	0.1495
		5	0.0544	0.0509	0.0951
		6	0.0382	0.0376	0.0569
		7	0.0180	0.0187	0.0389
		8	0.0160	0.0150	0.0228
		9	0.0076	0.0071	0.0152
		10	0.0053	0.0052	0.0100
5	6	1	0.0725	0.0705	0.9275
		2	0.2204	0.2258	0.7070
		3	0.2760	0.2657	0.4311
		4	0.1977	0.1981	0.2333
		5	0.0887	0.0908	0.1446
		6	0.0509	0.0521	0.0937
		7	0.0262	0.0268	0.0675
		8	0.0242	0.0242	0.0432
		9	0.0126	0.0129	0.0306
		10	0.0100	0.0103	0.0206

Table 4: $P(W > n)$ for $p = 0.9$, $k_l = 5$, $k_r = 3$ when the rewards from geometric distribution

p_l	p_r	n	$P(W = n)$	Simulated values	$P(W > n)$
0.6	0.3	1	0.4436	0.4456	0.5564
		2	0.3859	0.3857	0.1706
		3	0.1036	0.1047	0.0669
		4	0.0396	0.0373	0.0273
		5	0.0121	0.0136	0.0152
		6	0.0097	0.0080	0.0056
		7	0.0024	0.0023	0.0032
		8	0.0016	0.0012	0.0016
		9	0.0009	0.0008	0.0008
		10	0.0003	0.0003	0.0004
0.6	0.5	1	0.2276	0.2187	0.7724
		2	0.4302	0.4387	0.3423
		3	0.2255	0.2300	0.1168
		4	0.0574	0.0526	0.0594
		5	0.0245	0.0241	0.0349
		6	0.0215	0.0202	0.0134
		7	0.0054	0.0064	0.0080
		8	0.0038	0.0036	0.0042
		9	0.0022	0.0029	0.0020
		10	0.0009	0.0009	0.0011
0.6	0.7	1	0.0836	0.0859	0.9164
		2	0.3517	0.3534	0.5647
		3	0.3936	0.3878	0.1711
		4	0.0685	0.0725	0.1025
		5	0.0403	0.0391	0.0623
		6	0.0377	0.0375	0.0246
		7	0.0096	0.0098	0.0150
		8	0.0069	0.0070	0.0081
		9	0.0042	0.0035	0.0039
		10	0.0017	0.0015	0.0022
0.6	0.9	1	0.0116	0.0113	0.9884
		2	0.1505	0.1457	0.8379
		3	0.6082	0.6162	0.2298
		4	0.0730	0.0700	0.1568
		5	0.0596	0.0597	0.0972
		6	0.0581	0.0579	0.0391
		7	0.0149	0.0146	0.0242
		8	0.0110	0.0117	0.0132
		9	0.0068	0.0061	0.0064
		10	0.0027	0.0029	0.0037

Table 5: $P(W > n)$ for $p = 0.3$, $\beta_l = 3$, $\beta_r = 1$ when the rewards from exponential distribution

k_l	k_r	n	$P(W = n)$	Simulated values	$P(W > n)$
5	3	1	0.1471	0.1471	0.8529
		2	0.2139	0.2120	0.6390
		3	0.1608	0.1632	0.4782
		4	0.1166	0.1160	0.3616
		5	0.0723	0.0704	0.2893
		6	0.0576	0.0581	0.2317
		7	0.0393	0.0402	0.1924
		8	0.0325	0.0323	0.1599
		9	0.0248	0.0257	0.1351
		10	0.0200	0.0188	0.1152
		11	0.0162	0.0158	0.0990
		12	0.0133	0.0142	0.0857
		13	0.0110	0.0112	0.0747
		14	0.0092	0.0089	0.0655
		15	0.0078	0.0075	0.0577
5	4	1	0.1377	0.1388	0.8623
		2	0.2029	0.2035	0.6594
		3	0.1553	0.1556	0.5041
		4	0.1156	0.1159	0.3885
		5	0.0735	0.0725	0.3150
		6	0.0596	0.0592	0.2555
		7	0.0414	0.0403	0.2141
		8	0.0345	0.0351	0.1796
		9	0.0266	0.0260	0.1530
		10	0.0216	0.0205	0.1314
		11	0.0176	0.0189	0.1137
		12	0.0147	0.0153	0.0991
		13	0.0121	0.0115	0.0869
		14	0.0103	0.0099	0.0766
		15	0.0087	0.0092	0.0679
5	5	1	0.1342	0.1357	0.8658
		2	0.1978	0.1993	0.6679
		3	0.1518	0.1506	0.5161
		4	0.1143	0.1153	0.4018
		5	0.0735	0.0720	0.3284
		6	0.0602	0.0597	0.2681
		7	0.0422	0.0419	0.2259
		8	0.0354	0.0360	0.1905
		9	0.0275	0.0283	0.1631
		10	0.0224	0.0229	0.1406
		11	0.0184	0.0181	0.1223
		12	0.0154	0.0153	0.1069
		13	0.0128	0.0121	0.0941
		14	0.0109	0.0105	0.0833
		15	0.0093	0.0092	0.0740
5	6	1	0.1330	0.1295	0.8670
		2	0.1956	0.1981	0.6715
		3	0.1500	0.1518	0.5215
		4	0.1132	0.1102	0.4083
		5	0.0732	0.0722	0.3351
		6	0.0603	0.0597	0.2748
		7	0.0425	0.0409	0.2322

		8	0.0358	0.0358	0.1965
		9	0.0279	0.0294	0.1686
		10	0.0228	0.0231	0.1458
		11	0.0188	0.0194	0.1270
		12	0.0157	0.0160	0.1113
		13	0.0131	0.0129	0.0982
		14	0.0112	0.0113	0.0871
		15	0.0095	0.0098	0.0775

Table 6: $P(W > n)$ for $p = 0.3$, $k_l = 5$, $k_r = 2$ when the rewards from exponential distribution

β_l	β_r	n	$P(W = n)$	Simulated values	$P(W > n)$
3	1	1	0.1728	0.1747	0.8272
		2	0.2360	0.2369	0.5912
		3	0.1681	0.1644	0.4232
		4	0.1147	0.1130	0.3085
		5	0.0677	0.0681	0.2408
		6	0.0520	0.0521	0.1888
		7	0.0345	0.0342	0.1543
		8	0.0281	0.0291	0.1262
		9	0.0211	0.0215	0.1052
		10	0.0167	0.0177	0.0884
		11	0.0134	0.0134	0.0751
		12	0.0109	0.0110	0.0642
		13	0.0088	0.0084	0.0554
		14	0.0074	0.0079	0.0480
		15	0.0061	0.0056	0.0419
3	2	1	0.2426	0.2421	0.7574
		2	0.2751	0.2744	0.4823
		3	0.1730	0.1725	0.3094
		4	0.1024	0.1018	0.2070
		5	0.0537	0.0542	0.1533
		6	0.0379	0.0386	0.1153
		7	0.0237	0.0243	0.0917
		8	0.0190	0.0186	0.0727
		9	0.0137	0.0142	0.0590
		10	0.0106	0.0113	0.0484
		11	0.0083	0.0081	0.0401
		12	0.0066	0.0077	0.0335
		13	0.0052	0.0050	0.0282
		14	0.0043	0.0037	0.0240
		15	0.0035	0.0036	0.0205
2	3	1	0.2115	0.2129	0.7885
		2	0.2387	0.2360	0.5498
		3	0.1801	0.1803	0.3697
		4	0.1188	0.1201	0.2510
		5	0.0671	0.0672	0.1838
		6	0.0430	0.0419	0.1408
		7	0.0267	0.0261	0.1141
		8	0.0210	0.0204	0.0931
		9	0.0154	0.0156	0.0777
		10	0.0125	0.0125	0.0652
		11	0.0100	0.0103	0.0552
		12	0.0082	0.0081	0.0471
		13	0.0066	0.0069	0.0404
		14	0.0055	0.0055	0.0349

		15	0.0046	0.0045	0.0303
3	3	1	0.2862	0.2863	0.7138
		2	0.2918	0.2930	0.4220
		3	0.1722	0.1694	0.2497
		4	0.0931	0.0932	0.1567
		5	0.0450	0.0452	0.1117
		6	0.0297	0.0303	0.0820
		7	0.0178	0.0166	0.0642
		8	0.0141	0.0145	0.0501
		9	0.0100	0.0102	0.0401
		10	0.0077	0.0072	0.0324
		11	0.0059	0.0063	0.0265
		12	0.0047	0.0050	0.0218
		13	0.0036	0.0037	0.0182
		14	0.0030	0.0036	0.0152
		15	0.0024	0.0024	0.0129

Table 7: $P(W > n)$ for $p = 0.9$, $\beta_l = 3$, $\beta_r = 1$ when the rewards from exponential distribution

k_l	k_r	n	$P(W = n)$	Simulated values	$P(W > n)$
5	3	1	0.0637	0.0633	0.9363
		2	0.1439	0.1432	0.7924
		3	0.1886	0.1860	0.6038
		4	0.1802	0.1807	0.4236
		5	0.1317	0.1311	0.2920
		6	0.0902	0.0896	0.2018
		7	0.0526	0.0549	0.1492
		8	0.0380	0.0401	0.1112
		9	0.0232	0.0241	0.0880
		10	0.0196	0.0194	0.0684
		11	0.0131	0.0121	0.0553
		12	0.0116	0.0114	0.0437
		13	0.0079	0.0079	0.0358
		14	0.0070	0.0075	0.0288
		15	0.0051	0.0055	0.0237
5	4	1	0.0354	0.0343	0.9646
		2	0.0805	0.0819	0.8841
		3	0.1287	0.1283	0.7555
		4	0.1548	0.1549	0.6007
		5	0.1443	0.1432	0.4564
		6	0.1173	0.1191	0.3391
		7	0.0813	0.0820	0.2578
		8	0.0588	0.0601	0.1990
		9	0.0382	0.0381	0.1608
		10	0.0306	0.0305	0.1303
		11	0.0213	0.0205	0.1089
		12	0.0190	0.0188	0.0899
		13	0.0138	0.0133	0.0761
		14	0.0126	0.0132	0.0635
		15	0.0095	0.0090	0.0540
5	5	1	0.0250	0.0250	0.9750
		2	0.0478	0.0473	0.9272
		3	0.0814	0.0807	0.8458
		4	0.1142	0.1158	0.7316
		5	0.1281	0.1290	0.6035
		6	0.1225	0.1231	0.4811

		7	0.0998	0.0982	0.3813
		8	0.0778	0.0773	0.3035
		9	0.0548	0.0549	0.2487
		10	0.0425	0.0422	0.2063
		11	0.0304	0.0303	0.1759
		12	0.0263	0.0260	0.1496
		13	0.0198	0.0189	0.1298
		14	0.0182	0.0185	0.1116
		15	0.0142	0.0152	0.0973
5	6	1	0.0211	0.0208	0.9789
		2	0.0323	0.0322	0.9465
		3	0.0516	0.0515	0.8949
		4	0.0781	0.0780	0.8168
		5	0.0999	0.1007	0.7169
		6	0.1096	0.1098	0.6073
		7	0.1030	0.1025	0.5043
		8	0.0889	0.0903	0.4154
		9	0.0690	0.0697	0.3464
		10	0.0544	0.0534	0.2920
		11	0.0402	0.0405	0.2518
		12	0.0334	0.0330	0.2184
		13	0.0257	0.0254	0.1927
		14	0.0233	0.0234	0.1694
		15	0.0187	0.0179	0.1508

Table 8: $P(W > n)$ for $p = 0.9$, $k_l = 5$, $k_r = 2$ when the rewards from exponential distribution

β_l	β_r	n	$P(W = n)$	Simulated values	$P(W > n)$
3	1	1	0.1407	0.1396	0.8593
		2	0.2470	0.2472	0.6123
		3	0.2275	0.2288	0.3848
		4	0.1579	0.1570	0.2269
		5	0.0839	0.0839	0.1429
		6	0.0511	0.0514	0.0918
		7	0.0253	0.0248	0.0666
		8	0.0201	0.0199	0.0465
		9	0.0114	0.0115	0.0351
		10	0.0095	0.0094	0.0256
		11	0.0060	0.0060	0.0196
		12	0.0050	0.0053	0.0146
		13	0.0032	0.0030	0.0114
		14	0.0026	0.0028	0.0088
		15	0.0019	0.0018	0.0069
3	2	1	0.3500	0.3492	0.6500
		2	0.3387	0.3365	0.3113
		3	0.1660	0.1687	0.1453
		4	0.0765	0.0760	0.0688
		5	0.0271	0.0266	0.0417
		6	0.0185	0.0194	0.0232
		7	0.0073	0.0072	0.0159
		8	0.0062	0.0068	0.0097
		9	0.0031	0.0027	0.0066
		10	0.0022	0.0025	0.0044
		11	0.0013	0.0012	0.0031

		12	0.0010	0.0010	0.0021
		13	0.0006	0.0006	0.0015
		14	0.0004	0.0005	0.0011
		15	0.0003	0.0002	0.0008
2	3	1	0.4703	0.4710	0.5297
		2	0.3253	0.3246	0.2044
		3	0.1140	0.1145	0.0904
		4	0.0500	0.0490	0.0404
		5	0.0159	0.0162	0.0245
		6	0.0121	0.0121	0.0124
		7	0.0043	0.0043	0.0081
		8	0.0035	0.0031	0.0047
		9	0.0017	0.0021	0.0030
		10	0.0010	0.0012	0.0019
		11	0.0007	0.0006	0.0013
		12	0.0004	0.0005	0.0008
		13	0.0002	0.0003	0.0006
		14	0.0002	0.0003	0.0004
		15	0.0001	0.0001	0.0003
3	3	1	0.4810	0.4826	0.5190
		2	0.3261	0.3262	0.1929
		3	0.1118	0.1090	0.0811
		4	0.0462	0.0487	0.0349
		5	0.0140	0.0129	0.0209
		6	0.0105	0.0100	0.0104
		7	0.0036	0.0031	0.0068
		8	0.0030	0.0031	0.0039
		9	0.0014	0.0016	0.0025
		10	0.0009	0.0010	0.0016
		11	0.0005	0.0006	0.0010
		12	0.0004	0.0004	0.0007
		13	0.0002	0.0003	0.0005
		14	0.0001	0.0002	0.0003
		15	0.0001	0.0001	0.0002

Table 9. $P(W > n)$ for $p = 0.3$, $p_l = 0.6$, $p_r = 0.4$ when the rewards from binomial distribution

k_l	k_r	n	$P(W = n)$	Simulated values	$P(W > n)$
5	3	1	0.0000	0.0000	1.0000
		2	0.0000	0.0000	1.0000
		3	0.0017	0.0018	0.9983
		4	0.0021	0.0021	0.9961
		5	0.0153	0.0154	0.9809
		6	0.0244	0.0247	0.9564
		7	0.0269	0.0274	0.9295
		8	0.0262	0.0258	0.9033
		9	0.0246	0.0242	0.8787
		10	0.0234	0.0248	0.8553
		11	0.0219	0.0208	0.8334
		12	0.0213	0.0200	0.8121
		13	0.0202	0.0195	0.7919
		14	0.0196	0.0195	0.7723
		15	0.0187	0.0185	0.7536
5	4	1	0.0000	0.0000	1.0000
		2	0.0000	0.0000	1.0000
		3	0.0000	0.0000	1.0000

		4	0.0002	0.0002	0.9998
		5	0.0134	0.0124	0.9864
		6	0.0225	0.0227	0.9639
		7	0.0251	0.0253	0.9388
		8	0.0244	0.0254	0.9144
		9	0.0230	0.0238	0.8914
		10	0.0219	0.0217	0.8696
		11	0.0205	0.0201	0.8491
		12	0.0200	0.0202	0.8291
		13	0.0189	0.0191	0.8102
		14	0.0185	0.0185	0.7917
		15	0.0176	0.0187	0.7741
5	5	1	0.0000	0.0000	1.0000
		2	0.0000	0.0000	1.0000
		3	0.0000	0.0000	1.0000
		4	0.0000	0.0002	1.0000
		5	0.0131	0.0124	0.9869
		6	0.0223	0.0227	0.9646
		7	0.0248	0.0253	0.9398
		8	0.0241	0.0254	0.9157
		9	0.0227	0.0238	0.8930
		10	0.0216	0.0217	0.8714
		11	0.0203	0.0201	0.8511
		12	0.0197	0.0202	0.8314
		13	0.0187	0.0191	0.8127
		14	0.0183	0.0185	0.7944
		15	0.0175	0.0187	0.7770
5	6	1	0.0000	0.0000	1.0000
		2	0.0000	0.0000	1.0000
		3	0.0000	0.0000	1.0000
		4	0.0000	0.0000	1.0000
		5	0.0131	0.0128	0.9869
		6	0.0222	0.0221	0.9647
		7	0.0248	0.0261	0.9399
		8	0.0241	0.0237	0.9159
		9	0.0227	0.0227	0.8932
		10	0.0216	0.0210	0.8716
		11	0.0202	0.0202	0.8514
		12	0.0197	0.0194	0.8317
		13	0.0187	0.0188	0.8130
		14	0.0182	0.0182	0.7948
		15	0.0174	0.0175	0.7773

Table 10: $P(W > n)$ for $p = 0.3$, $k_l = 5$, $k_r = 3$ when the rewards from binomial distribution

p_l	p_r	n	$P(W = n)$	Simulated values	$P(W > n)$
0.6	0.3	1	0.0000	0.0000	1.0000
		2	0.0000	0.0000	1.0000
		3	0.0007	0.0007	0.9992
		4	0.0009	0.0011	0.9983
		5	0.0140	0.0139	0.9842
		6	0.0232	0.0229	0.9609
		7	0.0258	0.0253	0.9351
		8	0.0250	0.0250	0.9101
		9	0.0235	0.0243	0.8865
		10	0.0224	0.0240	0.8640
		11	0.0210	0.0216	0.8430

		12	0.0204	0.0202	0.8225
		13	0.0193	0.0187	0.8031
		14	0.0188	0.0190	0.7842
		15	0.0180	0.0175	0.7662
0.6	0.5	1	0.0000	0.0000	1.0000
		2	0.0000	0.0000	1.0000
		3	0.0034	0.0032	0.9966
		4	0.0039	0.0039	0.9927
		5	0.0170	0.0178	0.9758
		6	0.0261	0.0251	0.9497
		7	0.0286	0.0271	0.9212
		8	0.0277	0.0273	0.8934
		9	0.0261	0.0256	0.8673
		10	0.0247	0.0242	0.8426
		11	0.0232	0.0230	0.8194
		12	0.0224	0.0225	0.7970
		13	0.0212	0.0208	0.7758
		14	0.0206	0.0212	0.7552
		15	0.0196	0.0198	0.7356
0.6	0.7	1	0.0000	0.0000	1.0000
		2	0.0000	0.0000	1.0000
		3	0.9261	0.9340	0.9907
		4	0.8983	0.8760	0.9818
		5	0.2175	0.2222	0.9600
		6	0.3083	0.3152	0.9292
		7	0.3321	0.3448	0.8960
		8	0.3213	0.3306	0.8638
		9	0.3018	0.2996	0.8337
		10	0.2850	0.2816	0.8052
		11	0.2664	0.2672	0.7785
		12	0.2560	0.2540	0.7529
		13	0.2414	0.2524	0.7288
		14	0.2325	0.2254	0.7055
		15	0.2206	0.2168	0.6835
0.6	0.9	1	0.0000	0.0000	1.0000
		2	0.0000	0.0000	1.0000
		3	0.0197	0.0187	0.9803
		4	0.0155	0.0148	0.9648
		5	0.0282	0.0281	0.9366
		6	0.0373	0.0381	0.8993
		7	0.0395	0.0408	0.8598
		8	0.0380	0.0382	0.8217
		9	0.0356	0.0365	0.7862
		10	0.0334	0.0332	0.7528
		11	0.0311	0.0314	0.7216
		12	0.0297	0.0302	0.6920
		13	0.0279	0.0281	0.6641
		14	0.0266	0.0263	0.6374
		15	0.0252	0.0242	0.6123

Table 11: $P(W > n)$ for $p = 0.9$, $p_l = 0.6$, $p_r = 0.4$ when the rewards from binomial distribution

k_l	k_r	n	$P(W = n)$	Simulated values	$P(W > n)$
5	3	1	0.0000	0.0000	1.0000
		2	0.0000	0.0000	1.0000
		3	0.0467	0.0462	0.9533
		4	0.0802	0.0796	0.8731

		5	0.0939	0.0920	0.7792
		6	0.0939	0.0934	0.6854
		7	0.0838	0.0838	0.6015
		8	0.0749	0.0749	0.5266
		9	0.0615	0.0625	0.4651
		10	0.0540	0.0545	0.4110
		11	0.0436	0.0421	0.3675
		12	0.0389	0.0396	0.3286
		13	0.0314	0.0320	0.2972
		14	0.0287	0.0283	0.2685
		15	0.0237	0.0245	0.2448
5	4	1	0.0000	0.0000	1.0000
		2	0.0000	0.0000	1.0000
		3	0.0000	0.0000	1.0000
		4	0.0168	0.0178	0.9832
		5	0.0380	0.0386	0.9452
		6	0.0543	0.0546	0.8910
		7	0.0631	0.0616	0.8279
		8	0.0655	0.0674	0.7624
		9	0.0626	0.0603	0.6998
		10	0.0586	0.0599	0.6412
		11	0.0518	0.0512	0.5894
		12	0.0473	0.0470	0.5421
		13	0.0407	0.0403	0.5014
		14	0.0374	0.0386	0.4640
		15	0.0322	0.0330	0.4319
5	5	1	0.0000	0.0000	1.0000
		2	0.0000	0.0000	1.0000
		3	0.0000	0.0000	1.0000
		4	0.0000	0.0000	1.0000
		5	0.0060	0.0059	0.9940
		6	0.0169	0.0160	0.9770
		7	0.0287	0.0279	0.9483
		8	0.0382	0.0384	0.9101
		9	0.0442	0.0438	0.8659
		10	0.0468	0.0473	0.8191
		11	0.0464	0.0473	0.7727
		12	0.0448	0.0456	0.7279
		13	0.0415	0.0407	0.6864
		14	0.0388	0.0397	0.6477
		15	0.0349	0.0340	0.6127
5	6	1	0.0000	0.0000	1.0000
		2	0.0000	0.0000	1.0000
		3	0.0000	0.0000	1.0000
		4	0.0000	0.0000	1.0000
		5	0.0000	0.0000	1.0000
		6	0.0022	0.0020	0.9978
		7	0.0073	0.0073	0.9906
		8	0.0143	0.0142	0.9763
		9	0.0215	0.0226	0.9548
		10	0.0275	0.0278	0.9273
		11	0.0317	0.0310	0.8957
		12	0.0340	0.0350	0.8617
		13	0.0345	0.0341	0.8272
		14	0.0340	0.0342	0.7932
		15	0.0324	0.0327	0.7608

Table 12: $P(W > n)$ for $p = 0.9$, $k_l = 5$, $k_r = 3$ when the rewards from binomial distribution

p_l	p_r	n	n	$P(W = n)$	Simulated values
0.6	0.3	1	0.0000	0	1.0000
		2	0.0000	0	1.0000
		3	0.0197	0.0200	0.9803
		4	0.0392	0.0397	0.9411
		5	0.0526	0.0520	0.8886
		6	0.0596	0.0584	0.8290
		7	0.0604	0.0631	0.7686
		8	0.0594	0.0597	0.7092
		9	0.0543	0.0551	0.6549
		10	0.0509	0.0507	0.6040
		11	0.0447	0.0444	0.5594
		12	0.0413	0.0427	0.5181
		13	0.0357	0.0368	0.4824
		14	0.0330	0.0326	0.4494
		15	0.0286	0.0285	0.4207
0.6	0.5	1	0.0000	0.0000	1.0000
		2	0.0000	0.0000	1.0000
		3	0.0911	0.0907	0.9089
		4	0.1321	0.1323	0.7767
		5	0.1321	0.1310	0.6446
		6	0.1155	0.1148	0.5291
		7	0.0902	0.0899	0.4389
		8	0.0744	0.0766	0.3645
		9	0.0551	0.0559	0.3094
		10	0.0468	0.0453	0.2626
		11	0.0351	0.0338	0.2275
		12	0.0311	0.0324	0.1964
		13	0.0238	0.0232	0.1726
		14	0.0216	0.0225	0.1509
		15	0.0172	0.0164	0.1337
0.6	0.7	1	0.0000	0.0000	1.0000
		2	0.0000	0.0000	1.0000
		3	0.2500	0.2471	0.7500
		4	0.2275	0.2289	0.5224
		5	0.1546	0.1544	0.3678
		6	0.1054	0.1069	0.2624
		7	0.0628	0.0640	0.1995
		8	0.0506	0.0520	0.1490
		9	0.0314	0.0309	0.1175
		10	0.0268	0.0260	0.0908
		11	0.0180	0.0184	0.0728
		12	0.0154	0.0158	0.0574
		13	0.0106	0.0107	0.0468
		14	0.0091	0.0085	0.0378
		15	0.0068	0.0069	0.0310
0.6	0.9	1	0.0000	0.0000	1.0000
		2	0.0000	0.0000	1.0000
		3	0.5314	0.5316	0.4686
		4	0.1966	0.1964	0.2719
		5	0.0933	0.0929	0.1786
		6	0.0740	0.0736	0.1047
		7	0.0322	0.0324	0.0724
		8	0.0280	0.0285	0.0444
		9	0.0146	0.0146	0.0298

		10	0.0098	0.0099	0.0200
		11	0.0063	0.0063	0.0137
		12	0.0044	0.0049	0.0093
		13	0.0026	0.0024	0.0067
		14	0.0019	0.0018	0.0047
		15	0.0014	0.0015	0.0034

We also use the rewards Eqn. (6)-(7) in our study. [1] gives some numerical computation for survival function for rewards Eqn. (6) and Eqn. (7). Some extended numerical computations are presented in Tables 1-4 for survival probability $P(W > n)$ by using Eqn. (6)-(7) in Eqn. (3) for selected values of p, p_r, p_l, k_r, k_l. The simulated probabilities with 10000 trials are also included in the tables. From Tables 1-4, our theoretical and simulated probabilities can be observed as almost identical. This indicates that the survival function given in Eqn. (3) is correct.

Some numerical computations are presented in Tables 5-8 for survival probability $P(W > n)$ by using Eqn. (8)-(9) in Eqn. (3), for selected values of p, p_r, p_l, k_r, k_l. The simulated probabilities with 10000 trials are also included in the tables. From Tables 5-8, our theoretical and simulated probabilities can be observed almost identical.

Some numerical computations are presented in Tables 9-12 for survival probability $P(W > n)$ by using Eqn. (10)-(11) in Eqn. (3) for selected values of $p, \beta_r, \beta_l, k_r, k_l$. The simulated probabilities with 10000 trials are also included in the tables. From the Tables 9-12, our theoretical and simulated probabilities can be observed as almost identical. Matlab codes for theoretical probabilities can be requested from the authors.

3. Proportion Estimates for Generalized Geometric Distribution Parameters

In this section, we consider the estimation of parameters. The maximum likelihood estimation is not discussed here since the pmf of W is intractable. For this reason, we discuss the proportion type estimate for the parameters. We need the following probabilities to obtain the proportion estimation of the parameters.

$$P(W=1) = pP(Y_1 \geq k_r) + (1-p)P(Z_1 \geq k_l), \tag{12}$$

$$\begin{aligned}P(W=2)&=(1-p)P(Z_1<k_l)\,pP(Y_1\geq k_r)\\&+pP(Y_1<k_r)(1-p)P(Z_1\geq k_l)\\&+pP(Y_1<k_r)\,pP(Y_1+Y_2\geq k_r)\\&+(1-p)P(Z_1<k_l)(1-p)P(Z_1+Z_2\geq k_l),\end{aligned}\tag{13}$$

$$\begin{aligned}P(W=3)&=(1-p)P(Z_1<k_l)(1-p)P(Z_1+Z_2<k_l)\,pP(Y_1\geq k_r)\\&+(1-p)P(Z_1<k_l)\,pP(Y_1<k_r)\,pP(Y_1+Y_2\geq k_r)\\&+pP(Y_1<k_r)(1-p)P(Z_1<k_l)\,pP(Y_2\geq k_r)\\&+pP(Y_1<k_r)(1-p)P(Z_1<k_l)(1-p)P(Z_1+Z_2\geq k_l)\\&+pP(Y_1<k_r)\,pP(Y_1+Y_2<k_r)(1-p)P(Z_1\geq k_l)\\&+(1-p)P(Z_1<k_l)\,pP(Y_1<k_r)(1-p)P(Z_2\geq k_l)\\&+pP(Y_1<k_r)\,pP(Y_1+Y_2<k_r)\,pP(Y_1+Y_2+Y_3\geq k_r)\\&+(1-p)P(Z_1<k_l)(1-p)P(Z_1+Z_2<k_l)(1-p)\\&\times P(Z_1+Z_2+Z_3\geq k_l),\end{aligned}\tag{14}$$

Since the probabilities are too complicated, the estimation is performed under the conditions $p_l=p_r=p_J$ and $p_i=p, i=1,2,\ldots$. Let $Y_1,Y_2,\ldots$be the independent rewards with cumulative distribution function (cdf)

$$F_i(y)=P\{Y_i\leq y\}=1-(1-p_r)^y,\ \ y=1,2,\ldots$$

and $Z_1,Z_2,\ldots$ independent Type-II rewards with cdf

$$G_i(z)=P\{Z_i\leq z\}=1-(1-p_l)^z,\ \ z=1,2,\ldots.$$

for $i=1,2,\ldots.$

Under condition the $p_l=p_r=p_J,\ p_i=p$, it can be written by

$$\begin{aligned}P(Y_1\geq k_r)&=1-F_1(k_r-1)=(1-p_J)^{k_r-1},\\P(Z_1\geq k_l)&=1-G_1(k_l-1)=(1-p_J)^{k_l-1},\end{aligned}\tag{15}$$

and

$$\begin{aligned}P(Y_1+Y_2\geq k_r)&=nbincdf(k_r-3,2,p_J),\\P(Z_1+Z_2\geq k_l)&=nbincdf(k_l-3,2,p_J),\end{aligned}\tag{16}$$

where

$$nbincdf(a,b,c)=\sum_{i=0}^{a}\binom{b+i+1}{i}c^b(1-c)^i\tag{17}$$

which is cdf of negative binomial distribution. These probabilities can be calculated with Matlab function *nbincdf*. Using Eqn. (12)-(13) and Eqn. (15)-(17), we have

$$P(W=1)=p(1-p_J)^{k_r-1}+(1-p)(1-p_J)^{k_l-1} \tag{18}$$

and

$$\begin{aligned}P(W=2)&=p(1-p_J)^{k_r-1}(1-p)\,p\left(1-(1-p_J)^{k_l-1}\right)\\&+\left(1-nbincdf\left(k_r-3,2,p_J\right)-(1-p_J)^{k_l-1}\right)p^2\\&+(1-p_J)^{k_l-1}(1-p)\,p\left(1-(1-p_J)^{k_r-1}\right)\\&+\left(1-nbincdf\left(k_l-3,2,p_J\right)-(1-p_J)^{k_l-1}\right)(1-p)^2.\end{aligned} \tag{19}$$

Khan et al. [7] proposed the proportion type estimates for discrete Weibull distribution. In this section, we now use their methodology to get the estimates for parameters of distribution with survival function given in Eqn. (3).

Let $W_1,W_2,\ldots,W_n$ be a random sample from a distribution with survival function Eqn. (3). Furthermore, two types of rewards are independently distributed with pmfs Eqn. (4) and Eqn. (5), respectively.

Let us define the following indicator functions, for $i=1,2,\ldots n$,

$$\nu_1(W_i)=\begin{cases}1, & W_i=1\\0, & W_i>1\end{cases} \tag{20}$$

and

$$\nu_2(W_i)=\begin{cases}1, & W_i=2\\0, & W_i\neq 2\end{cases}. \tag{21}$$

It is noticed that the $\frac{1}{n}\sum_{i=1}^{n}\nu_1(W^i)$ and $\frac{1}{n}\sum_{i=1}^{n}\nu_2(W^i)$ are unbiased and consistent estimates for $P(W=1)$ and $P(W=2)$ respectively. Hence, the proportion estimates for parameters p and p_J are obtained by solving the following equations simultaneously

$$p(1-p_J)^{k_r-1}+(1-p)(1-p_J)^{k_l-1}=\tfrac{1}{n}\textstyle\sum_{i=1}^{n}\nu_1(W_i) \tag{22}$$

$$
\begin{aligned}
&h(p,p_J)=p(1-p_J)^{k_r-1}(1-p)\,p\left(1-(1-p_J)^{k_l-1}\right)\\
&+\left(1-nbincdf\left(k_r-3,2,p_J\right)-(1-p_J)^{k_l-1}\right)p^2\\
&+(1-p_J)^{k_l-1}(1-p)\,p\left(1-(1-p_J)^{k_r-1}\right)\\
&+\left(1-nbincdf\left(k_l-3,2,p_J\right)-(1-p_J)^{k_l-1}\right)(1-p)^2=\tfrac{1}{n}\textstyle\sum_{i=1}^{n}v_2(W_i)
\end{aligned}
\quad . \tag{23}
$$

From Eqn. (22) the parameter p can be expressed by

$$
p^*=\frac{\frac{1}{n}\sum_{i=1}^{n}v_1(W_i)-(1-p_J)^{k_L-1}}{(1-p_J)^{k_R-1}-(1-p_J)^{k_L-1}}. \tag{24}
$$

Using Eqn. (24) in Eqn. (23), we obtain the profile equation as

$$
h\left(p^*,p_J\right)=\tfrac{1}{n}\textstyle\sum_{i=1}^{n}v_2(W_i), \tag{25}
$$

which is a function of p_J. Eqn. (25) can be solved by using one-dimensional root searching methods Newton-Raphson or secant method. The approximate value of the iterative root finder is a proportion estimate of parameter p_J and we denote it by $\hat{p}_J$. Then the proportion estimate of p is given by

$$
\hat{p}=\frac{\frac{1}{n}\sum_{i=1}^{n}v_1(W_i)-(1-\hat{p}_J)^{k_L-1}}{(1-\hat{p}_J)^{k_R-1}-(1-\hat{p}_J)^{k_L-1}}. \tag{26}
$$

In our trials, we observe that the equation in Eqn. (25) has two roots. In the example section, we give a suggestion to overcome this issue. As a final comment, If the constraint $p_l=p_r=p_J$ is relaxed, then Eqn. (14) should be taken in consideration and three equations should also be solved simultaneously to get the proportion estimates p_r, p_l and p.

4. Illustrative Example

In this section, we give an example to illustrate the methodology given in the previous section. We generate random data $n=30$ sample of size from distribution in Eqn. (3) with the parameters $k_R=8$, $k_L=5$, $p_J=0.4$ and $p=0.3$. The generated data is presented in Table 13.

Table 13: Generated data

i	1	2	3	4	5	6	7
x_i	1	2	3	4	5	7	12
o_i	3	7	9	3	5	2	1

In Table 13, x_i and o_i denote the observed value and observed frequency, respectively. Using Eqn. (24)-(25), the proportion estimates of (p_J,p) are obtained by 0.4093 and 0.2252,

respectively. The initial value is used as $p_J^{(0)} = 0.9$ to solve the equation in Eqn. (25) and reach these estimates. It is noticed that these estimates are reasonable and they are around the true values of parameters. If the initial value is fixed by $p_J^{(0)} = 0.1$, in this case, the proportion estimates of (p_J, p) are obtained by 0.2973 and 0.9031. These estimates are far from the true values of parameters. At this point, the authors have a suggestion which is given as follows: Calculated the Chi-Square goodness of fit statistic for the two different estimates. Then the estimates can be accepted, which gives minimum Chi-squares statistic. From Fig.1, we can observe the function $h(p^*, p_J) - \frac{1}{n}\sum_{i=1}^{n} \nu_2(W^i)$ is non-monotone and the equation $h(p^*, p_J) = \frac{1}{n}\sum_{i=1}^{n} \nu_2(W^i)$ has two roots.

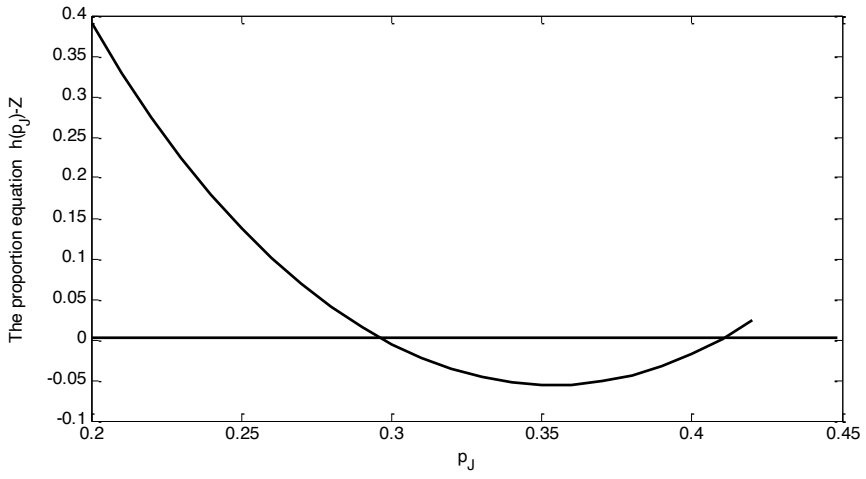

Figure 1: Graph of the $h(p_J) - \frac{1}{n}\sum_{i=1}^{n} \nu_2(W_i)$

5. Concluding Remarks and Future Researches

In this paper, the waiting time given by [1] is obtained in a different way. In this study, the survival function obtained by Eryılmaz et al. [1] based on geometric reward is extended for exponential and geometric rewards. An extensive Monte Carlo simulation study is carried for different parameter settings when the rewards are geometric, exponential and binomial. An estimation method is provided for the parameters of waiting time distribution under some constraints. An illustrative example is also carried out for sample of size $n = 30$. As a future study, the proportion estimates can be used without any constraints.

References

[1] Eryılmaz, S., Gong, M., Xie, M., *Generalized sooner waiting time problems in a sequence of trinary trials*, Statistics and probability Letters, 115, 70-78, 2016.

[2] Philippou, A.N., Georghiou, C., Philippou, G.N., *A generalized geometric distribution and some of its properties*, Statistics and probability Letters, 1, 171-175, 1983.

[3] Eryılmaz, S., *Geometric distribution of order k with a reward*, Statistics and Probability Letters, 92, 53-58, 2014.

[4] Koutras, M.V., Alexandrou, V.A., *Sooner waiting time problems in a sequence of trinary trials*, Journal Applied Probability, 34, 593-609, 1997.

[5] Demir, S., Eryılmaz, S., *Run statistics in a sequence of arbitrarily dependent binary trials*, Statistical Papers, 51(4), 959-973, 2010.

[6] Mallor, F., Santos, J., *Reliability of systems subject to shocks with a stochastic dependence for the damages*, Sociedad de Estadistica e Investigacion Opevativa Test, 12(2), 427-444, 2003.

[7] Khan, M.A., Khalique, A., Abouammoh, A.M., *On estimating parameters in a discrete Weibull distribution*, IEEE Transactions on Reliability, 38(3), 348-350, 1989.

Adıyaman University Journal of Science
https://dergipark.org.tr/en/pub/adyujsci
DergiPark AKADEMİK
ISSN 2147-1630
e-ISSN 2146-586X

Computation of Refractive Index Values of Inert Gases at Near-Infrared and XUV Region Based on Mathematica Software

Muhammed SAYRAC[1,*]

[1]*Sivas Cumhuriyet University, Faculty of Engineering, Department of Nanotechnology Engineering, Sivas, Turkey*
muhammedsayrac@cumhuriyet.edu.tr, ORCID: 0000-0003-4373-6897

Received: 18.06.2020 **Accepted:** 15.04.2021 **Published:** 30.06.2021

Abstract

In this study, refractive indices in the visible, near-infrared, and extreme ultraviolet (XUV) regions are calculated based on Mathematica software. Atomic scattering factors are simulated for a high photon energy range (20-60 eV). By using the atomic scattering factors, the real and imaginary part of the index of refraction values are plotted as a function of photon energy. This work aims to present a computational program, which calculates the index of refraction of the inert gases at different wavelength regions. The refractive indices of gases, namely helium (He), neon (Ne), argon (Ar), and xenon (Xe) in the near-infrared and XUV region are computed by using Mathematica software. The applications of the index of refraction are discussed in the paper. The Mathematica program calculating the refractive indices is presented in the Appendix.

Keywords: Refractive index; Inert gas; Infrared region; Extreme ultraviolet.

Mathematica Yazılımı Kullanılarak Yakın Kızılötesi ve XUV Bölgesinde Asal Gazların Kırılma İndisi Değerlerinin Hesaplanması

Öz

* Corresponding Author
DOI: 10.37094/adyujsci.754497

Bu çalışmada, görünür, kızılötesi ve aşırı ultraviyole (XUV) bölgesindeki kırılma indisleri Mathematica yazılımı kullanılarak hesaplanmıştır. Atomik saçılma faktörleri yüksek foton enerji aralığı (20-60 eV) için simülasyonu gerçekleştirilmiştir. Atomik saçılma faktörleri kullanılarak kırılma indisi değerlerinin gerçek ve sanal kısmı, foton enerjisinin bir fonksiyonu olarak hesaplandı. Bu çalışmanın amacı, farklı dalga boyu bölgelerinde asal gazların kırılma indisini hesaplayan bir simülasyon programı sunmaktır. Yakın kızılötesi ve XUV bölgesindeki helyum (He), neon (Ne), argon (Ar) ve xenon (Xe) kırılma indisleri Mathematica yazılımı kullanılarak hesaplandı. Kırılma indisinin uygulama alanları bahsedilmiştir. Kırılma indislerini hesaplayan Mathematica programı Ek'te sunulmaktadır.

Anahtar Kelimeler: Kırılma indisi; Asal gaz; Kızılötesi bölge; Aşırı ultraviole.

1. Introduction

The laser-matter interaction paves the path for a new avenue to many research areas. Laser light is modified while propagating in the nonlinear medium, i.e. gas species that affect the propagation of light in a medium. The refractive index of the medium gives information about the modification of the laser light. Thus, the variation of the refractive index at different wavelength regions must be determined in the near-infrared region (at around 800 nm) and extreme ultraviolet (XUV) region (10 nm – 60 nm) to predict how the laser beam propagates and is shaped through the medium. Spectroscopic measurements are usually taken in a gas medium. For accurate measurements, the corresponding wavelength needs to be known, $\lambda_{medium}=\lambda_{vac}/n_{medium}$, here n_{medium}, λ_{medium}, and λ_{vac} are the index of refraction of the medium, the wavelength of light in the medium and wavelength of light in the vacuum, respectively. For this reason, the refractive index value of the used medium is to be known to accurately determine the behavior of the corresponding wavelength.

Technological devices require detailed studies. For example, optoelectronic devices find a wide range of applications in electronic and optical devices such as laser diodes, photodetectors, and nanotechnology [1-8]. The optical and electronic properties of a device are determined by fundamental science, e.g. properties of refractive index, which is a measurement of how light behaves in the medium. Moreover, the electronic properties such as atomic polarizability and dielectric constant depend on the refractive index of the materials as well.

In this paper, the refractive index of the inert gases in the infrared and XUV region is determined by using Mathematica software. The calculations of refractive indices of helium (He), neon (Ne), argon (Ar), and xenon (Xe) are performed using the various models in the visible and near-infrared region presented in the literature [9-15]. In addition, the refractive indices of these

species in the XUV region are calculated using the atomic scattering factors [16-18]. The atomic scattering factors help calculate the real and imaginary part of the refractive indices in the XUV region. Wolfram Mathematica 10.0 program [19] has been used for calculation by using a personal computer. The complete Mathematica program is given in the Appendix.

2. Materials and Methods

The list of refractive index coefficients and atomic scattering factors has been obtained from Ref. [9, 10] and the official website of the physical measurement laboratory of the National Institute of Standards and Technology, https://www.nist.gov/. The refractive index constant in the IR region is obtained, and the atomic scattering factors calculate the index of refraction values in the XUV region.

3. Calculation of Index of Refraction in the Infrared Region

Refractive indices of inert gases have been calculated using the model at room temperature and pressure presented in Ref. [9]. The refractive index model for the inert gas is formulated by Eqn. (1) [9]

$$n = \sqrt{1 + a\left(1 + \frac{b}{\lambda^2} + \frac{c}{\lambda^4} + \frac{d}{\lambda^6} + \frac{e}{\lambda^8} + \frac{f}{\lambda^{10}}\right)} \tag{1}$$

where λ is the wavelength in angstroms, and a, b, c, d, e, and f are coefficients for each gas species. The coefficients are given in Table 1 [9, 10].

Table 1: Refractive index coefficients used to calculate refractive indices of different gases in the infrared region

Gas species	*a*	*b*	*c*	*d*	*e*	*f*
Helium	6.927×10^{-5}	2.24×10^{5}	5.94×10^{10}	1.72×10^{16}	0	0
Neon	1.335×10^{-4}	2.24×10^{5}	8.09×10^{10}	3.56×10^{16}	0	0
Argon	5.547×10^{-4}	5.15×10^{5}	4.19×10^{11}	4.09×10^{17}	4.32×10^{23}	0
Xenon	1.366×10^{-3}	9.02×10^{5}	1.81×10^{12}	4.89×10^{18}	1.45×10^{25}	4.34×10^{31}

Figure 1 shows the refractive indices (n-1) of inert gases in the infrared region (from 600 nm to 800 nm) at room temperature and pressure. The variation of refractive index (n-1) values in the visible and near-infrared region is small, Fig. 1. The refractive indices (n-1) are small and positive for all gas species, and they give refractivity of the gas species in the optical path.

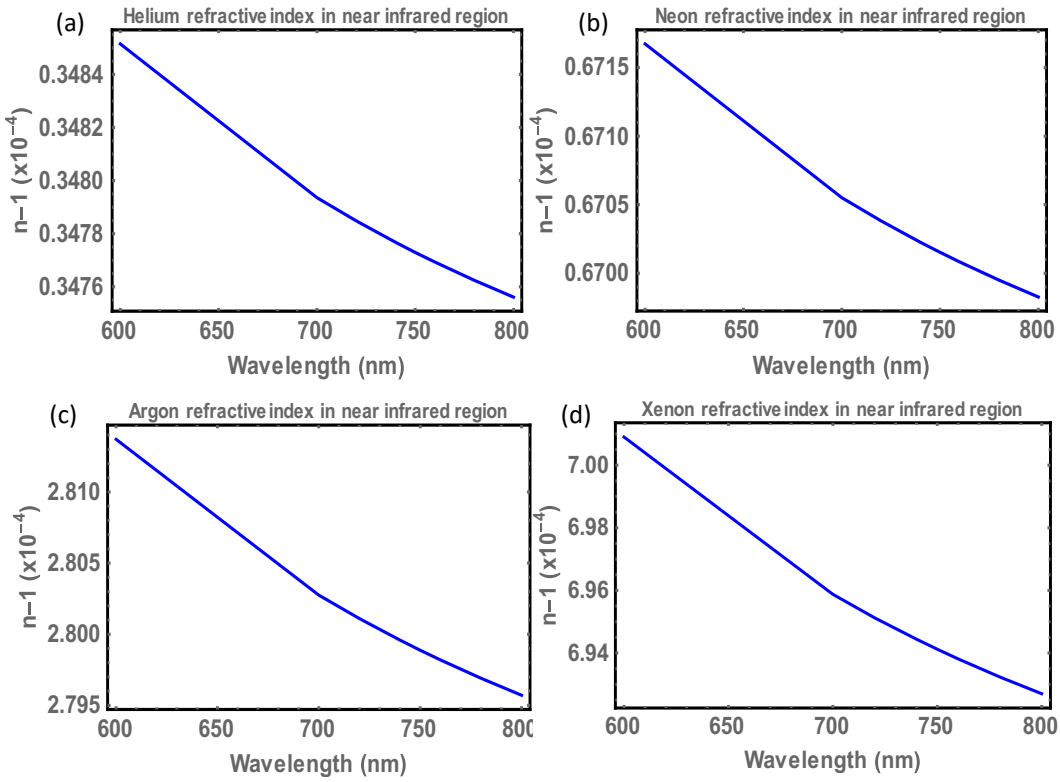

Figure 1: Simulation of refractive index (*n*-1) of inert gas species in the infrared region. (a) Helium, (b) Neon (c) Argon (d) Xenon

The index of refraction values is calculated at room temperature and pressure. If the refractivity of the gas species is required at a specific temperature and pressure, the conversion formula is given by Eqn. (2) [10, 20]

$$n = 1 + (n_0 - 1)\frac{T_0}{T}$$
$$n = 1 + (n_0 - 1)\frac{P_0}{P} \qquad (2)$$

here n_0, T_0, P_0 are the reference refractive index, temperature, and pressure, respectively.

4. Calculation of Refractive Index in the Extreme Ultraviolet Region

The refractive indices in the XUV region are not known very well compared to those in the infrared region. The estimation of the refractive index in the XUV region is obtained from the atomic scattering factors, f_1 and f_2 [16, 21]. The atomic scattering factors measure the scattering

power of individual atoms. Each species has a different scattering factor, which shows how X-ray radiation response to each species. Each component of atomic scattering factors gives information about the dispersive and absorptive components, f_1 and f_2, respectively.

The atomic scattering factors are defined as $f=f_1+if_2$ [10, 21]. The atomic scattering is described by the complex refractive index, n. The refractive index value is proportional to the atomic scattering factor, and it is given by [16, 21].

$$n = 1 - \frac{r_0}{2\pi}\lambda^2 \rho f \tag{3}$$

where ρ, f, and r_0 are the density of atoms, the atomic scattering factor, and the classical electron radius, respectively.

Figure 2 presents the scattering factors for the used gas species. The values are taken from the references [16-18] and are used as the input parameters in the simulation program, Appendix. f_1 and f_2 describe the refraction and absorption of the species. The refractive indices of the gases at the XUV region are determined from the scattering factors, Eqn. (3). The solid blue line shows scattering properties of the species, while the red dotted line gives information about the absorptive components of the species, Fig. 2.

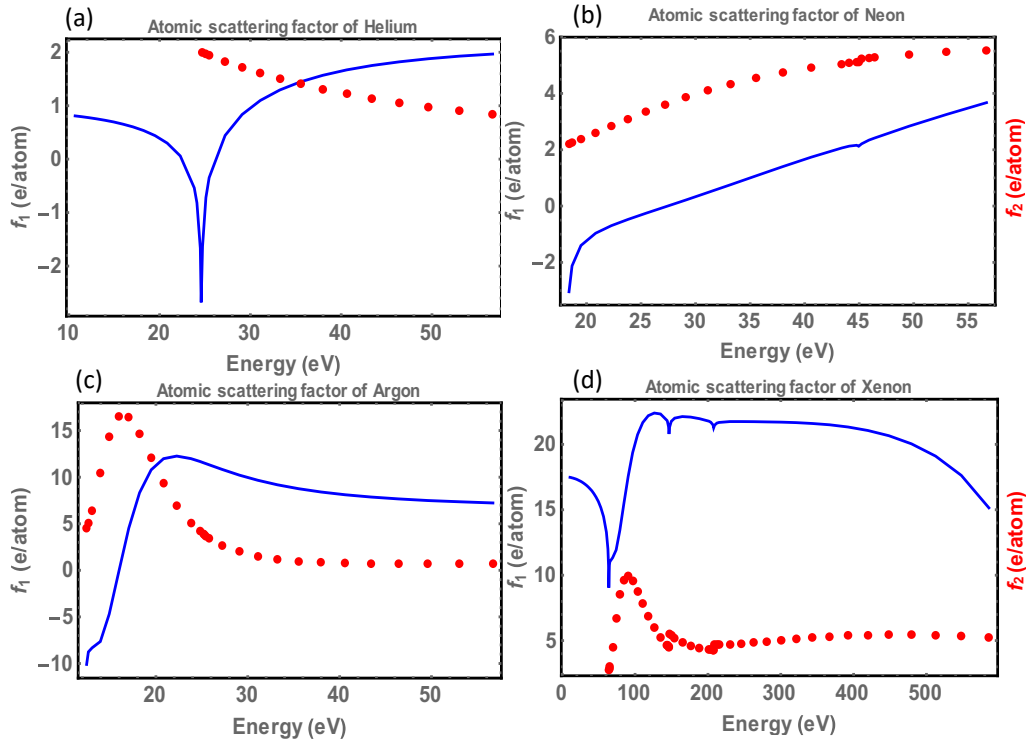

Figure 2: Atomic scattering factors of inert gases in the XUV region. (a) Helium, (b) Neon (c) Argon (d) Xenon. The solid blue line is for f_1, and the red dotted line is for f_2

The refractive indices in the XUV region are calculated using Eqn. (3) even though the refractive indices in the XUV region are not completely accurate in the energy range of interest. The simulation for refraction index values helps determine how a medium responds to a specific wavelength. The real and imaginary parts of the refractive indices are studied using Eqn. (3). Figure 3 presents the real part of the refractive indices for He, Ne, Ar, and Xe gas while Fig. 4 shows the imaginary part of the index of refraction values for these gas species. f_2 of xenon is plotted from 60 eV to 500 eV since f_2 is available for xenon gas at this range, Fig. 2 and 3.

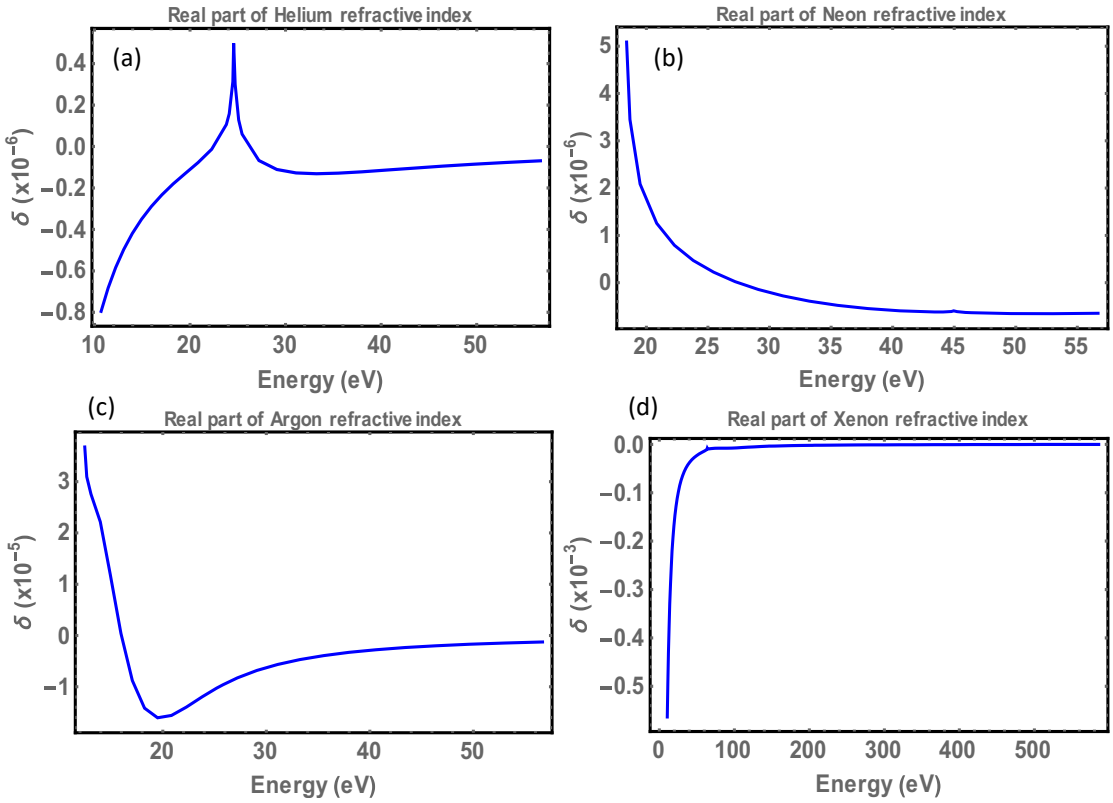

Figure 3: Simulation of the real part of the refractive index ($\delta = R(n) - 1$) in the XUV region for inert gases (a) Helium, (b) Neon, (c) Argon, (d) Xenon

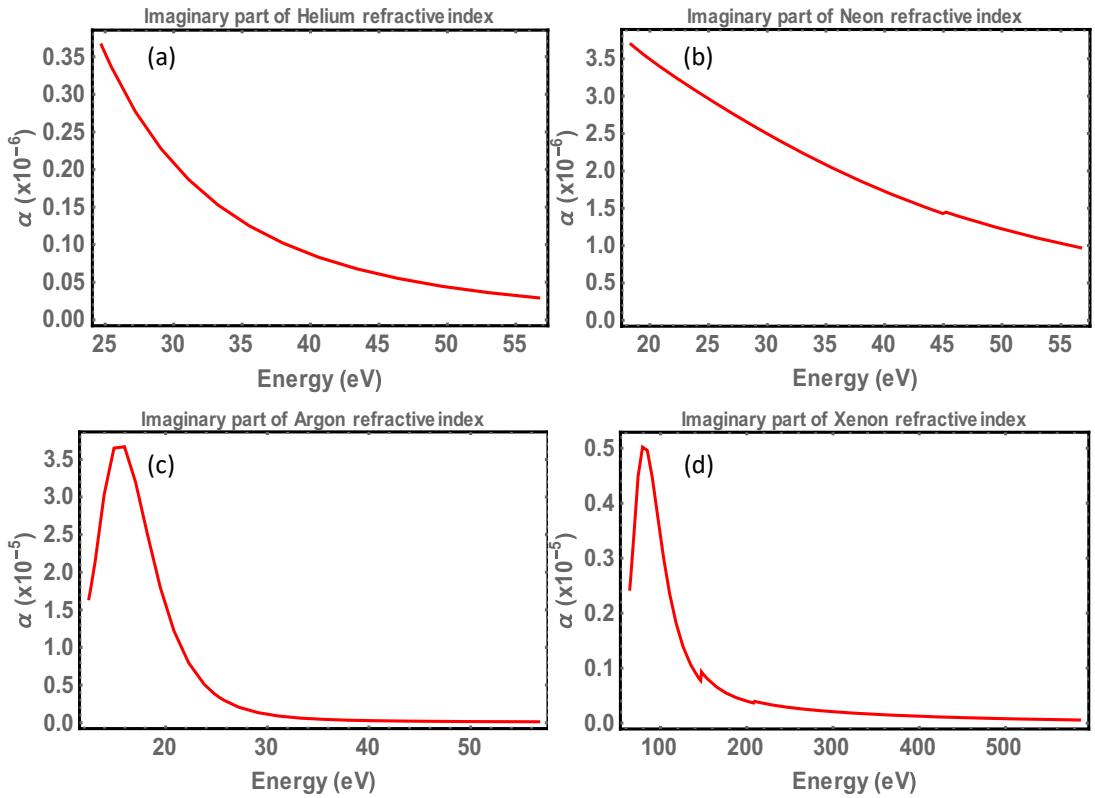

Figure 4: Simulation of imaginary part of the refractive index ($\alpha = Im(n)$) in the XUV region for inert gases (a) Helium, (b) Neon, (c) Argon, (d) Xenon

5. Conclusions

In this paper, refractive index values in the IR and XUV region are calculated using the Mathematica program. This paper is the comparison of refractive indices of different inert gases in different wavelength regions. An explanation of the index of refraction at the IR and XUV region is described for room temperature and pressure values. This paper provides a calculation of the real and imaginary part of refractive indices of inert gases and covers a wide range of wavelengths from IR to XUV region. The study of the refraction index values in the near-infrared and the extreme ultraviolet region has been carried out. The atomic scattering factors for gas species help calculate the real and imaginary part of the refractive index values in the XUV region. The gas species of helium, neon, argon, and xenon are used. The atomic scattering factors of these gas species are used as input parameters in the simulation program, and so the real and imaginary parts of the refractive indices in the XUV region are determined. As simulation software, the Wolfram Mathematica program is used for the calculation of refractive indices.

The estimation of the index of refraction values in the infrared and XUV region can be used for the phase matching calculation for the generation of coherent XUV pulses, absorption, or transmission of a material for a specific wavelength region.

Appendix: Mathematica Program

```
a=1.366*10^-3; b=9.02*10^5; c=1.81*10^12; d=4.89*10^18; ee=1.45*10^25; f=4.34*10^31;
(*Xe gas variables values*)
λ={6000,7000,7200,7400,7500,7600,7800,8000}; (*Wavelength angstrom*)
n=SetPrecision[Table[(1+a*(1+b/λ[[i]]^2+c/λ[[i]]^4+d/λ[[i]]^6+ee/λ[[i]]^8+f/λ[[i]]^10))^(1/2),
{i,1,8}],10];
Print["Refractive index of Xe at 800 nm = ",n," at 1 bar for Xe gas"]
n=n-1;
ListLinePlot[Table[{λ[[i]]/10,n[[i]]*10^4},{i,1,8}],Frame->True,Axes->False,PlotRange-
>All,FrameLabel->{"Wavelength (nm)","n-1 (x10-4)"},FrameStyle->Thick,LabelStyle-
>{Bold,15},PlotStyle->{Thick,Blue},PlotLabel->"Xenon refractive index in near infrared
region"]
MA=131.29; (*Xenon atomic weight gr/mol*) R=83.14; (*cm^3bar/Kmol*) T=22.8+273.15;
P=1; (*bar optimum presure for Xenon gas*) ρ=MA*P/R/T;Print["ρ=",ρ,"gr/cm^3"]
Nav=6.02*10^23; (*avagadro number*) natom=Nav*ρ/MA; (*number of atoms per cm^3*)
Print["natom= ",natom," atoms/cm^3"]

EEf1={10.69,11.4276,12.2161,13.059,13.9601,14.9234,15.9531,17.0538,18.2305,19.4884,20.8
331,22.2706,23.8073,25.45,27.2061,29.0833,31.09,33.2352,35.5285,37.9799,40.6005,43.402,4
6.3967,49.5981,53.0204,56.6788,60.5896,62.72,63.68,63.936,64.32,64.7703,65.28,69.2394,74.
017,79.1241,84.5837,90.42,96.6589,103.328,110.458,118.08,126.227,134.937,143.766,144.248
,145.967,146.553,147.433,149.634,154.201,164.84,176.214,188.373,201.371,203.938,207.06,2
07.892,209.141,212.262,215.266,230.119,245.997,262.971,281.116,300.513,321.248,343.414,3
67.11,392.441,419.519,448.466,479.41,512.489,547.851,585.653}; (*eV for f1*)

f1={17.4817,17.4729,17.4627,17.451,17.4376,17.4222,17.4044,17.3839,17.3603,17.333,17.301
4,17.2647,17.2221,17.1724,17.1143,17.046,16.9653,16.8696,16.7551,16.6169,16.4483,16.2392
,15.9749,15.631,15.1635,14.4787,13.2889,11.9994,10.5181,9.04168,10.1989,10.7681,11.0295,
11.3451,11.9353,13.4352,15.4567,17.5482,19.3672,20.7487,21.6728,22.1972,22.3982,22.3204,
21.8272,21.7629,21.3416,20.7968,21.3224,21.7567,22.0064,22.129,22.0852,21.9645,21.7702,2
1.6898,21.4862,21.2694,21.4691,21.6278,21.6791,21.7426,21.7454,21.7359,21.7211,21.6987,2
1.6617,21.5992,21.4951,21.3273,21.0644,20.6582,20.0448,19.1067,17.6322,15.1523}; (*Real
atomic scattering factor*)
```

```
EEf2={64.32,64.7703,65.28,69.2394,74.017,79.1241,84.5837,90.42,96.6589,103.328,110.458,118.08,126.227,134.937,143.766,144.248,145.967,146.553,147.433,149.634,154.201,164.84,176.214,188.373,201.371,203.938,207.06,207.892,209.141,212.262,215.266,230.119,245.997,262.971,281.116,300.513,321.248,343.414,367.11,392.441,419.519,448.466,479.41,512.489,547.851,585.653}; (*eV for f2*)

f2={2.7373,2.8683,3.0230,4.4855,6.6806,8.5363,9.6404,9.9217,9.5457,8.7673,7.8187,6.8627,5.9916,5.2451,4.6587,4.6310,4.5353,4.5038,5.5082,5.4034,5.2082,4.8526,4.5958,4.4226,4.3179,4.3047,4.2913,4.2883,4.6957,4.6923,4.6913,4.7129,4.7685,4.8475,4.9411,5.0418,5.1427,5.2375,5.3204,5.3862,5.4308,5.4507,5.4436,5.4084,5.3453,5.2553}; (*Imaginary atomic scattering factor*)

r0=2.82*10^-6;(*classical electron radius*);
λ=1240/EEf1 (*nm*);
nr=SetPrecision[1-((r0)/(2*π))*λ^2*(ρ*f1),40];
λ=1240/EEf2 (*nm*);
ni=SetPrecision[((r0)/(2*π))*λ^2*(ρ*f2),40];
b1=ListLinePlot[Table[{EEf1[[i]],(nr[[i]]-1)*10^3},{i,1,76}],Frame->True,Axes->False,PlotRange->All,FrameLabel->{"Energy (eV)","δ (x10-3)"},FrameStyle->Thick,LabelStyle->{Bold,15},PlotStyle->{Thick,Blue},PlotLabel->"Real part of Xenon refractive index"]

b2=ListLinePlot[Table[{EEf2[[i]],(ni[[i]]*10^5)},{i,1,46}],Frame->True,Axes->False,PlotRange->All,FrameLabel->{"Energy (eV)","α (x10-5)"},FrameStyle->Thick,LabelStyle->{Bold,15},PlotStyle->{Thick,Red},PlotLabel->"Imaginary part of Xenon refractive index"]
Show[b1,b2,PlotRange->All]

a1=ListLinePlot[Table[{EEf1[[i]],(f1[[i]])},{i,1,76}],Frame->True,Axes->False,PlotRange->All,FrameLabel->{"Energy (eV)","f1 (e/atom)"},FrameStyle->Thick,LabelStyle->{Bold,15},PlotStyle->{Thick,Blue},PlotLabel->"Atomic scattering factor of Xenon"]

a2=ListPlot[Table[{EEf2[[i]],(f2[[i]])},{i,1,46}],Frame->True,Axes->False,PlotRange->All,FrameLabel->{"Energy (eV)","f2 (e/atom)"},FrameStyle->Thick,LabelStyle->{Bold,15},PlotStyle->{Thick,Red},PlotLabel->"Atomic scattering factor of Xenon"]
```

```
Show[a1,a2,PlotRange->All]
```

The gas variables are taken from Table 1, Ref [9, 10].

References

[1] Paskov, P.P., *Refractive indices of InSb, InAs, GaSb, InAsxSb1−x, and In1−xGaxSb: Effects of free carriers*, Journal of Applied Physics, 81(4) 1890-1898, 1997.

[2] Rappl, P.H.O., McCann, P.J., *Development of a novel epitaxial-layer segmentation method for optoelectronic device fabrication*, IEEE Photonics Technology Letters, 15(3), 374-376, 2003.

[3] Tripathy, S.K., *Refractive indices of semiconductors from energy gaps*, Optical Materials, 46, 240-246, 2015.

[4] Penn, D.R., *Wave-number-dependent dielectric function of semiconductors*, Physical Review, 128(5), 2093-2097, 1962.

[5] Naccarato, F., Ricci, F., Suntivich, J., Hautier, G., Wirtz, L., Rignanese, G.M., *Searching for materials with high refractive index and wide band gap: A first-principles high-throughput study*, Physical Review Materials, 3(4), 044602, 2019.

[6] Reddy, R.R., Gopal, K.R., Narasimhulu, K., Reddy, L.S.S., Kumar, K.R., Reddy, C.V.K., Ahmed, S.N., *Correlation between optical electronegativity and refractive index of ternary chalcopyrites, semiconductors, insulators, oxides and alkali halides*, Optical Materials, 31(2), 209-212, 2008.

[7] Reddy, R.R., Gopal, K.R., Narasimhulu, K., Reddy, L.S.S., Kumar, K.R., Balakrishnaiah, G., Kumar, M.R., *Interrelationship between structural, optical, electronic and elastic properties of materials*, Journal of Alloys and Compounds, 473(1-2), 28-35, 2009.

[8] Ahmad, S., Ashraf, M., Ahmad, A., Singh, D.V., *Electronic and Optical Properties of Semiconductor and Alkali Halides*, Arabian Journal for Science and Engineering, 38(7), 1889-1894, 2013.

[9] Dalgarno, A., Kingston, A.E., *The refractive indices and Verdet constants of the inert gases*, Proceedings of the Royal Society of London. Series A. Mathematical and Physical Sciences, 259(1298), 424-431, 1960.

[10] Rogers, E.T.F., *Modelling of capillary high harmonic generation*, PhD thesis, University of Southampton, 2008.

[11] Cuthbertson, C., *XI. New determinations of some constants of the inert gases*, The London, Edinburgh, and Dublin Philosophical Magazine and Journal of Science, 21(121), 69-77, 1911.

[12] Cuthbertson, C., Cuthbertson, M., *The refraction and dispersion of neon and helium*, Proceedings of the Royal Society of London. Series A, Containing Papers of a Mathematical and Physical Character, 135(826), 40-47, 1932.

[13] Korff, S.A., Breit, G., *Optical dispersion*, Reviews of Modern Physics, 4(3), 471-503, 1932.

[14] Ingersoll, L.R., Liebenberg, D.H., *Faraday effect in gases and vapors II*, Journal of the Optical Society of America, 46(7), 538-542, 1956.

[15] Pekeris, C.L., *1^1S and 2^3S States of Helium*, Physical Review, 115(5), 1216-1221, 1959.

[16] Chantler, C.T., Olsen, K., Dragoset, R.A., Chang, J., Kishore, A.R., Kotochigova, S.A., Zucker, D.S., *X-ray form factor, attenuation, and scattering tables,* 22 Mayıs 2020 tarihinde https://www.nist.gov/pml/x-ray-form-factor-attenuation-and-scattering-tables web sitesinden alınmıştır.

[17] Chantler, C.T., *Detailed tabulation of atomic form factors, photoelectric absorption and scattering cross section, and mass attenuation coefficients in the vicinity of absorption edges in the soft x-ray (Z=30–36, Z=60–89, E=0.1 keV–10 keV), addressing convergence issues of earlier work*, Journal of Physical and Chemical Reference Data, 29(4), 597-1056, 2000.

[18] Chantler, C.T., *Theoretical form factor, attenuation, and scattering tabulation for Z=1–92 from E=1–10 eV to E=0.4–1.0 MeV*, Journal of Physical and Chemical Reference Data, 24(1), 71-643, 1995.

[19] *Mathematica Version 10.0.,* Wolfram Research, Inc., Champaign, Illinois, 2014.

[20] Ciddor, P.E., *Refractive index of air: 3. The roles of CO_2, H_2O, and refractivity virials:erratum*, Applied Optics, 41(33), 7036-7036, 2002.

[21] Henke, B.L., Gullikson, E.M., Davis, J.C., *X-ray interactions: photoabsorption, scattering, transmission, and reflection at E = 50-30,000 eV, Z = 1-92,* Atomic Data and Nuclear Data Tables, 54(2), 181-342, 1993.

Adıyaman University Journal of Science
https://dergipark.org.tr/en/pub/adyujsci
DergiPark AKADEMİK
ISSN 2147-1630
e-ISSN 2146-586X

G-banded Karyotypes of Some Species in Gliridae (Mammalia: Rodentia) from Turkey

Teoman KANKILIÇ[1,*], Perinçek Seçkinozan ŞEKER[2], Engin SELVİ[3], Beytullah ÖZKAN[4], Nuri YİĞİT[3], Ercüment ÇOLAK[3]

[1]*Niğde Ömer Halisdemir University, Faculty of Arts and Science, Department of Biotechnology, Niğde Turkey*
tkankilic@ohu.edu.tr, ORCID: 0000-0002-9576-5887
[2]*Artvin Çoruh University, Artvin Vocational School, Hunting and Wildlife Program, Artvin, Turkey*
seckinperincek@artvin.edu.tr, ORCID: 0000-0002-6103-4840
[3]*Ankara University, Faculty of Science, Department of Biology, Ankara, Turkey*
eselvi@ankara.edu.tr, ORCID: 0000-0001-5370-3023
colak@science.ankara.edu.tr, ORCID: 0000-0001-5826-1615
nyigit@science.ankara.edu.tr, ORCID: 0000-0001-8426-2144
[4]*Trakya University, Faculty of science, Department of Biology, Edirne, Turkey*
beytullahozkan@trakya.edu.tr, ORCID: 0000-0003-0050-7031

Received: 23.11.2020 **Accepted:** 16.04.2021 **Published:** 30.06.2021

Abstract

The results of a cytogenetic study on some representatives of Gliridae from Turkey were introduced. The G-, C-, and AgNOR banded karyotypes of *Muscardinus avellanarius abanticus* from Abant (Bolu), and the G-banded karyotype of *Myomimus roachi* from Thrace were presented for the first time. Additionally, the G-banded karyotypes of *Dryomys nitedula*, and *Myoxus glis* were analysed. Because of not including a secondary constriction and the smallest chromosome being metacentric instead of acrocentric in the autosomal set, the karyotype of *M. a. abanticus* was different from that of *M. a. trapezius.* With the comparison of obtained G-banded patterns belonging to the other Glirid species, it was detected that obtained karyotypes displayed consistency at a great extent with the previously determined karyotypes.

* Corresponding Author DOI: 10.37094/adyujsci.830056

Keywords: Gliridae; G-banding; Karyotype; Turkey.

Türkiye'de Yayılış Gösteren Gliridae (Mammalia: Rodentia) Familyasındaki Bazı Türlerin G-bantlı Karyotipleri

Öz

Bu çalışmada Türkiye'de yayılış gösteren bazı Gliridae temsilcileri üzerinde yapılan bir sitogenetik çalışmanın sonuçları sunuldu. Abant'tan (Bolu) *Muscardinus avellanarius abanticus*'un G-, C- ve AgNOR bantlı karyotipleri ile Trakya'dan *Myomimus roachi*'nin G-bantlı karyotipi ilk kez sunuldu. Ek olarak, *Dryomys nitedula* ve *Myoxus glis*'in G-bantlı karyotipleri analiz edildi. Otozomal sette ikincil bir daralma olmaması ve en küçük kromozomun akrosantrik yerine metasentrik olması nedeniyle, *M. a. abanticus*'un karyotipinin *M. a. trapezius*'un karyotipinden farklı olduğu tespit edildi. Farklı lokalitelerde yaşayan Glirid türlerinin elde edilen G-bantlı karyotiplerinin daha önceki çalışmalarda belirlenen karyotiplerle büyük ölçüde tutarlılık gösterdiği tespit edildi.

Anahtar Kelimeler: Gliridae; G-bantlama; Karyotip; Türkiye.

1. Introduction

Gliridae Thomas, 1897 is one of the oldest extant families of order Rodentia. Members of this family are known for their long-term (5-6 months) hibernation. They can occupy many different habitats; such as woods, thickets, orchards, rocky areas in the forest, steppes, and deserts. Species within this family are mostly found in Europe and Asia Minor, although some of them live in Africa, Russia, India, China, and Japan [1, 2]. The family consists of 9 genera including 28 living species [2]. There are 11 species in the family whose distribution range is limited to the western Palearctic; seven of them (*Myoxus glis*, *Dryomys nitedula, Dryomys laniger*, *Eliomys melanurus*, *Myomimus roachi*, *Muscardinus avellanarius*, and *Myomimus setzeri*) lived in Turkey [3]. Among all, the most common dormouse species in Turkey are *M. glis*, *D. nitedula,* and *M. avellanarius*. The remaining species have a more limited geographical distribution range. *M. roachi*, also known as Roach's mouse-tailed dormouse, is present only in a limited area in the western part of Thrace and Turkey. Another *Myomimus* species, *M. setzeri*, also known as Setzer's mouse-tailed dormouse, has been recorded from eastern Anatolia adjacent to Iran. Despite *E. melanurus* is found in Egypt, Iraq, Israel, Jordan, Lebanon, Libya, Saudi Arabia, Syria and Turkey (Şanlıurfa), *D. laniger* that is an endemic hibernator species has a limited distribution in the Taurus Mountains [3].

Until this time, there have been numerous studies that examine the characteristics of karyological of Glirid taxa in Europe and Turkey. [4, 5]. Beyond that the conventional karyotypes of most species in Gliridae from Turkey have been determined by previously performed studies [6, 7]. Notwithstanding, there is still lack of information about the banded and even conventional karyotypes of many taxa in this family. Heretofore, two subspecies of *M. avellanarius*, also called the hazel dormouse, in Turkey have been identified based on the morphological differences between geographically very distant populations of this species [8, 9]. The first one, *M. a. trapezius*, has been described from Coşandere (Trabzon), while, the second one, *M. a. abanticus*, has been identified from Abant (Bolu). Various karyotype studies including conventional, C- and G- banding techniques have often been focused on the European populations of *M. avellanarius* [10-16], and little has been known about the karyology of the Turkish populations [17, 18]. The C- and G-banded karyotypes in the populations of *M. a. trapezius* from Trabzon and Ordu have been previously reported [17, 18]. On the other hand, even conventional karyotype of the *M. a. abanticus* is still unknown. The conventional and AgNOR- banded karyotype of *M. roachi* has been studied by Civitelli et al. [19]. However, the C- and G-banded karyotypes of *M. roachi* from Turkey have not been reported up to the present. The conventional stained and banded karyotype of *D. nitedula* has been detected from various parts of its geographic distribution range in Turkey [6, 7, 19, 20]. In contrast to this, the C- and G- and AgNOR-banded karyotype of this species has been studied on the limited number of specimens from the restricted number of areas in Turkey [7, 19, 20]. The conventional karyotype of fat dormouse, *M. glis*, has been investigated in specimens from both Anatolia and Thrace [21, 19]. The C- and G- banded karyotype of this species have been studied from different parts of Black Sea regions [20, 22].

On the members of the Gliridae family from Turkey, the conventional karyotype studies have been performed more often, however, karyotype banding studies have been limited. The increase in the number of banding studies conducted on the members of this family, which has a wide range in our country, will make it easier to determine possible intraspecific variations within the species of this rodent family; and thus, this will enable us to directly contribute to the understanding of our country's biodiversity and hence global biodiversity. Based on this thought, the current study primarily presented the banded karyotypes of the representatives of Gliridae from Turkey (*M. a. abanticus, M. a. trapezius, M. roachi*, *D. nitedula*, and *Myoxus glis*) to fill the gaps in our knowledge about chromosome banding patterns of dormouse species. In addition, the G-, C-, and AgNOR-banded karyotypes of *M. a. abanticus* were introduced for the first time.

2. Materials and Methods

Karyotype analyses were carried out on 51 specimens belonging to *M. a. abanticus*, *M. roachi*, *D. nitedula*, and *M. glis* in the Gliridae family. The number of specimens, sample designations, and collecting sites for each species was identified in Table 1 and Fig. 1. Animal samples were captured by the fieldwork performed in accordance with the legal permission (no: 72784983-488.04-150036) given by the Republic of Turkey Ministry of Agriculture and Forestry, General Directorate of Nature Conservation and National Parks. Experimental processes were conducted according to the animal experiments local ethics committee decision provided by the Animal Experiments Local Ethics Committee of Ankara University (no. 2015-6-105).

Karyotype preparations were obtained from the fresh bone marrow of colchicine treated animals following the method of Ford and Hamerton [23]. To define autosomal and sexual chromosomes pairs, the C-, G- and AgNOR staining techniques were employed. The G-banding processes of the chromosomes were carried out in accordance with the process introduced by Seabright [24]. Constitutive heterochromatin and nucleolus organizer regions (NORs) were detected by following the staining techniques of Sumner [25] and Howell and Black [26], respectively. A total of 10 slides were made from each sample and nearly 20 well-spread metaphase plates were examined. The slides were photographed with the Nikon DS-Ri2 stereo binocular microscope. Chromosome numbers were determined by attentively counting of well-spreading metaphase plates. The most frequently observed chromosome counts were regarded as valid karyotypes. The diploid number of chromosomes (2n), the total numbers of chromosomal arms (NF), and the numbers of autosomal arms (NFa), as well as the X and the Y chromosomes, were classified. All chromosomes were arranged from bigger to smaller and noted to be the metacentric, submetacentric and acrocentric according to their centromere positions, consistent with the Levan et al. [27]. The skins, skulls, and karyotype preparations of all examined specimens were deposited at the Niğde Ömer Halisdemir University, Niğde, Turkey.

3. Results

The G-, C-, and AgNOR-banded karyotype of *M. a. abanticus* were studied for the first time. The karyotype of three populations from Abant (Bolu) - type locality of *M. a. abanticus*-, Uludağ (Bursa) and Yığılca (Düzce) in Turkey had 2n = 46, NF = 92 and NFA = 88 values. All the autosomal chromosomes were bi-armed (meta- and submetacentric or subtelocentric pairs) in gradually decreasing size. The X chromosome was a medium-sized metacentric, while the Y chromosome was a small-sized acrocentric. AgNOR staining revealed that the nucleolar organizer regions positioning in the secondary constrictions were localized in the 20^{th} and 22^{nd} autosomal pairs. All detected NORs were heteromorphic and observed only in one of the homologs. Most of the autosomal chromosomes enjoyed apparent C-positive bands in pericentromeric regions, while,

C-bands in some chromosomes were nebulous. The sexual chromosomes also had dark C-bands. (Fig. 2).

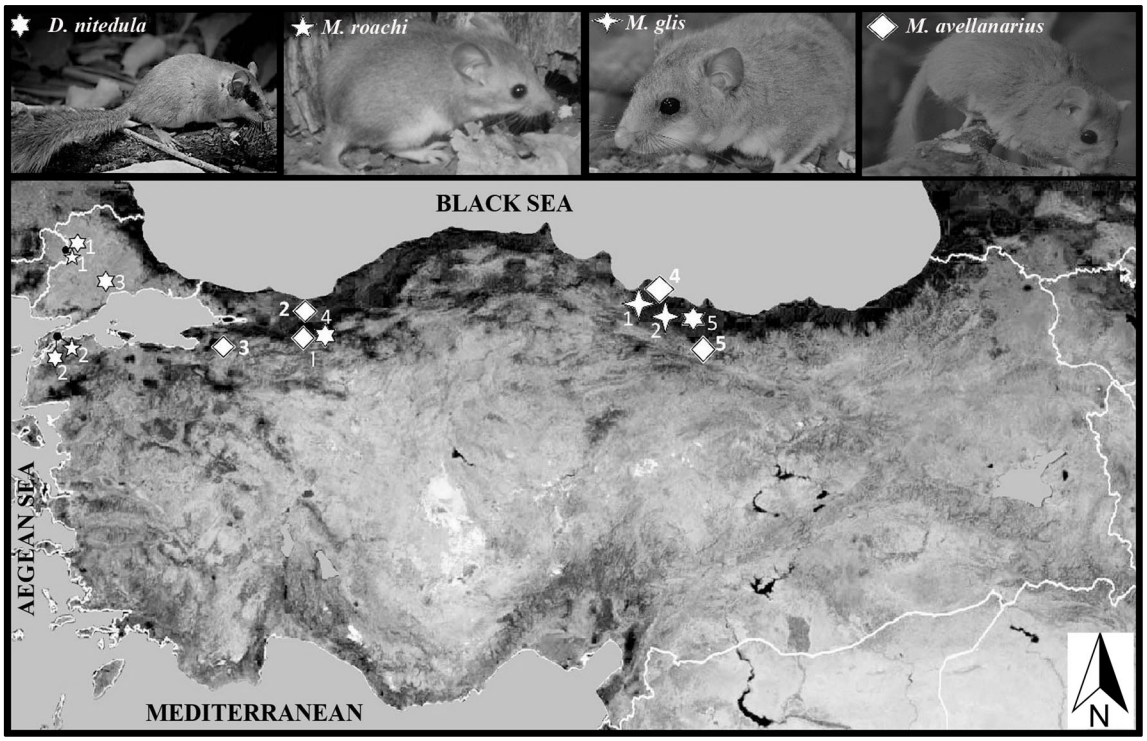

Figure 1: The map showing collecting sites of the samples, the numbers and symbols in the map correspond to the localities and species given in Table 1

Additionally, the G- banded karyotypes of *M. a. trapezius* from Ordu-Ulubey and Giresun-Bulancak were presented. The detected karyotype consisted of 2n = 46, NF = 90, and NFa = 86 values. The X chromosome was larger metacentric and Y chromosome was acrocentric. This karyotype was different from the karyotype of *M. a. abanticus*, because of including a secondary constriction in the 20th chromosome pair and the smallest chromosome being acrocentric instead of metacentric in the autosomal set (Fig. 3).

The G- banded karyotype of *M. roachi* was detected for the first time. The karyotype of three specimens from Edirne and Çanakkale from Thrace in the European part of Turkey had the karyotype including 2n = 44, NFa = 84 and NF = 88 values. All the autosomal chromosomes were bi-armed (meta- or submetacentric pairs) of decreasing size. In the karyotypes, the X chromosome was a medium-sized submetacentric, while the Y chromosome was a medium-sized metacentric (Fig. 4A).

Table 1: The number of specimens, sample designations, collecting sites and karyological characteristics for each species. (NFa: autosomal fundamental number NF: chromosome arm numbers)

Species	Map Number	Localities (Latitude/Longitude)	Total	♂	♀	2n	NFa	NF
Myoxus glis (✦	1	Giresun-Bulancak (40^0 56' 08" N / 38^0 13' 51" E)	1	1	-	62	120	124
	2	Ordu-Ulubey-Yukarıkızılen (40^0 46' 38" N / 37^0 42' 39" E)	2	1	1	62	120	124
Dryomys nitedula (✡	1	Edirne-Orhaniye-Bağlık (41^0 31' 07" N / 26^0 39' 09" E)	1	-	1	48	92	96
	2	Çanakkale-Gelibolu-Sütlüce (40^0 20' 35" N / 26^0 36' 03" E)	1	-	1	48	92	96
	3	Tekirdağ-Kumbağı-Naip (40^0 52' 25" N / 27^0 25' 31" E)	1	-	1	48	92	96
	4	Bolu-Abant (40^0 35' 41" N / 31^0 16' 57" E)	1	-	1	48	92	96
	5	Giresun-Bulancak (40^0 55' 12" N / 38^0 12' 56" E)	1	1	-	48	92	96
Myomimus roachi (★)	1	Edirne-Orhaniye-Bağlık (41^0 29' 50" N / 26^0 38' 49" E)	1	-	1	44	84	88
	1	Edirne-Azatlı (41^0 29' 38" N / 26^0 42' 03" E)	1	-	1	44	84	88
	2	Çanakkale-Gelibolu-Sütlüce (40^0 20' 54" N / 26^0 36' 47" E)	1	1	-	44	84	88
Muscardinus avellanarius (◇)	1	Bolu-Abant-Soğuksu (40^0 36' 49" N / 31^0 17' 56" E)	7	4	3	46	88	92
	2	Düzce-Yığılca (40^0 57' 31" N / 31^0 27' 04" E)	4	3	1	46	88	92
	3	Bursa-Uludağ (40^0 07' 06" N / 29^0 07' 11" E)	2	1	1	46	88	92
	4	Ordu-Ulubey (40^0 52' 36" N / 37^0 45' 32" E)	6	3	3	46	86	90
	5	Giresun-Bulancak (40^0 55' 57" N / 38^0 14' 52" E)	4	2	2	46	86	90

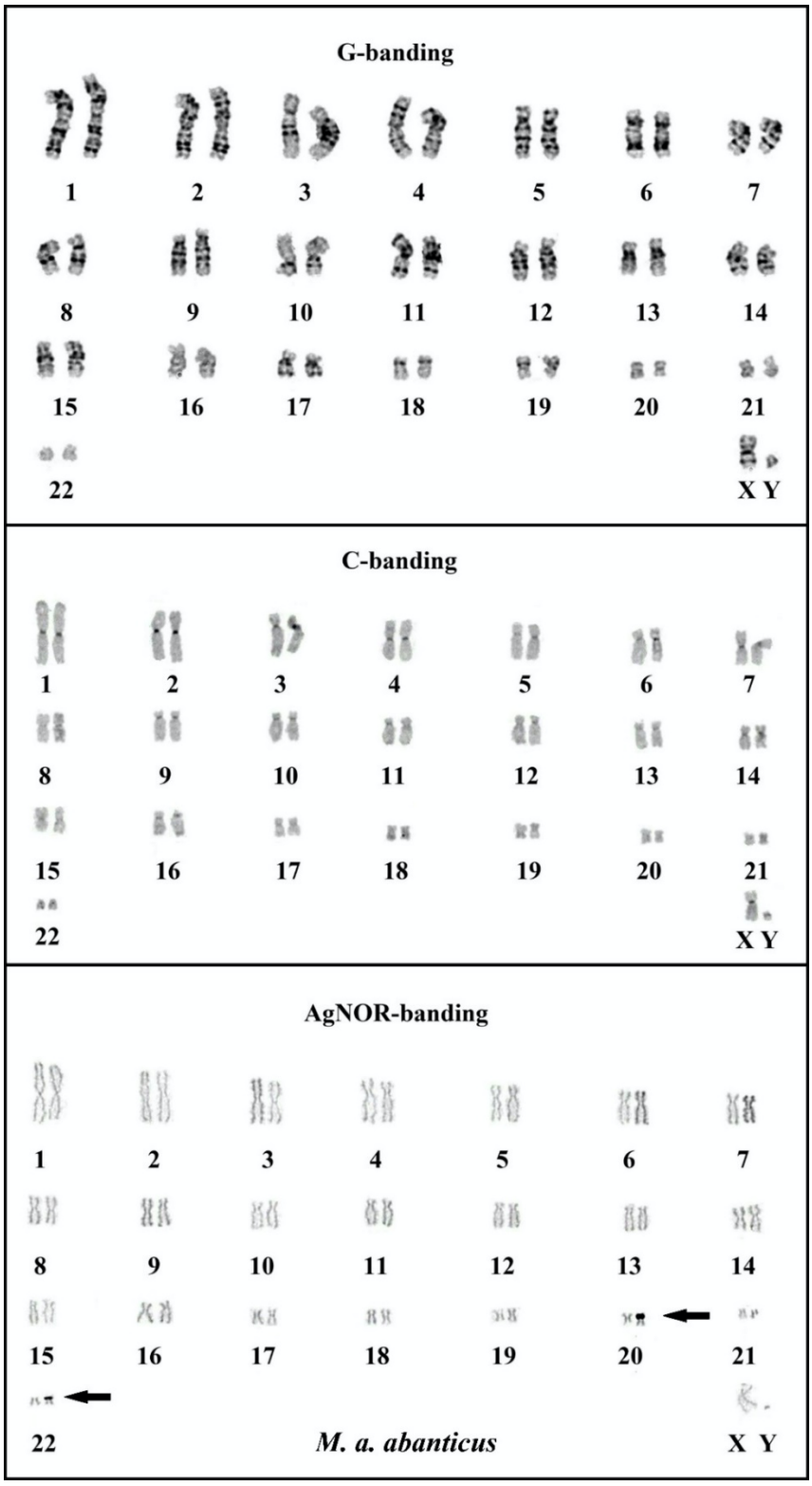

Figure 2: The G-, C- and AgNOR- banded karyotype of *M. a. abanticus* from Abant-Bolu. The arrows indicate the position of the heteromorphic active AgNOR regions

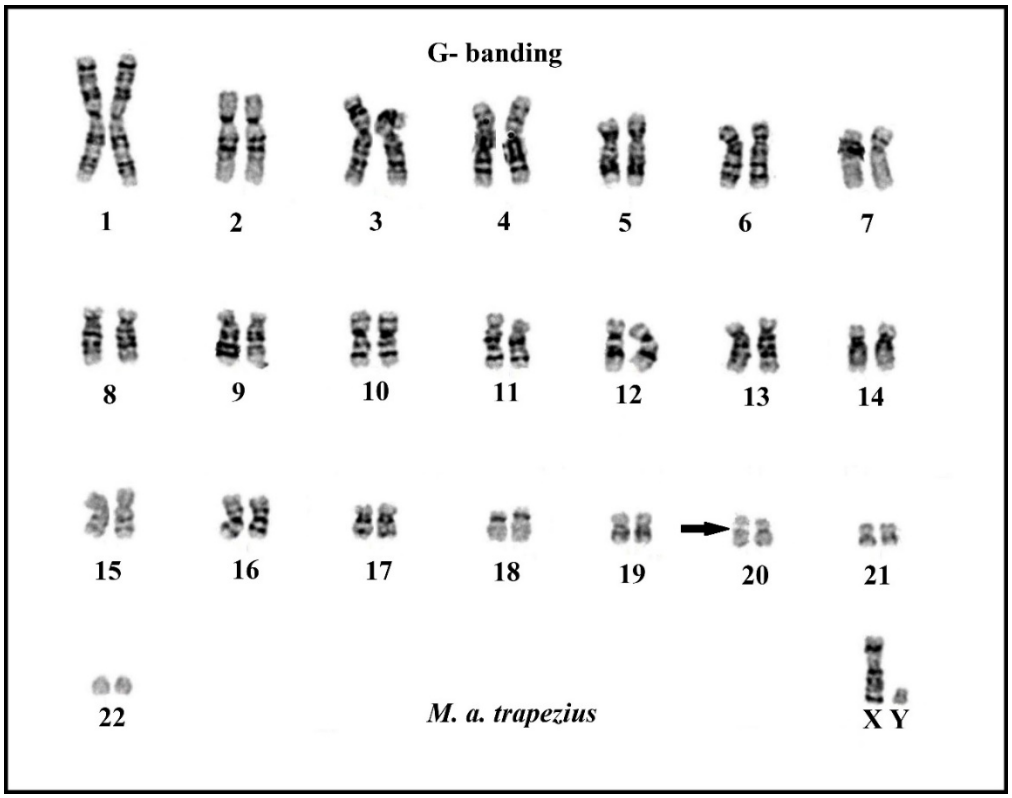

Figure 3: The G- banded karyotype of *M. a. trapezius* from Ulubey-Ordu. The arrow indicates the secondary construction

The karyotype of *D. nitedula* from Thrace located in the European Turkey and Anatolia was studied using the G-banding technique. The karyotypes of five specimens collected from five localities had the values of 2n = 48, NF = 96 and NFa = 92. It was determined that the karyotypes of all specimens consisted of 23 pairs of large and small meta-, submeta- and subtelocentric autosomal chromosomes. The first autosomal pair was frankly bigger than the other autosomal pairs in the complement. In conformity with the findings of previous studies, it was detected that 21st autosomal chromosomes were in a heterozygous secondary constriction condition in this karyotype. The X chromosomes were identified to be in the large and submetacentric shape (Fig. 4B).

The G-banded karyotype of *M. glis* from Turkey was investigated. The karyotype having the values of 2n = 62, FN = 124, NFa = 120 was found in two *M. glis* specimens from two different localities of Anatolia. Except for the Y- chromosome, all chromosomes, including X- as well, in the karyotype were noted to be bi-armed, meta- and submetacentric chromosomes. The 17th autosomal pair appeared to carry a secondary constriction in the karyotype. The X- chromosome was determined to be a large-sized and metacentric element, while the Y- chromosome was detected to be dot-like and most likely acrocentric element (Fig. 4C).

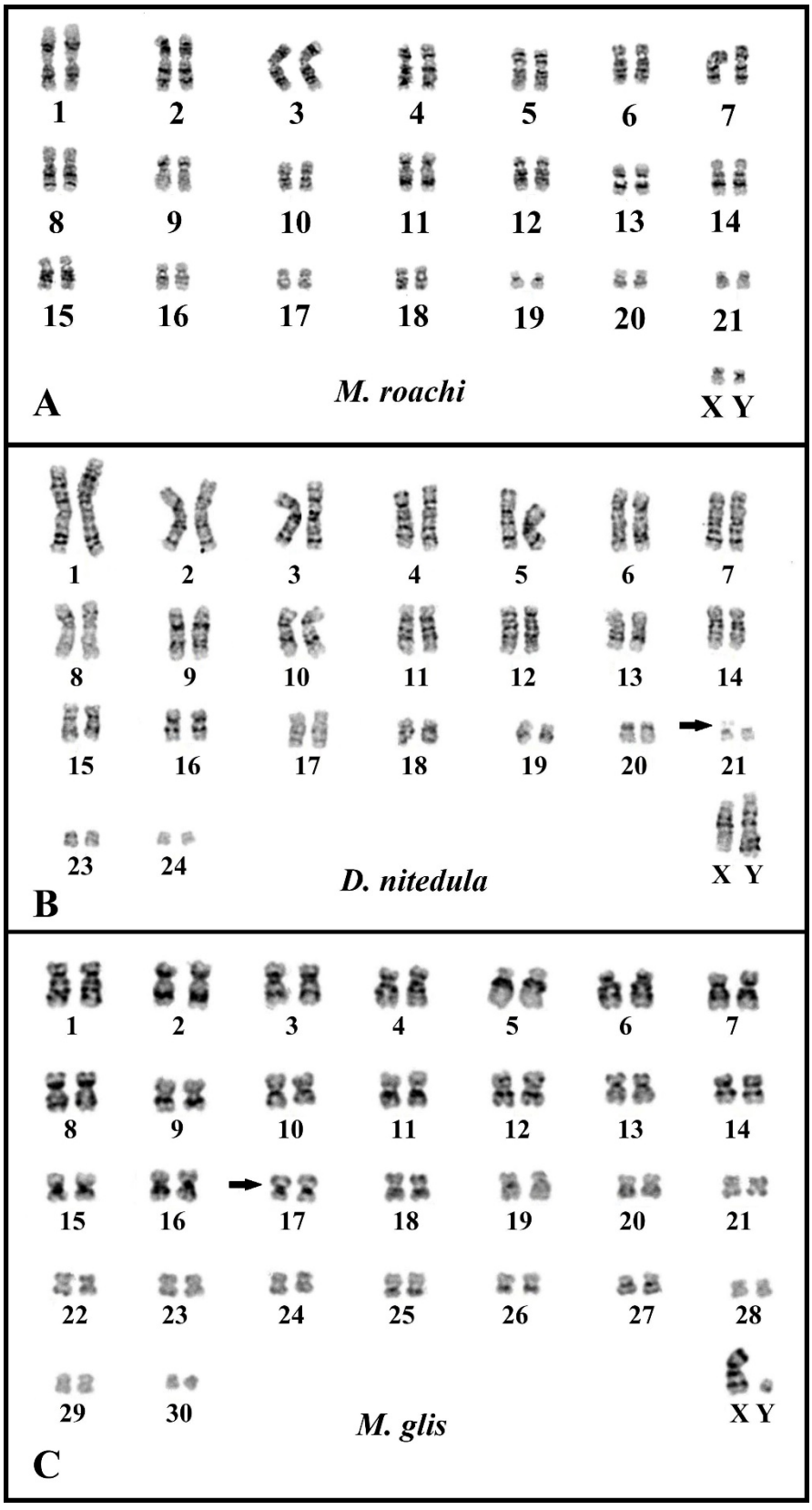

Figure 4: G- banded karyotypes of *M. roachi* from Edirne (A), *D. nitedula* from Tekirdağ (B), and *M. glis* from Ordu (C). The arrows indicate the secondary construction in the karyotypes

4. Discussion

Identifying intra-specific variations is the most fundamental step in documenting biodiversity in a particular region. In this sense, the variations hidden in the genome of both plant and animal species in our country are tried to be revealed by using a wide variety of markers, including karyotype analysis [7, 17, 19, 28, 29]. Karyotype variations are an easy-to-apply method used to determine genetic variation. In this study, carried out for this purpose, the G-, C-, and AgNOR-banded karyotypes of *M. a. abanticus* and the G-banded karyotypes of *M. roachi* from Turkey were presented for the first time. Additionally, the G-banded karyotypes of *M. a. trapezius, D. nitedula*, and *M. glis* were submitted as well.

The karyotype of *M. avellanarius* was investigated from only two localities in north-eastern Anatolia throughout Turkey until now. Those obtained karyotypes belonged to the *M. a. trapezius*, known subspecies of this species from the region. The smallest autosomal pair in investigated karyotypes was considered to be subtelocentric in the Trabzon population or acrocentric in the Ordu population. Accordingly, two karyotype forms with NFa = 86 or NFa = 88 values were determined for this subspecies based on the morphological difference of the smallest pair [17, 18]. The G- banded karyotype of *M. a. trapezius* presented by this study included the values of 2n = 46, NF = 90 and NFa = 86 to be compatible with the karyotype determined by Şekeroğlu et al. [17]. The karyotype we identified from Ulubey-Ordu included a secondary constriction in the 20th chromosome pair, similar to the karyotype of *M. a. trapezius* revealed by Şekeroğlu et al. [17] and Doğramacı and Kefelioğlu [18]. Also, the autosomal and sex chromosome morphologies in the karyotype of *M. a. trapezius* determined by this study and also those of previously presented one by Şekeroğlu et al. [17] were nearly the same as those of European populations of *M. avellanarius* except for the karyotype introduced by Doğramacı and Kefelioğlu [18] [4, 5]. In this context, it is necessary to open a separate parenthesis to the study of Peshev and Delov [15]. The researchers stated in their study that *M. a. avellanarius* had a value of NFa = 88. However, it is clearly seen in the presented idiogram and the text of the study that the smallest autosomal chromosome pair is acrocentric. We think that this (NFa = 88) may have arisen from a printing error. Therefore, this species should have an NFa of 86 instead of 88. Considering that, the NFa = 88 value is only seen in the populations of *M. avellanarius* from Turkey.

The karyotype of *M. a. abanticus* from Abant-Bolu was described for the first time by the current study and it was detected that the karyotype had 2n = 46, NF = 92 and NFA = 88 values. Obtained karyotype was substantially compatible with the karyotype of Doğramacı and Kefelioğlu [18] except to not include a secondary constriction. This karyotype was different from the karyotype of *M. a. trapezius* in two ways. The first was that the detected karyotype of *M. a.*

abanticus did not include a secondary constriction. The second was that the smallest chromosome in the autosomal set was metacentric instead of acrocentric. By using silver-nitrate staining, the nucleolar organizer region was localized in the secondary constrictions in autosomal pair no. 20 and 22. All observed NORs were heteromorphic and occurred in differ homologues (Fig. 2).

Although the conventional karyotype of *M. roachi* from Thrace was known, however, no information about the banded karyotype of this species has been imparted so far. This deficiency has been tried to be compensated to a certain extent by this study presenting the G-banded karyotype. The results related to autosomal chromosomal set complied with those of Civitelli et al. [19]. Unlike this study, Y chromosome in the sample from the same locality was identified as metacentric rather than acrocentric.

That the karyotype of *D. nitedula* from various parts of Turkey (both from Thrace and Anatolia) had a steady karyotype value of 2n = 48 FN = 96 and NFa = 92 consistent with the results of previous studies were determined. The autosomal complement was entirely composed of the variable numbers of large and small, bi-armed chromosomes in the form of meta-, submeta- or partly subtelocentric. In the karyotypes obtained by many previous studies, variations that were thought by us as not obvious in the shape and size of the chromosomes were found. Since it was thought that revealed chromosomal morphologies may have changed according to the researchers' perspective, no grouping attempts with respect to chromosome morphology were made in this study. Our results were found to be consistent with those of Doğramacı and Kefelioğlu [6], Şekeroğlu and Şekeroğlu [20], and Arslan et al. [7] including samples from Anatolia, and Mitsainas et al. [30] including the populations of *D. nitedula* from Greece. The karyotype introduced by the current study also comprised the secondary construction in the 21st chromosome pair, as it was detected by previous studies. Three *Dryomys* species, *D. laniger*, *D. nitedula* and *D. pictus* have been reported from Turkey until this time [2, 3]. From these species, *D. nitedula* populations in Turkish Thrace were mostly assigned to *D. n. wingei* [2]. Another subspecies of this species, *D. n. phrygius*, thought to be an endemic to Turkey, were firstly reported from western Anatolia [31], but so far, their taxonomic status has not been clarified in detail. Our results based on the sampling from both Thrace and Anatolia showed that there was no karyological difference between G- banded karyotypes of two subspecies.

Obtained karyotype having 2n = 62 diploid chromosome number in the two populations of *M. glis* by the current study was also previously determined in European and Asian populations [12-15, 19, 20, 21, 22, 30]. Some chromosomal differences in the karyotypes of this species have been found before, even if the karyotype structures were homogeneous on a large scale. For example, the presence of a pair of acrocentric chromosomes in the autosomal set has been reported

in Bulgarian populations [15]. However, a similar situation was not observed in the karyotypes presented by the current study; all the autosomal chromosomes were bi-armed, mostly congruent with the results of the previous studies. In addition, the secondary constriction in a small-sized pair has been frequently described in most examined populations of this species from Europe and Turkey [14, 20, 30]. Similar to them, the 17th autosomal pair appeared to carry a secondary constriction in the karyotype determined by the current study. Mitochondrial DNA sequence analyses revealed that there is an amazing genetic homogeneity within the distribution range of the populations of this species not only in Turkey, but also in the whole of Europe [32]. This may be considered to be an indicator that the İstanbul and Çanakkale straits, and the Marmara Sea, obstacles for the terrestrial connection between Europe and Asia continentals, are not an effective geographic barrier for the gene flow between the populations of the edible dormouse. However, it is clear that more evidence is required for the solution of such complex biogeographical events. The karyotype data reported here and supporting the aforesaid genetic homogeneity can be considered as evidence required for the explanation of the mentioned situation.

5. Conclusions

By the results of the current karyotype study on some representatives of Gliridae from Turkey, the G-, C-, and AgNOR banded karyotypes of *M. a. abanticus* from Abant (Bolu), and the G-banded karyotype of *M. roachi* from Thrace were presented for the first time. With the examination and comparison of the determined findings, it was demonstrated that the intraspecific variations can be easily revealed by the karyotype. Available karyological variations in the determined karyotypes should be considered to be the noteworthy steps for the populations' differentiation. Of course, a strong genetic difference at the subspecies level between *M. a. abanticus* and *M. a. trapezius* may not be mentioned at this stage. Therefore, obtained findings by current study and the results of further studies based on additional markers will allow a more accurate assessment. Additionally, those kinds of intraspecific variations should be taken into account as the major indicators the documenting of Turkey's biodiversity. On the other hand, the steady karyotypes that are compatible with the previous findings could indicate a genetic homogeneity for other species examined in the study.

Acknowledgement

This study was supported by The Scientific and Technological Research Council of Turkey (TUBITAK) [grant number: 113Z822].

References

[1] Corbet, G.B., The mammals of the Palearctic region: a taxonomic review. British Museum (Natural History), Cornell University Press, London and Ithaca, 1978.

[2] Wilson, D.E., Reeder, D.M., Mammal Species of the World: A Taxonomic and Geographic Reference. 3rd ed. The Johns Hopkins University Press, Baltimore, 2005.

[3] Kryštufek, B., Vohralík, V., Mammals of Turkey and Cyprus. Rodentia I: Sciuridae, Dipodidae, Gliridae, Arvicolinae. Založba Annales, Koper, 2005.

[4] Arslan, A., Zima, J., *Karyotypes of the mammals of Turkey and neighbouring regions: a review*, Folia Zoologica, 63(1), 1–62, 2014.

[5] Zima, J, Macholán, M., Filippucci, M. G., *Chromosomal variation and systematics of glirids*, Hystrix, 6, 73–86, 1995.

[6] Doğramacı, S., Kefelioğlu H., *The karyotype of Dryomys nitedula (Mammalia: Rodentia) from Turkey*, Turkish Journal of Zoology, 14, 316-328, 1990.

[7] Arslan, A., Kankılıç, T., Yorulmaz, T., Kankılıç, T., Zima, J., *Comparison of the chromosome banding patterns in Dryomys laniger and D. nitedula from Turkey*, Turkish Journal of Zoology, 40(3), 363-368, 2016.

[8] Kıvanç, E., *Die Haselmus, Muscardinus avellanarius L., in der Türkei*, Bonner Zoologische Beiträge, 34(4), 419–428, 1983.

[9] Doğramacı, S., *Türkiye Memeli Faunası*, Ondokuz Mayıs Üniversitesi Fen Dergisi, 1(3), 107–136, 1989.

[10] Savic, I., Soldatovic, B., *On the karyotype of Muscardinus avellanarius Linnaeus, 1758 (Rodentia, Gliridae),* Arhiv Bioloških Nauka, 24, 7-8, 1972.

[11] Zima, J., Kral, B., *Karyotypes of European mammals*, II. Acta Scientiarum Naturilium, Academiae Scientarum Bohemoslovacae, 18, 1–62, 1984.

[12] Zima, J., *Karyotypes of certain rodents from Czechoslovakia (Sciuridae, Gliridae, Cricetidae)*, Folia Zoologica, 36(4), 337–343, 1987.

[13] Belcheva, R.G., Topashka-Ancheva, M.N., Atanossov, N.I., *Karyological studies of five species of mammals from Bulgaria's fauna*, Comptes Rendus de I'Academie Bulgare des Sciences, 42, 125–138, 1988.

[14] Graphodatsky, A.S., Fokin, I.M., *Comparative cytogenetics of Gliridae (Rodentia)*, Zoologicheskii Zhurnal, 72(11), 104-113, 1993.

[15] Peshev, D., Delov, V., *Chromosome study of three species of dormice from Bulgaria*, Hystrix, 6(1-2), 151–153, 1995.

[16] Zima, J., Macholan, M., Filippucci, M.G., *Chromosomal variation and systematics of Myoxids*, Hystrix, 6(1-2), 63–76, 1995.

[17] Şekeroğlu, V., Kefelioğlu, H, Şekeroğlu, Z.A., *G- and C-banded karyotype of hazel dormouse, Muscardinus avellanarius trapezius (Mammalia: Rodentia) in Turkey*, Turkish Journal of Zoology, 35, 375–379, 2011.

[18] Doğramacı, S., Kefelioğlu, H., *Türkiye Muscardinus avellanarius (Mammalia: Rodentia) türünün karyotipi*, Doğa-Turkish Journal of Zoology, 16, 43–49, 1992.

[19] Civitelli, M.V., Filippucci, M.G., Kurtonur, C., Özkan, B., *Chromosome analysis of three species of Myoxidae*, Hystrix, 6, 117–126, 1995.

[20] Şekeroğlu, V., Şekeroğlu, Z.A., *A chromosomal study of two dormouse species from Turkey*, Hystrix 22, 301–309, 2011.

[21] Doğramacı, S., Tez, C., *Geographic variations and karyological characteristics of the species Glis glis (Mammalia: Rodentia) in Turkey*, Turkish Journal of Zoology, 18, 167–170, 1991.

[22] Arslan, A., Zima, J., Yorulmaz, T., Gözütok, S., Toyran, K., *Chromosome banding pattern in fat dormouse and bank vole (Mammalia: Rodentia) from Turkey*, Folia Biologica, 61, 47–51, 2013.

[23] Ford, C.E., Hamerton, J.L., *'A colchicine-hypotoniccitrate' squash sequence for mammalian chromosomes*, Stain Technology, 31, 247–251, 1956.

[24] Seabright, M., *A rapid technique for human chromosomes*, Lancet, 2, 971–972, 1971.

[25] Sumner, A.T., *A simple technique for demonstrating centromeric heterochromatin*, Experimental Cell Research, 75, 304-306, 1972.

[26] Howell, W.M., Black, D.A., *Controlled silver staining of nucleolus organizer regions with a protective colloidal developer: a 1-step method*, Experientia, 36, 1014–1015, 1980.

[27] Levan, A., Fredga, K., Sandberg, A.A., *Nomenclature for centromeric position on chromosomes*, Hereditas, 52, 201–220, 1964.

[28] Şeker, P.S, Arslan A., Selvi, E., Kankılıç, T., Zima J., *Variation in the Conventional and Banded Karyotypes among Populations of Arvicola amphibius (L., 1758) (Mammalia: Rodentia) from Turkey*, Acta Zoologica Bulgarica, 70(1), 19–30, 2018.

[29] Kankılıç, T., Arslan, A., Şeker, P.S., Kankılıç, T., Toyran, K., Zima, J., *A new chromosomal race (2n =44) of Nannospalax xanthodon from Turkey (Mammalia: Rodentia)*, Zoology in the Middle East, 63(3), 181–188, 2017.

[30] Mitsainas, G.P., Rovatsos, M.T., Karamariti, I., Giagia-Athanasopoulou, E.B., *Chromosomal studies on Greek populations of four small rodent species*, Folia Zoologica, 57(4), 337–346, 2008.

[31] Çağlar, M., *Dryomys nitedula phrygius'un Anadolu'da yeni tespit edilen yaşama yerleri*, İstanbul Üniversitesi Fen Fakültesi Mecmuası, 27, 16–18, 1962.

[32] Helvacı, Z., Renaud, S., Ledevin, R., Adriaens, D., Michaux, J., Çolak, R., Kankılıç, T., Kandemir, İ., Yiğit, N., Çolak, E., *Morphometric and genetic structure of the edible dormouse* (*Glis glis): a consequence of forest fragmentation in Turkey*, Biological Journal of the Linnean Society, 107, 611–623, 2012.

Adıyaman University Journal of Science
https://dergipark.org.tr/en/pub/adyujsci
DergiPark AKADEMİK
ISSN 2147-1630
e-ISSN 2146-586X

Evaluating Effects of Black Carrot Extract on Testicular Carboxylesterase Activity and Oxidative Stress Parameters in Rats Exposed to Bisphenol A

Ahmet ÖZKAYA[1], Zafer ŞAHİN[2,*], Yunus ŞAHİN[1], Özgür BULMUŞ[3], Miraç UÇKUN[4], Ertan YOLOĞLU[5]

[1]Adiyaman University, Faculty of Science and Art, Department of Chemistry, Adıyaman, Turkey
aozkaya@adiyaman.edu.tr, ORCID ID: 0000-0002-0173-3084; ynsshn49@gmail.com, ORCID ID: 0000-0003-3185-5282
[2]Karadeniz Technical University, Faculty of Medicine, Department of Physiology, Trabzon, Turkey
zafersahin55@yahoo.com, ORCID ID: 0000-0001-7982-7155
[3]Balikesir University, Faculty of Health Sciences, Department of Physical Therapy and Rehabilitation, Balıkesir, Turkey
obulmus@yahoo.com, ORCID ID:0000-0001-7736-402X
[4]Adiyaman University, Faculty of Engineering, Department of Food Engineering, Adıyaman, Turkey
miracuckun@gmail.com, ORCID ID: 0000-0002-9018-8515
[5]Adiyaman University, Faculty of Education, Department of Science Education, Adıyaman, Turkey
ertanyologlu82@gmail.com, ORCID: 0000-0002-9730-9471

Received: 20.09.2020 **Accepted:** 20.04.2021 **Published:** 30.06.2021

Abstract

We aimed to evaluate the effects of black carrot extract on testicular carboxylesterase (Ces) activity, malondialdehyde (MDA), glutathione S-transferases (GST) and reduced glutathione (GSH) in male rats exposed to bisphenol A (BPA). Adult Wistar albino male rats were divided into 4 groups as follows (n = 7/group): control, BPA, black carrot and BPA+Black carrot. Testicular Ces, MDA, GST and reduced GSH were analyzed by using a spectrophotometer system. Testicular Ces activity was significantly lower only in the BPA group than the control group ($p < 0.001$). Testicular MDA concentrations were higher only in the BPA group compared with the control group ($p < 0.001$). Reduced GSH level was higher in the black carrot and BPA+Black carrot groups than the control group ($p < 0.05$). GST activity was lower in the BPA

* Corresponding Author DOI: 10.37094/adyujsci.782874

group in comparison to the control group ($p < 0.05$). In the black carrot and BPA+Black carrot groups, the GST activities were higher than the control group ($p < 0.001$). Our results showed BPA suppresses testicular detoxification activity and increases lipid peroxidation in rats. We observed that black carrot extract has a beneficial effect on the toxic and oxidative stress-related parameters caused by BPA exposure.

***Keywords**:* Bisphenol A; Black carrot; Testis; Carboxylesterase; Oxidative stress; Rat.

Bisfenol A'ya Maruz Kalan Sıçanlarda Siyah Havuç Ekstresinin Testis Karboksilesteraz Aktivitesi ve Oksidatif Stres Parametreleri Üzerindeki Etkilerinin Değerlendirilmesi

Öz

Bu çalışmada Bisfenol A'ya (BPA) maruz kalan erkek sıçanlarda siyah havuç ekstraktının testiküler karboksilesteraz (Ces) aktivitesi, malondialdehit (MDA) düzeyi, indirgenmiş glutatyon (GSH) ve glutatyon S-transferaz (GST) aktiviteleri üzerine etkilerini değerlendirmeyi amaçladık. Yetişkin erkek Wistar albino sıçanlar kontrol, BPA, siyah havuç ve BPA+Siyah havuç olmak üzere 4 gruba ayrıldı ($n = 7$/grup). Testis dokusunda Ces, MDA, indirgenmiş GSH ve GST düzeyleri mikroplaka okuyucu spektrofotometre sistemi kullanılarak analiz edildi. Testis Ces aktivitesi sadece BPA grubunda kontrol grubuna kıyasla önemli düzeyde daha düşüktü ($p < 0.001$). Testis MDA konsantrasyonu sadece BPA grubunda kontrol grubuna kıyasla daha yüksekti ($p < 0.001$). İndirgenmiş GSH düzeyi siyah havuç ve BPA+Siyah havuç gruplarında kontrol grubuna kıyasla daha yüksekti ($p < 0.05$). GST aktivitesi BPA grubunda kontrol grubuna göre daha düşüktü ($p < 0.05$). Siyah havuç ve BPA + Siyah havuç gruplarında GST aktiviteleri kontrol grubuna kıyasla daha yüksekti ($p <0.001$). Sonuçlarımız, BPA'nın sıçan testis dokusunda detoksifikasyon aktivitesini baskıladığını ve lipit peroksidasyonunu arttırdığını gösterdi. Siyah havuç ekstraktının, BPA maruziyetinin neden olduğu toksik ve oksidatif stresle ilişkili parametreler üzerinde yaralı bir etkiye sahip olduğunu gözlemledik.

***Anahtar Kelimeler**:* Bisfenol A; Siyah havuç; Testis; Karboksilesteraz; Oksidatif stres; Sıçan.

1. Introduction

Fruits and vegetables are foods that have invaluable beneficial effects on both nutrition and health with their vitamins, minerals and other natural biological components. These food sources can be consumed as processed products, such as juices, canned foods or jams, and naturally unprocessed products. It has been understood that consuming them as natural as possible, especially unprocessed, is important for their health benefits to emerge as expected. *Carrot or*

Daucus carota is a member of the *Apiaceae* family (also called as *Umbelliferae*). This biennial vegetable can be classified into two groups as the carotene (*Daucus carota ssp. sativus*) and the anthocyanin (*Daucus carota subsp. sativus var. atrorubens*) groups [1]. Although the carotene group is grown in many countries across the world, the anthocyanin group, also known as black carrots, is grown in especially in Turkey, Egypt, Afghanistan and India [2]. Black carrots have a bluish-purple color due to their high anthocyanin levels and may be used as natural food coloring. Moreover, black carrot extracts offer an important alternative to synthetic colorants being a less toxic, more pH- and heat-stable food colorant [3]. Fresh black carrots have high anthocyanin content, which may be about 1750 mg/kg [4]. Additionally, acylated cyanidin-based anthocyanins in the content of black carrot are reported to be mainly cyanidin 3-feruloyl-xylosyl-glucosyl-galactoside (13.5%) and cyanidin 3-synapoyl-xylosyl-glucosyl-galactoside (27.5%) [3, 4]. Anthocyanin derivatives in black carrots have been suggested to have antioxidant activity [5, 6]. In some studies, carrot seed extract has been reported to contribute to reducing reproductive toxicity caused by toxic agents [7, 8].

Bisphenol A (BPA), a xenoestrogen and toxic agent, is the building block in the manufacture of several polycarbonate plastic products such as water tubes, drinking containers, toys and epoxy resins papers [9]. Important sources of BPA exposure in the human population are oral, through inhalation and transdermal [10]. In humans, there is a relationship between BPA levels in the body and health problems. BPA has been defined as a causative agent for various metabolic disorders such as hepatic dysfunction, cancer, type 2 diabetes and infertility [11]. Although scientific data from animal models show the adverse effects of BPA on reproductive function, there is an increasing literature investigating the destructive effects of it on the male reproductive system, but offering heterogeneous and sometimes contradictory findings between the animals and humans [12]. These reports indicate that BPA has complex toxic effects on the reproductive system. One of the negative effects of BPA on the reproductive system, it causes oxidative stress in the testicles and epididymis by stimulating lipid peroxidation and inhibiting antioxidant enzymes [13]. Despite the relatively low oxygen capacity compared to organs such as the brain, which characterize the testicular microenvironment, testes remain vulnerable to the oxidative stress due to high levels of unsaturated fatty acids (especially 20:4 and 22:6) and presence of potentially reactive oxygen species (ROS) [14]. High ROS production in the testes has been reported to cause important changes in the testicular physiological functions that may lead to infertility [15]. The interaction of BPA as a xenoestrogen and toxic agent with carboxylesterase (Ces), a xenobiotic metabolizing enzyme [16], may also play a role in the pathophysiological process associated with reproductive dysfunction. It is suggested that, based on a well-known role of Ces in the detoxification of chemicals and environmental pollutants, it is

possible that Ces in the male genital system may exhibit a similar physiological function capable of modulating dysfunction in the reproductive system against xenobiotic effects [17]. To the best of our knowledge, there has been no report on the effects of black carrot on testicular Ces activity. Therefore, in our study, it was aimed to determine the effects of black carrot on testis Ces activity, as well as malondialdehyde (MDA), glutathione S-transferases (GST) and reduced glutathione (GSH) levels in male rats exposed to BPA.

2. Materials and Methods

2.1. Animal models and experimental protocol

Adult male Wistar albino rats (230 ± 20 g) were obtained from the Experimental Research Center of Fırat University (FUDAM, Elazig, Turkey). The rats were housed under standard light-dark schedule (12h light: 12 h darkness from 19:00), at a standard humidity (55 ± 5%) and constant temperature (21 ± 1 °C). They were fed with ad libitum standard rat diet and fresh tap water. The approval for the experimental protocol was given by the Animal Experiments Local Ethics Committee of Fırat University (Protocol no: 2017/111). National and international laws and policies on experimental animals were cared.

The rats were divided into four groups as Control, BPA, Black carrot and BPA + Black carrot (n=7 for each group). The black carrots, which were thoroughly washed and cleaned, were passed through a juicer. BPA (20 μg/kg) and black carrot juice (4ml/kg) were administered orally to the rats via an orogastric gavage throughout 60 days with 1-day intervals [18, 19]. Black carrot juice was prepared fresh before each application. The rats were sacrificed at the end of 60 days. The testes were dissected from the animals.

2.2. Chemicals

BPA, potassium phosphate buffer (PPB), p-nitrophenyl acetate (PNPA), 1-chloro-2,4-dinitrobenzene (CDNB), 5,5′-dithio-bis (2-nitrobenzoic acid (DTNB), bovine serum albumin (BSA) and Bradford reagent were obtained from Sigma (Dorset, UK) unless otherwise stated.

2.3. Tissue homogenization

According to our previous method [20], homogenization of the testicular tissue was performed using a homogenizer (Heidolph RZ 2021, Germany) in a cooled homogenization buffer (pH 7.4 in 0.1 M PPB; 1mM DTT, 0.15M KCl, 1mM EDTA,). After homogenization, the homogenates were transferred into Eppendorf tubes and centrifuged at 16,000 g for 20 minutes at 4 °C (Sigma 2-16K, St. Louis, Missouri). Following this process, the supernatant fraction was removed, and analyzes were performed on these samples.

2.4. Total protein analyses

The total protein level in the supernatant samples was measured using a previously described method [21]. Briefly, 250 μL of Bradford reagent and 5 μL of diluted supernatant (1/4) were added into each microplate wells. After 15-minutes incubation period, absorbance was recorded at 595 nm.

2.5. Determination of testicular total Ces activity

A spectrophotometric method [22] adapted to the microplate reader spectrophotometer system (ThermoTM Varioskan Flash - Thermo Fisher Scientific, Vantaa, Finland) was used to measure the total Ces activity. In the activity analysis, PNPA was prepared in 26 mM ethanol (96%), and this prepared solution was used as substrate. Alterations in absorbance were recorded at 405 nm for 2 minutes at 25 °C.

2.6. MDA, reduced GSH and GST analyses

The testis MDA levels were determined based on relative production of reactive substances of the thiobarbituric acid [23]. The reduced GSH activity was measured by the substance's reaction with DTNB at 412 nm [24].

For determining GST activity, firstly, 20 mM of CDNB was prepared in ethanol (96%), and this chemical was used as substrate solution. 0.002 M reductive GSH solution was used as cofactor in the reaction [25]. 100 µL of the GSH mixture + 10 µL of the supernatant + 100 µL of the PBS (pH 6.5 and 0.1 M) and finally 10 µL of CDNB were transferred into microplate wells. In the following process, change in absorbance was monitored at 344 nm for 2 minutes at 25 °C.

2.7. Statistical analysis

The comparison of the groups was performed using one-way analysis of variance (ANOVA) followed by Tukey test. Statistical significance was accepted as $p < 0.05$.

3. Results

Figure 1 shows the results on the testicular tissue Ces activity. The testicular Ces activity was significantly lower only in the BPA group (812 ± 75 nmol/min/mg protein) than the control group (1430 ± 32 nmol/min/mg protein, $p < 0.001$). There was no significant difference in the Ces activity between the control group and the Black carrot (1661 ± 75 nmol/min/mg protein) and BPA+Black carrot (1573 ± 91 nmol/min/mg protein) groups. Moreover, there was a significant difference in the Ces activity between the BPA group and the BPA+Black carrot group ($p <0.001$).

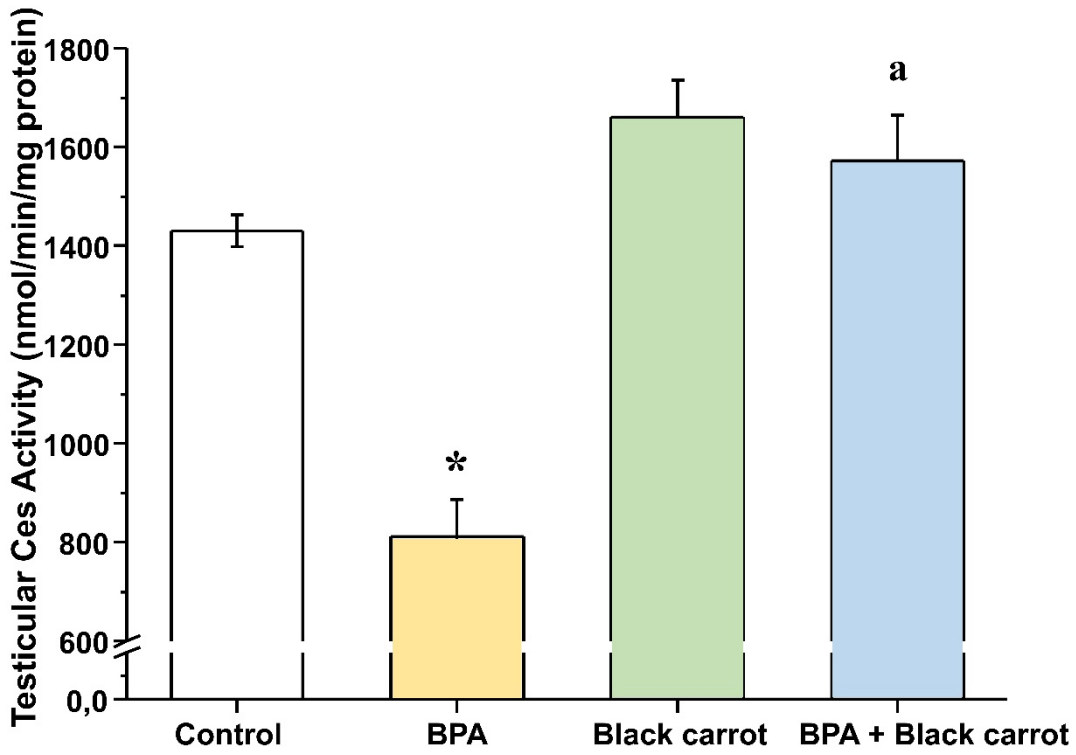

Figure 1: Results of testicular Ces activities for all groups. The data represent mean± SEM. *: $p < 0.001$ compared with the control group, a: $p < 0.001$ compared with the BPA group ($n = 7$ for each group). Ces: Carboxylesterase

Figure 2 shows the results on the testicular tissue MDA level. The MDA concentrations in the testes were higher in the BPA group (605±15 pmol/mg protein) in comparison to the control group (294±12 pmol/mg protein, $p < 0.001$). In the Black carrot (243±38 pmol/mg protein) and BPA+Black carrot (233±45 pmol/mg protein) groups, the MDA concentrations were at the same level as the control group value. Moreover, there was a significant difference in the MDA concentration between the BPA group and the BPA+Black carrot group ($p < 0.001$).

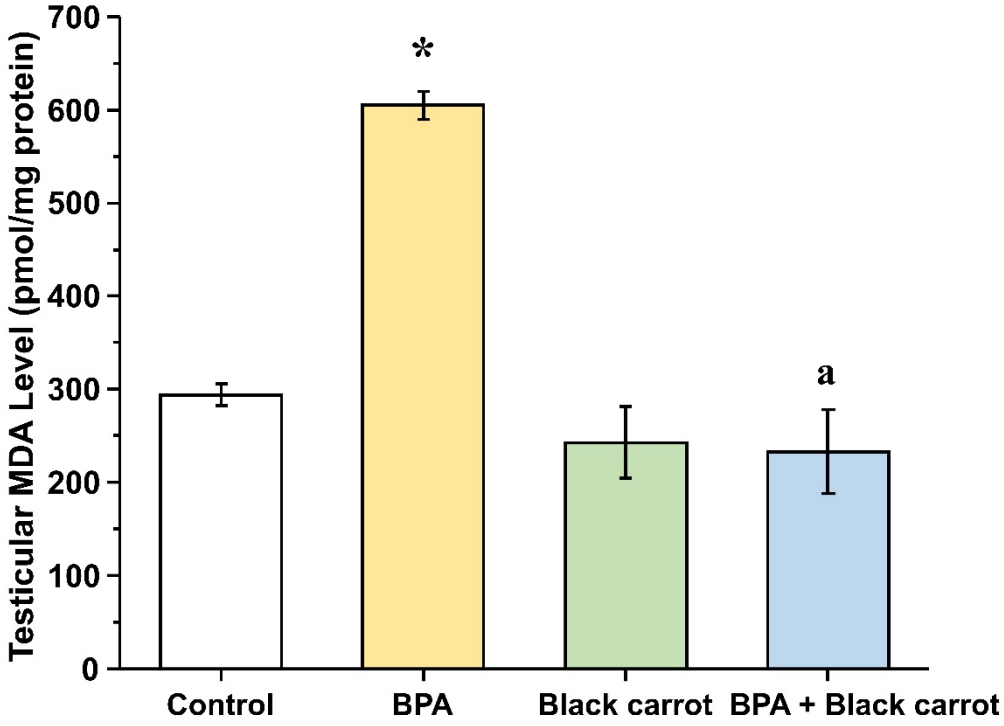

Figure 2: Results of testicular MDA levels for all groups. The data represent mean± SEM. *: $p < 0.001$ compared with the control group, a: $p < 0.001$ compared with the BPA group (n=7 for each group). MDA: Malondialdehyde.

Figure 3 shows the results on the testicular tissue reduced GSH level. The reduced GSH level was higher in the Black carrot (93±4 nmol/mg protein) and BPA+Black carrot (95±5 nmol/mg protein) groups than the control group (67±3 nmol/mg protein, $p<0.05$). In the BPA group (73±4 nmol/mg protein), reduced GSH level did not differ than the control group. However, there was a significant difference in the GSH level between the BPA group and the BPA+Black carrot group ($p < 0.05$).

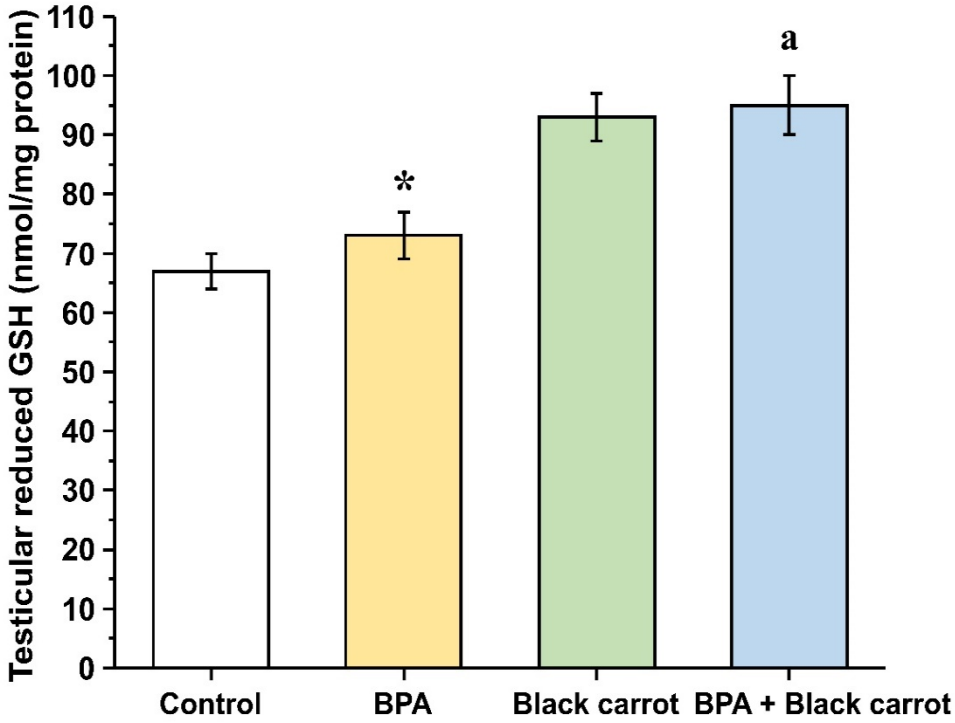

Figure 3: Results of testicular reduced GSH levels for all groups. The data represent mean± SEM. *****: $p < 0.05$ compared with the control group, a: $p < 0.05$ compared with the BPA group (n=7 for each group). GSH: Reduced Glutathione

Figure 4 shows the results on the testicular tissue GST activity. The GST activity was lower in the BPA group (56±3 nmol/min/mg protein) in comparison to the control group (68±3 nmol/min/mg protein, $p < 0.05$). In the Black carrot (88±7 nmol/min/mg protein) and BPA+Black carrot (83±3 nmol/min/mg protein) groups, the GST activities were higher than the control group ($p<0.001$). Moreover, there was a significant difference in the GST activity between the BPA group and the BPA+Black carrot group ($p<0.001$).

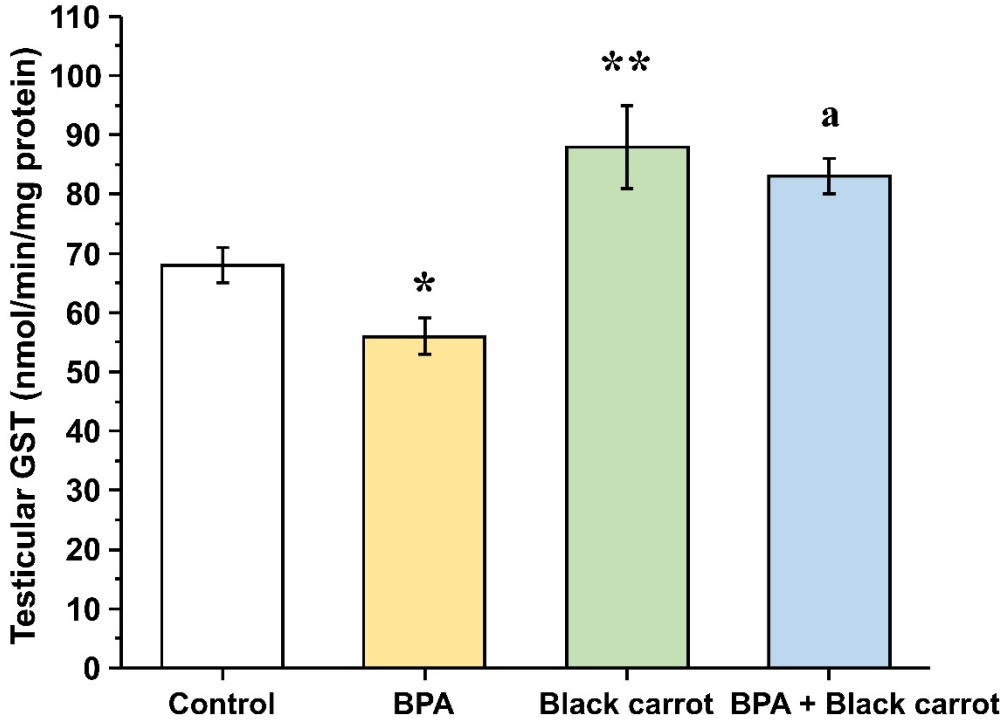

Figure 4: Results of testicular GST activities for all groups. The data represent mean± SEM. *: $p < 0.05$, **: $p < 0.001$ compared with the control group, a: $p < 0.001$ compared with the BPA group ($n = 7$ for each group). GST: Glutathione S-transferases

4. Discussion

This study was based on determination of the effects of black carrot extract on testicular Ces activity, as well as testicular MDA, reduced GSH and GST levels in male rats exposed to BPA. We determined that the testicular Ces activity was significantly lower only in the BPA group in comparison to the control group. The Ces activity of the Black carrot and BPA+Black carrot groups was not significantly different from control group. This result showed that BPA negatively affects Ces activity, a family of the detoxification enzymes, in the testes. These enzymes are a multigene family of serine-dependent enzymes which are localized in the endoplasmic reticulum of cells in the body. Ces enzymes play an substantial role in the metabolism of foreign substrates and endogenous lipids including environmental toxins and drugs [26, 27]. Therefore, a wide range of xenobiotics, drugs and chemicals is determined to alter the activity of Ces enzymes [26]. Comparative assessment of sex-dependent protein expression in the male reproductive tissue of humans and animals has revealed Ces expression in the male reproductive tract. However, very little is known about the functional significance of Ces activity in the male reproductive system. The Ces enzyme family is expressed mainly in the liver and other organs such as the kidney, heart, intestines, lungs, brain and testes [28]. A study reported that, with Ces5a-knockdown, a new Ces gene, male animals exhibited a reduction in fertility [29].

In rats, molinate is an herbicide used on rice, and this chemical covalently reacts with rat Hydrolase A (orthologue of human CES1) in a highly specific manner. This modification causes to remarkably reduced Ces activity in rat liver and testicular tissue in the case that Leydig cells could inhibit mobilization of cholesterol esters required for testosterone synthesis [30]. In the testes, the functional role of Ces is thought to be involved in testosterone biosynthesis and protecting testicular cells from the action of harmful and toxic agents. In rodents, typical "testicular tissue-specific" toxic substances, such as ethane dimethane sulfonate (alkylating antitumor agent) [31], tri-o-cresyl phosphate (plasticizer) [32], inhibit the testicular Ces activity and expression and significantly reduce testosterone levels and testicular functions. BPA has been reported to inhibit xenobiotic metabolizing enzymes and thereby Ces expression in the liver and alter the epigenetic regulation of genes encoding these enzymes [16]. Based on our results regarding Ces, we may state that BPA exposure affects the testicular tissue detoxification process, and black carrot extract modulates the BPA-related toxic effects because the activity of Ces in the BPA + black carrot group was at the same level as the control value.

Growing evidence draws attention to specific flavonoids from phytochemicals present in vegetables and fruits that have beneficial effects on the body [33]. It has been suggested that higher consumption habits of fruit / vegetable-based flavonoids are associated with a lower risk of metabolic and cardiovascular diseases in both gender [34, 35]. Anthocyanins as a group of colorful flavonoids are important biological components that are used as a natural dye sources in the food industry [36]. Pretreatment of rats exposed to cadmium with Hibiscus sabdarrifa L. anthocyanins has been reported to significantly normalize reproductive hormones, especially testosterone levels [37]. Studies on carrot seed extract have been reported to contribute to reducing reproductive problems such as low testosterone caused by toxic agents. In a study on the topic, carrot seed extract was reported to have a beneficial effect profile on decreased spermatogenesis and testosterone level by gentamicin administration [7]. In another study, it was stated that the ethanolic extract of *Daucus carota L.* seeds restores the acetaminophen-induced antiandrogenic effect in male rats and will be useful for drug research for treatment of androgen-related deficiencies due to this important effect [8].

Anthocyanin-rich extracts from fruits and vegetables, as well as purified anthocyanins, reduce lipid peroxidation and increase the body's antioxidant capacity [38]. Cyanidin-based anthocyanin pigments in the black carrots are known to have powerful antioxidant properties [5,6]. In our experiment, we determined that the testicular MDA concentration was higher only in the BPA group. Moreover, the GST activity was lower in the BPA group, but it was higher the black carrot group and the BPA+Black carrot group than the control group. Regarding the GSH levels, we showed that it was higher in the black carrot and the BPA+Black carrot groups in

comparison to the control group. The increased MDA level in the BPA group is an important indicator of oxidative stress. Moreover, GST is an enzyme that has both a detoxifying and antioxidant effect [39]. Therefore, a reduction in the GST activity of the BPA group indicated that this substance reduces the detoxification and antioxidant defense of the testes as both a toxic and oxidant agent. The MDA levels were the same as the control group value in both the black carrot and the BPA+Black carrot groups. There were also significant increases in the GST activity and GSH level of these groups. These results showed that BPA-induced oxidative stress can be reduced by the antioxidant effect of anthocyanins in black carrot extract. It was reported that anthocyanins have a much stronger antioxidant ability than α-tocopherol, vitamin C and some other antioxidants [40, 41]. No negative effects of anthocyanins up to 640 mg/day have been reported in humans [38]. A wide dose range in consumption of fruit or vegetable juices containing anthocyanins may be associated with a low potential for side effects. Additionally, it seems possible that pharmacological compounds to be obtained from such plants may be used in a wide dose range. This feature enriches drug development alternatives from substances in the composition of the black carrot.

5. Conclusions

To the best of our knowledge, this study is the first report to investigate the effects of black carrot extract on changes in testicular Ces activity and lipid peroxidation due to BPA exposure. Based on the results of this study, the Ces and GST activities in the testes decreased, and the MDA level increased as a result of BPA exposure. This indicates that BPA suppresses testicular detoxification activity and increases lipid peroxidation in male rats. We observed that black carrot extract has a curative effect on the toxic and oxidative stress-related parameters caused by BPA exposure. This indicates that black carrot extract may be beneficial in reducing BPA-related negative effects, alone or as a supportive treatment. It may also be stated that the active ingredients in black carrots have a significant potential for use as pharmacological compounds.

References

[1] Pistrick, K., Mansfeld's Encyclopedia of Agricultural and Horticultural Crops. 1st ed, 2001.

[2] Erten, H., Tanguler, H., Canbaş, A., *A traditional Turkish lactic acid fermented beverage: shalgam (salgam)*, Food Reviews International, 24(3), 352–359, 2008.

[3] Montilla, E.C., Arzaba, M.R., Hillebrand, S. et al., *Anthocyanin composition of black carrot (daucus carota ssp sativus var atrorubens alef) cultivars Antonina,* Beta Sweet, Deep Purple, and Purple Haze, Journal of Agricultural and Food Chemistry, 59(7), 3385–3390, 2011.

[4] Kırca, A., Özkan, M., Cemeroglu, B., *Stability of black carrot anthocyanins in various fruit juices and nectars*, Food Chemistry, 97(4), 598–605, 2006.

[5] Kaur, A., Singh Sogi, D., *Influence of development stages on the physicochemical properties of black carrots (Daucus carota L)*, Cogent Food & Agriculture, 6(1), 1841358, 2020.

[6] Yildiz, E., Guldas, M., Gurbuz, O., *Determination of in-vitro phenolics, antioxidant capacity and bio-accessibility of Kombucha tea produced from black carrot varieties grown in Turkey*, Food Science and Technology, 2020.

[7] Nouri, M., Khaki, A., Azar, F.F. et al., *The protective effects of carrot seed extract on spermatogenesis and cauda epididymal sperm reserves in gentamicin treated rats*, Yakhteh, 11(3), 327–333, 2009.

[8] Yakubu, M.T., Opakunle, F.K., Salimon, S.S., *Effects of the ethanolic extract of Daucus carota L seeds on acetaminophen-induced uremia and antiandrogenicity in male rats*, Tropical Journal of Health Sciences, 24(3), 33–40, 2017.

[9] Goodson, A., Robin, H., Summerfield, W. et al., *Migration of bisphenol A from can coatings—effects of damage, storage conditions and heating*, Food Additives and Contaminants, 21(10), 1015–1026, 2004.

[10] Geens, T., Aerts, D., Berthot, C. et al., *A review of dietary and non-dietary exposure to bisphenol-A*, Food and Chemical Toxicology, 50(10), 3725–3740, 2012.

[11] vom Saal, F.S., Akingbemi, B.T., Belcher, S.M. et al., *Chapel Hill bisphenol A expert panel consensus statement: Integration of mechanisms, effects in animals and potential to impact human health at current levels of exposure*, Reproductive Toxicology, 24(2), 131–138, 2007.

[12] Cariati, F., D'Uonno, N., Borrillo, F. et al., *Bisphenol A: an emerging threat to male fertility*, Reproductive Biology and Endocrinology, 17(1), 6, 2019.

[13] Manfo, F.P.T., Jubendradass, R., Nantia, E.A. et al., *Adverse effects of bisphenol A on male reproductive function*, Reviews of environmental contamination and toxicology, 228, 57–82, 2014.

[14] Aitken, R.J., Roman, S.D., *Antioxidant systems and oxidative stress in the testes,* Oxidative Medicine and Cellular Longevity, 1(1), 15–24, 2008.

[15] Doreswamy, K., Muralidhara, *Genotoxic consequences associated with oxidative damage in testis of mice subjected to iron intoxication*, Toxicology, 206(1), 169–178, 2005.

[16] Nahar, M.S., Kim, J.H., Sartor, M.A. et al., *Bisphenol A-associated alterations in the expression and epigenetic regulation of genes encoding xenobiotic metabolizing enzymes in human fetal liver*, Environmental and Molecular Mutagenesis, 55(3), 184–195, 2014.

[17] Mikhailov, A.T., Torrado, M., *Carboxylesterase overexpression in the male reproductive tract: a universal safeguarding mechanism*, Reproduction, Fertility and Development, 11(3), 133, 1999.

[18] Balasubramaniam, P., Pari, L., Menon, V.P., *Protective effect of carrot (daucus carota L) against lindane - induced hepatotoxicity in rats*, Phytotherapy Research, 12(6), 434–436, 1998.

[19] Bindhumol, V., Chitra, K.C., Mathur, P.P., *Bisphenol A induces reactive oxygen species generation in the liver of male rats*, Toxicology, 188(2–3), 117–124, 2003.

[20] Ozkaya, A., Sahin, Z., Kuzu, M. et al., *Role of geraniol against lead acetate-mediated hepatic damage and their interaction with liver carboxylesterase activity in rats*, Archives of Physiology and Biochemistry, 124(1), 80–87, 2018.

[21] Bradford, M., *A rapid and sensitive method for the quantitation of microgram quantities of protein utilizing the principle of protein-dye binding*, Analytical Biochemistry, 72(1–2), 248–254, 1976.

[22] Nousiainen, U., Törrönen, R., *Differentiation of microsomal and cytosolic carboxylesterases in the rat liver by in vivo and in vitro inhibition*, General Pharmacology: The Vascular System, 15(3), 223–227, 1984.

[23] Placer, Z.A., Cushman, L.L., Johnson, B.C., *Estimation of product of lipid peroxidation (malonyl dialdehyde) in biochemical systems,* Analytical Biochemistry, 16(2), 359–364, 1966.

[24] Moron, M., Depierre, J., Mannervik, B., *Levels of glutathione, glutathione reductase and glutathione S-transferase activities in rat lung and liver*, Biochimica et Biophysica Acta (BBA) - General Subjects, 582(1), 67–78, 1979.

[25] Habig, W.H., Pabst, M.J., Jakoby, W.B., *Glutathione S-transferases the first enzymatic step in mercapturic acid formation*, The Journal of Biological Chemistry, 249(22), 7130–7139, 1974.

[26] Satoh, T., Hosokawa, M., *The mammalian carboxylesterases: from molecules to functions*, Annual Review of Pharmacology and Toxicology, 38(1), 257–288, 1998.

[27] Holmes, R.S., Wright, M.W., Laulederkind, S.J.F. et al., *Recommended nomenclature for five mammalian carboxylesterase gene families: human, mouse, and rat genes and proteins*, Mammalian Genome, 21(9–10), 427–441, 2010.

[28] Sanghani, S.P., Sanghani, P.C., Schiel, M.A. et al., *Human carboxylesterases: an update on CES1, CES2 and CES3*, Protein & Peptide Letters, 16(10), 1207–1214, 2009.

[29] Zhou, Y.-C., Zhang, Y.-L., Ru, Y.-F. et al., *An epididymis-specific carboxyl esterase CES5A is required for sperm capacitation and male fertility in the rat,* Asian Journal of Andrology, 17(2), 292, 2015.

[30] Jewell, W.T., Miller, M.G., *Identification of a carboxylesterase as the major protein bound by molinate*, Toxicology and Applied Pharmacology, 149(2), 226–234, 1998.

[31] Hess, R.A., *Effects of environmental toxicants on the efferent ducts, epididymis and fertility*, Journal of Reproduction and Fertility. Supplement, 53, 247–259, 1998.

[32] Chapin, R.E., Phelps, J.L., Somkuti, S.G. et al., *The interaction of Sertoli and Leydig cells in the testicular toxicity of tri-o-cresyl phosphate*, Toxicology and Applied Pharmacology, 104(3), 483–495, 1990.

[33] Jiang, X., Li, X., Zhu, C. et al., *The target cells of anthocyanins in metabolic syndrome*, Critical Reviews in Food Science and Nutrition, 59(6), 921–946, 2019.

[34] Cassidy, A., Mukamal, K.J., Liu, L. et al., *High anthocyanin intake is associated with a reduced risk of myocardial infarction in young and middle-aged women*, Circulation, 127(2), 188–196, 2013.

[35] Cassidy, A., Bertoia, M., Chiuve, S. et al., *Habitual intake of anthocyanins and flavanones and risk of cardiovascular disease in men*, The American Journal of Clinical Nutrition, 104(3), 587–594, 2016.

[36] Scotter, M.J., *Methods for the determination of European Union-permitted added natural colours in foods: a review*, Food Additives & Contaminants: Part A, 28(5), 527–596, 2011.

[37] Orororo, O.C., Asagba, S.O., Tonukari, N.J. et al., *Hibiscus Sabdarrifa L anthocyanins-induced changes in reproductive hormones of cadmium-exposed rats*, International Journal of Scientific and Research Publications (IJSRP), 8(4), 2018.

[38] Wallace, T., Slavin, M., Frankenfeld, C., *Systematic review of anthocyanins and markers of cardiovascular disease*, Nutrients, 8(1), 32, 2016.

[39] Gu, X., Zhang, N., Xie, Y. et al., *Metarhizium anisopliae CQMa128 regulates antioxidant/detoxification enzymes and exerts acaricidal activity against Psoroptes ovis var cuniculi in rabbits: A preliminary study*, Veterinary Parasitology, 279, 109059, 2020.

[40] Kong, J.-M., Chia, L.-S., Goh, N.-K. et al., *Analysis and biological activities of anthocyanins*, Phytochemistry, 64(5), 923–933, 2003.

[41] Leong, S.Y., Burritt, D.J., Hocquel, A. et al., *The relationship between the anthocyanin and vitamin C contents of red-fleshed sweet cherries and the ability of fruit digests to reduce hydrogen peroxide-induced oxidative stress in Caco-2 cells*, Food Chemistry, 227, 404–412, 2017.

Adıyaman University Journal of Science
https://dergipark.org.tr/en/pub/adyujsci
DergiPark AKADEMİK
ISSN 2147-1630
e-ISSN 2146-586X

On the Harmonic Evolute Surfaces of Hasimoto Surfaces

Kemal EREN[1,*], Alev KELLECİ AKBAY[2]

[1]*Sakarya University, Department of Mathematics, Sakarya, Turkey*
kemal.eren1@ogr.sakarya.edu.tr, ORCID: 0000-0001-5273-7897
[2]*Fırat University, Department of Mathematics, Elazığ, Turkey*
alevkelleci@hotmail.com, ORCID: 0000-0003-2528-2131

Received: 03.11.2020 **Accepted:** 30.04.2021 **Published:** 30.06.2021

Abstract

In this study, firstly by considering the evolution of a moving space curve, we give some related definitions and some new results about Hasimoto surfaces in Euclidean 3-spaces. Secondly, we examine harmonic evolute surfaces of Hasimoto surfaces in Euclidean 3-spaces and also, we give some geometric properties of these type surfaces. Moreover, we express the properties of parameter curves of harmonic evolute surfaces in Euclidean space. Finally, we give an explicit example of Hasimoto surface and its harmonic evolute surface and also we plot these surfaces.

Keywords: Hasimoto surfaces; Harmonic evolute surface; Binormal motion; Evolution of curves and surfaces; Gaussian curvature; Mean curvature.

Hasimoto Yüzeylerin Harmonik Evrim Yüzeyleri Üzerine

Öz

Bu çalısmada, ilk olarak hareketli bir uzay eğrisinin evrimini ele alarak, Öklid 3-uzaylarında Hasimoto yüzeyleri ile ilgili bazı tanımlar ve yeni sonuçlar verilmiştir. İkinci olarak, Öklid 3-uzaylarında Hasimoto yüzeylerinin harmonik evrim yüzeyleri incelenmiştir ve ayrıca bu tip yüzeylerin bazı geometrik özellikleri verilmiştir. Ayrıca, Öklid uzayındaki harmonik evrim

* Corresponding Author DOI: 10.37094/adyujsci.820698

yüzeylerinin parametre eğrilerinin özelliklerini ifade edilmiştir. Son olarak Hasimoto yüzeyinin ve harmonik evrimsel yüzeyinin açık bir örneği verilmiş ve ayrıca bu yüzeyler çizilmiştir.

Anahtar Kelimeler: Hasimoto yüzeyler; Harmonik evrim yüzeyler; Binormal hareketi; Eğri ve yüzeylerin evrimi; Gaussian eğrilik; Ortalama eğrilik.

1. Introduction

The harmonic evolute surface of a given surface r is defined as the geometric location of points that are as far away as the opposite of the mean curvature from the surface in the direction of the normal of the surface. The harmonic surface of a surface must be non-minimal in order to be obtained. Let $r = r(s,t)$ be a surface and also u, its normal and H denotes its non-zero mean curvature. Then, the harmonic evolute surface of $r = r(s,t)$ is given by parametrically

$$h(s,t) = r(s,t) + \frac{1}{H(s,t)} u(s,t),$$

see for more details, [1-3].

In recent years, the theory of surfaces with the connection of the motion of space curves and differential equations is a subject of research attention, [4, 5]. At the same time, the applications of this subject in differential geometry and physics have attracted attention. In 1971, Hasimoto examined the movement of a vortex filament, and then in 1972, Hasimoto showed that vortex filament (smoke ring) equation is equivalent non-linear Schrodinger equation [6, 7]. The relationship between the integrable equations and the theory of surfaces produces new types of surfaces. Hasimoto surfaces are one of these surfaces. Let $r = r(s,t)$ be the position vector of a moving curve on a surface in Euclidean 3-space and for all $t-$parameter, $r = r(s,t)$ be a unit speed curve. If this surface is a Hasimoto surface, then, the position vector $r = r(s,t)$ satisfies the following condition

$$r_t = r_s \wedge r_{ss}, \tag{1}$$

where t is the time parameter, s is arc-length parameter and the subscripts indicate the partial differential. This equation is said to be smoke ring equation or the vortex filament. The geometric properties of Hasimoto surfaces are investigated in detail by [8, 9]. Hashimoto surfaces have been produced according to the Bishop frame in Euclidean space, see [10]; and in Minkowski space, see [11]. Also, parallel surfaces of Hasimoto surfaces in Euclidean space are investigated at [12].

The aim of this study is to investigate the geometric properties the harmonic evolute surfaces of Hasimoto surfaces. Also, the characterization of the s and t parameter curves of the harmonic evolute surfaces of the Hasimoto surface is examined.

2. Geometric Preliminaries

In Euclidean 3-space, Euclidean inner product is given by $< x, y >= x_1y_1 + x_2y_2 + x_3y_3$ for two vectors $x = (x_1, x_2, x_3)$ and $y = (y_1, y_2, y_3)$ in E^3. The norm of a given vector $x \in E^3$ is defined as $\|x\| = \sqrt{< x, x >}$. Also, for an arbitrary curve r in E^3, if $\|r'(s)\| = 1$, then the curve r is called as a unit speed curve or parametrized by arc-length parameter s in Euclidean 3-space, E^3.

Now, we summarize basic concepts about the evolution of a moving space curve in Euclidean 3-space and so we give the intrinsic equations expressing with curvatures of it corresponding with moving Frenet frame $\{T, N, B\}$, [8]. Let r be a moving space curve described in parametric form by a position vector $r(s, t)$ in Euclidean 3-space, where s is the arc-length parameter and t is the time parameter. Thus, the moving Frenet frame $\{T, N, B\}$ of the curve with respect to s and t can be written in matrix form as follows:

$$\begin{bmatrix} T \\ N \\ B \end{bmatrix}_s = \begin{bmatrix} 0 & \kappa & 0 \\ -\kappa & 0 & \tau \\ 0 & -\tau & 0 \end{bmatrix} \begin{bmatrix} T \\ N \\ B \end{bmatrix} \text{ and } \begin{bmatrix} T \\ N \\ B \end{bmatrix}_t = \begin{bmatrix} 0 & \alpha & \beta \\ -\alpha & 0 & \gamma \\ -\beta & -\gamma & 0 \end{bmatrix} \begin{bmatrix} T \\ N \\ B \end{bmatrix}. \tag{2}$$

Here α, β, and γ are some smooth functions of s and t. Moreover, the time evolution equation for the curvature κ and the torsion τ of a moving curve can be found as

$$\begin{aligned} \kappa_t &= \alpha_s - \tau\beta, \\ \tau_t &= \gamma_s + \kappa\beta, \end{aligned} \tag{3}$$

where

$$\gamma = \frac{\beta_s + \tau\alpha}{\kappa}. \tag{4}$$

2.1. Some well-known and new results for Hasimoto surfaces

In this section, firstly we mention about some known geometric properties of $r = r(s, t)$ Hasimoto surfaces (or called as NLS surfaces) in Euclidean 3-spaces swept out by the binormal motion $r_t = \kappa B$, (see for more details, [7-9]). As well known that, since the tangent vector of

$r(s,t)$ Hasimoto surfaces is $r_s = T$, so the unit normal vector field u of this surface is calculated by [9]

$$u = \frac{r_s \wedge r_t}{\|r_s \wedge r_t\|} = -N. \tag{5}$$

Moreover, the coefficients of the first and second fundamental form of the Hasimoto surfaces are obtained by [9], respectively,

$$\begin{aligned} &E = \langle r_s, r_s \rangle = 1,\ F = \langle r_s, r_t \rangle = 0,\ G = \langle r_t, r_t \rangle = \kappa^2, \\ &e = \langle r_{ss}, u \rangle = -\kappa,\ f = \langle r_{st}, u \rangle = \kappa\tau,\ g = \langle r_{tt}, u \rangle = \kappa_{ss} - \kappa\tau^2. \end{aligned} \tag{6}$$

Moreover, by using the compatibility conditions, $T_{st} = T_{ts}$, $N_{st} = N_{ts}$, $B_{st} = B_{ts}$ and Eqn. (2), one can easily get

$$\alpha = -\kappa\tau,\ \beta = \kappa_s,\ \gamma = \frac{\kappa_{ss} - \kappa\tau^2}{\kappa}, \tag{7}$$

where these smooth functions are defined as in Eqn. (2). So, the intrinsic equations given as in Eqn. (3) for a moving curve can be rewritten as

$$\begin{aligned} &\kappa_t = -2\kappa_s\tau - \kappa\tau_s, \\ &\tau_t = \kappa\kappa_s - 2\tau\tau_s + \left(\frac{\kappa_{ss}}{\kappa}\right)_s. \end{aligned} \tag{8}$$

In order to study the harmonic evolute surfaces of Hasimoto surfaces, first let's recall the Gaussian and the mean curvatues of these surfaces in terms of the cuvature and torsion of moving curve:

Corollary 1. [9] Let $r = r(s,t)$ be a Hasimoto surface in Euclidean 3-space. Then its the Gaussian curvature K and the mean the curvature H are given by

$$K = \frac{eg - f^2}{EG - F^2} = \frac{-\kappa_{ss}}{\kappa} \tag{9}$$

and

$$H = \frac{1}{2}\frac{Eg - 2Ff + Ge}{EG - F^2} = \frac{1}{2\kappa}\left(\frac{\kappa_{ss}}{\kappa} - \kappa^2 - \tau^2\right), \tag{10}$$

where $\kappa \neq 0$ and τ are the curvature and torsion of moving curve respectively.

Secondly, we would like to give some characterizations of parametric curves of Hasimoto surfaces in Euclidean 3-spaces.

Theorem 1. Let $r = r(s,t)$ be a Hasimoto surface in Euclidean 3-spaces such that $r = r(s,t)$ is a curve parametrized by arc-length for all t. Then s-parameter curves of the Hasimoto surface are

- geodesic,
- asymptotic if and only if $\kappa = 0$.

Proof. Assume that $r = r(s,t)$ is a Hasimoto surface in E^3. Thus by considering the tangent vector of r, we have $r_{ss} = T_s = \kappa N$. So the binormal component of r_{ss} is zero. From which, we conclude that $s-$parameter curves of the Hasimoto surfaces are geodesics.

On the other hand, as we know that $r_{ss} = \kappa N$, the normal component of r_{ss} is zero if and only if $\kappa = 0$ which shows that $s-$parameter curves of the Hasimoto surfaces are asymptotic ones if and only if $\kappa = 0$.

Theorem 2. Let $r = r(s,t)$ be a Hasimoto surface in Euclidean 3-spaces such that $r = r(s,t)$ is a curve parametrized by arc-length for all t. Then $t-$parameter curves of r are

- geodesic if and only if $2\kappa_s\tau + \kappa\tau_s = 0,$
- asymptotic if and only if $\frac{\kappa_{ss}}{\kappa} = \tau^2.$

Proof. The proof can be exactly done by similar way of the proof of previous Theorem.

Theorem 3. Let $r = r(s,t)$ be a Hasimoto surface in Euclidean 3-spaces such that $r = r(s,t)$ is a curve parametrized by arc-length for all t. Then, parameter curves of r are lines of curvature if and only if. $\kappa\tau = 0.$

Proof. From Eqn. (6), we have $F = 0$ and $f = \kappa\tau.$ Thus we conclude that these curves of the Hasimoto surfaces are lines of curvature if and only if $\kappa\tau = 0.$

3. Harmonic Evolute Surfaces of Hasimoto Surfaces

In this section, inspired by data from Section 2, we aimed to investigate the harmonic evolute surfaces of the Hasimoto surfaces whose mean curvature does not vanish. Let us assume that the Hasimoto surface $r = r(s,t)$ is not a minimal surface. Then we have harmonic evolute surface of the Hasimoto surface defined as

$$h(s,t)=r(s,t)+\frac{1}{H(s,t)}u(s,t), \tag{11}$$

where $H(s,t)=\frac{1}{2\kappa}\left(\frac{\kappa_{ss}}{\kappa}-\kappa^2-\tau^2\right)$ with $\kappa\neq 0$ and $u(s,t)=-N(s,t)$ are the mean curvature and the normal vector of Hasimoto surface, respectively. By considering Eqn. (2) and Eqn. (10) with Eqn. (11), we have

$$h_s(s,t)=\left(1+\frac{\kappa}{H}\right)T-\left(\frac{1}{H}\right)_s N-\frac{\tau}{H}B,$$
$$h_t(s,t)=\frac{\alpha}{H}T-\left(\frac{1}{H}\right)_t N+\left(\kappa-\frac{\gamma}{H}\right)B,$$

where α,γ are given in Eqn. (7). So, the normal vector field of the harmonic evolute surface is found as

$$u^*=\frac{h_s\wedge h_t}{\|h_s\wedge h_t\|}=\frac{\lambda_1 T+\lambda_2 N+\lambda_3 B}{\sqrt{\lambda_1{}^2+\lambda_2{}^2+\lambda_3{}^2}} \tag{12}$$

such that

$$\lambda_1=-\frac{\tau}{H}\left(\frac{1}{H}\right)_t-\left(\frac{1}{H}\right)_s\left(\kappa-\frac{\gamma}{H}\right),$$
$$\lambda_2=-\frac{\tau\alpha}{H^2}-\left(1+\frac{\kappa}{H}\right)\left(\kappa-\frac{\gamma}{H}\right),$$
$$\lambda_3=\frac{\alpha}{H}\left(\frac{1}{H}\right)_s-\left(1+\frac{\kappa}{H}\right)\left(\frac{1}{H}\right)_t.$$

Moreover, the coefficients first fundamental form of the harmonic evolute surface, $h(s,t)$ in Euclidean 3-space are found by

$$E^*=\langle h_s,h_s\rangle=\left(1+\frac{\kappa}{H}\right)^2+\left(\left(\frac{1}{H}\right)_s\right)^2+\left(\frac{\tau}{H}\right)^2,$$
$$F^*=\langle h_s,h_t\rangle=\frac{\alpha}{H}\left(1+\frac{\kappa}{H}\right)+\left(\frac{1}{H}\right)_s\left(\frac{1}{H}\right)_t-\frac{\tau}{H}\left(\kappa-\frac{\gamma}{H}\right), \tag{13}$$
$$G^*=\langle h_t,h_t\rangle=\left(\frac{\alpha}{H}\right)^2+\left(\left(\frac{1}{H}\right)_t\right)^2+\left(\kappa-\frac{\gamma}{H}\right)^2.$$

On the other hand, the second order derivative formulas of the harmonic evolute surface defined in Eqn. (11) are

$$
\begin{aligned}
h_{ss} &= \left(\left(1+\frac{\kappa}{H}\right)_s + \kappa\left(\frac{1}{H}\right)_{ss}\right)T + \left(\kappa\left(1+\frac{\kappa}{H}\right) - \left(\frac{1}{H}\right)_{ss} + \frac{\tau^2}{H}\right)N - \left(\tau\left(\frac{1}{H}\right)_{ss} + \left(\frac{\tau}{H}\right)_s\right)B,\\
h_{st} &= \left(\left(1+\frac{\kappa}{H}\right)_t + \alpha\left(\frac{1}{H}\right)_s + \frac{\beta\tau}{H}\right)T + \left(\alpha\left(1+\frac{\kappa}{H}\right) - \left(\frac{1}{H}\right)_{st} + \frac{\gamma\tau}{H}\right)N\\
&\quad + \left(\beta\left(1+\frac{\kappa}{H}\right) - \gamma\left(\frac{1}{H}\right)_s - \left(\frac{\tau}{H}\right)_t\right)B,\\
h_{tt} &= \left(\left(\frac{\alpha}{H}\right)_t + \alpha\left(\frac{1}{H}\right)_t - \left(\kappa - \frac{\gamma}{H}\right)\right)T + \left(\frac{\alpha^2}{H} - \left(\frac{1}{H}\right)_{tt} - \gamma\left(\kappa - \frac{\gamma}{H}\right)\right)N\\
&\quad + \left(\frac{\alpha\beta}{H} - \gamma\left(\frac{1}{H}\right)_t + \left(\kappa - \frac{\gamma}{H}\right)_t\right)B.
\end{aligned}
\tag{14}
$$

By considering last equations with Eqn. (12), we could find the coefficients of second fundamental form of the harmonic evolute surface $h(s,t)$ as

$$
\begin{aligned}
e^* &= \frac{\lambda_1\left(\left(1+\frac{\kappa}{H}\right)_s + \kappa\left(\frac{1}{H}\right)_{ss}\right) + \lambda_2\left(\kappa\left(1+\frac{\kappa}{H}\right) - \left(\frac{1}{H}\right)_{ss} + \frac{\tau^2}{H}\right) - \lambda_3\left(\tau\left(\frac{1}{H}\right)_{ss} + \left(\frac{\tau}{H}\right)_s\right)}{\sqrt{\lambda_1^{\,2}+\lambda_2^{\,2}+\lambda_3^{\,2}}},\\
f^* &= \frac{\lambda_1\left(\left(1+\frac{\kappa}{H}\right)_t + \alpha\left(\frac{1}{H}\right)_s + \frac{\beta\tau}{H}\right) + \lambda_2\left(\alpha\left(1+\frac{\kappa}{H}\right) - \left(\frac{1}{H}\right)_{st} + \frac{\gamma\tau}{H}\right) + \lambda_3\left(\beta\left(1+\frac{\kappa}{H}\right) - \gamma\left(\frac{1}{H}\right)_s - \left(\frac{\tau}{H}\right)_t\right)}{\sqrt{\lambda_1^{\,2}+\lambda_2^{\,2}+\lambda_3^{\,2}}},\\
g^* &= \frac{\lambda_1\left(\left(\frac{\alpha}{H}\right)_t + \alpha\left(\frac{1}{H}\right)_t - \left(\kappa - \frac{\gamma}{H}\right)\right) + \lambda_2\left(\frac{\alpha^2}{H} - \left(\frac{1}{H}\right)_{tt} - \gamma\left(\kappa - \frac{\gamma}{H}\right)\right) + \lambda_3\left(\frac{\alpha\beta}{H} - \gamma\left(\frac{1}{H}\right)_t + \left(\kappa - \frac{\gamma}{H}\right)_t\right)}{\sqrt{\lambda_1^{\,2}+\lambda_2^{\,2}+\lambda_3^{\,2}}}.
\end{aligned}
\tag{15}
$$

From the equations Eqn. (13) and Eqn. (15), the Gaussian curvature K^* and the mean curvature H^* of the harmonic evolute surface can be obtained as following

$$K^{*}=\frac{\left(\begin{array}{l}\left(\frac{1}{H}\left(\gamma\beta+\alpha_{t}\right)-\kappa\beta+2\left(\frac{1}{H}\right)_{t}\alpha\right)\lambda_{1}\\+\left(\frac{1}{H}\left(\alpha^{2}+\gamma^{2}\right)-\kappa\gamma-\left(\frac{1}{H}\right)_{tt}\right)\lambda_{2}\\+\left(\frac{1}{H}\left(\alpha\beta-\gamma_{t}\right)-2\left(\frac{1}{H}\right)_{t}\gamma+\kappa_{t}\right)\lambda_{3}\end{array}\right)\left(\begin{array}{l}\left(\frac{1}{H}\kappa_{s}+2\left(\frac{1}{H}\right)_{s}\kappa\right)\lambda_{1}\\+\left(\kappa+\frac{1}{H}\left(\kappa^{2}+\tau^{2}\right)-\left(\frac{1}{H}\right)_{ss}\right)\lambda_{2}\\-\left(2\left(\frac{1}{H}\right)_{s}\tau+\frac{1}{H}\tau_{s}\right)\lambda_{3}\end{array}\right)}{\left(\begin{array}{l}-\left(\frac{1}{H}\left(\alpha+\frac{1}{H}\left(\kappa\alpha+\gamma\tau\right)-\kappa\tau\right)+\left(\frac{1}{H}\right)_{s}\left(\frac{1}{H}\right)_{t}\right)^{2}\\+\left(\left(1+\frac{1}{H}\kappa\right)^{2}+\frac{1}{H^{2}}\tau^{2}+\left(\frac{1}{H}\right)_{s}^{2}\right)\left(\frac{1}{H^{2}}\alpha^{2}+\left(-\frac{1}{H}\gamma+\kappa\right)^{2}+\left(\frac{1}{H}\right)_{t}^{2}\right)\end{array}\right)\left(\lambda_{1}^{2}+\lambda_{2}^{2}+\lambda_{3}^{2}\right)}$$
$$-\left(\begin{array}{l}\left(\left(\frac{1}{H}\right)_{s}\alpha+\left(\frac{1}{H}\right)_{t}\kappa+\frac{1}{H}\left(\beta\tau+\kappa_{t}\right)\right)\lambda_{1}\\+\left(\alpha n+\frac{1}{H}\left(\gamma\tau+\kappa\alpha\right)-\left(\frac{1}{H}\right)_{st}\right)\lambda_{2}\\+\left(\beta+\frac{1}{H}\left(\kappa\beta-\tau_{t}\right)-\gamma H_{s}-\tau H_{t}\right)\lambda_{3}\end{array}\right)^{2} \tag{16}$$

and

$$H^{*}=\frac{\left(\left(\left(1+\frac{\kappa}{H}\right)^{2}+\left(\frac{\tau}{H}\right)^{2}+\left(\frac{1}{H}\right)_{s}^{2}\right)\begin{pmatrix}\left(\frac{\gamma\beta+\alpha_{t}}{H}-\kappa\beta+2\left(\frac{1}{H}\right)_{t}\alpha\right)\lambda_{1}\\+\left(\frac{\alpha^{2}+\gamma^{2}}{H}-\kappa\gamma-\left(\frac{1}{H}\right)_{tt}\right)\lambda_{2}\\+\left(\frac{\alpha\beta-\gamma_{t}}{H}-2\gamma\left(\frac{1}{H}\right)_{t}+\kappa_{t}\right)\lambda_{3}\end{pmatrix}\right.}{}$$
$$\left.+\left(\left(\frac{\alpha}{H}\right)^{2}+\left(-\frac{\gamma}{H}+\kappa\right)^{2}+\left(\frac{1}{H}\right)_{t}^{2}\right)\begin{pmatrix}\left(\frac{1}{H}\kappa_{s}+2\kappa\left(\frac{1}{H}\right)_{s}\right)\lambda_{1}\\+\left(\kappa+\frac{\kappa^{2}+\tau^{2}}{H}-\left(\frac{1}{H}\right)_{ss}\right)\lambda_{2}\\-\left(2\tau\left(\frac{1}{H}\right)_{s}+\frac{\tau_{s}}{H}\right)\lambda_{3}\end{pmatrix}\right.$$
$$\left.-2\left(\begin{matrix}\frac{1}{H}\left(\alpha+\frac{\kappa\alpha+\gamma\tau}{H}-\kappa\tau\right)\\+\left(\frac{1}{H}\right)_{s}\left(\frac{1}{H}\right)_{t}\end{matrix}\right)\begin{pmatrix}\left(\alpha\left(\frac{1}{H}\right)_{s}+\kappa\left(\frac{1}{H}\right)_{t}+\frac{\beta\tau+\kappa_{t}}{H}\right)\lambda_{1}\\+\left(\alpha n+\frac{\gamma\tau+\kappa\alpha}{H}-\left(\frac{1}{H}\right)_{st}\right)\lambda_{2}\\+\left(\beta+\frac{\kappa\beta-\tau_{t}}{H}-\gamma\left(\frac{1}{H}\right)_{s}-\tau\left(\frac{1}{H}\right)_{t}\right)\lambda_{3}\end{pmatrix}\right.$$
$$\left.2\left(\begin{matrix}\left(-\left(\frac{1}{H}(\alpha+\frac{\kappa\alpha+\gamma\tau}{H}-\kappa\tau\right)+\left(\frac{1}{H}\right)_{s}\left(\frac{1}{H}\right)_{t}\right)^{2}\\+\left(\left(1+\frac{\kappa}{H}\right)^{2}+\left(\frac{\tau}{H}\right)^{2}+\left(\frac{1}{H}\right)_{s}^{2}\right)\left(\left(\frac{\alpha}{H}\right)^{2}+\left(\kappa-\frac{\gamma}{H}\right)^{2}+\left(\frac{1}{H}\right)_{t}^{2}\right)\end{matrix}\right)\sqrt{\lambda_{1}^{2}+\lambda_{2}^{2}+\lambda_{3}^{2}}}. \tag{17}$$

Corollary 2. The harmonic evolute surface $h(s,t)$ of the Hasimoto surface $r(s,t)$ is neither a developed surface nor a minimal surface.

Let's give some theorems about geometric interpretation of parametric curves of the harmonic evolute surface of the Hasimoto surface.

Theorem 4. If we assume that $h(s,t)$ is a harmonic evolute surface of the Hasimoto surface $r(s,t)$ in Euclidean 3-space, then $s-$parameter curves of $h(s,t)$ are

- geodesic if and only if $\tau\left(\frac{1}{H}\right)_{ss}+\left(\frac{\tau}{H}\right)_{s}=0,$

- asymptotic if and only if $\kappa\left(1+\frac{\kappa}{H}\right)-\left(\frac{1}{H}\right)_{ss}+\frac{\tau^2}{H}=0.$

Proof. Let us assume that $h=h(s,t)$ is a harmonic evolute surface of a Hasimoto surface in Euclidean 3-space. Then by considering the first expression in Eqn. (14), we have the binormal component of h_{ss} is $\tau\left(\frac{1}{H}\right)_{ss}+\left(\frac{\tau}{H}\right)_{s}$. From which, we conclude that $s-$parameter curves of the harmonic evolute surfaces are geodesics if and only if $\tau\left(\frac{1}{H}\right)_{ss}+\left(\frac{\tau}{H}\right)_{s}=0.$

On the other hand, by considering the first expression in Eqn. (14), we have the normal component of h_{ss} is $\kappa\left(1+\frac{\kappa}{H}\right)-\left(\frac{1}{H}\right)_{ss}+\frac{\tau^2}{H}$, which means that $s-$parameter curves of the Hasimoto surfaces are asymptotics if and only if $\kappa\left(1+\frac{\kappa}{H}\right)-\left(\frac{1}{H}\right)_{ss}+\frac{\tau^2}{H}=0.$

Theorem 5. If we assume that $h(s,t)$ is a harmonic evolute surface of the Hasimoto surface $r(s,t)$ in Euclidean 3-space, then t-parameter curves of $h(s,t)$ are

- geodesic if and only if $\frac{\alpha\beta}{H}-\gamma\left(\frac{1}{H}\right)_{t}+\left(\kappa-\frac{\gamma}{H}\right)_{t}=0,$
- asymptotic if and only if $\frac{\alpha^2}{H}-\left(\frac{1}{H}\right)_{tt}-\gamma\left(\kappa-\frac{\gamma}{H}\right)=0,$

where $\alpha=-\kappa\tau$, $\beta=\kappa_s$ and $\gamma=\frac{\kappa_{ss}-\kappa\tau^2}{\kappa}$ are defined as in Eqn. (8).

Proof. Let us assume that $h=h(s,t)$ is a harmonic evolute surface of a Hasimoto surface in Euclidean 3-space. Then by considering the last expression in Eqn. (14), we have the binormal component of h_{tt} is $\frac{\alpha\beta}{H}-\gamma\left(\frac{1}{H}\right)_{t}+\left(\kappa-\frac{\gamma}{H}\right)_{t}$. From which, we conclude that $s-$parameter curves of the harmonic evolute surfaces are geodesics if and only if $\frac{\alpha\beta}{H}-\gamma\left(\frac{1}{H}\right)_{t}+\left(\kappa-\frac{\gamma}{H}\right)_{t}=0.$

On the other hand, by considering the last expression in Eqn. (14), we have the normal component of h_{tt} is $\frac{\alpha^2}{H}-\left(\frac{1}{H}\right)_{tt}-\gamma\left(\kappa-\frac{\gamma}{H}\right)$, which means that s-parameter curves of the Hasimoto surfaces are asymptotics if and only if $\frac{\alpha^2}{H}-\left(\frac{1}{H}\right)_{tt}-\gamma\left(\kappa-\frac{\gamma}{H}\right)=0.$

Corollary 3. Let $h(s,t)$ be a harmonic evolute surface of Hasimoto surface $r(s,t)$. Then the following statements are satisfied;

- while there is no conditions for the $s-$parameter curves of the Hasimoto surface to be geodesic, the $s-$parameter curves of the harmonic evolute surfaces are geodesic under the condition is $\tau\left(\frac{1}{H}\right)_{ss}+\left(\frac{\tau}{H}\right)_{s}=0.$
- the $t-$parameter curves of the Hasimoto surfaces are geodesic under the condition that $2\kappa_s\tau+\kappa\tau_s=0$, while the $t-$parameter curves of the harmonic evolute surfaces are geodesic under the condition is. $\frac{\alpha\beta}{H}-\gamma\left(\frac{1}{H}\right)_{t}+\left(\kappa-\frac{\gamma}{H}\right)_{t}=0.$

Theorem 9. Let $h(s,t)$ be a harmonic evolute surface of the Hasimoto surface $r(s,t)$. The parameter curves of harmonic evolute surface are lines of curvature if and only if $\tau=0$ and κ is a non-zero constant.

Proof. The parameter curves of the harmonic evolute surface $h(s,t)$ are lines of curvature if and only if F^* and f^* being the coefficients of the first and second fundamental form, respectively, must be vanish. From the equations Eqn. (13) and Eqn. (15), we yield $F^*=f^*=0$, if $\tau=0$ and κ is a non-zero constant. Thus the proof is completed.

4. Example

Now, we give and plot a nice example related with the Hasimoto surface satisfying the Eqn. (1) and also its harmonic evolute surface. For this, if one take $\kappa=2sech(s)$ and $\tau=0$ such that they satisfy the Eqn. (8), then the Hasimoto surface $r(s,t)$ (see in Fig. 1) is expressed as follows

$$r(s,t)=\left(s-2tanh(s),-2sech(s)cos(t),-2sech(s)sin(t)\right).$$

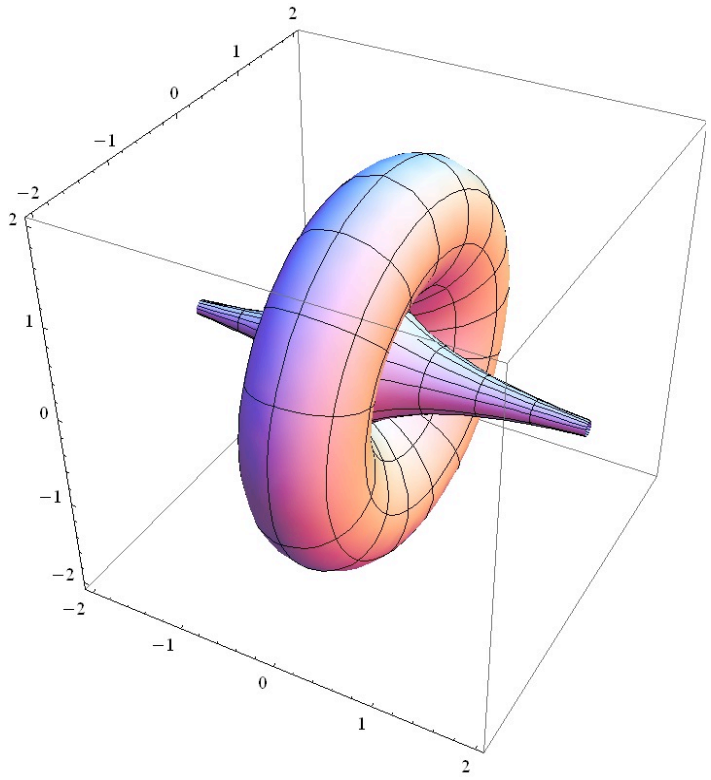

Figure 1: The Hasimoto surface $r(s,t)$ with $s \in (-4,4)$ and $t \in (0,2\pi)$

So, the normal vector field and the mean curvature of the Hasimoto surface r are given by, respectively,

$$u = \begin{pmatrix} -2\sqrt{sech\left(s^2\right)}tanh\left(s\right), \frac{1}{2}cos\left(t\right)\left(-3+cosh\left(2s\right)\right)sech\left(s\right)\sqrt{sech\left(s^2\right)}, \\ \frac{1}{2}\left(-3+cosh\left(2s\right)\right)sech\left(s\right)\sqrt{sech\left(s^2\right)}sin\left(t\right) \end{pmatrix}$$

and

$$H = \frac{1}{4}sech\left(s\right)\left(-5+sinh\left(s^2\right)\right).$$

Thus from Eqn. (11), we obtain the parametrization of the harmonic evolute surface $h\left(s,t\right)$ (see in Fig. 2) as

$$h(s,t)=\begin{pmatrix} s-\dfrac{8\sqrt{sech(s^2)}sinh(s)}{-5+sinh(s^2)}-2tanh(s), \\ 2cos(t)\left(-sech(s)+\dfrac{(-3+cosh(2s))\sqrt{sech(s^2)}}{-5+sinh(s^2)}\right), \\ 2sin(t)\left(-sech(s)+\dfrac{(-3+cosh(2s))\sqrt{sech(s^2)}}{-5+sinh(s^2)}\right) \end{pmatrix}.$$

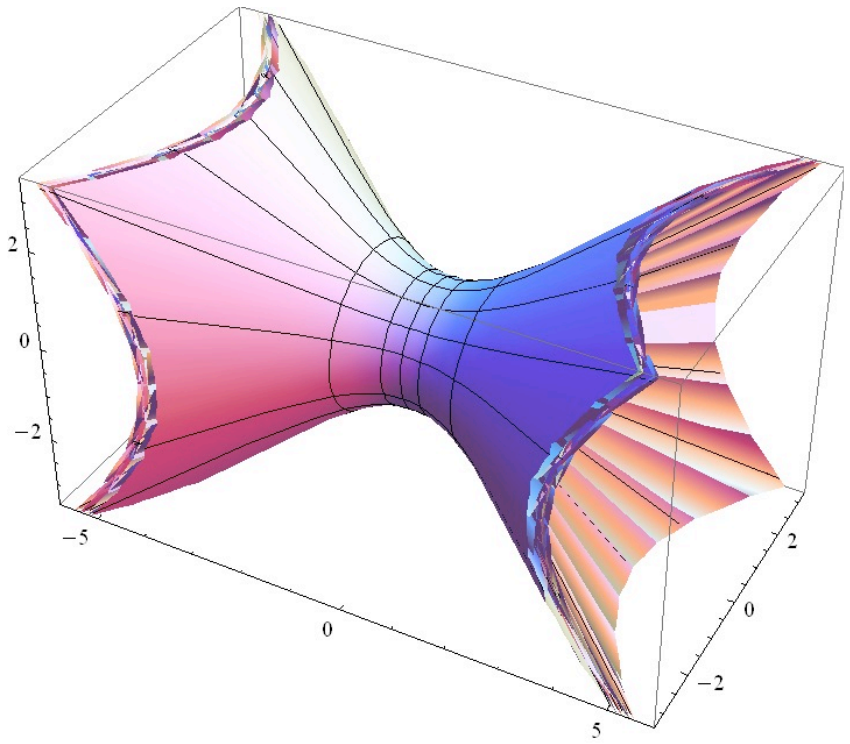

Figure 2: The harmonic evolute surface $h(s,t)$ with $s\in(-4,4)$ and $t\in(0,2\pi)$

References

[1] Sipus, Z.M., Vladimir, V., *The harmonic evolute of a surface in Minkowski 3-space*, Mathematical Communications, 19, 43-55, 2014.

[2] Lopez, R., Sipus, Z.M., Gajcic, L.P., Protrka, I., *Harmonic evolutes of B-scrolls with constant mean curvature in Lorentz-Minkowski space*, International Journal of Geometric Methods in Modern Physics, 16 (5), 1950076, 2019.

[3] Körpinar, T., Kaymanli, G.U., *On the harmonic evolute of quasi normal surfaces*, Journal of Science and Arts, 1 (50), 55-64, 2020.

[4] Eren, K., Kösal, H.H., *Evolution of space curves and the special ruled surfaces with modified orthogonal frame*, AIMS Mathematics, 5 (3), 2027-2039, 2020.

[5] Kelleci, A., Eren, K., *On evolution of some associated type ruled surfaces*, Mathematical Sciences and Applications E-Notes, 8 (2), 178-186, 2020.

[6] Hasimoto, H., *Motion of a vortex filament and its relation to elastica*, Journal of the Physical Society of Japan, 31, 293-294, 1971.

[7] Hasimoto, H., *A soliton on a vortex filament*, Journal of Fluid Mechanics, 51 (3), 477-485, 1972.

[8] Rogers, C., Schief, W.K., *Bäcklund and Darboux transformations*, Cambridge University Press, 432, 2002.

[9] Abdel-All, N.H., Hussien, R.A., Youssef, T., *Hasimoto surfaces*, Life Science Journal, 9 (3), 556-560, 2012.

[10] Kelleci, A., Bektaş, M., Ergüt, M., *The Hasimoto surface according to Bishop frame*, Adıyaman University Journal of Science, 9 (1), 13-22, 2019.

[11] Erdoğdu, M., Özdemir, M., *Geometry of Hasimoto surfaces in Minkowski 3-space*, Mathematical Physics, Analysis and Geometry, 17, 169-181, 2014.

[12] Çakmak, A., *Öklid 3-uzayında Hasimoto yüzeylerinin paralel yüzeyleri*, Bitlis Eren Üniversitesi Fen Bilimleri Dergisi, 7 (1), 125-132, 2018.

Adıyaman University Journal of Science
https://dergipark.org.tr/en/pub/adyujsci
DergiPark AKADEMİK
ISSN 2147-1630
e-ISSN 2146-586X

Response Surface Methodology Based Nickel Bioremoval by *Penicillium citrinum* Grown in Dilute Acid Pretreated Lignocellulosic Material

Ekin DEMİRAY[1,2]*

[1]*Adıyaman University, Faculty of Science and Literature, Department of Biology, Adıyaman, Turkey*
[2]*Ankara University, Science Faculty and Literature, Biology Department, Ankara, Turkey*
edemiray@ankara.edu.tr, ORCID: 0000-0003-2675-134X

Received: 29.12.2020 **Accepted:** 09.05.2021 **Published:** 30.06.2021

Abstract

The present study demonstrates the effectiveness of Ni (II) bioremoval by *Penicillium citrinum* fungus cultivated in carrot pomace medium. Experimental model for Ni (II) removal was developed using central composite design (CCD) based on response surface methodology (RSM). According to the model, the effects of some key parameters such as pH, initial Ni (II) loading, and initial carrot pomace loading on Ni (II) bioremoval was found as significant ($p < 0.05$). The highest bioremoval was oberved as 82.01% in the presence of pH 5, 50 mg/L initial Ni (II), and 100 g/L initial biomass loadings, respectively. Results revelaed that the usage of *Penicillium citrinum* were proven to be effective in removing of Ni (II).

Keywords: *Penicillium citrinum;* Bioremoval; Response surface methodology.

* Corresponding author
DOI: 10.37094/adyujsci.849704

Seyreltik Asit Ön-İşlemi ile Muamele Edilen Lignoselülozik Materyalde Geliştirilen *Penicillium citrinum*'un Yüzey Tepki Metodolojisi Temelli Nikel Biyogiderimi

Öz

Bu çalışma, havuç posası içeren besiyerinde geliştirilen *Penicillium citrinum* fungusunun Ni (II) biyogiderimini etkin bir şekilde gerçekleştirdiğini göstermektedir. Çalışmada Ni (II) giderimi adına yanıt yüzey metodolojisine (RSM) dayalı merkezi bileşik tasarım (CCD) kullanılarak deneysel bir model geliştirilmiştir. Modele göre, başlangıç Ni (II) ve havuç posası konsantrasyonu ile pH gibi bazı önemli parametrelerin Ni (II) biyogiderimi üzerindeki etkileri anlamlı bulunmuştur ($p < 0.05$). En yüksek giderim 50 mg/L Ni (II), 100 g/L biyokütle ve pH 5'te %82.01 olarak gözlenmiştir. Sonuçlar, *Penicillium citrinum* kullanımının Ni (II) 'nin gideriminde etkili olduğunu ortaya koymaktadır.

Anahtar Kelimeler: *Penicillium citrinum*; Biyogiderim; Tepki yüzey metodolojisi.

1. Introduction

As a result of industrialization, hazardous substances such as heavy metals cause serious problems for the environment, animals, and plants. These molecules can be harmful when the proper treatment methods are not performed [1]. The toxic effects of heavy metals are well known in the literature. They affect the brain, kidney, skin, or lung negatively, and they also have carcinogenic effects on certain organisms [2]. Therefore, different removal techniques such as physical, chemical, and biological are carried out for bioremoval of heavy metals from the wastewaters.

Although physicochemical methods can provide effective heavy metal removal, high capital costs and expensive regeneration processes limit their usage [3]. On the other hand, bioremoval is a cheap and effective alternative to the other techniques. Microorganisms produce high biomass yields; they have a fast growth rate and suitable for genetic manipulations [4]. For these reasons, different microorganisms such as fungi are used for textile dye or heavy metal removal from aquatic environments [5]. *Penicillium citrinum* is a widespread mesophilic fungus naturally found on different plants such as wheat or citrus species. Biotechnological applications of *P. citrinum* such as uranium (IV) biosorption [6], metabolite and enzyme production [7, 8], or textile dye removal [9] were shown in the literature previously.

Lignocellulosic biomass is one of the most abundant and underutilized raw materials on Earth. Cellulose and hemicellulose present in the lignocellulose contain fermentable sugars, which are very suitable for microbial growth. However, to obtain fermentable sugars from

lignocellulose, efficient pretreatment techniques are required [10]. Carrot pomace is an essential by-product of the juice and food industries. Millions of tons of carrot pomace are generated each year. After carrot processing, 50% of the raw material remains as pomace and this pomace contains neutral sugars, carotenoids, macroelements, and minerals (N, P, K, Mg, Na, Ca, Cu, Mn, Fe and Zn) which are essential for microbial growth and metabolic activity. Furthermore, carrot pomace has high sugar and nutritional content, and it can also accumulate the free sugars in its vacuoles [11, 12]. Therefore, numerous studies about the carrot pomace are carried out in the literature [13, 14].

Most of the biological optimization studies focus on the evaluation of one variable at a time. However, the combined effect of different variables is significant for optimization. Response Surface Methodology (RSM) allows identifying the interaction between controllable factors. RSM also defines the effects of different factors on the response alone or combined [15]. For these reasons, RSM studies have been used in many other areas such as biofuel production [16], dye biosorption [17], or heavy metal bioremoval [18].

The aim of the current study was to investigate the experimental model for Ni (II) bioremoval by *P. citrinum*. Within this context, effects of initial Ni (II) concentration, pH and initial biomass loading were optimized by response surface methodology. This is the first report about the Ni(II) bioremoval of *P. citrinum* cultivated in carrot pomace by RSM optimization.

2. Materials and Methods

2.1. Raw materials and pretreatment

Ground carrot pomace (approximately smaller than 0.2 mm particle size) was obtained from BELSO Co./Ankara and was dried in an oven at 70 ºC overnight. Dried carrot pomace was kept in screw cap bottles until pretreatment. Pretreatment was carried out in autoclave with 1% H_2SO_4 for 15 min at 121 ºC. The slurry was filtered through Whatman No:1 paper and was used in bioremoval experiments. The sugar concentration of carrot pomace was also determined before and after the experiments.

2.2. Microorganisms

P. citrinum was obtained from Ankara University Culture Collection. The fungus was kept in Potato Dextrose Agar (PDA) at +4 ºC until experiments.

2.3. Culture conditions

250 mL Erlen-Meyer flasks working volume with 100 mL were used for the experiments. Agitation speed and temperature were set as 125 rpm. and 30 °C, respectively. Uninoculated flasks with different pH, initial biomass nickel loadings were used as control. All experiments were performed triplicate.

2.4. Bioremoval with RSM studies

Design Expert Software® 12 was used for RSM experiments. Central composite design (CCD) with three levels was used to evaluate the effects of three variables on Ni(II) bioremoval of *P. citrinum*. Total 17 runs were created for RSM. pH (3-7), initial nickel loading (50-150 mg/L), and initial biomass loading (50-150 g/L) were selected as independent factors. The data obtained from experiments, was statistically evaluated using analysis of variance (ANOVA) at significance level of $p < 0.05$ by using Design Expert Software® 12.

2.5. Analytical methods

Ni(II) removal was measured spectrophotometrically (Shimadzu) at 340 nm. wavelength, according to Snell and Snell [19]. Total reducing sugar concentrations were measured according to the DNS method [20].

3. Results

3.1. Composition of carrot pomace

In the current study, carrot pomace was used for Ni (II) bioremoval of *P. citrinum*. Carrot pomace was pretreated with dilute acid (1% H_2SO_4 v/v). Reducing sugar concentrations of different carrot pomace loadings were examined. Results were shown in Fig. 1. It was observed that increasing biomass loadings resulted in increased sugar contents. The highest sugar was obtained from 150 g/L carrot pomace as 52.72 g/L. Sugar concentrations reduced to 24.69 g/L when 50 g/L carrot pomace was used. Moreover, in 100 g/L carrot pomace loading, 38.63 g/L sugar was detected.

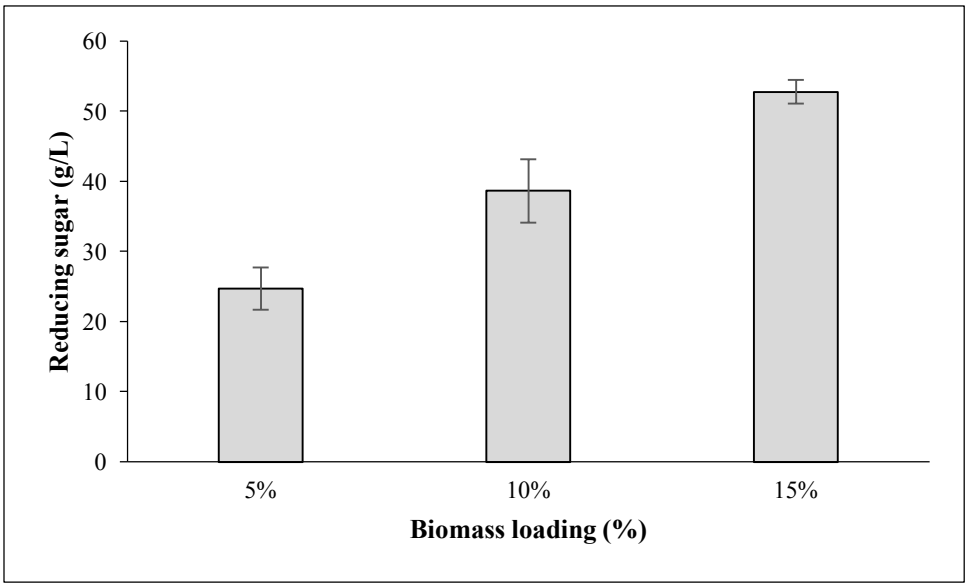

Figure 1: Reducing sugar concentrations of different carrot pomace loadings (Pretreatment: 1% H_2SO_4 for 15 min at 121 ºC)

3.2 Response Surface Methodology for Ni(II) Bioremoval

In RSM experiments, central composite design was employed to investigate the effect of pH, initial nickel, and biomass loadings. The descriptive table of the independent variables and bioremoval were shown as coded values in Table 1.

Table 1: Descriptive table of coded level for RSM analysis

Factor	Name	Minimum	Maximum	Coded Low	Coded High
A	**pH**	3	7	3	7
B	**Initial nickel concentration**	50	150	50	150
C	**Biomass loading**	5	15	5	15

The equation for the bioremoval yield was given in Eq (1). The final equation in terms of coded factors:

Eq (1): Bioremoval = -231.79 + 102.33*A + 0.26*B +2.48*C – 0.028*AB + 1.095*AC – 0.025*BC -10.39*A^2 + 0.000030*B^2 – 0.152*C^2

where A, B, C are the coded values of pH, initial nickel loading (mg/L), and biomass loading (%), respectively.

The effects of different variables on bioremoval were shown in Table 2. Response surface graphs were also shown in Fig. 2 A, B, and C. The highest removal was found at the end of the 3rd day of incubation. Therefore, RSM studies were carried out for the results of the 3rd day of incubation.

Table 2: Effect of different variables on Ni(II) bioremoval of *P. citrinum*

Std	Run	Factor 1 A: pH	Factor 2 B: Initial nickel concentrations (mg/L)	Factor 3 C: Biomass loading (%)	Response 1 Bioremoval (%)
4	**1**	7	150	5	20.71
12	**2**	5	150	10	59.06
10	**3**	7	100	10	40.43
2	**4**	7	50	5	15.68
6	**5**	7	50	15	81.72
15	**6**	5	100	10	73.54
9	**7**	3	100	10	17.31
11	**8**	5	50	10	82.01
8	**9**	7	150	15	46.00
3	**10**	3	150	5	14.08
16	**11**	5	100	10	77.64
5	**12**	3	50	15	19.82
17	**13**	5	100	10	75.09
13	**14**	5	100	5	53.87
7	**15**	3	150	15	11.18
1	**16**	3	50	5	13.22
14	**17**	5	100	15	79.45

According to model *p* values of the pH, initial nickel and biomass loading were found as 0.0003, 0.0155, and 0.0004, respectively, and pH was found as the most significant parameter and was followed by initial biomass loading. The highest Ni (II) removal was observed as 82.01% when pH, initial nickel, and biomass loadings were adjusted as 5, 50 mg/L, and 100 g/L. Moreover, it was found that increasing Ni (II) concentrations caused lower removal yields. The lowest removal was 11.18% in pH 3, 150 mg/L initial Ni (II) loading, and 150 g/L biomass loading, respectively. According to the data in Fig. 2 A, B, and C, higher removal rates were observed in pH 5 and lower Ni (II) loadings. Furthermore, higher Ni (II) removal was observed from increased biomass loadings.

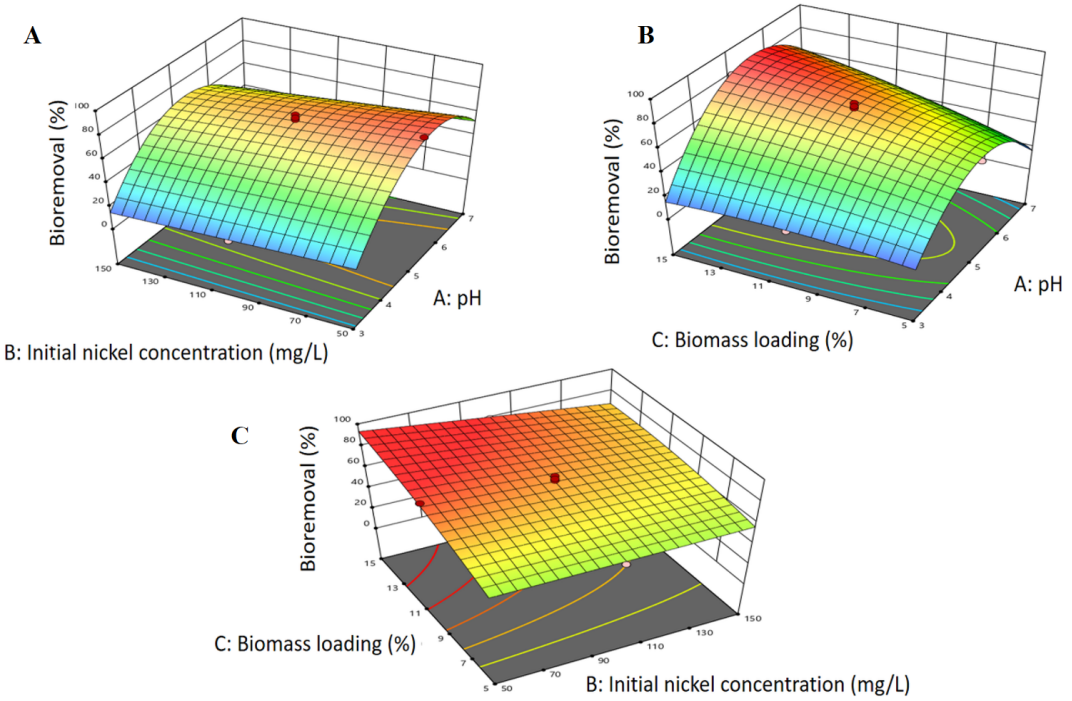

Figure 2: Response surface graphs of Ni bioremoval by *P. citrinum* in the presence of different conditions. **A:** Effect of pH and initial nickel concentration on bioremoval, **B:** Effect of pH and biomass loading on bioremoval, **C:** Effect of biomass loading and initial nickel concentration on bioremoval (Pretreatment: 1% H_2SO_4 for 15 min at 121 ºC, incubation time 72 hours, agitation speed: 125 rpm, T: 30 ºC)

Bioremoval of Ni (II) in the presence of pH 5, 50 mg/L initial Ni (II), and 50 g/L initial carrot pomace loadings were also given in Fig. 3. According to the figure, it was observed that *P. citrinum* consumed reducing sugars, and almost complete depletion occurred at the end of the 96 hours incubation period. Moreover, the highest removal was detected at the end of the 72 hours of incubation. After 72 hours, a slight decrease was found in the removal rates. Ni (II) removal was obtained as 22.84%, 72.69%, 82.01%, and 71.76% at the end of the 24, 48, 72, and 96 hours of incubation.

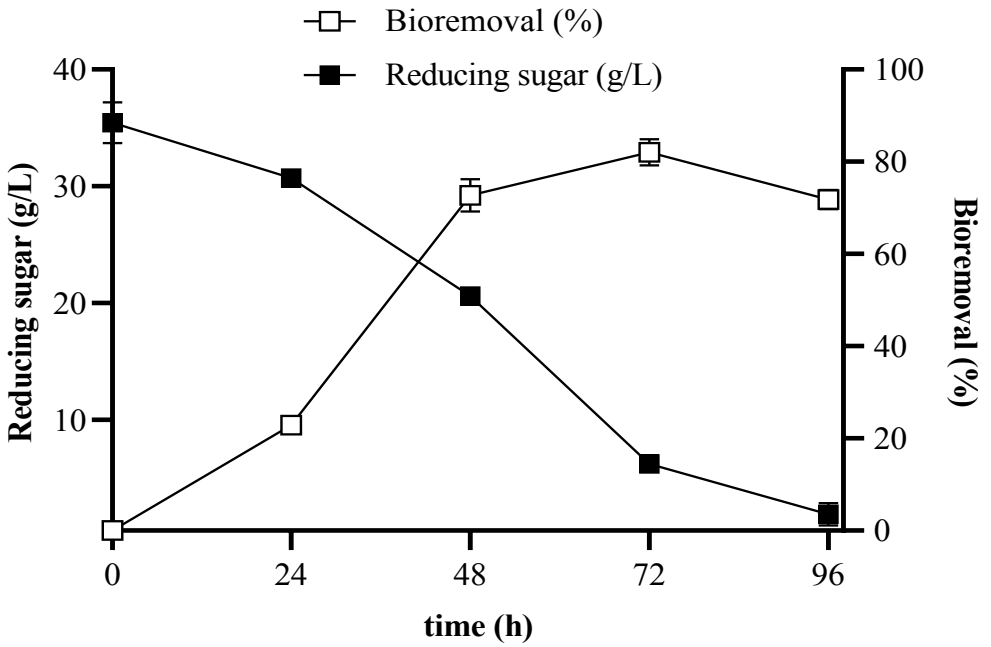

Figure 3: Time course of Ni (II) removal and reducing sugars during incubation of *P. citrinum* (Pretreatment: 1% H_2SO_4 for 15 min at 121 ºC, pH:5, initial Ni (II) concentration: 50 mg/L, initial carrot pomace loading: 100 g/L, agitation speed: 125 rpm, T: 30 ºC)

4. Discussion

During acidic pretreatment, some inhibitory compounds derived from biomass such as phenolics, weak acids, or furan derivatives can be released into the medium. These molecules have a negative impact on microbial growth and metabolism [21]. Therefore, the concentration of reducing sugars from acid pretreated carrot pomace was determined. It was observed that increasing biomass loadings resulted in higher sugar. In the literature, similar reports showed that increased biomass loading caused higher sugar amounts. In a study about switchgrass, approximately 15 g/L reducing sugar was observed in the presence of 50 g/L initial biomass loading. This value increased around 45 g/L when biomass loading was increased to 200 g/L [22].

Despite the higher biomass loadings, such as 150 g/L, any lagging or inhibition was not observed in the growth of *P. citrinum*. This tolerance can be attributed to the inhibitor-resistant nature of *P. citrinum* cells. Similarly, Karpe et al. [23] reported that *P. citrinum* could virtually degrade hydrothermally pretreated grape wastes, which contained inhibitors such as 5-HMF. Furthermore, Tejas et al. [24] showed that *P. citrinum* could remove 70% phenolic substances from paper mill wastewaters with fungal fermentation. These results indicate that *P. citrinum* is a suitable microorganism for bioremoval studies.

During RSM studies, it was indicated that *P. citrinum* effectively removed Ni(II) from carrot pomace medium, and pH 5 was favorable for *P. citrinum*. Similarly, in one study, the highest Cu, Pb, and Zn removal rates of *P. citrinum* were observed in pH 6 [25]. Medium pH is one of the most critical elements of metal uptake. In lower pH values, repulsive forces between the fungal cell surface and metal ions causedecreased metal binding to the surface. On the other hand, when pH increased, precipitation can occur, which may lead to reduction in bioremoval yields [26].

Moreover, lower bioremoval rates were observed when initial Ni(II) loading was increased (Figure 1a). This decline can be explained by the inhibitory effect of Ni(II). In the literature, it was previously shown that increased Ni(II) loadings led to lower bioremoval by *Aspergillus versicolor* [27]. Moreover, in a study about Cu(II) and Ni(II) bioremoval of *Aspergillus sp*., the highest removal in the presence of 50 mg/L initial Ni(II) was found as 86%. On the other hand, when the initial Ni(II) loading increased to 100 mg/L, bioremoval decreased to 78% [28].

Initial biomass loading is an essential parameter for microbial growth and bioremoval. Lower biomass loading can cause lower microbial growth. On the other hand, in higher biomass loading, inhibitory compounds can be released into the removal environment. Therefore, the effect of initial biomass loading on bioremoval was also investigated in the present study. According to Figure 1c, increased biomass loadings resulted in higher Ni(II) removal. In the literature, it was reported that higher sugar concentrations caused higher bioremoval rates. For instance, Kapdan and Kargi [29] found the decolorization of dyestuff by *Coriolus versicolor* as 54% in the presence of 5 mg/L glucose. Decolorization increased to 77% when the initial glucose loading was 10 mg/L.

5. Conclusions

In the present study, response surface methodology was applied for Ni(II) removal by *P. citrinum*. Carrot pomace, which is a cheap and abundant by-product of food and juice industries, was used as a growth environment. Some critical parameters such as pH, initial nickel loading, and initial biomass loading were optimized. *P. citrinum* effectively removed Ni(II) from carrot pomace medium. The highest bioremoval was observed as 82.01% in the presence of 50 mg/L Ni(II), pH 5, and 100 g/L initial carrot pomace loading. It was also detected that increased biomass loading resulted in higher removal rates, and removal rates decreased in the presence of increasing Ni(II) concentrations. This study reveals that the carrot pomace is a suitable raw material for the growth of microorganisms such as fungi, and *P. citrinum* is a promising bioagent for heavy metal removal.

Acknowledgement

The author thankfull to Prof. Dr. Sevgi ERTUĞRUL KARATAY and Prof. Dr. Gönül DÖNMEZ for their valuable contributions to writing of the manuscript.

References

[1] Akbal, F., Camcı, S., *Copper, chromium and nickel removal from metal plating wastewater by electrocoagulation*, Desalination, 269(1-3), 214-222, 2011.

[2] Axtell, N.R., Sternberg, S.P., Claussen, K., *Lead and nickel removal using Microspora and Lemna minor*, Bioresource technology, 89(1), 41-48, 2003.

[3] Villaescusa, I., Fiol, N., Martínez, M., Miralles, N., Poch, J., Serarols, J., *Removal of copper and nickel ions from aqueous solutions by grape stalks wastes*, Water research, 38(4), 992-1002, 2004.

[4] Fu, F., Wang, Q., *Removal of heavy metal ions from wastewaters: a review*, Journal of environmental management, 92(3), 407-418, 2011.

[5] Agarwal, M., Singh, K., *Heavy metal removal from wastewater using various adsorbents: a review*, Journal of Water Reuse and Desalination, 7(4), 387-419, 2017.

[6] Pang, C., Liu, Y.H., Cao, X.H., Li, M., Huang, G. L., Hua, R., An, X.F., *Biosorption of uranium (VI) from aqueous solution by dead fungal biomass of Penicillium citrinum*, Chemical Engineering Journal, 170(1), 1-6, 2011.

[7] Tashiro, Y., Ueno, H., Takaba, M., Hayashi, S., *Production of functional inulin-type fructooligosaccharides by an Enzyme from Penicillium citrinum*, Current microbiology, 74(9), 1114-1117, 2017.

[8] Gu, Y., Ding, P., Liang, Z., Song, Y., Liu, Y., Chen, G., Li, J.L., *Activated production of silent metabolites from marine-derived fungus Penicillium citrinum,* Fitoterapia, 127, 207-211, 2018.

[9] Demiray, E., *Assessment of apple and carrot pomaces for cost-effective reactive black 5 bioremoval by Penicillium citrinum*, Journal of the Chilean Chemical Society, 65(3), 4914-4918, 2020.

[10] Paul, S., Dutta, A., *Challenges and opportunities of lignocellulosic biomass for anaerobic digestion, Resources,* Conservation and Recycling, 130, 164-174, 2018.

[11] Aimaretti, N.R., Ybalo, C.V., Rojas, M.L., Plou, F.J., Yori, J.C., *Production of bioethanol from carrot discards,* Bioresource technology, 123, 727-732, 2012.

[12] Surbhi, S., Verma, R.C., Deepak, R., Jain, H.K., Yadav, K.K. *A review: Food, chemical composition and utilization of carrot (Daucus carota L.) pomace*. International Journal of Chemical Studies, 6(3), 2921-2926, 2018.

[13] Singh, B., Panesar, P.S., Nanda, V., *Utilization of carrot pomace for the preparation of a value added product,* World Journal of Dairy & Food Sciences, 1(1), 22-27, 2006.

[14] Karatay, S.E., Dönmez, G., *An economical phenol bioremoval method using Aspergillus versicolor and agricultural wastes as a carbon source*, Ecological engineering, 73, 224-228, 2014.

[15] Yolmeh, M., Jafari, S.M., *Applications of response surface methodology in the food industry processes*, Food and Bioprocess Technology, 10(3), 413-433, 2017.

[16] Uyan, M., Alptekin, F.M., Cebi, D., Celiktas, M.S., *Bioconversion of hazelnut shell using near critical water pretreatment for second generation biofuel production*, Fuel, 273, 117641, 2020.

[17] Mona, S., Kaushik, A., Kaushik, C.P., *Biosorption of reactive dye by waste biomass of Nostoc linckia,* Ecological Engineering, 37(10), 1589-1594, 2011.

[18] Gönen, F., Aksu, Z., *Single and binary dye and heavy metal bioaccumulation properties of Candida tropicalis: Use of response surface methodology (RSM) for the estimation of removal yields*, Journal of hazardous materials, 172(2-3), 1512-1519, 2009.

[19] Snell, F.D., Snell, C.T., *Colorimetric Methods of Analysis*, third ed., vol. 2. D Van Nostrand Company, New York, 1959.

[20] Miller, G.L*., Use of dinitrosalicylic acid reagent for determination of reducing sugar,* Analytical chemistry, 31(3), 426-428, 1959.

[21] Palmqvist, E., Hahn-Hägerdal, B., *Fermentation of lignocellulosic hydrolysates. II: inhibitors and mechanisms of inhibition,* Bioresource technology, 74(1), 25-33, 2000.

[22] Ioelovich, M., Morag, E., Study of enzymatic hydrolysis of pretreated biomass at increased solids loading, *Bioresources*, *7*(4), 4672-4682, 2012.

[23] Karpe, A.V., Harding, I.H., Palombo, E.A., *Comparative degradation of hydrothermal pretreated winery grape wastes by various fungi*, Industrial Crops and Products, *59*, 228-233, 2014.

[24] Namboodiri, M.T., Pakshirajan, K., *Sustainable and green approach of chitosan production from Penicillium citrinum biomass using industrial wastewater as a cheap substrate*, Journal of environmental management, 240, 431-440.

[25] Bourzama, G., Rihani, A., Ennaghra, N., Ouled-Haddar, H., Soumati, B., *Kinetic modeling for the biosorption of copper, lead and zinc by Penicillium citrinum isolated from polluted algerian beaches*, *Scientific Study Research. Chemistry Chemical Engineering, Biotechnology*, Food Industry, 21(3), 321-332, 2020.

[26] Choudhary, S., Sar, P., *Characterization of a metal resistant Pseudomonas sp. isolated from uranium mine for its potential in heavy metal (Ni2+, Co2+, Cu2+, and Cd2+) sequestration*, Bioresource technology, 100(9), 2482-2492, 2009.

[27] Taştan, B.E., Ertuğrul, S., Dönmez, G., *Effective bioremoval of reactive dye and heavy metals by Aspergillus versicolor,* Bioresource technology, 101(3), 870-876, 2010.

[28] Pundir, R., Chary, G.H.V.C., Dastidar, M.G., *Application of Taguchi method for optimizing the process parameters for the removal of copper and nickel by growing Aspergillus sp.*, Water resources and industry, 20, 83-92, 2018.

[29] Kapdan, I.K., Kargi, F., *Biological decolorization of textile dyestuff containing wastewater by Coriolus versicolor in a rotating biological contactor*, Enzyme and Microbial Technology, 30(2), 195-199, 2002.

Adıyaman University Journal of Science
https://dergipark.org.tr/en/pub/adyujsci
DergiPark AKADEMİK
ISSN 2147-1630
e-ISSN 2146-586X

Analysis of Interactions of NHC Type Molecules and NHC-Ag Complexes with VEGFR-2 and DNA: A Molecular Docking Study

Elvan ÜSTÜN[1], Neslihan ŞAHİN[2,*]
[1]*Ordu University, Faculty of Art and Science, Department of Chemistry, 52200, Ordu, Turkey*
elvanustun@odu.edu.tr, ORCID: 0000-0002-0587-7261
[2]*Cumhuriyet University, Faculty of Education, Department of Basic Education, 58140, Sivas, Turkey*
neslihan4458@gmail.com, ORCID: 0000-0003-1498-4170

Received: 13.12.2020 **Accepted:** 12.05.2021 **Published:** 30.06.2021

Abstract

Molecular docking is an important tool in drug research. Thanks to these calculations, the type and magnitude of interactions of the molecules with target molecules are evaluated. It is also possible to perform more detailed analyzes than known experimental methods in an easy and economical way by using the results obtained with current scientific developments and examine interactions with different target molecules depending on bioactivity type. Cancer researches show that vascular endothelial growth factor is effective in the growth and proliferation of cancer cells. Inhibition of the receptor that regulates the release of this factor may be an efficient method for designing an anticancer agent. One of these receptors is VEGFR-2. This receptor can be used as a target molecule in cancer research. In addition, the interaction of molecules with DNA is important in terms of getting insight for future studies. In this study, the interaction of 1-allyl-3-benzylbenzimidazolium, 1-allyl-3-(naphthylmethyl)benzimidazolium, 1-allyl-3-(anthracen-9-yl-methyl)benzimidazolium,chloro[1-allyl-3-benzylbenzimidazolium-2-ylidene]silver(I), chloro[1-allyl-3-(naphthylmethyl)benzimidazolium-2-ylidene]silver(I), chloro[1-allyl-3-(anthracen-9-yl-methyl)benzimidazolium-2-ylidene]silver(I) with VEGFR-2 and DNA were analyzed by molecular docking methods.

Keywords: Molecular docking; N-Heterocyclic carbenes; VEGFR-2; Silver complexes.

* Corresponding Author DOI: 10.37094/adyujsci.838918

NHC Tipi Moleküllerin ve NHC-Ag Komplekslerin VEGFR-2 ve DNA ile Etkileşimlerinin Analizi: Moleküler Doking Çalışması

Öz

Moleküler doking, ilaç araştırmalarında önemli bir araçtır. Bu hesaplamalar sayesinde moleküllerin hedef moleküllerle olan etkileşimlerinin türü ve büyüklüğü değerlendirilir. Güncel bilimsel gelişmelerle elde edilen sonuçlar kullanılarak, bilinen deneysel yöntemlere göre daha detaylı analizleri kolay ve ekonomik bir şekilde gerçekleştirmek ve biyoaktivite tipine bağlı olarak farklı hedef moleküller ile etkileşimleri incelemek de mümkündür. Kanser araştırmaları vasküler endotelyal büyüme faktörünün, kanser hücrelerinin büyümesi ve çoğalmasında etkili olduğunu göstermektedir. Bu faktörün salımını düzenleyen reseptörün inhibisyonu, bir antikanser ajanı tasarlamak için etkili bir yöntem olabilir. Bu reseptörlerden biri VEGFR-2'dir. Bu reseptör, kanser araştırmalarında bir hedef molekül olarak kullanılabilir. Ayrıca moleküllerin DNA ile etkileşimi ileride yapılacak çalışmalara ışık tutması açısından önemlidir. Bu çalışmada, VEGFR-2 ve DNA ile 1-allil-3-benzilbenzimidazolyum, 1-allil-3-(naftilmetil)benzimidazolyum, 1-allil-3 (antrasen-9-il-metil)benzimidazolyum, kloro[1-allil-3-benzilbenzimidazolyum-2-iliden]gümüş(I), kloro[1-allil-3-(naftilmetil)benzimidazolyum-2-iliden]gümüş (I), kloro[1-allil-3-(antrasen-9-il-metil)benzimidazolium-2-iliden]gümüş(I) bileşiklerinin etkileşimi moleküler doking yöntemleriyle analiz edildi.

***Anahtar Kelimeler**:* Moleküler doking; N-Heterosiklik karbenler; VEGFR-2; Gümüş kompleksleri.

1. Introduction

Angiogenesis which is defined as the formation of new blood vessels from pre-existing vasculature takes place in processes such as cell growth and wound healing [1, 2]. However, recent studies display that excessive angiogenesis causes pathological problems such as tumor formation, increase in existed tumor and metastasis [3, 4]. In this case, controlling the systems that regulate angiogenesis could be a hopeful way for cancer therapy. Vascular endothelial growth factor (VEGF) is a signal protein that positively regulates vascular endothelial cells [5]. The activity of VEGF is controlled by vascular endothelial growth factor receptors (VEGFR) that are structurally similar to each other and these are VEGFR-1 (Flt-1), VEGFR-2 (KDR / Flk-1) and VEGFR-3. VEGFR-2 is a type of tyrosine kinase and is major regulator of endothelial cells in both physiological and pathological angiogenesis [6]. Studies confirmed that overexpression of VEGFR-2 has been monitored in breast, colorectal, ovarian, and thyroid cancers [7-9]. Indeed,

VEGFR-2 could be considered as a target for fighting against cancer, and many articles on this strategy have been published recently [10-14].

DNA is the essential target for designing more effective molecules and the detection of the interaction of new molecules with DNA is still an active scientific field [15-17]. Understanding the interactions of metal complexes with DNA sequences is important for the analysis of tumor inhibition mechanisms and design new molecules for effecting the selected parts of DNA [18].

N-heterocyclic carbenes (NHCs) is a family of molecules whose many properties have been studied since the first synthesized [19, 20]. NHCs, which are well-known for their catalytic activity, can be easily synthesized and modified due to their electron-rich and neutral sigma donor properties [21, 22]. In addition, many NHC-metal complexes have been synthesized, and their bioactivities have been frequently studied. Particularly, the antibacterial activity of the ruthenium and rhodium complexes is well known [23, 24]. After the improvement in metal-based anti-cancer drugs, the anti-cancer properties of metal-NHC complexes have also been frequently studied [25, 26]. Good results have been especially obtained from anti-cancer activity studies of Au-NHC complexes [27]. Moreover, the anti-cancer research of Ag-NHC complexes that are generally known as anti-infective has positively progressed [28].

Molecular docking method is accepted as an essential tool for investigating the interactions between new molecules and biological macromolecules such as DNA, proteins, enzymes [29-32]. It is possible to have an idea about the properties of molecules that have not been synthesized with this method [33]. Moreover, it is very useful to have foresight for designing new molecules by comparing the experimental bioactivity results. In this study, VEGFR-2 and DNA were selected as a cancer target molecule and interaction of previously synthesized [34] 1-allyl-3-benzylbenzimidazolium [**1a**], 1-allyl-3-(naphthylmethyl)benzimidazolium [**1b**], 1-allyl-3-(anthracen-9-yl-methyl)benzimidazolium [**1c**], chloro[1-allyl-3-benzylbenzimidazolium-2-ylidene] silver(I) [**2a**], chloro[1-allyl-3-(naphthylmethyl) benzimidazolium-2-ylidene]silver(I) [**2b**], chloro[1-allyl-3-(anthracen-9-yl-methyl)benzimidazolium-2-ylidene]silver(I) [**2c**] (Fig. 1) with VEGFR-2 and DNA were analyzed by molecular docking methods.

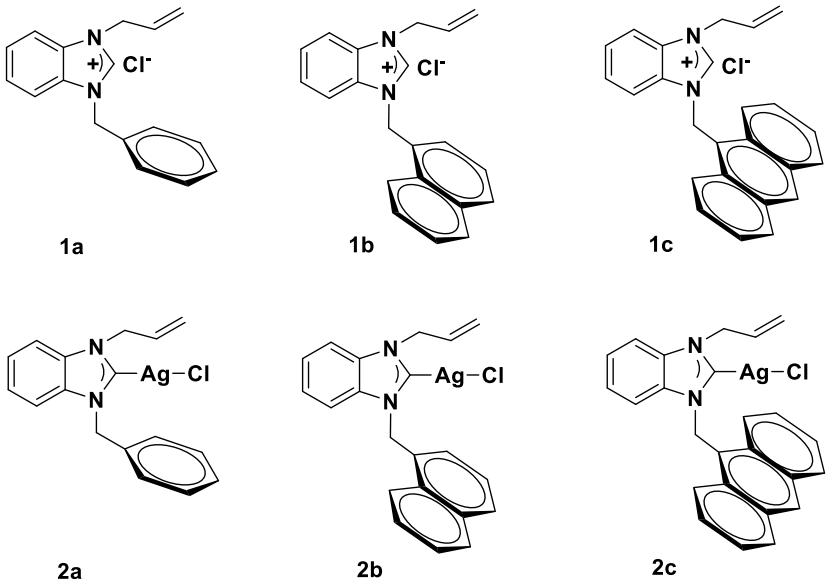

Figure 1: Allyl substituted benzimidazolium molecules and their Ag complexes

2. Materials and Methods

2.1. Molecular docking method

Before the molecular docking process, molecules are optimized with ORCA package program. DFT calculations were performed with ORCA version 2.8 using the BP86 functional with a def2-SVP def2-SVP/J basis set, the tightscf, and KDIIS SOSCF options for geometry optimizations [35, 36]. Molecular dockings were performed by using AutoDock 4.2. with both vascular endothelial growth factor receptor-2 (PDB id: 1YWN) and DNA dodecamer (PDB id: 1BNA) crystal structures which are obtained from RCSB protein data bank [37]. Water in the proteins was removed and polar hydrogen atoms and Kollman charges were evaluated for target molecules in the docking process. Gasteiger charges, randomized starting positions, optimizations, and torsions have been evaluated for ligand molecules. The genetic algorithm population was used as 150 while applying Lamarkian genetic algorithms.

3. Results

Molecular docking became a common method for bioactivity and drug design studies [38, 39]. In many published texts, experimental studies are supported by computational methods such as molecular docking [40, 41]. The action mechanisms and interactions of the molecules with biological macromolecules such as proteins and enzymes can be analyzed with this method. Besides, unlike the well-known and frequently used methods, these computational methods guide the future studies by using different target molecules [42, 43]. Due to the positive results obtained

from drug research of metal-based molecules, the bioactivity analysis of newly synthesized and characterized complexes is one of the important fields of chemical research and promising results have been obtained for many complexes. Cancer is still one of the major health problems in the world [44]. Therefore, it is important to investigate the anti-cancer activity of inorganic molecules. In cancer research, the standard procedures are in vitro [45, 46]. The studies show that anti-cancer agents affect with different mechanisms in different cancer types. For example, the vascular endothelial growth factor that is controlled by VEGF receptors is effective in cell growth, the proliferation of cancer cells, and metastasis. Among receptors, VEGFR-2 is efficient in thyroid, colorectal, and breast cancer cases. VEGFR-2 has also become a target molecule since the inhibition of VEGFR-2 can be used as a method in cancer treatment [47, 48].

In this study, the interactions between VEGFR-2 and NHC/Ag-NHC molecules that were previously analyzed for anti-cancer activities were investigated by the molecular docking method. **1a** has interacted with the region that formed by Leu887, Ile890, Val896, Val897, Leu1017, Cys1043, Cys1022, and Arg 1025 amino acids of VEGFR-2 with the binding energy of -5.74 kcal/mol. Effective alkyl and pi-alkyl interactions were noted, while no H-bond interaction was detected. The amide-pi stacked with Arg1025 and pi-cation with Cys1043 interactions of the molecule are remarkable. Although it is not high enough, van der Waals interactions have been noted for **1a** with Glu883, Ile1023, His1024, Ile1042, and Asp1044. **2a**, which is the silver complex of the **1a**, interacts with approximately the same region of VEGFR-2 with -6.18 kcal/mol binding energy. While the **2a** molecule represented pi-anion interactions with Glu 883 and Asp1044, amide-pi stacked interaction between benzimidazole ring of the molecule and Cys1043 was recorded. **2a** showed effective alkyl and pi-alkyl interactions, like **1a**. While alkyl and pi-alkyl interactions were calculated between Ile886, Ile890, Val896, Leu1017, Cys1022, and **2a**, van der Waals interactions were recorded with Leu887, Val897, Ile1023, His1024, Arg1025, and Ile1042. Binding properties and areas of **1b** and VEGFR-2 are different from **1a** and **2a**. The alkyl and pi-alkyl interactions of Val897, Leu887, Val846, Lys866, Ala864, and Cys917 with **1b** are efficient (Table 1, Fig. 2, and Fig. 3).

Table 1: Molecular docking results of the molecules for VEGFR-2 target

Molecules	Bind. Aff.*	Amino Acids Residue
		VEGFR-2 (1ywn)
1a	-5.74	Arg1025 (Pi-Cation), Cys1043 (Amide-Pi Stacked), Leu887, Ile890, Val896, Val897, Leu1017, Cys1022 (Pi-Alkyl), Glu883, His1024, Ile1023, Ile1042, Asp1044 (van de Waals)
1b	-6.97	Val914, Leu1033 (Pi-Sigma), Phe916 (Pi-Pi Stacked), Val846, Ala864, Lys866, Leu887, Val897, Cys917 (Pi-Alkyl), Glu883, Asp1044 (Carbon Hydrogen Bond), Val865, Val912, Glu915 (van der Waals)
1c	-7.40	Ile886 (Pi-Sigma), Arg1025 (Pi-Cation), Leu887, His889, Val896, Leu1017, Cys1022 (Pi-Alkyl), Glu883, Val897, His1024, Ile1042, Asp1044 (van der Waals)
2a	-6.18	Glu883, Asp1044 (Pi-Anion), Cys1043 (Amide-Pi Stacked), Ile886, Ile890, Val896, Leu1017, Cys1022 (Pi-Alkyl), Leu887, Val897, Ile1023, His1024, Arg1025, Ile1042 (van der Waals)
2b	-6.76	Ile886 (Pi-Sigma), Arg1025 (Pi-Cation), Cys1043 (Amide-Pi Stacked), Val896, Leu1017 (Pi-Alkyl), Glu883, Ile890, Val897, Ile1023, His1024, Ile1042, Asp1044 (van der Waals)
2c	-7.03	Leu1033 (Pi-Sigma), Leu838, Val846, Ala864, Val914, Cys917 (Pi-Alkyl), Gly839, Val897, Glu915, Phe916, Lys918, Gly920, Asn921 (van der Waals)

* Binding Affinity in kcal/mol.

Furthermore, the pi-sigma interactions between the benzimidazole residue and Val914, between naphthalene and Phe916 and, also pi-pi stacked interactions with Leu1033 can be examined in Fig. 2. In addition, carbon hydrogen-bonds of **1b** with Glu883 and Asp1044 were recorded. The binding energy of **1b** molecule with VEGFR-2 was calculated as -6.97 kcal/mol. The **2b**, which is the Ag complex of the **1b** ligand, differs from **1b** in terms of both binding site and binding types. Pi-alkyl interactions with Cys1022, Leu1017, and Val896, pi-cation interaction with Arg1025, pi-sigma interaction with Ile886, and amide-pi stacked interaction with Cys1043 contributed to the binding energy of **1b** with -6.76 kcal/mol. In addition, van der Waals interactions of the molecule can be pursued in the Fig. 2. It is noteworthy that **1c** performs less van der Waals interaction compared to other ligands. The binding energy was calculated for **1c** as -7.40 kcal/mol with the contribution of pi-cation, pi-sigma, amide-pi stacked and alkyl interactions. It can also be analyzed in Fig. 2 that **2c** makes only van der Waals, pi-sigma, and alkyl interactions. The binding energy of **2c** was calculated as -7.03 kcal/mol (Table 1, Fig. 2, and Fig. 3).

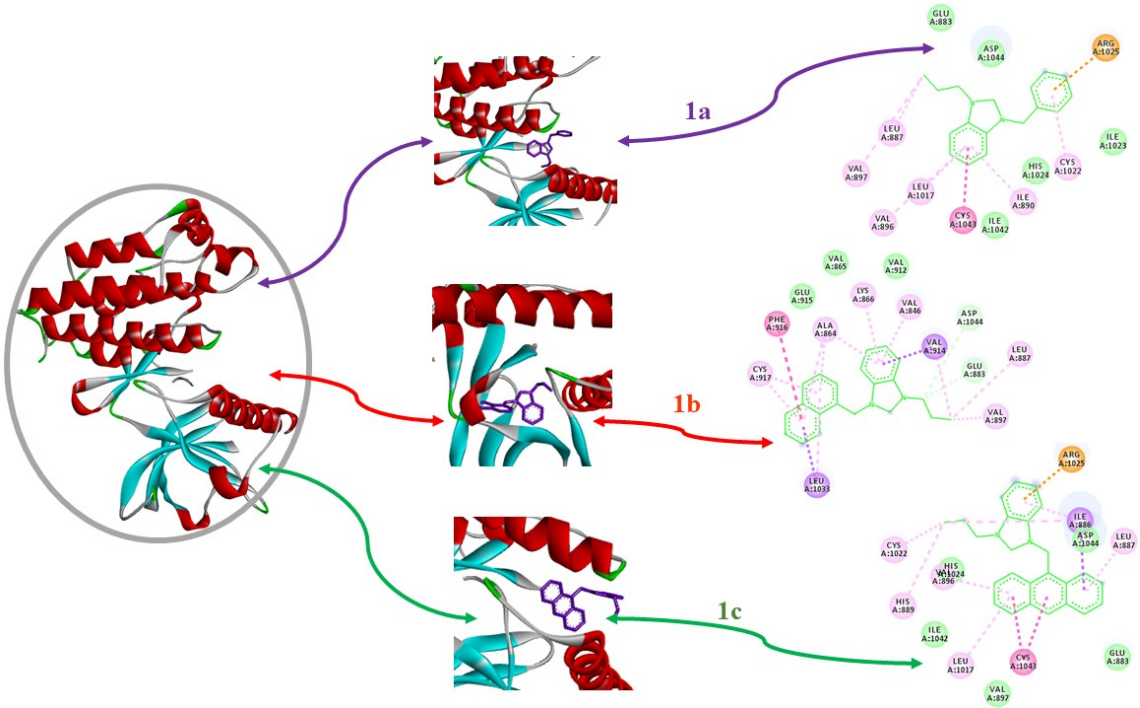

Figure 2: Graphical illustration of the interactions between VEGFR-2 and the molecules (center: ribbon style crystallographic structure of VEGFR-2; the arrows guided the interactions, purple: **1a**; red: **1b**; green: **1c**)

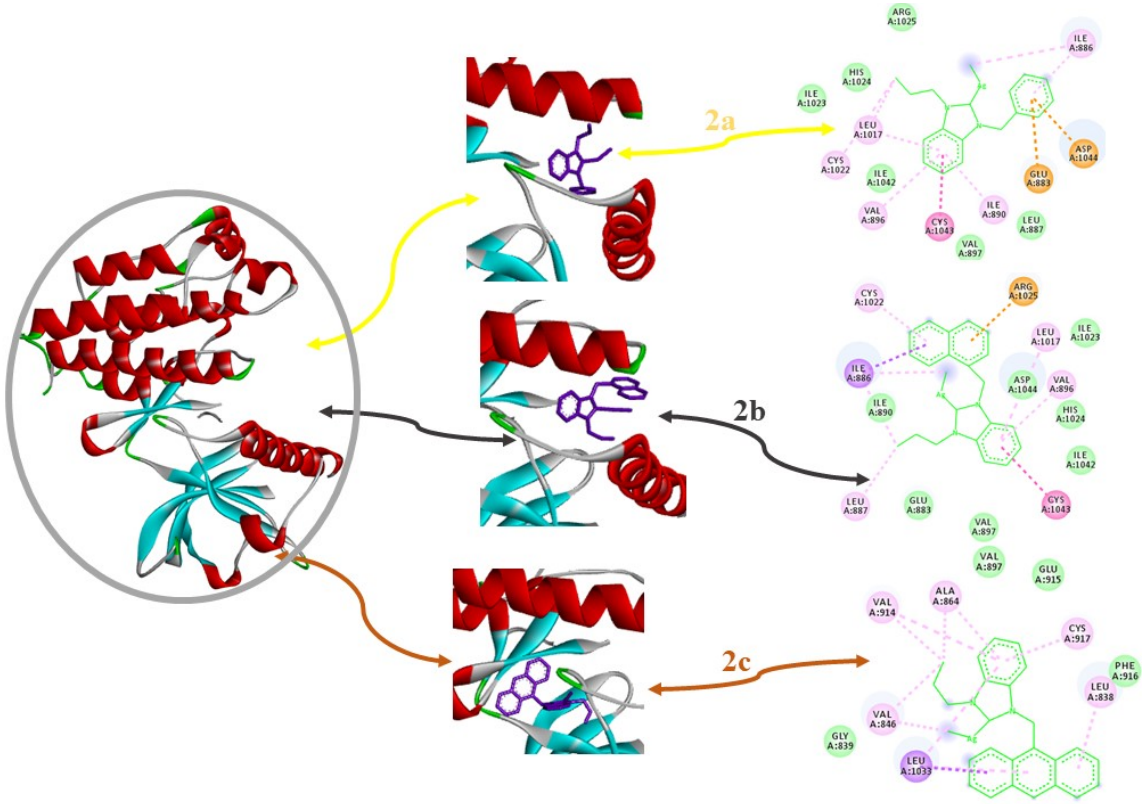

Figure 3: Graphical illustration of the interactions between VEGFR-2 and the molecules (center: ribbon style crystallographic structure of VEGFR-2; the arrows guided the interactions, yellow: **2a**; grey: **2b**; brown: **2c**)

In experimental studies of the molecules, activity values were examined both for different cancer types and different intervals. Binding energies are generally considered as a suitable criterion for comparing experimental and theoretical results. According to the theoretical results detailed above, it is possible to say that **1c** is the most active of the ligands while the most active complex is **2c**. These results agree with experimental results [34]. On the other hand, the experimental activity results of complex molecules were higher than the ligands, but the theoretical results were not compatible with this result.

One of the most frequently used analyzes when examining the activity of molecules is evaluating the position of the interactions of molecules with DNA [49]. The interaction of molecules with DNA is important in terms of getting insight for future studies [50]. DNA Dodecamer structure (pdb id:1BNA) was used to analyze the interaction (Fig. 4). All of the molecules interact with nearly the same region of DNA. **1a** with Cyt9 and Gua10, **1b** was interacted with Thy7 and Thy8, **1c** was interacted with Gua10 and Cyt11. The Ag complexes of these molecules were interacted with the similar region of DNA. **2a**, **2b**, and **2c** were interacted with Cyt9 and Gua10. It is noteworthy that unlike **2a** and **2b**, **2c** was also interacted with Thy7.

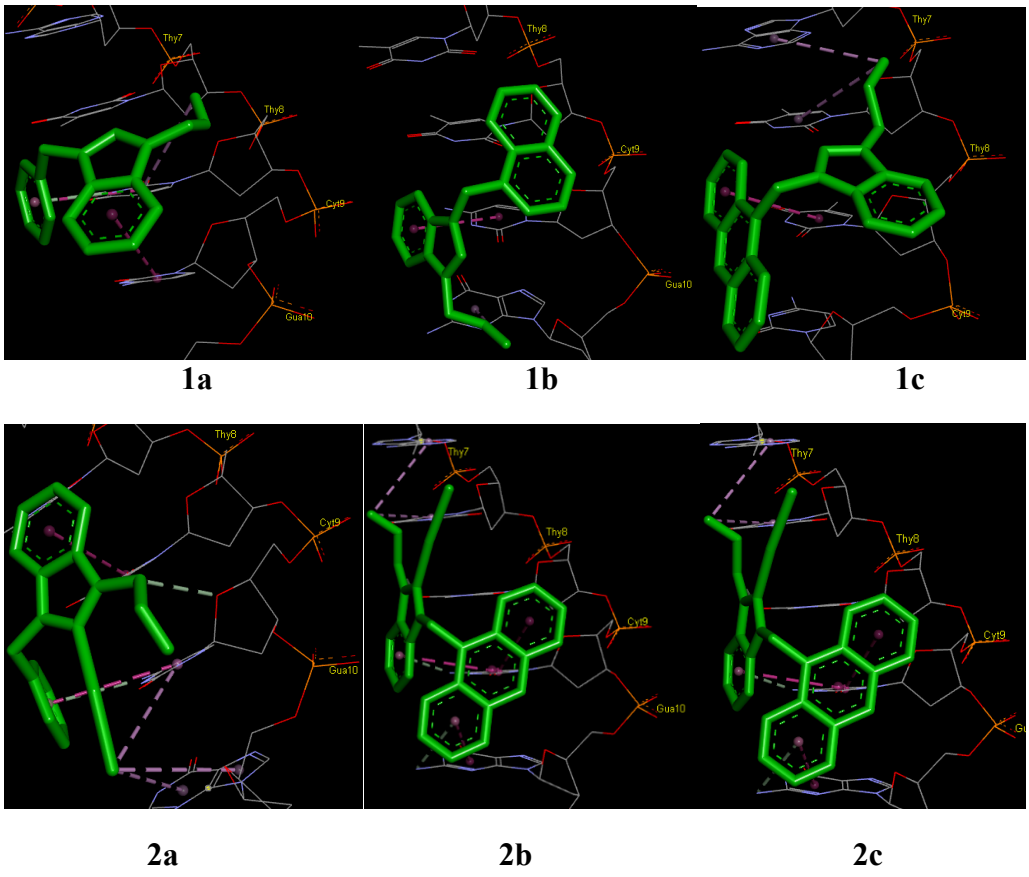

Figure 4: Graphical illustration of the interactions between DNA dodecamer and the molecules

5. Conclusions

The developments in *in-silico* studies in recent years are remarkable. Therefore, these methods are considered essential tools in bioactivity and drug design studies. Most of the empirical work is now supported by theoretical calculations. Molecular docking studies are one of the leading *in-silico* studies. In this study, molecular docking analysis of the complexes, whose activity was experimentally investigated previously, was performed. The first molecular docking analysis was performed using VEGFR-2, which is effective in the cell growth, proliferation of cancer cells, and metastasis. The obtained results are partially consistent with the experimental results. Secondly, the interaction of molecules with DNA was analyzed. As it is known, many mechanisms of action are known to be effective in cancer treatments. One of them is analyzed in this study. The augmentation of these studies is important in terms of getting foresight in future studies. In the future, it is planned to continue *in-silico* studies with different target molecules of different effect mechanisms.

Acknowledgement

The authors would like to thank the Technological and Scientific Research Council of Turkey (TÜBİTAK-3001, Project Number: 118R045).

References

[1] Auerbach, W., Auerbach, R., *Angiogenesis inhibition: a review,* Pharmacology & Therapeutics, 63(3), 265-311, 1994.

[2] Otrock, Z.K., Mahfouz, R.A., Makarem, J.A., Shamseddine, A.I., *Understanding the biology of angiogenesis: review of the most important molecular mechanisms,* Blood Cells, Molecules, and Diseases, 39(2), 212-220, 2007.

[3] Weidner, N., *Tumor angiogenesis: review of current applications in tumor prognostication,* In Seminars in Diagnostic Pathology, 10(4), 302-313, 1993.

[4] Shahi, P.K., Pineda, I.F., *Tumoral angiogenesis: review of the literature,* Cancer Investigation, 26(1), 104-108, 2008.

[5] Ferrara, N., *Vascular endothelial growth factor and the regulation of angiogenesis,* Recent Progress in Hormone Research, 55, 15-35, 2000.

[6] Chung, A.S., Ferrara, N., *Developmental and pathological angiogenesis*, Annual Review of Cell and Developmental Biology, 27, 563-584, 2011.

[7] Matulonis, U.A., Berlin, S., Ivy, P., Tyburski, K., Krasner, C., Zarwan, C., Lee, H., Cediranib, *An oral inhibitor of vascular endothelial growth factor receptor kinases, is an active drug in recurrent epithelial ovarian, fallopian tube, and peritoneal cancer,* Journal of clinical oncology, 27(33), 5601-5606, 2009.

[8] Parr, C., Watkins, G., Boulton, M., Cai, J., Jiang, W.G., *Placenta growth factor is over-expressed and has prognostic value in human breast cancer,* European Journal of Cancer, 41(18), 2819-2827, 2005.

[9] Strumberg, D., *Preclinical and clinical development of the oral multikinase inhibitor sorafenib in cancer treatment,* Drugs Today (Barc), 41(12), 773-784, 2005.

[10] Zhang, P.C., Liu, X., Li, M.M., Ma, Y.Y., Sun, H.T., Tian, X.Y., Chen, H.Y., *AT-533, a novel Hsp90 inhibitor, inhibits breast cancer growth and HIF-1α/VEGF/VEGFR-2-mediated angiogenesis in vitro and in vivo,* Biochemical Pharmacology, 172, 113771, 2020.

[11] Sana, S., Reddy, V.G., Bhandari, S., Reddy, T.S., Tokala, R., Sakla, A.P., Shankaraiah, N., *Exploration of carbamide derived pyrimidine-thioindole conjugates as potential VEGFR-2 inhibitors with anti-angiogenesis effect,* European Journal of Medicinal Chemistry, 112457, 2020.

[12] Abdel-Mohsen, H.T., Abdullaziz, M.A., Kerdawy, A.M.E., Ragab, F.A., Flanagan, K.J., Mahmoud, A.E., Senge, M.O., *Targeting Receptor Tyrosine Kinase VEGFR-2 in Hepatocellular Cancer: Rational Design, Synthesis and Biological Evaluation of 1, 2-Disubstituted Benzimidazoles*, Molecules, 25(4), 770, 1-37, 2020.

[13] El- Adl, K., El- Helby, A.G.A., Sakr, H., Ayyad, R.R., Mahdy, H.A., Nasser, M., El-Hddad, S.S., *Design, synthesis, molecular docking, anticancer evaluations, and in silico pharmacokinetic studies of novel 5- [(4- chloro/2, 4- dichloro) benzylidene] thiazolidine- 2, 4-dione derivatives as VEGFR- 2 inhibitors*, Archiv der Pharmazie, e2000279, 2020.

[14] Abou-Seri, S.M., Eldahna, W.M. Ali, M.M., and Ella, A.E., *1-Piperazinylphthalazines as potential VEGFR-2 inhibitors and anticancer agents: Synthesis and in vitro biological evaluation,* European Journal of Medicinal Chemistry, 107, 165-179, 2016.

[15] Michalak, E.M., Burr, M.L., Bannister, A.J., Dawson, M.A., *The roles of DNA, RNA and histone methylation in ageing and cancer,* Nature Reviews Molecular Cell Biology, 1, 2019.

[16] Zhang, J., Yang, C., Wu, C., Cui, W., and Wang, L., *DNA Methyltransferases in Cancer: Biology, Paradox, Aberrations, and Targeted Therapy*, Cancers, 12(8), 2123, 2020.

[17] Alhmoud, J.F., Woolley, J.F., Moustafa, A.E.A., Malki, M.I., *DNA Damage/Repair Management in Cancers,* Cancers, 12(4), 1050, 2020.

[18] Goessl, C., Müller, M., Straub, B., and Miller, K., *DNA alterations in body fluids as molecular tumor markers for urological malignancies*, European Urology, 41(6), 668-676, 2002.

[19] Öfele, K., 1*, 3-Dimethyl-4-imidazolinyliden-(2)-pentacarbonylchrom ein neuer Übergangsmetall-carben-komplex,* Journal of Organometallic Chemistry, 12(3), 42-43, 1968.

[20] Wanzlick, H.W., Schönherr, H.J., *Direct synthesis of a mercury salt- carbene complex,* Angewandte Chemie International Edition in English, 7(2), 141-142, 1968.

[21] Diez-Gonzalez, S., Marion, N., Nolan, S.P., *N-heterocyclic carbenes in late transition metal catalysis,* Chemical Reviews, 109(8), 3612-3676, 2009.

[22] Feller, D., Borden, W.T., Davidson, E.R*., Dependence of the singlet-triplet splitting in heterosubstituted carbenes on the heteroatom electronegativity and conformation,* Chemical Physics Letters, 71(1), 22-26, 1980.

[23] Sarı, Y., Gürses, C., Celepci, D.B., Keleştemur, Ü., Aktaş, A., Yüksel, Ş., Gök, Y., *4-Vinylbenzyl and 2-morpholinoethyl substituted ruthenium (II) complexes: Design, synthesis, and biological evaluation*, Journal of Molecular Structure, 1202, 127355, 2020.

[24] Simpson, P.V., Schmidt, C., Ott, I., Bruhn, H., Schatzschneider, U., *Synthesis, Cellular Uptake and Biological Activity Against Pathogenic Microorganisms and Cancer Cells of Rhodium and Iridium N- Heterocyclic Carbene Complexes Bearing Charged Substituents*, European Journal of Inorganic Chemistry, 2013(32), 5547-5554, 2013.

[25] Şahin, N., Şahin-Bölükbaşı, S., Tahir, M.N., Arıcı, C., Cevik, E., Gürbüz, N., Cummings, B.S., *Synthesis, characterization and anticancer activity of allyl substituted N-Heterocyclic carbene silver(I) complexes,* Journal of Molecular Structure, 1179, 92-99, 2019.

[26] Rehm, T., Rothemund, M., Muenzner, J. K., Noor, A., Kempe, R., Schobert, R., *Novel cis-[(NHC)^1 (NHC)^2(L)Cl]platinum(II) complexes–synthesis, structures, and anticancer activities,* Dalton Transactions, 45(39), 15390-15398, 2016.

[27] Hackenberg, F., Müller-Bunz, H., Smith, R., Streciwilk, W., Zhu, X., Tacke, M., *Novel ruthenium (II) and gold (I) NHC complexes: Synthesis, characterization, and evaluation of their anticancer properties*, Organometallics, 32(19), 5551-5560, 2013.

[28] Düşünceli, S.D., Ayaz, D., Üstün, E., Günal, S., Özdemir, N., Dinçer, M., Özdemir, İ., *Synthesis, antimicrobial properties, and theoretical analysis of benzimidazole-2-ylidene silver(I) complexes,* Journal of Coordination Chemistry, 73(13), 1967-1986, 2020.

[29] Hosseini, F.S., & Amanlou, M., *Anti-HCV and anti-malaria agent, potential candidates to repurpose for coronavirus infection: Virtual screening, molecular docking, and molecular dynamics simulation study,* Life Sciences, 258, 118205, 2020.

[30] Akkoç, S., Yavuz, S.Ç., Türkmenoğlu, B., İlhan, İ.Ö., Akkurt, M., *Single Crystal, DFT and Docking Studies of a Benzimidazolium Salt*, Crystallography Reports, 65, 1173-1178, 2020.

[31] Velihina, Y., Scattolin, T., Bondar, D., Pil'o, S., Obernikhina, N., Kachkovskyi, O., Semenyuta, I., Caligiuri, I., Rizzolio, F., Brovarets, V., Karpichev, Y., Nolan, S.P., *Synthesis, in silico and in vitro Evaluation of Novel Oxazolopyrimidines as Promising Anticancer Agents,* Helvetica Chimica Acta, 103(12), ee2000169, 2020.

[32] Yavuz, S.Ç., Akkoç, S., Türkmenoğlu, B., Sarıpınar, E., *Synthesis of novel heterocyclic compounds containing pyrimidine nucleus using the Biginelli reaction: Antiproliferative activity and docking studies,* Journal of Heterocyclic Chemistry, 57(6), 2615-2627, 2020.

[33] Radwan, M.A., Alshubramy, M.A., Abdel-Motaal, M., Hemdan, B.A., El-Kady, D. S., *Synthesis, molecular docking and antimicrobial activity of new fused pyrimidine and pyridine derivatives,* Bioorganic Chemistry, 96, 103516, 2020.

[34] Çevik-Yıldız, E., Şahin, N., Şahin-Bölükbaşı, S., *Synthesis, characterization, and investigation of antiproliferative activity of novel Ag(I)-N-Heterocyclic Carbene (NHC) compounds,* Journal of Molecular Structure, 1199, 126987, 2020.

[35] Neese, F., *A critical evaluation of DFT, including time-dependent DFT, applied to bioinorganic chemistry*, JBIC Journal of Biological Inorganic Chemistry, 11(6), 702-711, 2006.

[36] Neese, F.*, Prediction of molecular properties and molecular spectroscopy with density functional theory: From fundamental theory to exchange-coupling,* Coordination Chemistry Reviews, 253(5-6), 526-563, 2009.

[37] https://www.rcsb.org/ Protein Data Bank (PDB)

[38] Islam, M.A., & Pillay, T.S., *Identification of promising anti-DNA gyrase antibacterial compounds using de novo design, molecular docking and molecular dynamics studies,* Journal of Biomolecular Structure and Dynamics, 38(6), 1798-1809, 2020.

[39] Sivakumar, K.C., Haixiao, J., Naman, C.B., & Sajeevan, T.P., *Prospects of multitarget drug designing strategies by linking molecular docking and molecular dynamics to explore the protein–ligand recognition process,* Drug Development Research, 81(6), 685-699, 2020.

[40] Vidhya, V., Austine, A., & Arivazhagan, M., *Experimental approach, theoretical investigation and molecular docking of 2-chloro-5-fluoro phenol antibacterial compound,* Heliyon, 6(11), e05464, 2020.

[41] Qiu, Y., Li, X., He, X., Pu, J., Zhang, J., Lu, S., *Computational methods-guided design of modulators targeting protein-protein interactions (PPIs),* European Journal of Medicinal Chemistry, 207, 112764, 2020.

[42] Dana, H., Chalbatani, G.M., Gharagouzloo, E., Miri, S.R., Memari, F., Rasoolzadeh, R., Marmari, V., *In silico Analysis, Molecular Docking, Molecular Dynamic, Cloning, Expression and Purification of Chimeric Protein in Colorectal Cancer Treatment,* Drug Design, Development and Therapy, 14, 309, 2020.

[43] Acharya, R., Chacko, S., Bose, P., Lapenna, A., Pattanayak, S.P., *Structure based multitargeted molecular docking analysis of selected furanocoumarins against breast cancer,* Scientific Reports, 9(1), 1-13, 2019.

[44] Hashim, D., Carioli, G., Malvezzi, M., Bertuccio, P., Waxman, S., Negri, E., Boffetta, P., *Cancer mortality in the oldest old: a global overview*, Aging (Albany NY), 12(17), 16744, 2020.

[45] Meng, X., Ye, L., Yang, Z., Xiang, R., Wang, J., *Adsorption behavior of melphalan anti-ovarian cancer drug onto boron nitride nanostructures, Studying MTT assay: in vitro cellular toxicity and viability*, Chemical Papers, 1-6, 2020.

[46] Vetrivel, P., Kim, S.M., Ha, S.E., Kim, H.H., Bhosale, P.B., Senthil, K., Kim, G.S., *Compound Prunetin Induces Cell Death in Gastric Cancer Cell with Potent Anti-Proliferative Properties: In Vitro Assay, Molecular Docking, Dynamics, and ADMET Studies,* Biomolecules, 10(7), 1086, 2020.

[47] Ahmed, E.Y., Latif, N.A.A., El-Mansy, M.F., Elserwy, W.S., Abdelhafez, O.M., *VEGFR-2 inhibiting effect and molecular modeling of newly synthesized coumarin derivatives as anti-breast cancer agents,* Bioorganic & Medicinal Chemistry, 28(5), 115328, 2020.

[48] Cheng, K., Liu, C.F., Rao, G.W., Anti-angiogenic Agents: A Review on Vascular Endothelial Growth Factor Receptor-2 (VEGFR-2) Inhibitors, Current Medicinal Chemistry, 20(1), 2020. Doi:10.2174/092986732766620051408242 5

[49] Jackson, S.P., *The DNA-damage response: new molecular insights and new approaches to cancer therapy,* Biochemical Society Transactions, 37(3), 483-494, 2009.

[50] Gupta, R.K., Sharma, G., Pandey, R., Kumar, A., Koch, B., Li, P.Z., Pandey, D.S., *DNA/protein binding, molecular docking, and in vitro anticancer activity of some thioether-dipyrrinato complexes*, Inorganic Chemistry, 52(24), 13984-13996, 2013.

Adıyaman University Journal of Science
https://dergipark.org.tr/en/pub/adyujsci
DergiPark AKADEMİK
ISSN 2147-1630
e-ISSN 2146-586X

Optical Solutions of the Kundu-Eckhaus Equation via Two Different Methods

Melike KAPLAN[1,*]

[1]*Kastamonu University, Faculty of Art and Science, Department of Mathematics, 37150, Kastamonu, Turkey*
mkaplan@kastamonu.edu.tr, ORCID: 0000-0001-5700-9127

Received: 10.12.2020 **Accepted:** 14.05.2021 **Published:** 30.06.2021

Abstract

This work is devoted to obtaining new optical solutions to the Kundu-Eckhaus (KE) equation which is believed to play a crucial part in the area of nonlinear optics. Two different methods, the $\exp(-\varphi(\varepsilon))$ method with the exponential rational function approach have been utilized. Both methods are efficient in finding the analytical solutions of many nonlinear partial differential equations and fractional differential equations. Results obtained in this research are dissimilar to the ones in the literature and the solutions are controlled by relocating them back to the primary equation. Finally, it can be stated that optical solutions have a promising future.

Keywords: Nonlinear equation; Symbolic computation; Optical solutions.

Kundu-Eckhaus Denkleminin İki Farklı Yöntemle Optik Çözümleri

Öz

Bu çalışmada, lineer olmayan optik alanında önemli bir yere sahip olan Kundu-Eckhaus (KE) denkleminin optik çözümlerinin elde edilmesine yer verilmiştir. $\exp(-\varphi(\varepsilon))$ yöntemi ve üstel rasyonel fonksiyon yöntemi ilgili denkleme uygulanmıştır. Bahsedilen her iki yöntem de lineer olmayan kısmi diferensiyel denklemler ve kesir mertebeden diferensiyel denklemlerin tam çözümlerinin elde edilmesinde oldukça etkili olduğu bilinen yöntemlerdir. Bu çalışmada elde

* Corresponding Author DOI: 10.37094/adyujsci.838536

edilen sonuçlar, literatürde daha önce var olanlardan farklıdır. Elde edilen çözümler, Maple yardımıyla yerine konularak kontrol edilmiştir. Sonuç olarak, optik çözümlerin literatürde önemli bir geleceğinin olduğunu belirtmeliyiz.

Anahtar Kelimeler: Lineer olmayan denklem; Sembolik hesaplama; Optik çözümler.

1. Introduction

A lot of real-world problems in the vast areas of engineering and science are modeled by nonlinear evolution equations (NLEEs). Looking for the exact solutions of NLEEs is quite crucial for one to understand the phenomena described by the NLEEs. The analytical expressions of NLEEs were researched using various powerful techniques. Some of these methods are Auto-Backlund transformations[1], modified simple equation method [2], transformed rational function method [3], trial method [4], the sine-Gordon expansion method [5], the (G'/G)- expansion method [6], (G'/G,1/G)-expansion method [7], auxiliary equation method [8, 9], exp-function method [10], F-expansion method [11], sine-cosine method [12], ansatz method [13], sub equation method [14], exponential rational function method [15], Lie group analysis [16], Hirota bilinear method [17], Backlund transformation method [18], Wronskian technique [19], homogeneous balance method [20], inverse scattering method [21], and so on [22]. Regarding the domain of research in photonics sciences, optical solitons is considered among the most rapidly emerging fields. Recently, this technique is widely used by scientists [23, 24, 25].

The $\exp(-\varphi(\varepsilon))$ method is a new and useful method that gives many solutions to NLEEs. The supremacy of the suggested technique toward the (G'/G)-expansion scheme requires to give fresh travelling wave solutions while using arbitrary additional parameters [26, 27]. The other technique utilized in the paper, the exponential function method, is a straight method.

The style implemented in this article can be described as follows: In the Part of Materials and Methods, the primary stages of methods are introduced. In Section III, the implementation of the techniques to the Kundu-Eckhaus is given. Finally, the conclusion of the paper is provided.

2. Materials and Methods

A general NLEE of the formula will be taken into consideration:

$$P(u, u_{x,} u_t, u_{xx}, u_{xt}, u_{tt}, \dots) = 0, \quad (1)$$

The polynomial and derivates of $u = u(x,t)$ are represented by P, where the nonlinear terms and the highest order derivatives are comprised. In a suitable manner of the following travelling wave transformation

$$\xi = x - ct, u(x,t) = U(\xi),$$

where c represents the velocity of the wave, Eqn. (1) is reduced thereby forming an ordinary differential equation (ODE) in the form

$$Q(U, U', U'', U''', \dots) = 0. \tag{2}$$

It is noted that, in Eqn. (2) the differentiation of U with respect to ξ is represented by prime. All the terms in Eqn. (2) will be integrated.

2.1.The exp(−φ(ξ)) method

Conforming to this technique [27], the desired solution for the reduced equation is formed by a polynomial in exp(−φ (ξ)) as

$$\mathrm{U}(\xi) = \sum_{\mathrm{n}=0}^{\mathrm{m}} a_n \left(\exp\left(-\varphi(\xi)\right)\right)^{\mathrm{n}},$$

where $a_n, (a_m \neq 0)$ are constants which will be found afterwards and φ (ξ) is the solution of the following ODE below

$$\varphi^{\iota}(\xi) = exp\left(-\varphi(\xi)\right) + \mu\, exp\left(\varphi(\xi)\right) + \lambda. \tag{3}$$

The supplementary equation Eqn. (3) possesses distinct solutions below:

Case 1: When $\lambda^2 - 4\mu > 0$ and $\mu \neq 0$, the hyperbolic function solutions,

$$\varphi_1(\xi) = \ln\left(\frac{-\sqrt{\lambda^2-4\mu}\tanh\left(\sqrt{\frac{\lambda^2-4\mu}{2}}(\xi+C)\right)-\lambda}{2\mu}\right). \tag{4}$$

Case 2: When $\lambda^2 - 4\mu < 0$ and $\mu \neq 0$, trigonometric function solutions,

$$\varphi_2(\xi) = \ln\left(\frac{\sqrt{4\mu-\lambda^2}\tan h\sqrt{\frac{4\mu-\lambda^2}{2}}(\xi+C))-\lambda}{2\mu}\right). \tag{5}$$

Case 3: When $\lambda^2 - 4\mu > 0$, $\mu \neq 0$ and $\lambda \neq 0$, hyperbolic function solutions,

$$\varphi_3(\xi) = -\ln\left(\frac{\lambda}{\cosh\left(\lambda(\xi+C)\right)+\sinh\left(\lambda(\xi+C)\right)-1}\right). \tag{6}$$

Case 4: When $\lambda^2 - 4\mu = 0$, $\mu \neq 0$ and $\lambda \neq 0$, rational function solutions,

$$\varphi_4(\xi) = \ln\left(-\frac{2(\lambda+(\xi+C)+2)}{\lambda^2(\xi+C)}\right). \tag{7}$$

Case 5: When $\lambda^2 - 4\mu = 0$, $\mu = 0$ and $\lambda = 0$,

$$\varphi_5(\xi) = \ln(\xi + C). \tag{8}$$

2.2. The exponential rational function method

In agreement with this technique, Eqn. (2)'s solitary wave solution is assumed as [21, 22]:

$$U(\xi) = \sum_{n=0}^{N} \frac{a_n}{(1+\exp(\xi)^n}, \tag{9}$$

where $a_n (a_N \neq 0)$ are constants which will be determined afterwards. It can be noted that congruently N is a balancing number. Here the same logic steps in and, on subrogating Eqn. (9) in Eqn. (2), then gathering all the terms in the similar order of exp(iξ), (i = 0,1,2, ...), the left-hand side of Eqn. (2) is converted into a new polynomial in exp(iξ). Later on, one can equate every coefficient of the obtained polynomial to zero in order to solve the system. Consequently, the solutions of the system can be calculated using the assistance of the Maple that gives the desired solitary wave solutions of Eqn. (1).

3. Results and Discussion

3.1. Mathematical analysis

Kundu-Eckhaus (KE) equation, founded by Kundu [28] and Eckhaus [29], is chosen to implement how the methods work. This equation supplies a different model for the solitons transmission along optical fibers. This equation, within the nonlinear Schrödinger class, is a fundamental model which is modelling optical soliton promulgation in Kerr media. The magnitude of the incident light field to generate ultrashort (femtosecond) optical pulses in optic fiber communications systems must be adjusted [30].

$$i\frac{\partial^{\alpha} q(x,t)}{\partial t^{\alpha}} + a\frac{\partial^2 q(x,t)}{\partial x^2} + b|q(x,t)|^4 q(x,t) + c\frac{\partial(|q(x,t)|^2)}{\partial x} q(x,t) = 0. \tag{10}$$

Here complex-valued wave profile represents by $q(x,t)$. Eqn. (10)'s first term involves the temporal evolution of the nonlinear wave, whereas the real-valued constants c, b and a denote, nonlinear effect, quintic nonlinearity, group velocity dispersion and respectively.

Analysis of Eqn. (10) gives:

$$q(x,t) = \sqrt{v(s)}e^{i\Phi(x,t)}, \tag{11}$$

where $v(s)$ denotes the form of the pulse and

$$s = k(x + 2a\kappa\ \frac{t^{\alpha}}{\alpha}),$$

and the phase component is denoted as shown below.

$$\Phi(x,t) = -\kappa x + \omega((t^{\alpha})/\alpha) + \theta_0,$$

where $\omega =$ wave number of the soliton, $\kappa =$ soliton frequency, and $\theta_0 =$ phase constant.

Then by subrogating Eqn. (11) in Eqn. (10) and dividing them into imaginary and real parts the following equation is obtained.

$$2ak^2vv'' + 4ckv^2v' - ak^2(v')^2 - 4(\omega + a\kappa^2)v^2 + 4bv^4 = 0. \quad (12)$$

According to homogenous balance principle, balancing vv'' with v^4 gives $N = 1$.

3.2. The exp(−φ(ξ)) method

In accordance with idea of the adopted method gives the solution of Eqn. (12) below.

$$v(\xi) = a_0 + a_1 exp(-\varphi(\xi)). \quad (13)$$

The equation system consisting of $a, b, c, k, a_0, a_1, \lambda, \mu, \omega, \kappa$ could be found by substituting Eqn. (13) into Eqn. (12), gathering the coefficient of every term of $\exp(-\varphi(\xi))^n$ and equating all coefficients to zero.

$$\exp(4\xi): -ak^2{a_1}^2\mu^2 - 4cka_1{a_0}^2\mu + 4b{a_0}^4 - 4\omega{a_0}^2 - 4a\kappa^2{a_0}^2 + 2ak^2a_0a_1\mu\lambda = 0,$$

$$\exp(3\xi): -8\omega a_0a_1 + 16b{a_0}^3a_1 + 2ak^2a_0a_1\lambda^2 - 8a\kappa^2a_0a_1 - 4cka_1{a_0}^2\lambda - 8cka_1{a_1}^2a_0\mu + 4ak^2a_0a_1\mu = 0,$$

$$\exp(2\xi): -4cka_1{a_0}^2 + 6ak^2a_0a_1\lambda - 4cka_1{}^3\mu - 8cka_1{a_1}^2a_0\lambda - 4a\kappa^2{a_1}^2 - 4\omega{a_1}^2 + 24b{a_0}^2{a_1}^2 + a{a_0}^2{a_1}^2\lambda^2 + 2ak^2{a_1}^2\mu = 0,$$

$$\exp(1\xi): 4ak^2a_0a_1 + 16ba_0{a_1}^3 - 8cka_1{}^2a_0 - 4cka_1{}^3\lambda + 4ak^2{a_1}^2\lambda = 0,$$

$$\exp(0\xi): 3ak^2{a_1}^2 - 4cka_1{}^3 + 4b{a_1}^4 = 0.$$

Utilisation of software programs gives the solution as follows:

$$a_0 = \frac{\left(\frac{\lambda}{2} + \frac{\sqrt{\lambda^2 - 4\mu}}{2}\right)ck}{4b}, \quad a_1 = \frac{ck}{4b}, \quad a = \frac{c^2}{4b}, \quad \omega = -\frac{(4\kappa^2 - k^2\lambda^2 + 4k^2\mu)c^2}{16b}.$$

These obtained values, the algorithm of the method and its auxiliary equations, gives the various optical solutions for KE equation:

Case 1: $\lambda^2 - 4\,\mu > 0$ and $\mu \neq 0$, according to Eqn. (4),

The hyperbolic function solutions:

$$q_1(x,t) = \sqrt{\frac{\left(\frac{\lambda}{2}+\frac{\sqrt{\lambda^2-4\mu}}{2}\right)ck}{4b} - \frac{2ck\mu}{4b\sqrt{\lambda^2-4\mu}\tanh\left(\frac{\sqrt{\lambda^2-4\mu}}{2}\left(kx+2ak\kappa\frac{t^\alpha}{\alpha}\right)\right)+4b\lambda}} \times exp\left(i(-\kappa x+\omega\frac{t^\alpha}{\alpha}+\theta_0)\right).$$

Case 2: $\lambda^2 - 4\,\mu < 0$ and $\mu \neq 0$, according to Eqn. (5),

The trigonometric function solutions:

$$q_2(x,t) = \sqrt{\frac{\left(\frac{\lambda}{2}+\frac{\sqrt{\lambda^2-4\mu}}{2}\right)ck}{4b} + \frac{2ck\mu}{4b\sqrt{4\mu-\lambda^2}\tan\left(\frac{\sqrt{4\mu-\lambda^2}}{2}\left(kx+2ak\kappa\frac{t^\alpha}{\alpha}\right)\right)-\lambda}} \times exp\left(i(-\kappa x+\omega\frac{t^\alpha}{\alpha}+\theta_0)\right).$$

Case 3: $\lambda^2 - 4\,\mu > 0$, $\mu = 0$ and $\lambda \neq 0$, according to Eqn. (6),

The hyperbolic function solutions:

$$q_3(x,t) = \sqrt{\frac{\left(\frac{\lambda}{2}+\frac{\sqrt{\lambda^2-4\mu}}{2}\right)ck}{4b} + \frac{ck\lambda}{4b\cosh(\lambda(kx+2ak\kappa\frac{t^\alpha}{\alpha}+C))+4b\sinh(\lambda(kx+2ak\kappa\frac{t^\alpha}{\alpha}+C))-4b}}$$
$$\times exp\left(i(-\kappa x+\omega\frac{t^\alpha}{\alpha}+\theta_0)\right).$$

Case 4: When $\lambda^2 - 4\,\mu = 0$, $\mu \neq 0$ and $\lambda \neq 0$, according to Eqn.(7),

The rational function solutions:

$$q_4(x,t) = \sqrt{\frac{\left(\frac{\lambda}{2}+\frac{\sqrt{\lambda^2-4\mu}}{2}\right)ck}{4b} - \frac{\lambda^2 ck(kx+2ak\kappa\frac{t^\alpha}{\alpha}+C)}{8b\lambda kx+16b\lambda ak\kappa\frac{t^\alpha}{\alpha}+8bC+16b}} \times exp\left(i(-\kappa x+\omega\frac{t^\alpha}{\alpha}+\theta_0)\right).$$

Case 5: $\lambda^2 - 4\,\mu = 0$, $\mu = 0$ and $\lambda = 0$, according to Eqn.(8),

$$q_5(x,t) = \sqrt{\frac{ck}{4bkx+8bak\kappa\frac{t^\alpha}{\alpha}+4bC}} \times exp\left(i(-\kappa x+\omega\frac{t^\alpha}{\alpha}+\theta_0)\right).$$

3.3 The exponential rational function method

Optical solutions of the reduced form of KE equation which is Eqn. (12) can be assumed as follows:

$$v(\xi) = a_0 + \frac{a_1}{1+exp(\xi)}, \tag{14}$$

a polynomial of exp(iξ) (i = 0,1, ...4) can be obtained. Then by adjusting the powers of the obtained polynomial to zero, one can find the equation system below.

$$\begin{aligned}
&\exp(4\xi): -4a\kappa^2{a_0}^2 - 4\omega{a_0}^2 + 4b{a_0}^4 = 0\\
&\exp(3\xi): 2ak^2a_0a_1 + 16b{a_0}^3a_1 - 16a\kappa^2{a_0}^2 - 16\omega{a_0}^2 - 8\omega a_0a_1\\
&\qquad -8a\kappa^2a_0a_1 - 4cka_1{a_0}^2 + 16b{a_0}^4 = 0,\\
&\exp(2\xi): -24a\kappa^2a_0a_1 - 24a\kappa^2{a_0}^2 + 24b{a_0}^2{a_1}^2 + 48b{a_0}^3a_1 - 4a\kappa^2{a_1}^2 - 4\omega{a_1}^2\\
&\qquad -24\omega{a_0}^2 - 24\omega a_0a_1 + 24b{a_0}^4 + ak^2{a_1}^2 - 8cka_1{}^2a_0 - 8cka_1{a_0}^2 = 0,\\
&\exp(1\xi): -2ak^2a_0a_1 - 4cka_1{a_0}^2 - 16a\kappa^2{a_0}^2 - 2ak^2{a_1}^2 - 4cka_1{}^3\\
&\qquad -24a\kappa^2a_0a_1 - 8a\kappa^2{a_1}^2 + 48b{a_0}^2{a_1}^2 + 48b{a_0}^3a_1\\
&\qquad +16ba_0{a_1}^3 - 8cka_1{}^2a_0 - 16\omega{a_0}^2 - 24\omega a_0a_1 + 16b{a_0}^4 - 8\omega{a_1}^2 = 0,\\
&\exp(0\xi): -4\omega{a_0}^2 + 4b{a_0}^4 - 4\omega{a_1}^2 + 4b{a_1}^4 - 4a\kappa^2{a_0}^2 - 8\omega a_0a_1 - 4a\kappa^2{a_1}^2\\
&\qquad +16b{a_0}^3a_1 + 24b{a_0}^2{a_1}^2 + 16ba_0{a_1}^3 - 8a\kappa^2a_0a_1 = 0.
\end{aligned}$$

From the solutions of the algebraic equations using Maple, two different cases can be verified as follows:

Case 1:

$$a_0 = 0,\ a_1 = -\frac{ck}{4b}, a = \frac{c^2}{4b},\quad \omega = \frac{c^2(-4\kappa^2+k^2)}{16b}$$

Then, on substituting these results into Eqn. (14) in order to obtain the optical solutions of KE equation gives

$$q_6(x,t) = \sqrt{-\frac{ck}{4b(1+exp(k(x+2a\kappa\frac{t^\alpha}{\alpha})))}}\,exp\left(i\left(-\kappa x + \omega\frac{t^\alpha}{\alpha} + \theta_0\right)\right).$$

Case 2:

$$a_0 = \frac{ck}{4b},\ a_1 = -\frac{ck}{4b},\ a_2 = \frac{c^2}{4b},\ \omega = \frac{c^2(-4\kappa^2+k^2)}{16b}$$

Then, on substituting these results into Eqn. (14) in order to obtain the optical solutions of KE equation gives

$$q_7(x,t) = \sqrt{\frac{ck}{4b} - \frac{ck}{4b(1+exp(k(x+2a\kappa\frac{t^\alpha}{\alpha})))}}\,exp\left(i\left(-\kappa x + \omega\frac{t^\alpha}{\alpha} + \theta_0\right)\right).$$

The KE equation was considered successful according to the exp(−φ(ξ)) and the exponential rational methods. As an upshot, several wave solutions have been previously acquired. Also, one must note that the accuracy of the acquired optical solutions was checked by subrogating every solution to KE equation. Since the exp(−φ(ξ)) method gives various types of solutions, it can be applied to additional models that will be considered in near future. Since the exponential rational function method is direct and effective, it is more simple to implement.

4. Conclusion

The results in this paper were dissimilar to the existing ones in the literature, and the results/they were checked thanks to Maple by resubstituting the solutions into the Kundu-Eckhaus equation. Finally, it could be stated that optical solutions have a promising future. Since both methods are applicable for many nonlinear partial differential equations, further applications are implementable for future studies. Also, different types of exact solutions can be founded for the dealt equation by using different methods.

References

[1] Kaplan M., Ozer, M.N., *Auto-Bäcklund transformations and solitary wave solutions for the nonlinear evolution equation,* Optical and Quantum Electronics, 50(1), 33, 2018.

[2] Akter, J., Akbar, M.A., *Exact solutions to the Benney-Luke equation and the Phi-4 equations by using modified simple equation method*, Results in Physics, 5, 125-130, 2015.

[3] Ma, W.X., Lee, J.H*., A transformed rational function method and exact solutions to the 3+1 dimensional Jimbo-Miwa equation*, Chaos, Solitons and Fractals, 42, 1356-1363, 2009.

[4] Mirzazadeh, M., Arnous, A.H., Mahmood, M.F. Zerrad, E. Biswas, A., *Soliton solutions to resonant nonlinear Schrödinger's equation with time-dependent coefficients by trial solution approach,* Nonlinear Dynamics, 81, 277-282, 2015.

[5] Bulut, H., Akturk, T., Gurefe, Y., *An application of the new function method to the generalized double sinh-Gordon equation*, AIP Conference Proceedings 1648, 370014, 2015.

[6] Islam, M.S., Khan, K., Akbar, M. A., *An analytical method for finding exact solutions of modified Korteweg-de Vries equation*, Results in Physics, 5, 131-135, 2015.

[7] Inan, I.E., Ugurlu, Y., Inc, M., *New Applications of the (G'/G,1/G)-Expansion Method,* Acta Physica Polonica A, 128, 245-251, 2015.

[8] Abdou, M.A., *A generalized auxiliary equation method and its applications*, Nonlinear Dynamics, 52, 95-102, 2008.

[9] Adem, A.R., Khalique, C.M., *Conserved quantities and solutions of a (2+1)-dimensional Haragus-Courcelle-Il'ichev model,* Computers and Mathematics with Applications, 71, 1129-1136, 2016.

[10] He, J.H., Abdou, M.A., *New periodic solutions for nonlinear evolution equations using Exp-function method,* Chaos, Solitons and Fractals, 34, 1421-1429, 2007.

[11] Abdou, M.A., *Further improved F-expansion and new exact solutions for non- linear evolution equations,* Nonlinear Dynamics, 52, 277-288, 2008.

[12] Mirzazadeh, M., Eslami, M., Zerrad, E., Mahmood, M.F., Biswas, A., Belic, M., *Optical solitons in nonlinear directional couplers by sine-cosine function method and Bernoulli's equation approach*, Nonlinear Dynamics, 81, 1933-1949, 2015.

[13] Younis, M., Ali, S. , Mahmood, S.A., *Solitons for compound KdV-Burgers equation with variable coefficients and power law nonlinearity*, Nonlinear Dynamics, 81, 1191-1196, 2015.

[14] Durur, H., Kurt, A., Tasbozan, O., *New Travelling Wave Solutions for KdV6 Equation Using Sub Equation Method,* Applied Mathematics and Nonlinear Sciences, 5(1), 455-460, 2020.

[15] Yusufoğlu, E., *New solitonary soltions for the MBBM equatios using Exp-function Method,* Physic Letters A, 372, 442-446, 2008.

[16] Biswas, A., Khalique, C.M., *Stationary solutions for nonlinear dispersive Schrödinger's equation,* Nonlinear Dynamics, 63, 623-626, 2011.

[17] Wazwaz, A.M., *Multiple-soliton solutions for the Boussinesq equation,* Applied Mathematics and Computation, 192, 479-486, 2007.

[18] Lü, X., Tian, B., Zhang, H.Q., Xu, T., Li, H., *Generalized (2+1)-dimensional Gardner model: bilinear equations, Bäcklund transformation,* Lax representation and interaction mechanisms, Nonlinear Dynamics, 67, 2279-2290, 2012.

[19] Ma, W.X., Abdeljabbar, A., Asaad, M.G., *Wronskian and Grammian solutions to a (3+1)-dimensional generalized KP equation,* Applied Mathematics and Computation, 217, 10016-10023, 2011.

[20] Wang, M.L., *Solitary wave solutions for variant Boussinesq equations*, Physics Letters A, 199, 169-172, 1995.

[21] Ablowitz, M.J., Segur, H., *Solitons and Inverse Scattering Transformation*, SIAM, Philadelphia, 1981.

[22] Thabet, H., Kendre, S., Peters, J., Kaplan, M., *Solitary wave solutions and traveling wave solutions for systems of time-fractional nonlinear wave equations via an analytical approach,* Computational and Applied Mathematics, 39, 2020, 144 .

[23] Zayed, E.M.E., Alngar, M.E.M., Al-Nowehy, A.G., *On solving the nonlinear Schrödinger Equation with an anti-cubic nonlinearity in presence of Hamiltonian perturbation terms,*Optik - International Journal for Light and Electron Optics, 178, 488-508, 2019.

[24] Biswas, A., Jawad, A.J.M. and Zhou, Q., *Resonant optical solitons with anti-cubic nonlinearity*, Optik, 157, 525-531, 2018.

[25] Biswas, A., *Optical soliton perturbation with Radhakrishnan-Kundu-Lakshmanan equation by traveling wave hypothesis*, Optik, 171, 217-220, 2018.

[26] Kaplan, M., *Application of two reliable methods for solving a nonlinear conformable time-fractional equation,* Optical and Quantum Electronics, 49, 312, 2017.

[27] Roshid, H.O., Kabir, M.R., Bhowmik, R.C., Datta, B.K., *Investigation of Solitary wave Solutions for Vakhnenko-Parkes equation via exp-function and exp(−φ(ξ))-expansion method.* SpringerPlus, 3, 692, 2014.

[28] Kundu, A., *Landau-Lifshitz and higher-order nonlinear systems gauge generated from nonlinear Schrödinger type equations*, Journal of Mathematical Physics, 25, 3433-3438, 1984.

[29] Eckhaus, W., *The long-time behaviour for perturbed wave-equations and related problems,* Preprint no. 404, Department of Mathematics, University of Utrecht, 1985.

[30] Mirzazadeh, M., Yıldırım, Y., Yas, E., Triki, H., Zhoud, Q., Moshokoa, S.P., Ullah, M.Z., Seadawy, A.R., Biswas, A., Belic, M., *Optical solitons and conservation law of Kundu-*

Eckhaus equation, Optik, 154, 551-557, 2018.

Adıyaman University Journal of Science
https://dergipark.org.tr/en/pub/adyujsci
DergiPark AKADEMİK
ISSN 2147-1630
e-ISSN 2146-586X

Assessing the Renewable Energy Efficiency Levels of BRICS Countries and Turkey Using Stochastic Frontier Analysis and Information Complexity Criteria

Haydar KOÇ[1,*]

[1]*Çankırı Karatekin University, Faculty of Science, Department of Statistics,18100, Çankırı, Turkey*
haydarkoc@karatekin.edu.tr, ORCID: 0000-0002-8568-4717

Received: 19.06.2020 **Accepted:** 14.05.2021 **Published:** 30.06.2021

Abstract

Renewable energy is a sustainable energy source that can be produced repeatedly by using the resources that exist in nature's own evolution. Renewable energy sources occupy an important place in the world and our country due to their renewability, minimal environmental impact, low operating and maintenance costs, and their national qualifications, and reliable energy supply features. In this study renewable energy efficiency levels for the BRICS countries and Turkey were examined. In the study covering the period 2006-2015, we used the SFA method for efficiency analysis in input selection. We used information complexity criteria to decide which input set is the best on renewable energy efficiency process. The selection results pointed out to the CO_2 emission and Energy intensity as the most explanatory inputs. We observed that the selected inputs have significant effect on the renewable energy efficiencies. According to results, the renewable energy efficiency values follow approximately the same pattern for each country and do not vary significantly between the years. When comparing the renewable energy efficiencies among the countries, Brazil has the best performance with approximately 97% efficiency level, and Russia has the worst one. The efficiency level of Turkey is rather weak, but it is not the worst and the average efficiency is very close to China.

* Corresponding Author DOI: 10.37094/adyujsci.755048

Keywords: Renewable energy; Stochastic frontier analysis; Information complexity criteria; BRICS; Turkey.

BRICS Ülkelerinin ve Türkiye'nin Yenilenebilir Enerji Verimliliği Düzeylerinin Stokastik Sınır Analizi ve Bilgi Karmaşıklığı Kriterleri Kullanılarak Değerlendirilmesi

Öz

Yenilenebilir enerji, doğanın kendi evriminde var olan kaynaklar kullanılarak tekrar tekrar üretilebilen sürdürülebilir bir enerji kaynağıdır. Yenilenebilir enerji kaynakları, yenilenebilirlik, minimum çevresel etki, düşük işletme ve bakım maliyetleri, ulusal nitelikleri ve güvenilir enerji tedarik özellikleri nedeniyle dünyada ve ülkemizde önemli bir yer tutmaktadır. Bu çalışmada BRICS ülkeleri ve Türkiye için yenilenebilir enerji verimliliği düzeyleri incelenmiştir. 2006-2015 dönemini kapsayan çalışmada, girdi seçiminde verimlilik analizi için SFA yöntemini uygulandı. Yenilenebilir enerji verimliliği sürecinde hangi girdi setinin en iyi olduğuna karar vermek için bilgi karmaşıklığı kriterlerini kullandık. Seçim sonuçları CO_2 emisyonunu ve enerji yoğunluğunu en açıklayıcı girdiler olarak ortaya koymaktadır. Ayrıca seçilen girdilerin yenilenebilir enerji verimliliği üzerinde önemli etkisi olduğu gözlemlendi. Sonuçlara göre, yenilenebilir enerji verimliliği değerleri her ülke için yaklaşık olarak aynı kalıbı takip etmektedir ve yıllar arasında önemli bir farklılık göstermemektedir. Ülkeler arasında yenilenebilir enerji verimliliği karşılaştırıldığında, Brezilya yaklaşık %97 verimlilik seviyesi ile en iyi performansa sahiptir ve Rusya en kötü performansa sahiptir. Türkiye'nin verimlilik seviyesi oldukça zayıf olmakla birlikte en kötü değil ve ortalama verimlilik Çin'e çok yakındır.

Anahtar Kelimeler: Yenilenebilir enerji; Stokastik sınır analizi; Bilgi karmaşıklığı kriterleri; BRICS, Türkiye.

1. Introduction

Energy is an important factor for the social wealth and economic development of countries. Economic developments, the rapidly growing population, and the developing industry have further increased the energy requirement and energy use. Despite the fact that energy requirement is increasing, fossil sources of energy will be exhausted in the near future [1]. The irregular use of fossil fuels is a danger for our future as well as to the present. Unconsciously used of these fuels to meet the energy needs, ecological balance and global climate change cause disruption. Emissions that show up with consumption threaten the environment and human health.

With renewable energy, it is possible to meet increasing energy sources safely and cleanly. Renewable energy is the energy obtained from natural sources such as sun and wind, which can renew itself quickly after consumption and is not exhausted as it is used. Renewable energy sources are the ones that are renewed in a continual motion and are ready to be used in nature. Since these sources are not fossil-derived (coal, oil and carbon derivatives), and CO_2 emissions are generated at a low level when generating electrical energy, their impact and harm to the environment are much lower than that of conventional energy sources.

In order to meet the increasing energy demand, the studies on renewable energy sources and energy efficiency should be increased. Increasing energy efficiency is a worldwide problem and naturally depends heavily on energy use. High-income developing countries known as BRICS (Brazil, Russia, India, China and S. Africa) countries and Turkey are the leading countries in renewable energy sector investment. The performance measurement of renewable energy sources is as important as the investment and production of these resources. Some of the studies in the literature on energy efficiency are given below.

Song et al. [2] used a Super SBM model to measure and calculate the energy efficiency of BRICS. They also applied Bootstrap to change values based on DEA obtained from small sample data and finally measured the relationship between energy efficiency and carbon emissions. The results show that BRICS has low energy efficiency as a whole but tends to increase rapidly.

Menegaki [3] used data envelopment analysis and Malmquist method in the study within the scope of European Union countries. Only national income per capita is used as output variable, while input variables are the percentage of renewable energy sources in electricity generation, energy consumption, CO_2 emission, employment rate, and capital. Kupeli and Alp [4] demonstrated the renewable energy performance of G20 countries by data envelopment analysis (DEA) and balanced performance weights method. They concluded that the results of the analysis with the balanced weights model gave more distinctive results than the classical model. Wang [5] demonstrated the performance of 109 countries using multi-criteria data envelopment analysis. In the study, CO_2 emission intensity and energy density were used as input variable, and ratio of renewable energy in electricity generation (%) was used as output variable. The study was conducted to cover the period 2005-2010. Sozen et al. [6] presented an approach for site selection of wind farms using data envelopment analysis (DEA) and TOPSIS approaches. By sorting 12 months efficiency values, they determined the most appropriate place for establish a wind farm in Turkey as examining by multi-parameter.

Lin and Long [7] applied the stochastic frontier analysis method to examine the average energy efficiency and energy saving potential of the chemical industry. The results show that energy price and operating scale are suitable for improving energy efficiency but property structure has an adverse effect. Using the stochastic frontier analysis model, Honma and Hu [8] estimated TFEE (total factor energy efficiency) scores for 47 regions across Japan between 1996 and 2008. Zhou et al. [9] extended the proposed cross-sectional stochastic frontier model. Hsiao et al. [10], using the SFA, measured TFEE for 10 countries across the Baltic Sea between 2004 and 2014.

Flippini and Hunt [11] estimated a panel "frontier" whole economy aggregate energy demand function for 29 countries over the period 1978 to 2006 using parametric stochastic frontier analysis (SFA). In this study, the energy efficiency of each country was also modeled, and it was argued that this represents a measure of the underlying efficiency for OECD countries. Lin and Du [12] presented a latent class stochastic frontier approach to measure energy efficiency under heterogeneous technologies. The proposed model has been applied to Chinese energy economy. The results show that the total energy efficiency of Chinese provinces is not high, with an average of 0.632 points from 1997 to 2010. Jin and Kim [13], to investigate energy efficiency in both economic and ecological aspects using Cobb-Douglas production function-based energy consumption, economic complexity index, and other production factors for 21 developing countries selected from Morgan Stanley Capital International in the period 1995-2016 applied a stochastic boundary analysis method. The parametric SFA method used for performance measurement is a very powerful technique.

In this study, the renewable energy efficiency levels for the BRICS countries and Turkey are assessed using the SFA method and information complexity criteria. To our knowledge, this study is the first attempt to use information complexity criteria for input-output selection task within SFA models. This paper includes two main originality since it investigates the popular assertions about “BRICST” and implements model selection procedures via the information complexity criteria in efficiency analysis.

The remainder of the study is organized as follows. In section 2, we introduce SFA methods and information criteria. Section 3 explains the application of the SFA model with renewable energy efficiency for BRICS countries and Turkey. Finally, a brief discussion is given in Section 4.

2. Materials and Methods

2.1. Stochastic frontier analysis

Stochastic frontier Analysis (SFA) is a frontier estimation method that accepts a functional form for the relationship between inputs and outputs [14]. By the SFA method, the errors occurring during production are estimated with econometric models, and the inefficiency resulting from these errors is minimized as much as possible. The SFA method is described and developed by Aigner et al. [15], Battase and Cora [16], Meusen and Vanden Browck [17]. Subsequently, Krumbhakar et al. [18], Huang and Liu [19] proposed stochastic production models that predict parameters of both stochastic frontier and inefficiency functions.

The SFA model proposed by Aigner et al. [15] is as follows:

$$\ln y_{it} = f(x_{j,it}, t, \beta) + v_{it} - u_{it} \quad (1)$$

where $\varepsilon_{it} = v_{it} - u_{it}$ shows the error term with $v_{it} \sim N(0, \sigma_v^2)$ for $u_{it} \geq 0$.

In this functional structure, the components are defined as follows:
f(.) is parametric production function (eg. Cobb- Douglas, Translog)
y_{it} : At time t, i-th output amount of decision making unit
$x_{j,it}$: At time t, i-th Vector showing entries of decision making unit
β: Unknown parameter vector

The stochastic production frontier model assumes that ε_{it} is a combined error consisting of two independent variables represented by v_{it} and u_{it}. v_{it} is independent and identically distributed error term, and $u_{it} \geq 0$ is technical inefficiency. For inefficiency, one of the semi-normal, exponential, and truncated normal and gamma distributions is used [15], Stevensen [20], Meeusen and van den Broeck [17], Greene [21]. In this study, u is inefficiency terms assumed to be an iid nonnegative truncated normal distribution.

The most common production functions used in the SFA method are Translog and Cobb-Douglas production forms [22]. In this study, Cobb - Douglas production function frontier analysis model is discussed.
Cobb-Douglas stochastic frontier model is as follows:

$$\ln y_{it} = \beta_0 + \sum_{j=1}^{k} \beta_j \ln x_{j,it} + v_{it} - u_{it} \quad (2)$$

2.2. Information criteria

The most commonly used measurements in statistical model selection are information criteria. Each criterion has different penalization terms. There are many information criteria used

in the selection of statistical models. In this study, we considered three information complexity criteria ICOMP [23-26].

$$\text{CICOMP} = -2logL\left(\widehat{M}\right) + d[\log(n) + 1] + 2C(\hat{\Sigma}_{\text{model}}) \quad (3)$$

$$\text{ICOMP}_{\text{IFIM}} = -2logL\left(\widehat{M}\right) + 2C\left(\hat{\Sigma}_{\text{model}}\right) \quad (4)$$

$$\text{ICOMP}_{\text{PEULN}} = -2\text{logL}\left(\widehat{\text{M}}\right) + \text{d} + \log(\text{n})\text{C}\left(\hat{\Sigma}_{\text{model}}\right) \quad (5)$$

where $L\left(\widehat{M}\right)$ is likelihood function, d is the total number of parameters, n is the sample size, C is a real-valued measure of complexity [23], and $\hat{\Sigma}_{\text{model}}$ represents the predicted covariance matrix of the parameter vector of the model. ICOMP information criteria penalize the covariance complexity of the model rather than directly penalizing the number of free parameters [27].

3. Application Part

In this part, we implemented the SFA to evaluate the renewable energy efficiency levels of BRICS countries and Turkey. We collected the data set from https://data.worldbank.org for the period of 2006-2015. The data set includes four inputs and one input variable. We encountered with some missing values and imputed the missing data with interpolation method for time series [28].

Firstly, we determined four potential inputs and then we eliminated them inside the SFA models. We performed the variable selection using three information complexity criteria and selected the most convenient model among all possible combinations of the input variables. The applications were conducted with R software (R Core Team, 2019). During the analysis, we benefited three R packages plm, frontier and imputeTS [28-30]. Table 1 shows the description of the input variables (x_1, x_2, x_3, x_4) and the output variable (y).

Table 1: Description of the variables

Variable	Description
x_1	CO_2 emission (metric ton per capita)
x_2	Primary energy (%)
x_3	Unemployment (%)
x_4	Energy intensity (level of primary energy)
y	Renewable energy (% of total final energy consumption)

Table 2 and 3 indicate the summary statistics correlation matrix for the input-output variables, respectively.

In Table 4, we reported the information criteria values for the all subsets of the input variables in SFA models. The selection results denote that all the information complexity criteria chose two inputs such as the CO_2 emissions and energy intensity for conducting the renewable energy efficiency analysis.

Table 5 shows the SFA model results for the selected inputs. In this model, the selected two inputs have significant impact on the output variable. When checking the coefficients, we can see that the CO_2 emission has the negative impact on the renewable energy efficiencies. The energy intensity provides a positive contribution on the renewable energy efficiencies.

However, time effect is not significant on the six country's efficiency levels. The Gamma parameter is also found significant and close to 1. This fact points out to the reason of the deviation of the renewable energy efficiencies which occurred because of the technical inefficiencies of the countries.

Table 2: Correlation matrix for the input and output variables

	x_1	x_2	x_3	x_4	y
x_1	1	0.224708	0.319632	0.626327	-0.779227
x_2	0.224708	1	-0.771190	0.407381	-0.277025
x_3	0.319632	-0.771190	1	0.026126	-0.014327
x_4	0.626327	0.407381	0.026126	1	-0.226474
y	-0.779227	-0.277025	-0.014327	-0.226474	1

Table 3: Summary statistics for the variables

Variable	$\bar{X}$	Med	SD	Min	Max
x_1	5.890	4.735	3.784	1.120	12.780
x_2	30.612	11.375	35.621	1.140	114.790
x_3	9.393	7.125	7.400	2.440	28.490
x_4	6.526	6.175	2.445	2.950	10.160
y	22.064	15.690	15.650	3.230	49.110

Table 4: Information criteria values for all the subsets of SFA models

Subset	ICOMPpeu	ICOMPpeuln	CICOMP
x_1	-93.430	-92.775	-72.958
x_2	-117.791	-107.395	-97.319
x_3	-86.938	-77.009	-66.467
x_4	-95.381	-85.057	-74.909
x_1, x_2	-123.237	-107.835	-98.671
x_1, x_3	-118.297	-103.656	-93.731
x_1, x_4	-123.797	-108.761	-99.231
x_2, x_3	-78.600	-77.972	-54.034
x_2, x_4	-77.109	-68.962	-52.543
x_3, x_4	-91.986	-76.610	-67.420
x_1, x_2, x_3	-117.202	-96.508	-88.541
x_1, x_2, x_4	-77.150	-63.624	-48.490
x_1, x_3, x_4	-117.709	-97.337	-89.049
x_2, x_3, x_4	-107.996	-87.737	-79.336
x_1, x_2, x_3, x_4	-111.545	-84.835	-78.790

Table 5: SFA results for the selected model

Coefficient	Estimate	SE	z-value	Sig.
(Intercept)	3.861395	0.084629	45.627600	<0.001
x_1	-0.086673	0.012298	-7.047500	<0.001
x_4	0.043810	0.016509	2.653700	<0.01
σ^2	1.112438	0.638565	1.742100	0.081492
Gamma	0.997640	0.001461	683.043600	<0.001
Time	0.001556	0.002687	0.579200	0.562422

Table 6 shows the yearly (2006-2015) renewable energy efficiency values, the average efficiencies (AE), and the ranks of BRICS countries and Turkey. According to results, the renewable energy efficiency values follow approximately the same pattern for each country and do not vary significantly between the years. When comparing the renewable energy efficiencies among the countries, Brazil has the best performance with approximately 97% efficiency level,

and Russia has the worst one. The efficiency level of Turkey is rather weak, but it is not the worst and the average efficiency is very close to China.

Table 6: Efficiency values and the ranks for BRICS countries and Turkey

Year	BRA	RUS	IND	CHN	ZAF	TUR
2006	0.970855	0.137442	0.763710	0.339994	0.496299	0.337774
2007	0.970899	0.137866	0.764030	0.340565	0.496840	0.338345
2008	0.970944	0.138292	0.764350	0.341136	0.497381	0.338915
2009	0.970988	0.138718	0.764669	0.341707	0.497921	0.339486
2010	0.971032	0.139144	0.764988	0.342278	0.498461	0.340057
2011	0.971077	0.139572	0.765307	0.342849	0.499001	0.340627
2012	0.971121	0.140000	0.765625	0.343420	0.499541	0.341198
2013	0.971165	0.140428	0.765943	0.343991	0.500080	0.341769
2014	0.971209	0.140858	0.766261	0.344562	0.500619	0.342340
2015	0.971253	0.141288	0.766578	0.345133	0.501158	0.342911
AE	0.971054	0.139361	0.765146	0.342563	0.498730	0.340342
Rank	1	6	2	4	3	5

4. Conclusion and Discussion

Renewable energy management has been recently received great attention worldwide. Therefore, it becomes very important to use the resources efficiently for maintaining renewable energy process in terms of countries. In this paper, we measured the renewable energy efficiencies of BRICS countries compared with Turkey. We used SFA for the efficiency analysis within input selection. The information complexity criteria assisted us to decide which input set is the best on renewable energy efficiency process. The selection results pointed out to the CO_2 emission and Energy intensity as the most explanatory inputs. We observed that the selected inputs have significant effect on the renewable energy efficiencies.

According to average efficiency values, Brasilia is superior to all BRICS countries and Turkey regarding the renewable energy. Turkey's renewable energy efficiency level is very close to China and higher than Russia. Turkey is 5th country among all BRICS countries in terms of the average renewable energy efficiency scores. The renewable energy efficiency levels of BRICS

and Turkey do not pretty much differ, and Turkey's performance is not the worse one. Consequently, we believe that this study will shed light on the views about the possibility of "BRICST" association.

References

[1] Çapik, M., *Present situation and potential role of renewable energy in Turkey;* Renewable Energy, 46, 01-13, 2012.

[2] Song, M.L., Zhang, L.L., Liu, W., Fisher, R., *Bootstrap-DEA analysis of BRICS' energy efficiency based on small sample data*, Applied Energy, 112, 1049-1055, 2013.

[3] Menegaki, A.N., *Growth and renewable energy in Europe: benchmarking with data envelopment analysis,* Renewable Energy, 60, 363-369, 2013.

[4] Kupeli, M., İhsan, A., *G20 Ülkelerinin yenilenebilir enerji etkinliğinin dengeli performans ağirliklari ve veri zarflama analizi ile değerlendirilmesi*, Uluslararası İktisadi ve İdari İncelemeler Dergisi, 207-218, 2018.

[5] Wang, H., *A generalized MCDA–DEA (multi-criterion decision analysis–data envelopment analysis) approach to construct slacks-based composite indicator*, Energy, 80, 114-122, 2015.

[6] Sozen, A., Mirzapour, A., Cakır, M.T., İskender, Ü., Çipil, F., *Selecting best location of wind plants using DEA and TOPSIS approach in Turkish cities*, Gazi J. Eng. Sci, 1, 174-193, 2016.

[7] Lin, B., Long, H., *A stochastic frontier analysis of energy efficiency of China's chemical industry,* Journal of Cleaner Production, 87, 235-244, 2015.

[8] Honma, S., Hu, J.L., *A panel data parametric frontier technique for measuring total-factor energy efficiency: an application to Japanese regions*, Energy, 78, 732-739, 2014.

[9] Zhou, P., Ang, B.W., Zhou, D.Q., *Measuring economy-wide energy efficiency performance: a parametric frontier approach*, Applied Energy, 90(1), 196-200, 2012.

[10] Hsiao, W. L., Hu, J. L., Hsiao, C., Chang, M. C., *Energy efficiency of the Baltic Sea Countries: an application of stochastic frontier analysis*, Energies, 12(1), 104, 2019.

[11] Filippini, M., Hunt, L.C., *Energy demand and energy efficiency in the OECD countries: a stochastic demand frontier approach,* The Energy Journal, 59-80, 2011.

[12] Lin, B., Du, K., *Measuring energy efficiency under heterogeneous technologies using a latent class stochastic frontier approach: an application to Chinese energy economy*, Energy, 76, 884-890, 2014.

[13] Jin, T., Kim, J., *A comparative study of energy and carbon efficiency for emerging countries using panel stochastic frontier analysis*, Scientific Reports, 9(1), 6647, 2019.

[14] Coelli, T.J., Rao, D.S.P., O'Donnell, C.J., Battese, G.E., *An introduction to efficiency and productivity analysis,* 2nd ed, Springer, New York, 2005.

[15] Aigner, D.J., Lovelly, C.A.K., Schmidt, P.J., *Formulation and estimation of stochastic frontier production function models,* Journal of Econometrics, 6, 1977.

[16] Battese, G.E., Corra, G.S., *Estimation of a production frontier model: with application to the pastoral zone of Eastern Australia'*, Australian Journal of Agricultural Economics, 21, 169-179, 1977.

[17] Meeusen, W., Van den Broeck, J., *Efficiency estimation from Cobb Douglas production functions with composed error,* International Economic Review,18, 435–444, 1977.

[18] Kumbhakar, S.C., Ghosh S., McGuckin J.T., *A generalized production frontier approach for estimating determinants of inefficiency in U.S. dairy farms*, Journal of Business and Economics Statistics, 9(3), 279-286, 1991.

[19] Huang, C. J., Liu, J.T., *Estimation of a non-neutral stochastic frontier production function*, Journal of Productivity Analysis, 5(2), 171-180, 1994.

[20] Stevenson, R.E., *Likelihood function for generalized stochastic frontier estimation*, Journal of Econometrics, 13, 57-66, 1980.

[21] Greene, W.M., *The econometric approach to efficiency analysis, the measurement of productive efficiency: techniques and applications*, published in Harold O. Fried, Lovell, C.A.K. and Schmidt, S.S. (eds.), Oxford University Press: 68–119, 1993.

[22] Battese, G.E., Broca, S.S., *Functional forms of stochastic frontier production functions and models for technical inefficiency effects: a comparative study for wheat farmers in Pakistan,* Journal of Productivity Analysis, 8(4), 395-414,1977.

[23] Bozdogan, H., *Akaike's information criterion and recent developments in information complexity,* Journal of Mathematical Psychology, 44 (1), 2000.

[24] Bozdogan, H., *Intelligent statistical data mining with information complexity and genetic algorithms,* Statistical Data Mining and Knowledge Discovery, 15-56, 2004.

[25] Pamukçu, E., Bozdogan, H., Çalık, S., *A novel hybrid dimension reduction technique for undersized high dimensional gene expression data sets using information complexity criterion for cancer classification*, Computational and Mathematical Methods in Medicine, 2015(2015).

[26] Deniz, E., Akbilgic, O., Howe, J.A., *Model selection using information criteria under a new estimation method: Least squares ratio*, Journal of Applied Statistics, 38 (9), 2011.

[27] Koç, H., Dünder, E., Gümüştekin, S., Koç, T., Cengiz, M.A., *Particle swarm optimization-based variable selection in Poisson regression analysis via information complexity-type criteria,* Communications in Statistics-Theory and Methods, 47(21), 5298-5306, 2018.

[28] Moritz, S., Bartz-Beielstein, T, *ImputeTS: time series missing value imputation in R*, The R Journal, 9(1), 207-218, 2017.

[29] Croissant, Y., Millo, G., *Panel data econometrics in R: The plm package,* Journal of Statistical Software, 27(2), 1-43, 2008.

[30] Coelli, T., Henningsen, A., Henningsen, M.A., *Package 'frontier*', Available in ftp://gnu.cs.pu.edu.tw/network/CRAN/web/packages/frontier/frontier. pdf. Accessed, 2017.

Adıyaman University Journal of Science
https://dergipark.org.tr/en/pub/adyujsci
DergiPark AKADEMİK
ISSN 2147-1630
e-ISSN 2146-586X

Investigation of the DKP Equation for A Two-Dimensional Black Hole

Evrim Ersin KANGAL[1,*], Ali HAVARE[2]

[1]*Mersin University, School of Applied Technology and Management of Erdemli, Department of Computer Technology and Information Systems, 33740, Mersin, Turkey*
evrimersin@gmail.com, ORCID: 0000-0001-5906-3143
[2]*Mersin University, Faculty of Arts and Sciences, Department of Physics, 33343, Mersin, Turkey*
ahavare@gmail.com, ORCID: 0000-0002-6476-7708

Received: 06.03.2021 **Accepted:** 17.05.2021 **Published:** 30.06.2021

Abstract

In the present study, we firstly investigated the spatial properties of event horizon of a two-dimensional black hole. Then we solve Duffin-Kemmer-Petiau (DKP) equation for such a black hole metric depending on the signs of spatial variable. After obtaining the exact solutions, we determine thermal parameters related to this metric. Finally, the harmonic oscillation behavior of the system is evaluated.

Keywords: DKP equation; Black hole; Thermal parameters; Harmonic oscillation.

İki Boyutlu Bir Karadelik için DKP Denkleminin Araştırılması

Öz

Bu çalışmada ilk olarak iki boyutlu bir kara deliğin olay ufkunun uzaysal özellikleri incelendi. Daha sonra böyle bir karadelik metriği için uzaysal değişkenin işaretine bağlı olarak DKP denklemi çözüldü. Tam çözümler elde edildikten sonra bu metrik ile ilişkili ısıl nicelikler belirlendi. Son olarak sistemin harmonik salınım davranışı değerlendirildi.

Anahtar Kelimeler: DKP Denklemi; Kara delik; Isıl parametreler; Harmonik osilasyon.

* Corresponding Author DOI: 10.37094/adyujsci.892038

1. Introduction

General relativity is one of the most attractive topics in modern theoretical physics [1-3]. In 1915, Einstein proposed that the gravity is a result of geometry and formulated it with the following equation,

$$G_{\mu\nu} = 8\pi G T_{\mu\nu} \tag{1}$$

where $T_{\mu\nu}$ is the stress-energy tensor of matter fields, G is the Newtonian constant of gravitation and $G_{\mu\nu}$ is the Einstein tensor given by

$$G_{\mu\nu} = R_{\mu\nu} - \frac{1}{2} g_{\mu\nu} R \tag{2}$$

$R_{\mu\nu}$ is the Ricci curvature tensor, $g_{\mu\nu}$ is the metric tensor, and R is the scalar curvature. Black hole is generally evaluated as a new mathematical or physical mechanism used to construct a link between gravity and quantum theory [4-5]. However, the dynamics of physical properties of a black hole existing in a four-dimensional curved spacetime can be sometimes extremely hard to understand thanks to some difficulties in quantizing gravity. For this reason, one of the best ways of overcoming these challenges is to reduce to a two-dimensional spacetime [6-7]. In such a spacetime, the Einstein field equation reduces to,

$$R - \Lambda = 8\pi G T \tag{3}$$

where T is the trace of two-dimensional energy momentum tensor and Λ is cosmological constant. Mann proposed to employ the following line element for a black hole by solving the above Einstein field equation in two dimensional spacetime [8]

$$ds^2 = -\alpha(x) dt^2 + \frac{1}{\alpha(x)} dx^2 \tag{4}$$

where

$$\alpha(x) = -\frac{\Lambda}{2} x^2 + 2M|x| - C \tag{5}$$

C is an arbitrary constant and M represents a positive energy source. Here, the number of distinct classes of solutions is dependent on the signs of Λ, C, and M. For Λ =0, the location of event horizon is [8]

$$|x| = \frac{C}{2M} \tag{6}$$

According to this equation, the existence of an event horizon appears if C and M are of the same sign. If Eqn. (6) is plotted for $\Lambda = 0$ [8], we obtain

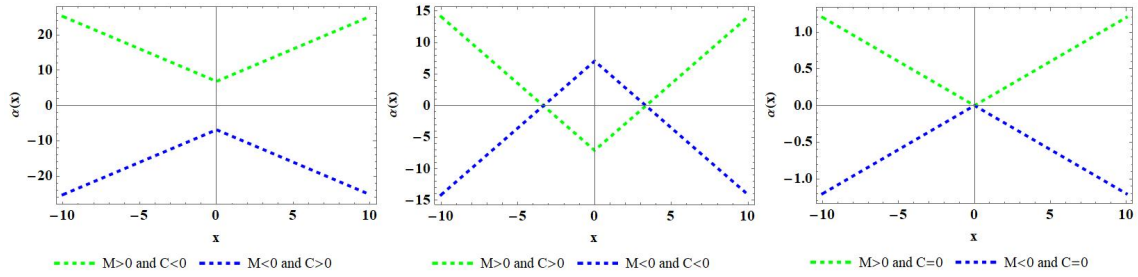

Figure 1: Dependence of $\boldsymbol{\alpha(x)}$ scale factor for setting $\boldsymbol{\Lambda = 0}$ and different values of M and C

As shown in Fig. 1, the horizon is surrounded by a timelike region for positive $\boldsymbol{M}$ while it is enclosed by a spacelike region for negative $\boldsymbol{M}$ at $\boldsymbol{C = 0}$ case or right-side graph. In addition, we see two distinct horizons for $\boldsymbol{C \neq 0}$ case or center-side graph. Finally, any horizon has not been observed for left-side graph since the absolute value of $\boldsymbol{x}$ is greater than zero.

If $\boldsymbol{\Lambda \neq 0}$, event horizon is placed at [8]

$$|\boldsymbol{x}| = \frac{\boldsymbol{2M \pm \sqrt{4M^2 - 2C\Lambda}}}{\boldsymbol{\Lambda}} \tag{7}$$

From the above equation, one can say that the existence of an event horizon is mainly in accordance with the $\boldsymbol{C\Lambda \leq 2M^2}$ equality. If we make a plot of Eqn. (7) under this circumstance [8], we get

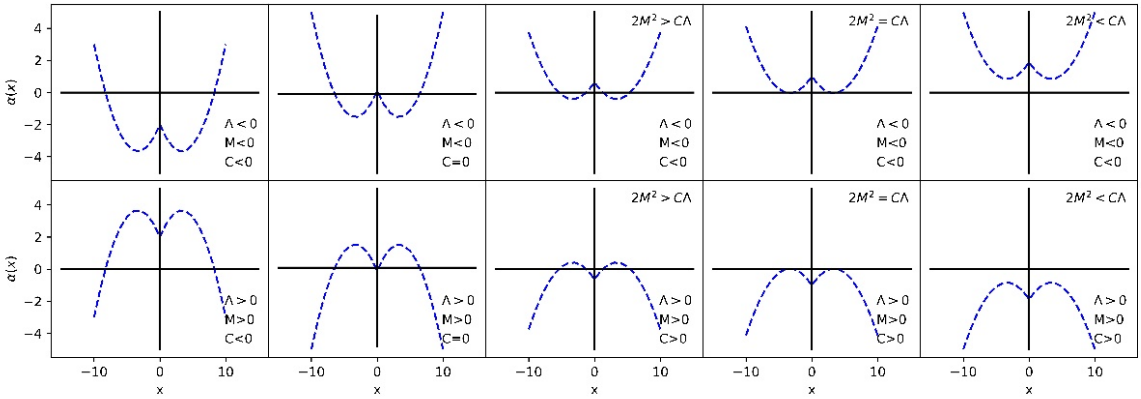

Figure 2: Type of solutions for running values of $\boldsymbol{\Lambda}$

From Fig. 2, we can easily say that $\alpha(x)$ equation have ten distinct of solutions whose behaviour are anti-symmetric structure with respect to each other. Further, any exist of restriction does not appear in the first two columns while the presence of a restriction exists in the other columns.

The DKP equation was proposed by Duffin, Kemmer and Petiau [9-11] and is mathematically identical to the general form of Dirac equation but it is uniquely characterized by $\boldsymbol{\beta}$ matrices instead of $\boldsymbol{\gamma}$ matrices. However, we sometimes encounter some difficulties to solve the DKP equation in (3 + 1) dimensions since it is a 16-component wave equation. An alternative way to overcome this problem is to evaluate the DKP equation in the lower dimensions in order to obtain the behavior of semi-classical and quantum gravity. In the literature, we find many studies related to the general relativity in (1 + 1)-dimensions [12-15].

In this work, we firstly obtained the exact solution of the DKP equation for the line element of a two-dimensional black hole described at Eqn. (4). In the second section, we investigate thermal parameters related to these solutions. Then the harmonic oscillation frequency is obtained in section 4. Last section is devoted to discussing our results.

2. The Exact Solution of the DKP Equation in (1+1) - Dimensions

The DKP equation in curved spacetime is given by [16-18]

$$\left[i\beta^{\mu}\left(\partial_{\mu}-\Sigma_{\mu}\right)-m\right]\Psi_{K}(t,x)=0 \tag{8}$$

where m is particle mass, $\beta^{\mu}=\gamma^{\mu}\otimes I+I\otimes\gamma^{\mu}$ are the Kemmer matrices, $\gamma^{\mu}=e^{\mu}_{(i)}\gamma^{(i)}$, $\Psi_{K}(t,x)$ shows the 16-component Kemmer wave function and Σ_{μ} are generally known as the spinorial connections defined by

$$\Sigma_{\mu}=\Gamma_{\mu}\otimes I+I\otimes\Gamma_{\mu} \tag{9}$$

where I is the $4\otimes 4$ identity matrices and Γ_{μ} are the spin connections for spin-1/2 particle calculated with the following equation

$$\Gamma_{\lambda}=-\frac{1}{8}g_{\mu\alpha}\Gamma^{\alpha}_{\nu\lambda}[\gamma^{\mu},\gamma^{\nu}] \tag{10}$$

and $\Gamma^{\alpha}_{\nu\lambda}$ are the Christoffel symbols that are directly written in terms of the metric tensor as

$$\Gamma^{\alpha}_{\mu\nu}=\frac{1}{2}g^{\alpha\beta}\left(\partial_{\mu}g_{\beta\nu}+\partial_{\nu}g_{\beta\mu}-\partial_{\beta}g_{\mu\nu}\right) \tag{11}$$

Unal [19-21] proved that the Kemmer wave function does not change under local Lorentz transformations, when the DKP particles are mathematically considered as a system of the product of two-identical spin-1/2 particles. Hence, the Kemmer wave function and β^{μ} matrices are reduced to

$$\Psi_K(t,x) = \Psi_D(t,x) \otimes \Psi_D(t,x) = \begin{bmatrix}\rho\\ \varphi\end{bmatrix} \otimes \begin{bmatrix}\rho\\ \varphi\end{bmatrix} = \begin{bmatrix}\rho\rho\\ \rho\varphi\\ \rho\varphi\\ \varphi\varphi\end{bmatrix} = \begin{bmatrix}h_1\\ h_0\\ h_0\\ h_2\end{bmatrix} e^{-iwt} \tag{12}$$

$$\beta^{\mu}(x) = \sigma^{\mu}(x) \otimes I + I \otimes \sigma^{\mu}(x) \tag{13}$$

since the usual Dirac matrices are replaced with the Pauli spin matrices, and also the Kemmer wave function oscillates freely with time. If we choose the Pauli matrices as $\sigma^{\mu} = \left(\sigma^3 = \begin{pmatrix}1 & 0\\ 0 & -1\end{pmatrix}, -i\sigma^2 = \begin{pmatrix}0 & -1\\ 1 & 0\end{pmatrix}\right)$ and substitute Eqn. (12) and Eqn. (13) into Eqn. (8), we get the following set of coupled differential equations:

$$\left(2iw\alpha^{-\frac{1}{2}} - m\right)h_1 + 2\left(\alpha^{\frac{1}{2}}\partial_x - \frac{\alpha'}{2\alpha^{\frac{1}{2}}}\right)h_0 = 0$$

$$\left(2iw\alpha^{-\frac{1}{2}} + m\right)h_2 + 2\left(\alpha^{\frac{1}{2}}\partial_x - \frac{\alpha'}{2\alpha^{\frac{1}{2}}}\right)h_0 = 0 \tag{14}$$

$$h_0 = \frac{\alpha^{\frac{1}{2}}}{m}\partial_x(h_2 - h_1)$$

After some mathematical algebra, the above equations yields

$$h_1 + h_2 = 2iw\alpha^{-\frac{1}{2}}(h_2 + h_1) \tag{15}$$

$$\left(\frac{\partial^2}{\partial x^2} + \frac{w^2}{\alpha^2} + \frac{m^2}{4}\frac{1}{\alpha}\right)\Phi = 0 \tag{16}$$

where $\Phi = h_2 - h_1$. If we insert Eqn. (5) into Eqn. (16), we find the following equation

$$\left(\frac{\partial^2}{\partial x^2} + \frac{4w^2}{(\Lambda x^2 - 4M|x| + 2C)^2} - \frac{m^2}{2}\frac{1}{\Lambda x^2 - 4M|x| + 2C}\right)\Phi(x) = 0 \tag{17}$$

The exact solution of Eqn. (17) depends on the sign of the x variable:

- $\boldsymbol{x < 0}$ **case:** Eqn. (17) becomes

$$\left(\frac{\partial^2}{\partial x^2} + \frac{4w^2}{(\Lambda x^2 + 4Mx + 2C)^2} - \frac{m^2}{2}\frac{1}{\Lambda x^2 + 4Mx + 2C}\right)\Phi(x) = 0 \tag{18}$$

This second order differential equation resembles the associated Legendre differential equation, and solutions are obtained as follows [22]

$$\Phi(x) = \sqrt{\Lambda x^2 + 4Mx + 2C}\left[C_1 P_n^m\left(\frac{x+\frac{M}{\Lambda}}{\sqrt{\left(\frac{M}{\Lambda}\right)^2 - \frac{2C}{\Lambda}}}\right) + C_2 Q_n^m\left(\frac{x+\frac{M}{\Lambda}}{\sqrt{\left(\frac{M}{\Lambda}\right)^2 - \frac{2C}{\Lambda}}}\right)\right] \tag{19}$$

- $\boldsymbol{x > 0}$ **case:** Eqn. (17) takes

$$\left(\frac{\partial^2}{\partial x^2} + \frac{4w^2}{(\Lambda x^2 - 4Mx + 2C)^2} + \frac{m^2}{2}\frac{1}{\Lambda x^2 - 4Mx + 2C}\right)\Phi(x) = 0 \tag{20}$$

Similarly, for the solution of this equation, we find the following result [22]

$$\Phi(x) = \sqrt{\Lambda x^2 - 4Mx + 2C}\left[C_1 P_n^m\left(\frac{x-\frac{M}{\Lambda}}{\sqrt{\left(\frac{M}{\Lambda}\right)^2 - \frac{2C}{\Lambda}}}\right) + C_2 Q_n^m\left(\frac{x-\frac{M}{\Lambda}}{\sqrt{\left(\frac{M}{\Lambda}\right)^2 - \frac{2C}{\Lambda}}}\right)\right] \tag{21}$$

where

$$n = \frac{1}{2}\left(-1 + \sqrt{1 + 2m^2\Lambda}\right) \tag{22}$$

$$m = \sqrt{1 + \frac{\left(\frac{2w}{\Lambda}\right)^2}{-\left(\frac{M}{\Lambda}\right)^2 + \frac{2C}{\Lambda}}} \tag{23}$$

The values of m parameter are integers because of definition. Thus, the energy is obtained as

$$E_l = \hbar\sqrt{2M^2 - C\Lambda}\,l \tag{24}$$

where l is a positive integer number.

3. Calculation of the Thermal Quantities

The partition function of the DKP particle is given by [23]

$$Z(\beta) = \sum_{l=0}^{\infty} e^{-\beta(E_l - E_0)} = \sum_{l=0}^{\infty} e^{-\hbar\beta\sqrt{2M^2 - C\Lambda}\,l} \tag{25}$$

Before determining the thermal quantities, we need to test the convergence of series of Eqn. (25) by using the integral test which shows whether the integral converges or diverges. The function from Eqn. (25) is

$$f(x) = e^{-\hbar\beta\sqrt{2M^2 - C\Lambda}\,l} \tag{26}$$

where $\hbar = 1$ is adopted. If the integral test is performed to Eqn. (26), we obtain

$$\int_0^{\infty} f(l)\,dl = \frac{1}{\sqrt{2M^2 - C\Lambda}}\frac{1}{\beta} \tag{27}$$

so, function is convergent. In the meantime, the numerical partition function is calculated with the help of a method depending on the Euler–MacLaurin formula [24] defined by the following equation

$$\sum_{l=0}^{\infty} f(x) = \frac{1}{2} f(0) + \int_0^{\infty} f(x)dx - \sum_{p=1}^{\infty} \frac{B_{2p}}{(2p)!} f^{2p-1}(0) \tag{28}$$

where B_{2p} are the Bernoulli numbers, f^{2p-1} is the derivative of order $2p-1$. If we write the exact form of partition function Z by using Eqn. (28), we get

$$Z(\beta) = \frac{1}{2} + \frac{1}{\sqrt{2M^2 - C\Lambda}} \frac{1}{\beta} + \frac{\sqrt{2M^2 - C\Lambda}}{12} \beta - \frac{\left(\sqrt{2M^2 - C\Lambda}\right)^3}{720} \beta^3 \tag{29}$$

where the terms up to $p = 2$, with $B_2 = \frac{1}{6}$, and $B_6 = -\frac{1}{30}$ are chosen. If the following thermal quantities like the Helmholtz free energy, the mean energy, the entropy, and the specific heat are calculated by using the partition function,

$$F = -\frac{1}{\beta} \ln Z \tag{30}$$

$$S = \beta^2 \frac{\partial F}{\partial \beta} \tag{31}$$

$$< E >= -\frac{\partial \ln Z}{\partial \beta} \tag{32}$$

$$C_v = -\beta^2 \frac{\partial < E >}{\partial \beta} \tag{33}$$

the resulting solutions are messy, so we will discuss these quantities numerically with the help of MATHEMATICA [25] and thermal quantities given by Eqn. (30-33) are plotted depending on some values of C parameter for $M \neq 0$ and $\Lambda \neq 0$ by considering $C\Lambda \leq 2M^2$ restriction and are shown in Fig. 3. From Fig. 3, we can say that thermal capacity is going to a fixed value at high temperature since a physical system has always a constant thermal capacity and also, we observe the same behavior in the entropy. Besides, the behaviour of mean energy is reasonable because the contribution coming from every dimension is almost $\frac{kT}{2}$, and then total energy is approximately equal to kT like graph.

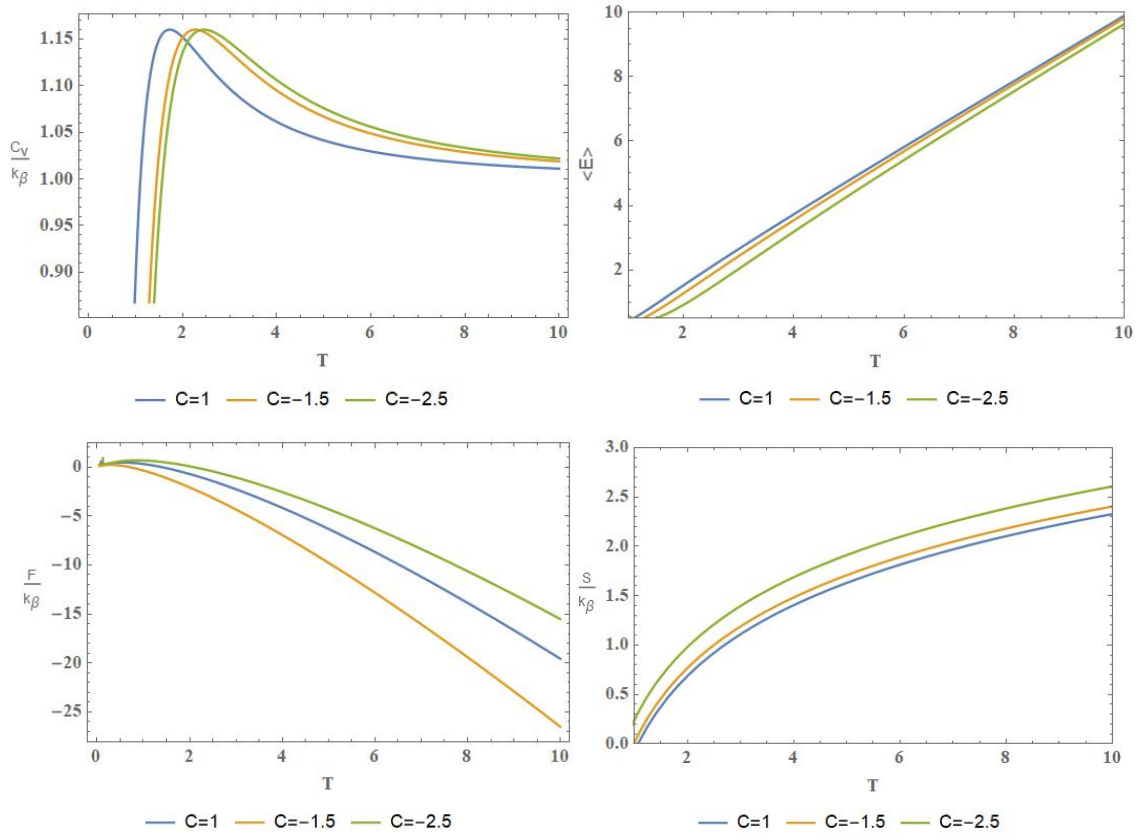

Figure 3: Thermal quantities depending on C for $M \neq 0$ and $\Lambda \neq 0$

4. The Harmonic Oscillator Behavior of the DKP Particles

To determine the range of oscillations of DKP particles, the form of the quadratic differential equation must be transformed to resemble the form of the differential equation of the harmonic oscillator given by

$$\left[\frac{\partial^2}{\partial x^2} + w^2\right] y(x) = 0 \tag{34}$$

where w represents the behavior of harmonic oscillation frequency. If we compare Eqn. (34) with Eqn. (17), we get

$$w^2 = \frac{4w^2}{(\Lambda x^2 - 4M|x| + 2C)^2} - \frac{m^2}{2}\frac{1}{\Lambda x^2 - 4M|x| + 2C} \tag{35}$$

and the following inequality corresponds to the range of above equation:

$$\frac{2M}{\Lambda} - \sqrt{\left(\frac{M}{\Lambda}\right)^2 + \left(\frac{2w}{\Lambda}\right)^2 - \frac{2C}{\Lambda}} < |x| < \frac{2M}{\Lambda} + \sqrt{\left(\frac{M}{\Lambda}\right)^2 + \left(\frac{2w}{\Lambda}\right)^2 - \frac{2C}{\Lambda}} \quad . \tag{36}$$

5. Conclusions

In this study, we solved the DKP equation for a two-dimensional black hole. In this case, the general solution is obtained by means of the associated Legendre Polynomials based on the signs of the x variable. Energy spectrum was obtained with the help of m parameter of Associated Legendre polynomials, and thermal quantities were calculated from energy spectrum. When the thermal quantities are graphically examined depending on the temperature, it is seen that the increases in the temperature alter these quantities. In addition, these changes show shifts depending on the different values of the C parameter of the metric. After all, we obtained the harmonic behavior of the DKP particles by determining the oscillation range. The oscillator behavior of particle is restricted in a spatial regime given by Eqn. (36). In conclusion, we can say that studying in the lower dimensions provides insights into the higher dimensions.

References

[1] Koyama, K., *Gravity beyond general relativity*, International Journal of Modern Physics D, 27 (15), 1848001, 2018.

[2] Gupta, S.N., *Gravitation and electromagnetism*, Physical Review, 96(6), 1683–1685, 1954.

[3] Boulware, D.G., Deser, S., *Classical general relativity derived from quantum gravity*, Annals of Physics, 89(1), 193–240, 1975.

[4] Hawking, S.W., *Black holes in general relativity*, Communications in Mathematical Physics, 25(2), 152–166, 1972.

[5] Hawking, S.W., *Black holes and thermodynamics*, Physical Review D, 13(2), 191–197, 1976.

[6] Teitleboim, C., *Gravitation and Hamiltonian structure in two spacetime dimensions*, Physics Letters B, 126(2), 41–45, 1983.

[7] Jackiw, R., *Lower Dimensional Gravity*, Nuclear Physics B, 252, 343–356, 1985.

[8] Mann, R.B., Shiekh, A., Tarasov, L., *Classical and quantum properties of tow-dimensional black holes*, Nuclear Physics B, 341(1),134-154, 1989.

[9] Duffin, R.J., *On the characteristic matrices of covariant systems*, Physical Review, 54, 1114, 1938.

[10] Kemmer, N., *The particle aspect of meson theory*, Proceeding of the Royal Society A, 173, 91-116, 1939.

[11] Petiau, G., *PhD thesis,* Academie Royale de Belgique, Classe des Sciences, Memoires, Collection 8, 1936.

[12] Lunardi, J.T., *A note on the Duffin-Kemmer-Petiau equation in (1+1) space-time dimensions,* Journal of Mathematical Physics, 58, 123501-123505, 2017.

[13] Lunardi, J.T., Pimentel, B.M., Teixeiri, R.G., Valverde, J.S., *Remarks on Duffin–Kemmer–Petiau theory and gauge invariance*, Physics Letter A, 268(3), 165-173, 2000.

[14] Sogut, K., Havare, A., *Transmission resonances in the Duffin–Kemmer–Petiau equation in (1+1) dimensions for an asymmetric cusp potential*, Physica Scripta, 82(4), 045013, 2010.

[15] Parker, L., Toms, D.J., *Quantum Field Theory in curved spacetime*, Cambridge University Press, 2009.

[16] Merad, M., *DKP equation with smooth potential and position-dependent mass*, International Journal of Theoretical Physics, 46, 2105-2118, 2007.

[17] Cheraitia, B.B., Boudjedaa, T., *Solution of DKP equation in Woods–Saxon potential*, Physics Letter A, 338(2), 97-107, 2005.

[18] Yasuk, F., Berkdemir, A., Onem, C., *Exact Solutions of the Duffin–Kemmer–Petiau Equation for the Deformed Hulthen Potential*, Physica Scripta, 71(4), 340-343, 2005.

[19] Unal, N., *Duffin–Kemmer–Petiau equation, Proca equation and Maxwells equation in (1+1) D*, Concepts of Physics, 2, 273, 2005.

[20] Unal, N., *Path integral quantization of a spinning particle*, Foundations of Physics, 28, 755-762, 1998.

[21] Unal, N., *A simple model of the classical Zitterbewegung: Photon wave function*, Foundations of Physics, 27, 731-746, 1997.

[22] Abramowitz, M., Stegun, I.A., *Handbook of mathematical functions*, National Bureau of Standards Applied Mathematics, 55, 1964.

[23] Boumali, A., *One-dimensional thermal properties of the Kemmer oscillator*, Physica Scripta, 76(6), 669–673, 2007.

[24] Pacheco, M.H., Landim, R.R., Almeida, C.A.S., *One-dimensional Dirac oscillator in a thermal bath*, Physics Letters A, 311, 93–96, 2003.

[25] Wolfram Research Company, Mathematica 9.0, 2012.

Adıyaman University Journal of Science
https://dergipark.org.tr/en/pub/adyujsci
DergiPark AKADEMİK
ISSN 2147-1630
e-ISSN 2146-586X

Solitary Wave Solutions of the Generalized (3+1)-Dimensional Shallow Water-Like Equation by Using Modified Kudryashov Method

Asıf YOKUŞ[1,*]

[1]*Fırat University, Faculty of Science, Department of Mathematics, Elazığ, 23100, Turkey*
asfyokus@yahoo.com, ORCID: 0000-0002-1460-8573

Received: 22.02.2021 **Accepted:** 24.05.2021 **Published:** 30.06.2021

Abstract

In this study, the generalized (3+1)-dimensional Shallow Water-Like (SWL) equation, which is one of the evolution equations, is taken into consideration. With the help of this evolution equation discussed, the modified Kudryashov method, traveling wave solutions are successfully obtained. In these solutions, graphs of solitary waves to be obtained by giving special values to arbitrary parameters are presented. At the same time, the effect of change of velocity parameter on the behavior on the solitary wave is examined in the solution obtained. The breaking of the wave is discussed. In this study, complex operations and graphic presentations are presented with the use of a ready-made package program.

Keywords: Generalized (3+1)-dimensional Shallow Water-Like equation; Modified Kudryashov method; Traveling wave solution.

Modifiye Kudryashov Metodu Kullanılarak Genelleştirilmiş (3 + 1)-Boyutlu Sığ Su Benzeri Denkleminin Solitary Dalga Çözümleri

* Corresponding Author DOI: 10.37094/adyujsci.883428

Öz

Bu çalışmada evrim denklemlerinden biri olan genelleştirilmiş (3+1) boyutlu sığ su benzeri denklemi dikkate alınır. Ele alınan bu evrim denklemi modifiye Kudryashov metodu yardımıyla yürüyen dalga çözümleri başarılı bir şekilde elde edilir. Bu çözümlerde keyfi parametrelere özel değerler verilerek elde edilecek solitary dalgaların grafikleri sunulur. Aynı zamanda elde edilen çözümde hız parametresinin değişiminin solitary dalga üzerindeki davranışlara olan etkisi incelenir. Dalganın kırılma olayı tartışılır. Bu çalışmada karmaşık işlemler ve grafik sunumları hazır paket programının kullanımıyla sunulur.

Anahtar Kelimeler: Genelleştirilmiş (3+1) boyutlu Sığ Su Benzeri denklem; Modifiye Kudryashov metodu, Yürüyen dalga çözümü.

1. Introduction

Nonlinear partial differential equations (NLPDEs) have many application areas such as fluid dynamics, hydromagnetic, optics, physics, chemistry, biology and others [1-5]. With the solutions of these NLPDEs and the values given to the special parameters in these solutions, many physical phenomena we encounter in daily life are modelled [6-10]. Therefore, there has been an increasing interest in the solution methods of NLPDEs by many scientists. Especially the methods existing in the last twenty years are updated and applied to these differential equations. With the help of these methods, many traveling wave solutions that satisfy the equation have been obtained [11-14]. Some of the methods are very efficient in NLPDEs and generate solutions from many different types. These properties of the methods are very important for the application area. Some of these methods are $\left(G'/G\right)$-expansion method [15], $\left(G'/G^2\right)$-expansion method [16], $\left(1/G'\right)$-expansion method [17-19], $\left(m+G'/G\right)$-expansion method [20], $\left(m+1/G'\right)$-expansion method [21], $\left(G'/G,1/G\right)$-expansion method [22] and so on [23].

$(3+1)$-dimensional Shallow Water-Like (SWL) equation is a nonlinear evolution equation that has become quite popular recently [24].

$$u_{xxxy}+3u_{xx}u_y+3u_xu_{xy}-u_{yt}-u_{xz}=0. \tag{1}$$

There have been many studies on this equation recently. The $\left(G'/G\right)$-expansion method was obtained by Zayed in 2010 [25], and the traveling wave solutions were obtained with the help of the generalized binary operator by Zhang in 2017 [26]. In 2019, the traveling wave solutions of Eqn. (1) were obtained by Dusunceli with the help of the Bernoulli sub equation method [24].

Then, by applying the sine-Gordon method, traveling wave solutions in complex form were reached by Baskonus and Eskitascıoglu in 2020 [27].

In this study, we aimed to reach traveling wave solutions for Eqn. (1) with the help of the the modified Kudryashov method [28]. At the same time, in the solutions obtained, special values are given to the parameters and presented with the help of graphics.

2. Materials and Methods

2.1. Methodology of the modified Kudryashov method

Assume you have a NLPDE in the form below

$$T\left(u,u_t,u_x,u_y,u_z,u_{xx},...\right)=0, \tag{2}$$

where T is a function in $u\left(x,y,z,t\right)$and its partial derivatives in which nonlinear terms and highest-order derivatives. We give the basic steps of this method in the following.

Step 1. Using the wave transmutation

$$u\left(x,y,z,t\right)=U\left(\xi\right),\quad \xi=x+ky+mz-wt, \tag{3}$$

we can transform it the following nODE for $U\left(\xi\right)$:

$$S\left(U,U',U'',...\right)=0, \tag{4}$$

where Eqn. (4) is the ODE, where k,w,m are constants. Here w is a physical quantity and is the speed parameter of the wave.

Step 2. We assume that Eqn. (4) has the formal solution

$$U\left(\xi\right)=a_0+\sum_{i=1}^{n}(a_iQ\left(\xi\right)^i+a_{-i}Q\left(\xi\right)^{-i}), \tag{5}$$

where $a_i,a_{-i},\quad i=\left\{1,...,n\right\}$are constants to be determined, such that $a_n\neq 0\ or\ a_{-n}\neq 0,$ and $Q\left(\xi\right)$is the solution of the equation

$$Q'\left(\xi\right)=\left[Q^2\left(\xi\right)-Q\left(\xi\right)\right]\ln a, \tag{6}$$

Eqn. (6) has solutions

$$Q(\xi)=\frac{1}{1\pm a^{\xi}}, \tag{7}$$

where $a>0, a\neq 1$ is a real number.

Step 3. In Eqn. (4), a positive integer *n* is calculated according to the balance principle.

Step 4. Substitute Eqn. (5) with Eqn. (6) into Eqn. (4), we compute all the required derivatives $U',U'',...$ of the function $U(\xi)$. Thus, we get a polynomial of $Q^{j}(\xi),(j=0,1,2,...)$. Computed polynomial, we add all the terms of the same powers of $Q^{j}(\xi)$ and equal them to zero, we get a system of algebraic equations that can be solved by a computer package program to attain the unknown parameters $a_i, a_{-i}, \quad i=\{1,...,n\}$, *k* and *w*. As a result, we get exact solutions of the Eqn. (2).

2.2. Application of modified Kudryashov method

We consider Eqn. (1). By using

$$u(x,y,z,t)=U(\xi), \quad \xi=x+ky+mz-wt, \tag{13}$$

Inserting Eqn. (13) into Eqn. (1), we obtain

$$kU^{(4)}+6kU'U''+(kw-m)U''=0, \tag{14}$$

Once the Eqn. (14) is integrated

$$kU'''+3k(U')^{2}+(kw-m)U'=0. \tag{15}$$

In the Eqn. (15), we get the balancing term $n=2$ and by considering in the Eqn. (5),

$$U(\xi)=a_0+a_1Q(\xi)+a_2Q(\xi)^{-1}+b_1Q(\xi)^{2}+b_2Q(\xi)^{-2}, \tag{16}$$

if Eqn. (16) is written in Eqn. (15) and if necessary adjustments are made, the following systems of equations can be written:

$$
\begin{aligned}
Const: \quad & m\log[a]a_2 - kw\log[a]a_2 - k\log[a]^3 a_2 - 6k\log[a]^2 a_1a_2 + 3k\log[a]^2 a_2^2 \\
& + 6k\log[a]^3 b_2 + 24k\log[a]^2 a_1b_2 - 24k\log[a]^2 b_1b_2 = 0, \\
\frac{1}{Q[\xi]}: \quad & -m\log[a]a_2 + kw\log[a]a_2 + k\log[a]^3 a_2 - 6k\log[a]^2 a_2^2 + 2m\log[a]b_2 \\
& - 2kw\log[a]b_2 - 14k\log[a]^3 b_2 - 12k\log[a]^2 a_1b_2 + 12k\log[a]^2 a_2b_2 = 0, \\
\frac{1}{Q[\xi]^2}: \quad & 3k\log[a]^2 a_2^2 - 2m\log[a]b_2 + 2kw\log[a]b_2 + 8k\log[a]^3 b_2 \\
& - 24k\log[a]^2 a_2b_2 + 12k\log[a]^2 b_2^2 = 0, \\
\frac{1}{Q[\xi]^3}: \quad & 12k\log[a]^2 a_2b_2 - 24k\log[a]^2 b_2^2 = 0, \\
\frac{1}{Q[\xi]^4}: \quad & 12k\log[a]^2 b_2^2 = 0,
\end{aligned}
\tag{17}
$$

$$
\begin{aligned}
Q[\xi]: \quad & m\log[a]a_1 - kw\log[a]a_1 - k\log[a]^3 a_1 + 12k\log[a]^2 a_1a_2 \\
& - 12k\log[a]^2 a_2b_1 - 12k\log[a]^2 a_1b_2 + 48k\log[a]^2 b_1b_2 = 0, \\
Q[\xi]^2: \quad & -m\log[a]a_1 + kw\log[a]a_1 + 7k\log[a]^3 a_1 + 3k\log[a]^2 a_1^2 \\
& - 6k\log[a]^2 a_1a_2 + 2m\log[a]b_1 - 2kw\log[a]b_1 - 8k\log[a]^3 b_1 \\
& + 24k\log[a]^2 a_2b_1 - 24k\log[a]^2 b_1b_2 = 0, \\
Q[\xi]^3: \quad & -12k\log[a]^3 a_1 - 6k\log[a]^2 a_1^2 - 2m\log[a]b_1 + 2kw\log[a]b_1 \\
& + 38k\log[a]^3 b_1 + 12k\log[a]^2 a_1b_1 - 12k\log[a]^2 a_2b_1 = 0, \\
Q[\xi]^4: \quad & 6k\log[a]^3 a_1 + 3k\log[a]^2 a_1^2 - 54k\log[a]^3 b_1 - 24k\log[a]^2 a_1b_1 + 12k\log[a]^2 b_1^2 = 0, \\
Q[\xi]^5: \quad & 24k\log[a]^3 b_1 + 12k\log[a]^2 a_1b_1 - 24k\log[a]^2 b_1^2 = 0, \\
Q[\xi]^6: \quad & 12k\log[a]^2 b_1^2 = 0.
\end{aligned}
$$

a_1, a_2, b_1, b_2 and m, k, w constants are obtained from Eqn. (17) the system utilizing a software program.

Case 1: If

$$
a_1 = -2log[a], \quad a_2 = 0, \quad b_1 = 0, \quad b_2 = 0, \quad m = k\left(w + log[a]^2\right), \tag{18}
$$

replacing values Eqn. (18) into Eqn. (16), we get traveling wave soliton for Eqn. (1)

$$u_1(x,y,z,t) = -\frac{2\,log[a]}{1+a^{-tw+x+ky+kz\left(w+log[a]^2\right)}} + a_0. \tag{19}$$

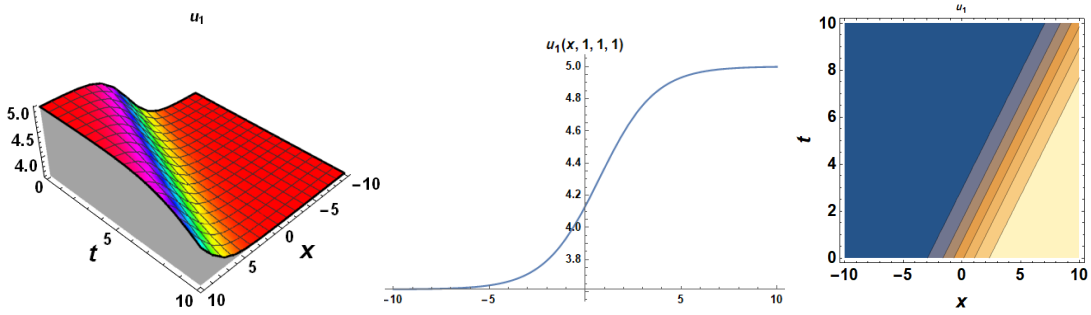

Figure 1: 3D, 2D and contour graphs for the Eqn. (19) for $a_0 = 5, w = 1, k = 0.1, y = 1, z = 1,\ a = 2$

3. Results and Discussions

In this study, we have obtained the traveling wave solution of the SWL equation with the modified Kudryashov method. It can be said that the solution obtained by this method is general from the solutions obtained in $(1/G')$-expansion method. This is usually because the base of the exponential function contains an arbitrary parameter. It is the *"e"* expression defined as the base exponential function in the $(1/G')$-expansion method. However, the term without exponential expression is constant in modified Kudryashov method, while it contains arbitrary parameters in $(1/G')$-expansion method [29]. When the solutions obtained are examined physically, let's examine the effect of the change of velocity parameter on the traveling wave solution obtained. The *"w"* expression in the classical wave transformation is a parameter representing the frequency of the wave and therefore its speed. We can present the effect of velocity on the wave with the following 3D simulation provided that other parameters except *"w"* are taken as constant Fig. 2 as seen in the simulation, as the speed increases, the changes in the behavior of the wave and the refraction phenomenon occur. Here is $w = 2.05$. The distortions at the end point of the value of the wave and the breaking event at $w = 2.055$ are clearly seen. In the future, the effect of other parameters on the wave can be observed.

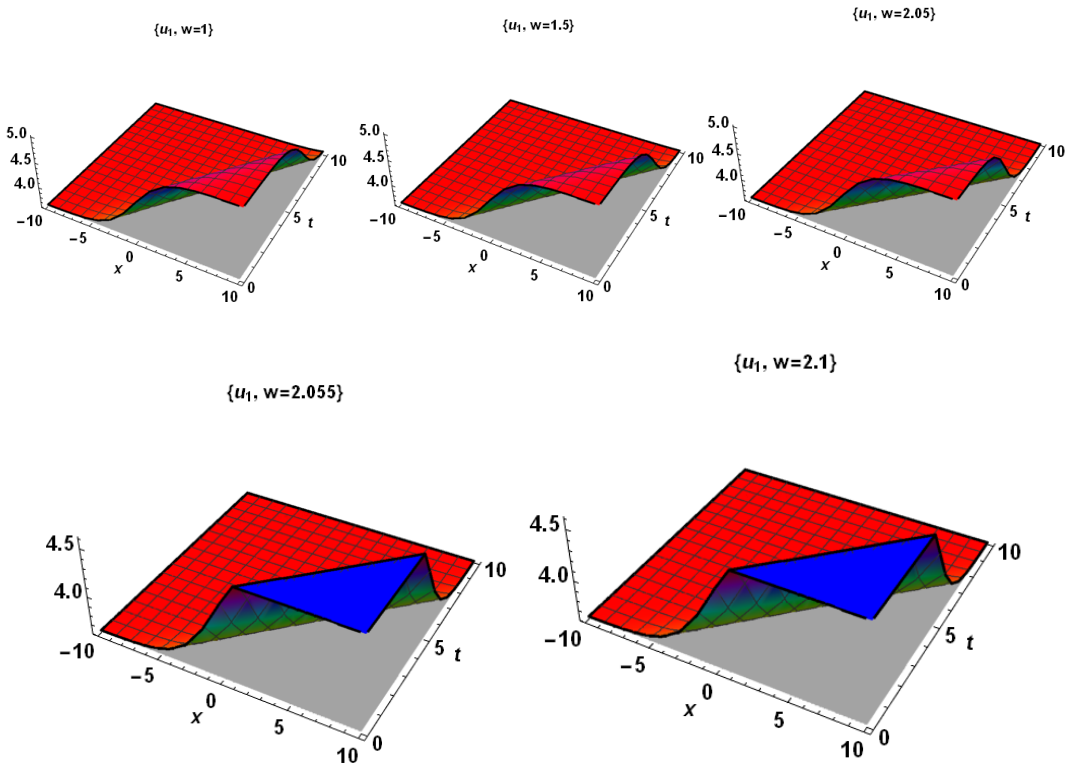

Figure 2: Simulation graphs of the Eqn. (19) for $a_0 = 5, k = 0.1, y = 1, z = 1,\ a = 2$

4. Conclusions

In this study, the traveling wave solution of the generalized SWL equation has been successfully obtained. Solitary wave solutions were created for specific values of arbitrary parameters in the traveling wave solution. 2D, 3D and contour graphics of these solitary waves are presented. At the same time, the effect of the change of velocity parameter on the behavior on the solitary wave in the solution obtained. Fig. 2 also presented and discussed. In addition, the value in the speed parameter at which the breakage of the wave occurred was determined. It was concluded that the modified Kudryashov method is valid, reliable and applicable. In future studies, many studies can be done on non-linear evolution equations with the help of this method.

References

[1] Yavuz, M., Sene, N., *Approximate solutions of the model describing fluid flow using generalized ρ-laplace transform method and heat balance integral method*, Axioms, 9(4), 123, 2020.

[2] Dungey, J.W., *Hydromagnetic Waves. In Physics of the Magnetosphere,* Based upon the Proceedings of the Conference Held at Boston College, Springer Science & Business Media, 10, 218, 2012.

[3] Rezazadeh, H., Mirhosseini-Alizamini, S.M., Eslami, M., Rezazadeh, M., Mirzazadeh, M., Abbagari, S., *New optical solitons of nonlinear conformable fractional Schrödinger-Hirota equation*, Optik, 172, 545-553, 2018.

[4] Alam, M.N., Akbar, M.A., *Traveling wave solutions for the mKdV equation and the Gardner equations by new approach of the generalized (G'/G)-expansion method*, Journal of the Egyptian Mathematical Society, 22(3), 402-406, 2014.

[5] Duran, S., Askin, M., Sulaiman, T.A., *New soliton properties to the ill-posed Boussinesq equation arising in nonlinear physical science*, An International Journal of Optimization and Control: Theories & Applications (IJOCTA), *7*(3), 240-247, 2017.

[6] Duran, S., *Solitary Wave Solutions of the Coupled Konno-Oono Equation by using the Functional Variable Method and the Two Variables (G'/G, 1/G)-Expansion Method*, Adıyaman Üniversitesi Fen Bilimleri Dergisi, 10(2), 585-594, 2020.

[7] Durur, H., *Different types analytic solutions of the (1+ 1)-dimensional resonant nonlinear Schrödinger's equation using (G'/G)-expansion method,* Modern Physics Letters B, 34(03), 2020.

[8] Saleem, S., Hussain, M.Z., Aziz, I., *A reliable algorithm to compute the approximate solution of KdV-type partial differential equations of order seven*. *Plos one*, *16*(1), e0244027, 2021.

[9] Duran, S., *Exact Solutions for Time-Fractional Ramani and Jimbo—Miwa Equations by Direct Algebraic Method*, Advanced Science, Engineering and Medicine, 12(7), 982-988, 2020.

[10] Yokus, A., Durur, H., Ahmad, H., Yao, S.W., *Construction of different types analytic solutions for the Zhiber-Shabat equation*, Mathematics, 8(6), 908, 2020.

[11] Yokuş, A., Durur, H., Abro, K.A., Kaya, D., *Role of Gilson–Pickering equation for the different types of soliton solutions: a nonlinear analysis*, The European Physical Journal Plus, 135(8), 1-19, 2020.

[12] Duran, S., Kaya, D., *Applications of a new expansion method for finding wave solutions of nonlinear differential equations*, World Applied Sciences Journal, 18(11), 1582-1592, 2012.

[13] Sulaiman, T.A., Bulut, H., Yokus, A., Baskonus, H.M., *On the exact and numerical solutions to the coupled Boussinesq equation arising in ocean engineering*, Indian Journal of Physics, 93(5), 647-656, 2019.

[14] Durur, H., Yokuş, A., *Analytical solutions of Kolmogorov–Petrovskii–Piskunov equation*, Balıkesir Üniversitesi Fen Bilimleri Enstitüsü Dergisi, 22(2), 628-636, 2020.

[15] Zhang, J., Wei, X., Lu, Y., *A generalized (G' G)-expansion method and its applications*, Physics Letters A, 372(20), 3653-3658, 2008.

[16] Rehman, S.U., Yusuf, A., Bilal, M., Younas, U., Younis, M., Sulaiman, T.A., *Application of (G'/G^ 2)-expansion method to microstructured solids, magneto-electro-elastic circular rod and (2+ 1)-dimensional nonlinear electrical lines*, Journal| MESA, 11(4), 789-803, 2020.

[17] Yokuş, A., Durur, H., Ahmad, H., *Hyperbolic type solutions for the couple Boiti-Leon-Pempinelli system*, Facta Universitatis, Series: Mathematics and Informatics, 35(2), 523-531, 2020.

[18] Durur, H., Yokuş, A., *Vakhnenko-Parkes denkleminin hiperbolik tipte yürüyen dalga çözümü*, Erzincan Üniversitesi Fen Bilimleri Enstitüsü Dergisi, 13(2), 550-556, 2020.

[19] Yokuş, A., Durur, H., *Complex hyperbolic traveling wave solutions of Kuramoto-Sivashinsky equation using (1/G') expansion method for nonlinear dynamic theory,* Balıkesir Üniversitesi Fen Bilimleri Enstitüsü Dergisi, 21(2), 590-599, 2019.

[20] Ismael, H.F., Bulut, H., Baskonus, H.M., *Optical soliton solutions to the Fokas–Lenells equation via sine-Gordon expansion method and (m+ ({G'}/{G}))-expansion method,* Pramana, 94(1), 35, 2020.

[21] Durur, H., Ilhan, E., Bulut, H., *Novel complex wave solutions of the (2+1)-dimensional hyperbolic nonlinear Schrödinger equation*, Fractal and Fractional, 4(3), 41, 2020.

[22] Yokus, A., Durur, H., Ahmad, H., Thounthong, P., Zhang, Y.F., *Construction of exact traveling wave solutions of the Bogoyavlenskii equation by (G'/G, 1/G)-expansion and (1/G')-expansion techniques,* Results in Physics, 19, 103409, 2020.

[23] Duran, S., Doğan, K., *New wave solutions for nonlinear differential equations using an extended Bernoulli equation as a new expansion method*, In ITM Web of Conferences (Vol. 22, p. 01035). EDP Sciences (2018).

[24] Dusunceli, F., *Exact solutions for generalized (3+ 1)-dimensional Shallow Water-Like (SWL) equation*, In Conference Proceedings of Science and Technology, 2(1), 55-57, 2019.

[25] Zayed, E.M.E., *Traveling wave solutions for higher dimensional nonlinear evolution equations using the G'/G-expansion method*, Journal of Applied Mathematics & Informatics, 28(1_2), 383-395, 2010.

[26] Zhang, Y., Dong, H., Zhang, X., Yang, H., *Rational solutions and lump solutions to the generalized (3+1)-dimensional Shallow Water-Like equation*, Computers & Mathematics with Applications, 73(2), 246-252 2017.

[27] Baskonus, H.M., Eskitascioglu, E.I., *Complex wave surfaces to the extended shallow water wave model with (2+1)-dimensional*, Computational Methods for Differential Equations, 8(3), 585-596, 2020.

[28] Kumar, D., Seadawy, A.R., Joardar, A.K., *Modified Kudryashov method via new exact solutions for some conformable fractional differential equations arising in mathematical biology.* Chinese journal of physics, 56(1), 75-85, 2018.

[29] Yokus, A., Tuz, M., Güngöz, U., *On the exact and numerical complex travelling wave solution to the nonlinear Schrödinger equation,* Journal of Difference Equations and Applications, 1-12, 2021.

Adıyaman University Journal of Science
https://dergipark.org.tr/en/pub/adyujsci
DergiPark AKADEMİK
ISSN 2147-1630
e-ISSN 2146-586X

Reduction of *Salmonella* Typhimurium, *Escherichia coli*, and *Staphylococcus aureus* Biofilms by Electrolysis

Başar KARACA[1,*]

[1]*Ankara University, Faculty of Science, Biology Department, Ankara, Turkey*
karaca@ankara.edu.tr, ORCID: 0000-0001-6943-8965

Received: 29.12.2020 **Accepted:** 27.05.2021 **Published:** 30.06.2021

Abstract

Adherence of microorganisms to food contact surfaces and subsequent biofilm formation leads to equipment damage, food spoilage, and foodborne diseases. Biofilms in food processing plants may exhibit resistance to routine disinfectants and sanitation procedures. Extensive studies have been conducted to reduce the risks of food biofilms. Since electrolysis is an inexpensive and effective approach, it has recently become the focus of interest among researchers in this context. In the related study, the removal (eradication) of major food pathogens such as *Escherichia coli*, *Salmonella* Typhimurium and *Staphylococcus aureus* biofilms was evaluated using low electric current. Experimental studies were conducted in an easy-to-install electrolysis setup containing electrodes capable of integrating metal surfaces on which biofilms develop. *E. coli* and *S.* Typhimurium biofilm cells on stainless steel surfaces were eliminated, while a significant decrease (2.5 log reduction) in the number of *S. aureus* biofilm cells was observed in the electrolysis process performed in 2M NaCl solution (10 V, 0.3 A, 1, 2 and 5 min). The viability of biofilm cells was controlled using colony count method. However, the removal of biofilm matrix residues from the surface was not possible

* Corresponding Author
DOI: 10.37094/adyujsci.849694

with the preferred electrolysis procedure. The biofilm matrix remaining on the surface after the procedure was detected by the crystal violet binding assay.

Being a low-cost and easy-to-use process, it became clear that electrolysis and the resulting biocidal agents produced by the reactions in the electrolyte buffer can be used in the food industry to control biofilms.

Keywords: Biofilm; Electrolysis; *Escherichia coli*; *Salmonella* Typhimurium; *Staphylococcus aureus.*

***Salmonella* Typhimurium, *Escherichia coli* ve *Staphylococcus aureus* Biyofilmlerinin Elektrolizle Giderimi**

Öz

Mikroorganizmaların gıdaların temas ettikleri yüzeylere tutunması ve devamında biyofilm üretmeleri, ekipman hasarına, gıda bozulmalarına ve gıda kaynaklı hastalıklara neden olmaktadır. Gıdaların işlendiği çevrelerdeki biyofilmler rutin dezenfektanlara ve sanitasyon işlemlerine direnç gösterebilmektedir. Gıda biyofilmlerinin neden oldukları riskleri azaltmak adına çok sayıda çalışma yürütülmüştür. Bu bağlamda elektroliz, ucuz ve etkili bir yaklaşım olması itibariyle son zamanlarda araştırmacıların odağında bulunmaktadır. İlgili çalışmada önemli gıda patojenleri olan *Escherichia coli*, *Salmonella* Typhimurium ve *Staphylococcus aureus* biyofilmlerinin düşük elektrik akımı ile giderimi (eradikasyon) değerlendirilmiştir. Deneysel çalışmalar, biyofilm örneklerinin geliştirileceği metalik yüzeylerin entegre edilebildiği elektrotları ihtiva eden ve kolaylıkla kurulabilir elektroliz düzeneğinde gerçekleştirilmiştir. 2M NaCl çözeltisi tercih edilerek gerçekleştirilen elektroliz işlemiyle (10 V, 0.3 A, 1, 2 ve 5 dakika süresince) paslanmaz çelik yüzeyler üzerindeki *E. coli* ve *S.* Typhimurium biyofilm hücreleri bütünüyle elimine edilirken, *S. aureus* biyofilm hücrelerinin sayısında önemli ölçüde bir azalma saptanmıştır (2.5 log azalma). Biyofilm hücrelerindeki canlılık koloni sayım yöntemiyle kontrol edilmiştir. Ancak biyofilm matriks kalıntılarını yüzeyden bütünüyle temizlemek tercih edilen elektroliz prosedürüyle mümkün olmamıştır. İşlemden sonra yüzeyde kalan matriks yapıları kristal viyole bağlanma uygulamasıyla gösterilmiştir.

Ucuz ve kolay uygulanabilir bir işlem olması itibariyle elektrolizin ve onun sonucunda elektrolit tampondaki reaksiyonlar sonucunda elde edilen biyosidal ajanların gıda endüstrisinde biyofilmler mücadelede kullanılabileceği açıkça anlaşılmıştır.

Anahtar Kelimeler: Biyofilm; Elektroliz; *Escherichia coli; Salmonella* Typhimurium*; Staphylococcus aureus.*

1. Introduction

The majority of microorganisms organize themselves as biofilms in their natural environment. Biofilms are found in artificial environments as well as in their natural environment. Biofilms are aggregates of microorganisms surrounded by three-dimensional complex extracellular polymeric components that form on surfaces [1]. Food safety is a vital issue that directly affects public health and encompasses all segments of the food industry [2]. Biofilm formation causes problems in many areas of the food industry through energy loss, reduction in flow and heat transfer, and clogging of membranes. Many bacteria, both harmless and pathogenic, can form biofilms in the food environment [2, 3].

Even with careful cleaning of food processing equipment, it is very difficult or impossible to produce a microorganism-free food. This difficulty is due to the presence of biofilms in the units where the product is processed [4]. Biofilms can form in moist environments with minimal food debris. Once the biofilm has formed, the surfaces are much more difficult to clean due to the presence of extracellular components. Many cleaning procedures involve the removal of food residue from surfaces with chemical agents applied with hot or cold water. The cleaning process is accomplished with a single chemical or a combined application of chemicals and physical agitation (water turbulence or scrubbing) [5]. However, conventional cleaning and disinfection procedures may not be effective in biofilm control due to the high resistance of biofilms. There are many studies evaluating new biofilm control strategies in the food industry. In addition to mechanical and chemical applications, biological approaches such as enzymes, phages, interspecies interactions, and antimicrobial molecules of microbial origin are also being evaluated [6-8].

Numerous microorganisms can colonize on metal surfaces and form biofilms. Routine sanitation procedures prefer chemical agents or biocides to clean metal surfaces. Nevertheless, these strategies, including the addition of substances from outside, have some disadvantages [9]. Electrolysis is the direct electric current passing through an electrolyte, causing chemical reactions and decomposition of substances at the electrodes. The basic components needed to perform electrolysis are an electrolyte, electrodes, and a power source. The generation of electrolysis products such as chlorine, hydrogen peroxide, and sudden pH changes with direct current prevents the adhesion of bacteria or facilitates the detachment of biofilms from surfaces [10-13]. Electrochemical biofilm control is a technology for delaying or preventing the adhesion of microorganisms to a surface by

altering their reactive properties or by removing adherent cells. This technology can be applied to surfaces which have electrical conductivity. These conductive surfaces behave like electrodes where electrochemical reactions occur. Thus, by applying a constant electric current to the surface, biofilm control can be possible continuously or for a certain period of time [14]. Current studies on electrochemical interactions of microbial biofilms include approaches to delaying the attachment of microbial cells or removing existing biofilms from surfaces. The generation of antimicrobial or antibiofilm agents on the adherent surface of biofilms may be a strategy to combat biofilms [15]. Antimicrobial agents may have difficulty diffusing into the inner layers of a biofilm when delivered from the fluid surrounding the biofilm. In situ generation of an antimicrobial or antibiofilm agent at the adherent site of a biofilm may be more efficient [10]. Electrolysis is one of the simplest ways to generate antimicrobial agents at a surface. Electrolysis of water can lead to local pH changes that can affect biofilms. Chlorine, an antimicrobial agent, can be generated by electrolysis in the presence of chlorine [16]. Electrolysis of aqueous solutions such as NaCl solution results in the generation of molecular oxygen, molecular hydrogen, hydrogen cations, hydroxyl anions and other reactive oxygen species as well as heat [17].

Damage to food processing equipment, product contamination, energy loss, and infectious diseases in clinical settings caused by microbial biofilms result in significant economic losses. Microbial biofilms that develop in food units cause significant financial losses by disrupting the textural properties of food products and leading to the spread of food-borne infection and intoxication diseases by being the source of continuous contamination. Attempting to remove biofilms using existing sanitation methods entails a financial burden due to the use of expensive chemicals and leads to contamination of food products due to intensive use of chemicals despite rinsing processes [18].

Electrochemical removal of biofilms is one of the most studied topics in the literature in the context of biofilm control. The aim of the study reported in this article was to shed light on the role of electrolysis products and biofilm removal at the anode or cathode. In this study, it was aimed to control and remove biofilms of some important food pathogens such as *E. coli*, *S.* Typhimurium and *S. aureus*, which significantly affect both human health and food quality.

2. Materials and Methods

2.1. Bacterial strains

The bacterial strains evaluated in the study were obtained from Ankara University, Faculty of Science, Department of Biology, Microbiology Research Laboratory Culture Collection. Two Gram-

negative (*Escherichia coli* ATCC 25922, *Salmonella* Typhimurium DMC4) and one Gram-positive (*Staphylococcus aureus* ATCC 25923) reference strains were used in the studies.

2.2. Optimization of biofilm formation

First, the ideal biofilm production conditions for the three reference strains were optimized. 316 L type stainless steel surfaces, which are widely used in the food industry, were preferred as the surface for biofilm sampling [18].

E. coli colonies grown overnight at 37 °C on BHI (Brain Heart Infusion, Merck, Germany) agar medium were harvested with a sterile loop and suspended in diluted (1:250) BHI (Brain Heart Infusion, Merck, Germany) medium to adjust MacFarland 2 (approximately 6.0×10^8). 5 mL of the suspended culture was taken and transferred to sterile glass tubes with 316 L type stainless steel coupons (2.5 cm × 0.8 cm × 0.1 cm). The tubes containing only medium and coupons were designed as negative controls. The test tubes were then incubated for 24 h at 37 °C under static conditions [19].

An overnight *S.* Typhimurium culture (cultured in LB; Luria-Bertani without NaCl) was reinoculated at a ratio of 5% (v/v) (2.5×10^8 CFU/mL) into a new tube containing 5 mL of LB without NaCl medium. 5 mL of inoculated cultures were transferred to sterile glass tubes with 316 L type stainless steel coupons (2.5 cm × 0.8 cm × 0.1 cm). The test tubes were incubated for 24 h at 28 °C under static conditions [20].

An overnight *S. aureus* culture (cultured in TSB; Tryptic Soy Broth, Merck, Germany) was reinoculated at a ratio of 5% (v/v) (2.5×10^7 CFU/mL) into a new tube containing 5 mL of TSB supplied with 1.5% NaCl). 5 mL of the cultures were transferred to sterile glass tubes with 316 L type stainless steel coupons (2.5 cm × 0.8 cm × 0.1 cm). The test tubes were then incubated for 24 h at 37 °C under static conditions [21].

For the current study 316L type stainless steel surface was preferred, which is widely used in the food industry. This material can be considered as a good electrode due to its high conductivity [22].

2.3. Electrolysis of biofilms sampled on stainless steel surfaces

After biofilm production was performed for each reference strain, the coupons were removed from the glass tubes under aseptic conditions and rinsed twice with sterile distilled water to remove planktonic cells. The experiment designed according to the method of Rabinovitch and Stewart [10] was modified. The rinsed coupons were connected to both the anode and cathode poles in a closed-

circuit system in which a direct electrical current was provided for each biofilm. The electrolysis setup with biofilm samples at different poles is shown in Fig. 1. The coupons containing the biofilm samples were connected to the poles and immersed in a sterile 2 M NaCl buffer. The circuit was completed with a power supply and a 10 V potential was applied (0.3 A). Individual electrolysis setups were prepared for 1, 2, and 5 min treatment as test groups. The coupons were separately attached to both the anode and cathode, and the effects of different poles on biofilm removal were evaluated.

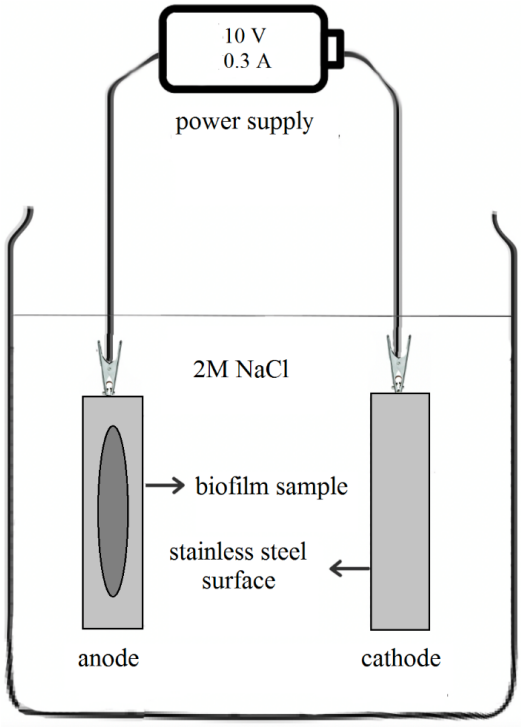

Figure 1: Schematic illustration of electrolysis setup

After applying a direct current, the coupons were washed and transferred under aseptic conditions to 50 mL-Falcon tubes containing 5 mL of sterile saline (0.9% NaCl) and 10 grams of glass beads. The tubes were vortexed at the highest intensity for 2 min and serial dilutions were prepared from the biofilm suspensions. Colony forming units (CFU) were calculated using the spread plate method on TSA agar plates (Tryptic Soy Agar, Merck, Germany). The plates were incubated at 37 °C for 24 h. As positive control groups, no electric current was applied and the coupons were immersed in 2 M NaCl buffer for 1, 2, and 5 min. The decrease in biofilm production compared to the control groups was determined by colony counting. Using the colony count results of the control

groups, the log percent (%) reductions of the test groups were calculated using the formula given: [(1-10- LR)] x 100 (LR: Logarithmic reduction; Logarithmic colony count of positive control groups-Logarithmic colony count of test groups).

2.4. Determination of remaining biofilm matrix after electrolysis

The crystal violet binding assay was used to detect the residual biofilm matrix remaining on the coupons after electrolysis. In the related study, the method proposed by [23] was modified. Biofilm sampling on the coupons was performed as described above. After incubation, the coupons were rinsed and subjected to the electrolysis process described above. After the process, the coupons were transferred to glass test tubes each containing 5 mL of 95% methanol and fixed for 10 min at room temperature. After this step, the coupons were transferred to glass test tubes containing 5 mL of 0.1% crystal violet solution (Merck, Germany). After the 30-min incubation, the coupons were rinsed under running tap water to remove the remaining crystal violet dye. Following rinsing, the coupons were transferred to tubes each containing 5 mL of 33% glacial acetic acid solution. After a 15 min-incubation period, 200 µL of the dissolved crystal violet dye was removed from the tubes and transferred to the wells of U-bottom microtiter plate (LP Italiana, Italy). The plates were read at 595 nm using an ELISA reader. As positive control groups, coupons were treated in the same way with biofilm samples that were not subjected to electrolysis. The sterile coupons were used as negative controls. The percentage reduction of biofilm matrix formation was calculated according to the given formula: {[(C-B)-(T-B)]/(C-B)} * 100 (C; OD values from control group wells, B; OD values from blank well, T; OD values from test group wells). The crystal violet binding assay is an indirect method and provides information on the accumulation of extracellular polymeric components associated with the biofilm matrix on surfaces. In this context, it was possible to determine the remaining matrix components on surfaces after electrolysis.

2.5. Antimicrobial effects of electrolyzed eater on planktonic bacterial cells

In this study, 2M NaCl solution electrolyzed according to the conditions in biofilm studies was applied to bacterial cells in planktonic form (10 V, 0.3 A, 5 min). 1 mL of the active bacterial cultures were removed and transferred to the tubes containing 1 mL of fresh electrolyzed solution. After the tubes were incubated for 5 min at room temperature, serial dilutions were prepared from the suspensions and inoculation was performed using the spread plate method on TSA agar plates. The logarithmic and percentage reduction of colony number was calculated as described above.

2.6. Statistical analysis

The results of the test and control groups were analyzed using One-WAY ANOVA and T tests. The changes in mean values were given as standard deviation. The results of biofilm cell eradication and matrix removal were compared using Pearson correlation. The confidence interval for tests was taken as $p < 0.01$.

3. Results

3.1. Electrolysis of biofilms sampled on stainless steel surfaces

To test the efficacy of electrolysis treatment, 24 h-old *S.* Typhimurium, *S. aureus*, and *E. coli* biofilms were treated at the anode and cathode. The viable cell counts of the biofilms exposed to electrolysis were enumerated using the CFU assay. The reduction of viable cells (LR) for each treatment was then calculated by subtracting the number of viable cells of the untreated control biofilms. The logarithmic reduction was also calculated (Table 1). A graph of the log reduction is displayed in Fig. 2. The biofilm cells of *S.* Typhimurium and *E. coli* on the cathode pole were eliminated at all treatment intervals. The biofilms of *S.* Typhimurium and *E. coli* on the anode were eradicated only during prolonged treatment (Fig. 2a and Fig. 2c). Although mature S. *aureus* biofilms on the cathode were removed more, they could not be eradicated under the applied electrolysis conditions and in the preferred electrolysis buffer. However, a strong decrease in cell viability was observed for cathode samples (approximately 2 log reduction) (Fig. 2b). Thus, all of the data indicated an increased trend of biofilm cell elimination for the compared anode samples.

Table 1: Logarithmic reductions (%) of biofilm cells and removal (%) of biofilm matrix after electrolysis

Strain	Cathode Biofilm Cell Log Reduction (%)			Anode Biofilm Cell Log Reduction (%)		
	1 min	2 min	5 min	1 min	2 min	5 min
S. Typhimurium DMC4	100.00	100.00	100.00	99.57 ± 0.057	92.76 ± 1.54	100.00
S. aureus ATCC 25923	99.29 ± 0.27	99.80 ± 1.54	99.66 ± 2.01	95.46 ± 0.41	97.70 ± 2.50	99.42 ± 3.41
E. coli ATCC 25922	100.00	100.00	100.00	99.999 ± 2.52	100.00	100.00
Strain	**Cathode Biofilm Matrix Reduction (%)**			**Anode Biofilm Matrix Reduction (%)**		
	1 min	2 min	5 min	1 min	2 min	5 min
S. Typhimurium DMC4	94.67 ± 4.57	97.81 ± 3.22	100.00	86.36 ± 7.57	88.75 ± 6.55	95.16 ± 9.51
S. aureus ATCC 25923	72.27 ± 3.44	85.69 ± 6.41	93.79 ± 7.83	75.88 ± 5.55	80.53 ± 6.41	84.22 ± 4.15
E. coli ATCC 25922	88.30 ± 2.42	100.00	100.00	83.74 ± 4.47	86.26 ± 3.77	100.00

Results were given as mean values with standard deviations.

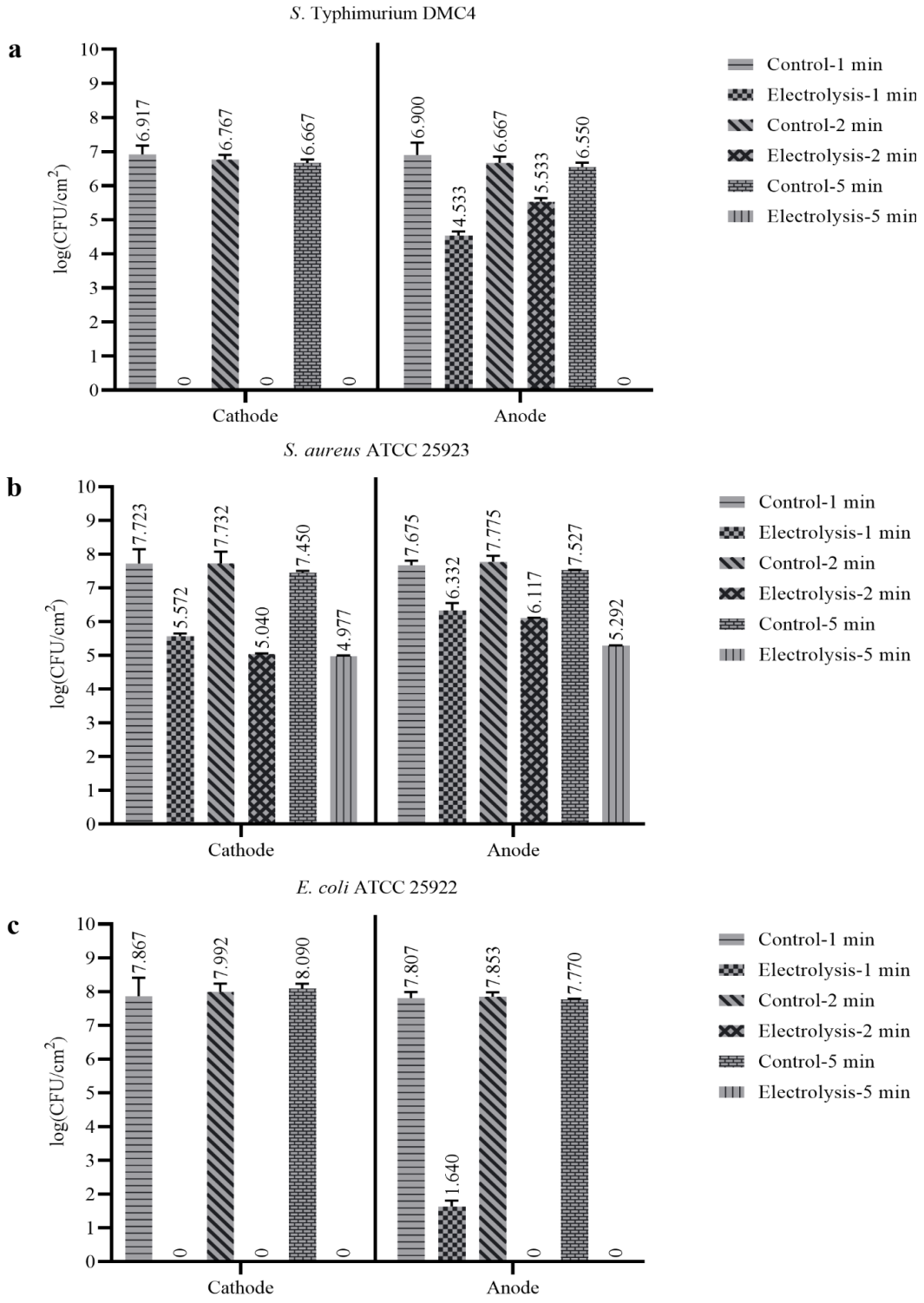

Figure 2: Effects of electrolysis on biofilm cells (a) Log reduction of *S.* Typhimurium biofilm cells on the cathode and anode (b) Log reduction of *S. aureus* biofilm cells on the cathode and anode (c) Log reduction of *E. coli* biofilm cells on the cathode and anode. Drastic log reductions have been observed in test groups compared with control groups (One-WAY ANOVA and T-Test; $p < 0.01$)

3.2. Determination of remaining biofilm matrix after electrolysis

After treatment with electrolysis, biofilms were quantified by the crystal violet staining method. The controls, treatment with only 2M NaCl solution for 1, 2, and 5 min, were also stained. The results of this experiment are shown in Fig. 3 and Table 1. Figure 3 shows the total matrix of biofilms for the different treatments applied. Efficient removal of the biofilm matrix was achieved only at the cathode. *E. coli* and S. Typhimurium biofilm matrix were removed from the stainless-steel surfaces with 5 min electrolysis treatment (Fig. 3a and 3c). It was also demonstrated that the efficacy of electrolysis, as measured by the crystal violet staining method and the colony forming unit assay, was proportional to the application time. Thus, a positive correlation was found between biofilm cell eradication rates and matrix removal of biofilms (Pearson correlation, $p < 0.01$). It was not possible to remove the *S. aureus* biofilm matrix from the surfaces by electrolysis.

3.3. Antimicrobial effects of electrolyzed water on planktonic bacterial cells

Planktonic cells of *S.* Typhimurium, *E. coli*, and *S. aureus* could be completely killed when treated with 2M NaCl solution electrolyzed at 10 V direct current for 5 min. A 10-log reduction in populations compared to the control groups indicated that the respective electrolyte buffer and electrolysis procedure were effective on planktonic cultures of these pathogens (Table 2).

Table 2: Antibacterial effects of electrolyzed NaCl solution on planktonic bacterial cells

Strain	Control Log (CFU/mL)	Treatment Log (CFU/mL)	Log Reduction	Log Reduction (%)
***S.* Typhimurium DMC 4**	10.55 ± 0.069	0.00	10.55	100.00
***S. aureus* ATCC 25923**	10.34 ± 0.189	0.00	10.34	100.00
***E. coli* ATCC 25922**	10.50 ± 0.281	0.00	10.50	100.00

Results were given as mean values with standard deviations.

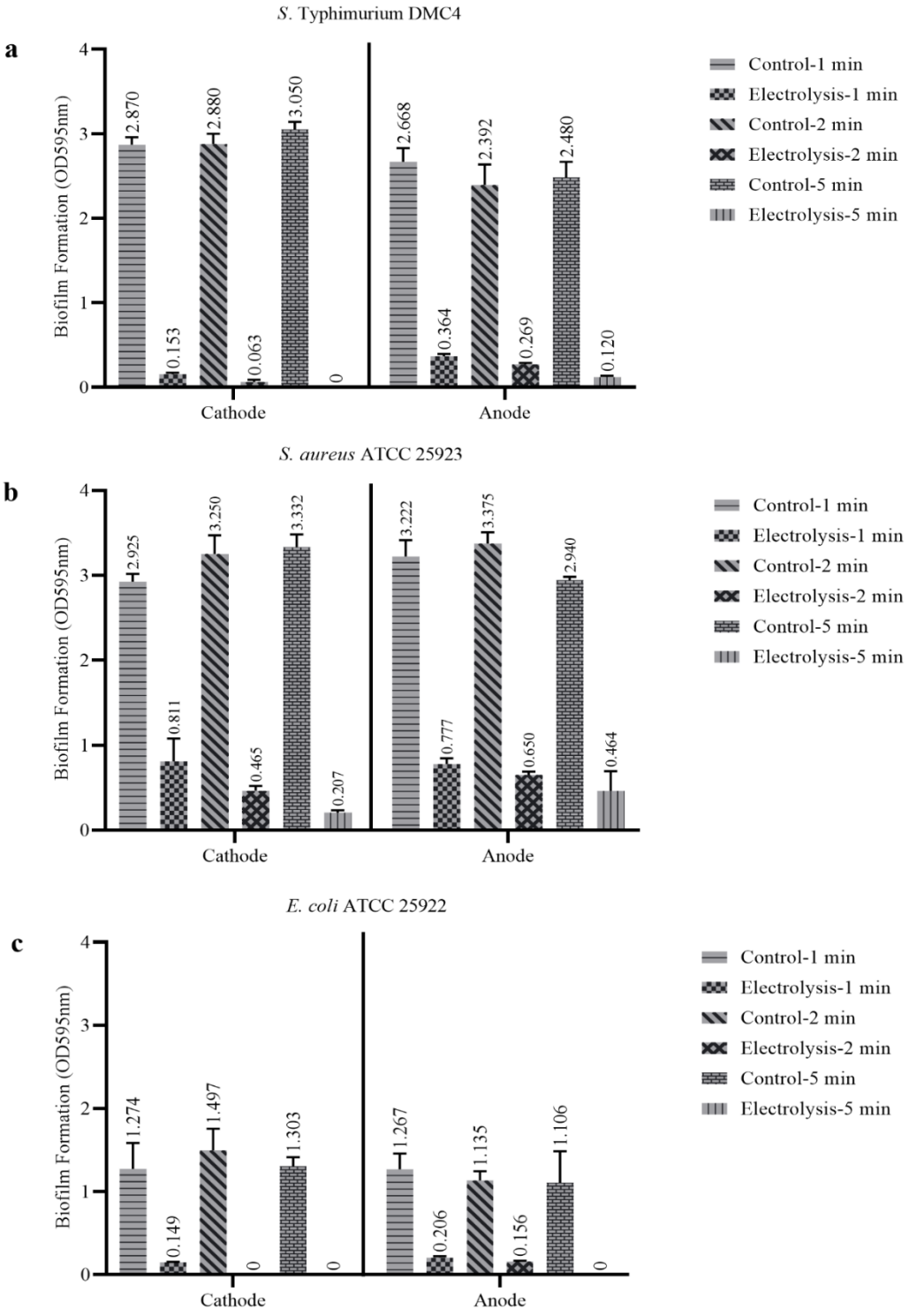

Figure 3: Effects of electrolysis on biofilm matrix (a) Matrix reduction of *S.* Typhimurium biofilm on the cathode and anode (b) Matrix reduction of *S. aureus* biofilm on the cathode and anode (c) Matrix reduction of *E. coli* biofilm on the cathode and anode. Biomass reductions have been observed in test groups compared with control groups (One-WAY ANOVA and T-Test; $p < 0.01$)

4. Discussion

There are several ways to control biofilm development depending on electrochemical strategies considered in the literature. Most of these methods focus either on delaying/preventing cell adhesion or removing/eradicating the biofilm [24]. An effective strategy for electrochemical biofilm control is the application of a steady potential that results in the formation of biocides on the electrodes. As a result of this phenomenon, a constant current can remove established biofilms from electrode surfaces [25]. The generation of potent antimicrobial agents from NaCl buffer is possible by electrolysis. The expected reaction is $2H_2O + 2e^- \rightarrow 2OH^- + H_2$ at the anodic site. Thus, pH increase and hydrogen gas production may occur at the anode. On the other hand, the essential reaction is $H_2O + Cl^- \rightarrow HOCl + H^+ + 2e^-$. This reaction leads to a pH decrease and the formation of hypochlorous acid, a strong antimicrobial substance. [10, 24]. The hypochlorous acid that can be generated at the cathode has a remarkable effect on viable cells found in biofilms [10]. The results of this study are similar to the results of the study by Rabinovitch and Stewart [10] in terms of better elimination of biofilm cells at the cathode than at the anode. The direct current efficacy observed in this study is also explained by the electrolytic production of chlorine. However, the DC biocidal agents produced were more effective in terms of removing Gram-negative biofilms such as *E. coli* and *S.* Typhimurium (Fig. 2). As an effective antimicrobial agent, chlorine has been documented to partially destroy biofilms of *S. aureus* and this study further confirms these findings [26].This research investigated the use of direct current under highly concentrated NaCl (2M NaCl). Although previous biofilm studies in this area typically used a chloride-free solution to mitigate electrolysis effects, a standard saline solution (0.9 percent NaCl) was also used to simulate physiologically important conditions. [27]. In contrast to these existing approaches, the high concentration of NaCl used in our experiments provided the best results in terms of eliminating *E. coli*, *S.* Typhimurium and *S. aureus* biofilms. In the preliminary study design, NaCl solutions of different concentrations were first subjected to electrolysis, and the most optimal result was obtained for 2M NaCl (data not shown).

In addition, our results showed improved detachment of the biofilm matrix by electrolysis. With direct current application due to locally charged molecular vibrations, these findings also indicated increased permeability of the exopolysaccharide matrix. Giladi et al. [28] confirmed this finding. In other studies, thermal stimuli generated at the electrodes during electrolysis have been found to have an enhanced effect on biomass removal [29]. In general, due to their complex structures and diverse stimuli, it is difficult to investigate the mechanisms underlying the effect of electrolysis on biofilms [30, 31]. Matrix-assembling extracellular polymeric substances (EPS) immobilize biofilm

cells, holding them in close proximity in the long term and thus enabling intense interactions, including cell-cell contact, horizontal gene transfer, and the formation of synergistic microconsortia [32]. Plastics, rubber, glass, wood, paper, cement and stainless steel are commonly used materials in the food industry, the latter being the most commonly used material for food machinery and utensils due to its hygienic properties [33, 34]. The low hygienic level of contact surfaces leads to the accumulation of organic material, which contributes to the attachment of microbes. When the biofilm formation is allowed to occur, the presence of adherent EPS makes surface cleaning more difficult. If the organic residues on the surface are not effectively cleaned, microorganisms can continuously adhere to these areas [35]. Although *E. coli* and *S*. Typhimurium biofilm matrix structures in particular were shown to be effectively removed from stainless steel surfaces by electrolysis, this application alone could not destroy a biofilm with all its components (Fig. 3 and Table 1).

5. Conclusion

In this study, it was clarified that it was possible to electrochemically control biofilms of some important food pathogenic bacteria such as *E. coli*, *S*. Typhimurium, and *S. aureus*, which significantly affect both human health and food quality due to the presence of biofilms in food processing facilities. To increase the electrochemical removal efficiency, NaCl was used in the electrolyte buffer because it is cheap and reliable. In this way, a low-cost approach and electrochemical reactions were used to obtain reliable doses of biocidal agents and test their efficacy on biofilm samples. The result is an alternative to highly toxic and expensive chemicals commonly used in cleaning-in-place processes in the food industry.

References

[1] Sutherland, I.W., *The biofilm matrix–an immobilized but dynamic microbial environment*, Trends in Microbiology, 9(5), 222-227, 2001.

[2] Mizan, M.F.R., Jahid, I.K., Ha, S.D., *Microbial biofilms in seafood: a food-hygiene challenge*, Food Microbiology, 49, 41-55, 2015.

[3] Poulsen, L.V., *Microbial biofilm in food processing*, LWT-Food Science and Technology, 32(6), 321-326, 2001.

[4] Brooks, J.D., Flint, S.H., *Biofilms in the food industry: problems and potential solutions,* International Journal of Food Science & Technology, 43(12), 2163-2176, 2008.

[5] Chmielewski, R.A.N., Frank, J.F., *Biofilm formation and control in food processing facilities*, Comprehensive Reviews in Food Science and Food Safety, 2(1), 22-32, 2003.

[6] Simões, M., Simões, L.C., Vieira, M.J., *A review of current and emergent biofilm control strategie*s, LWT-Food Science and Technology, 43(4), 573-583, 2010.

[7] Jahid, I.K., Ha, S.D., *A review of microbial biofilms of produce: future challenge to food safety*, Food Science and Biotechnology, 21(2), 299-316, 2012.

[8] Srey, S., Jahid, I.K., Ha, S.D., *Biofilm formation in food industries: a food safety concern,* Food Control, 31(2), 572-585, 2013.

[9] Lewandowski, Z., Beyenal, H., *Fundamentals of biofilm research*, CRC Press. Boca Raton, FL. 2014.

[10] Rabinovitch, C., Stewart, P.S., *Removal and inactivation of Staphylococcus epidermidis biofilms by electrolysis*, Applied and Environmental Microbiology, 72(9), 6364-6366, 2006.

[11] Liu, W.K., Brown, M.R., Elliott, T.S., *Mechanisms of the bactericidal activity of low amperage electric current (DC)*, The Journal of Antimicrobial Chemotherapy, 39(6), 687-695, 2001.

[12] Stoodley, P., deBeer, D., Lappin-Scott, H.M., *Influence of electric fields and pH on biofilm structure as related to the bioelectric effect*, Antimicrobial Agents and Chemotherapy, 41(9), 1876-1879, 1997.

[13] Poortinga, A.T., Smit, J., van der Mei, H.C., Busscher, H.J., *Electric field induced desorption of bacteria from a conditioning film covered substratum*, Biotechnology and Bioengineering, 76(4), 395-399, 2001.

[14] Hong, S.H., Jeong, J., Shim, S., Kang, H., Kwon, S., Ahn, K.H., Yoon, J., *Effect of electric currents on bacterial detachment and inactivation*, Biotechnology and Bioengineering, 100(2), 379-386, 2008.

[15] Stewart, P.S., G.A. McFeters, C.T., J.D., Bryers (ed.), Huang, *Biofilm control by antimicrobial agents*, Biofilms II: process analysis and applications. Wiley-Liss, New York, N.Y., 373p-405p, 2000.

[16] Lim, T.K., Murakami, T., Tsuboi, M., Yamashita, K., Matsunaga, T., *Preparation of a colored conductive paint electrode for electrochemical inactivation of bacteria*, Biotechnology and Bioengineering, 81(3), 299-304, 2003.

[17] Stewart, P.S., Wattanakaroon, W., Goodrum, L., Fortun, S.M., McLeod, B.R., *Electrolytic generation of oxygen partially explains electrical enhancement of tobramycin efficacy against Pseudomonas aeruginosa Biofilm*, Antimicrobial Agents and Chemotherapy, 43(2), 292-296, 1999.

[18] Kumar, C.G., Anand, S.K., *Significance of microbial biofilms in food industry: a review*, International Journal of Food Microbiology, 42(1-2), 9-27, 1998.

[19] Crémet, L., Corvec, S., Batard, E., Auger, M., Lopez, I., Pagniez, F., Caroff, N., *Comparison of three methods to study biofilm formation by clinical strains of Escherichia coli*, Diagnostic Microbiology and Infectious Disease, 75(3), 252-255, 2013.

[20] Vestby, L.K., Møretrø, T., Langsrud, S., Heir, E., Nesse, L.L., *Biofilm forming abilities of Salmonella are correlated with persistence in fish meal-and feed factories*, BMC Veterinary Research, 5(1), 20, 2009.

[21] Onbas, T., Osmanagaoglu, O., Kiran, F., *Potential properties of Lactobacillus plantarum F-10 as a Bio-control strategy for wound infections*, Probiotics and Antimicrobial Proteins, 11(4), 1110-1123, 2018.

[22] Istanbullu, O., Babauta, J., Duc Nguyen, H., Beyenal, H*., Electrochemical biofilm control: mechanism of action*, Biofouling, 28(8), 769-778, 2012.

[23] Stepanović, S., Vuković, D., Dakić, I., Savić, B., Švabić-Vlahović, M., *A modified microtiter-plate test for quantification of staphylococcal biofilm formation,* Journal of Microbiological Methods, 40(2), 175-179, 2000.

[24] Sultana, S.T., Babauta, J.T., Beyenal, H., *Electrochemical biofilm control: a review*, Biofouling, 31(9-10), 745-758, 2015.

[25] Dhar, H.P., Bockris, J.O., Lewis, D.H., E*lectrochemical inactivation of marine bacteria*, Journal of the Electrochemical Society, 128(1), 229, 1981.

[26] Ueda, S, Kuwabara, Y., *Susceptibility of biofilm Escherichia coli, Salmonella enteritidis and Staphylococcus aureus to detergents and sanitizers*, Biocontrol Science 12(4), 149-153, 2007.

[27] Sandvik, E.L., McLeod, B.R., Parker, A.E., Stewart, P.S., *Direct electric current treatment under physiologic saline conditions kills Staphylococcus epidermidis biofilms via electrolytic generation of hypochlorous acid*, PloS one, 8(2), e55118, 2013.

[28] Giladi, M., Porat, Y., Blatt, A., Shmueli, E., Wasserman, Y., Kirson, E.D., and Palti, Y., *Microbial growth inhibition by alternating electric fields in mice with Pseudomonas aeruginosa lung infection*, Antimicrobial Agents and Chemotherapy, 54(8), 3212-3218, 2010.

[29] Caubet, R., Pedarros-Caubet, F., Chu, M., Freye, E., de Belem Rodrigues, M., Moreau, J.M., Ellison, W.J., *A radio frequency electric current enhances antibiotic efficacy against bacterial biofilms*, Antimicrobial Agents and Chemotherapy, 48(12), 4662-4664, 2004.

[30] Del Pozo, J.L., Rouse, M.S., Patel, R., *Bioelectric effect and bacterial biofilms. A systematic review*, The International Journal of Artificial Organs, 31(9), 786-795, 2008.

[31] Del Pozo, J.L., Rouse, M.S., Euba, G., Greenwood-Quaintance, K.E., Mandrekar, J.N., Steckelberg, J.M., Patel, R., *Prevention of Staphylococcus epidermidis biofilm formation using electrical current*, Journal of Applied Biomaterials & Functional Materials, 12(2), 81-83, 2014.

[32] Flemming, H.C., Wingender, J., *The biofilm matrix*, Nature Reviews Microbiology, 8(9), 623-633, 2010.

[33] Holah, J.T., Thorpe, R.H., *Cleanability in relation to bacterial retention on unused and abraded domestic sink material*s, Journal of Applied Bacteriology, 69(4), 599-608, 1990.

[34] Van Houdt, R., Michiels, C.W., *Biofilm formation and the food industry, a focus on the bacterial outer surface*, Journal of Applied Microbiology, 109(4), 1117-1131, 2010.

[35] Boyd, R.D., Cole, D., Rowe, D., Verran, J., Paul, A.J., West, R.H., *Cleanability of soiled stainless steel as studied by atomic force microscopy and time of flight secondary ion mass spectrometry*, Journal of Food Protection, 64(1), 87-93, 2001.

Adıyaman University Journal of Science
https://dergipark.org.tr/en/pub/adyujsci
DergiPark AKADEMİK
ISSN 2147-1630
e-ISSN 2146-586X

Investigation of Analytical Solutions of the Nonlinear Mathematical Model Representing Gas Overflowing

Tolga AKTÜRK[1,*], Yusuf GÜREFE[2]

[1]*Ordu University, Faculty of Education, Department of Mathematics and Science Education, Ordu, Turkey*
tolgaakturk@odu.edu.tr, ORCID: 0000-0002-8873-0424
[2]*Uşak University, Faculty of Economics and Administrative Sciences, Department of Econometrics, Uşak, Turkey*
ygurefe@gmail.com, ORCID: 0000-0002-7210-5683

Received: 26.01.2021 **Accepted:** 28.05.2021 **Published:** 30.06.2021

Abstract

In this study, traveling wave soliton solutions of hyperbolic and trigonometric functions are successfully obtained by using the modified exponential function method of the Buckley-Leverett equation. In addition to these, there are also rational function solutions. Two and three-dimensional graphs of real and imaginary parts are included with contour simulations to physically analysis of the solution functions of the equation analyzed as a mathematical model using Mathematica software.

Keywords: Buckley-Leverett Equation; Traveling wave solution; Modified exponential function method.

Gaz Taşmasını Temsil Eden Doğrusal Olmayan Matematiksel Modelin Analitik Çözümlerinin Araştırılması

Öz

* Corresponding Author DOI: 10.37094/adyujsci.868800

Bu çalışmada, modifiye edilmiş üstel fonksiyon metodu kullanılarak Buckley-Leverett denkleminin hiperbolik ve trigonometrik fonksiyon gezici dalga soliton çözümleri başarıyla elde edilmiştir. Bunların yanı sıra rasyonel fonksiyon çözümleri de elde edilmiştir. Matematiksel model olarak incelenen denklemin çözüm fonksiyonlarını fiziksel olarak analiz etmek için Mathematica yazılımı kullanılarak kontur simülasyonları ile birlikte gerçek ve sanal parçaların iki ve üç boyutlu grafiklerine yer verilmiştir.

Anahtar Kelimeler: Buckley-Leverett denklemi; Yürüyen dalga çözümleri; Geliştirilmiş Üstel Fonksiyon Metodu.

1. Introduction

Nonlinear partial differential equations have an important place in all areas of life. This equation is based on the motion, density, fluidity of behavior or object in fields such as physics, chemistry, engineering, health, biology, etc. It provides the opportunity to evaluate. It is essential to obtain analytical solutions to such mathematical models. Because, with the solutions of these types of mathematical models, it will be easier to evaluate the physical conditions of the object being investigated in the desired time interval. For example, various mathematical models have been developed for the Covid-19 outbreak, which has affected worldwide recently. With the help of these models, obtaining information about the course of the epidemic in advance has emerged. For this reason, there are various methods or techniques in the literature about establishing such mathematical models and analyzing their solutions [1-14].

This article aims to obtain the analytical solution or solutions of the Buckley-Leverett equation with the help of the modified exponential function method (MEFM) by determining the appropriate parameters for gas flooding under varying constant pressure boundary conditions [15]. The Buckley-Leverett equation analyzed in the article is as follows [16-18],

$$U_t + \left(U - U^3\right)_x = \beta U_{xx} + \alpha U_{xxt}. \tag{1}$$

2. Analysis of Modified Exponential Function Method (MEFM)

In this section, general information about MEFM is given as follows. According to the method, the general form of the analyzed nonlinear partial differential equation is as follows;

$$P\left(U, U^3, U_x, U_t, U_{xx}, U_{xxt}, \cdots\right) = 0, \tag{2}$$

where $U = U(x,t),$ is unknown function.

Step 1. If the following nonlinear wave transformation is applied to partial differential equations representing the mathematical model;

$$U(x,t) = u(\xi),\ \xi = k.\left(x - ct\right), \tag{3}$$

c and k are real values that are not zero. The k term in wave transformation represents the height of the wave, and c represents the frequency of the wave. If the required derivative terms in Eqn. (1) are obtained from the wave transform Eqn. (3) and replaced by the following, the following nonlinear ordinary differential equation is obtained,

$$N\left(u, u', u'', \cdots\right) = 0. \tag{4}$$

Step 2: The solution function U analyzed in the Eqn. (4) obtained above is as follows;

$$U\left(\xi\right) = \frac{\sum_{i=0}^{n} A_i \left[\exp\left(-\Omega\left(\xi\right)\right)\right]^i}{\sum_{j=0}^{m} B_j \left[\exp\left(-\Omega\left(\xi\right)\right)\right]^j} = \frac{A_0 + A_1 \exp\left(-\Omega\right) + \cdots + A_n \exp\left(n\left(-\Omega\right)\right)}{B_0 + B_1 \exp\left(-\Omega\right) + \cdots + B_m \exp\left(m\left(-\Omega\right)\right)}, \tag{5}$$

where $A_i \neq 0, \left(0 \leq i \leq n\right)$ and $B_j \neq 0, \left(0 \leq j \leq m\right)$ are real and complex constants. The term $\Omega = \Omega\left(\xi\right)$ given above provides the following differential equation,

$$\Omega'\left(\xi\right) = \exp\left(-\Omega\left(\xi\right)\right) + \mu \exp\left(\Omega\left(\xi\right)\right) + \lambda. \tag{6}$$

If Eqn. (6) is solved under the following conditions [19],

Family 1: If $\mu \neq 0,\ \lambda^2 - 4\mu > 0,$

$$\Omega\left(\xi\right) = \ln\left(\frac{-\sqrt{\lambda^2 - 4\mu}}{2\mu} \tanh\left(\frac{\sqrt{\lambda^2 - 4\mu}}{2}(\xi + E)\right) - \frac{\lambda}{2\mu}\right). \tag{7}$$

Family 2: If $\mu \neq 0,\ \lambda^2 - 4\mu < 0,$

$$\Omega\left(\xi\right) = \ln\left(\frac{\sqrt{-\lambda^2 + 4\mu}}{2\mu} \tan\left(\frac{\sqrt{-\lambda^2 + 4\mu}}{2}(\xi + E)\right) - \frac{\lambda}{2\mu}\right). \tag{8}$$

Family 3: If $\mu = 0,\ \lambda \neq 0$ and $\lambda^2 - 4\mu > 0,$

$$\Omega\left(\xi\right) = -\ln\left(\frac{\lambda}{\exp\left(\lambda(\xi + E)\right) - 1}\right). \tag{9}$$

Family 4: If $\mu \neq 0,\ \lambda \neq 0$ and $\lambda^2 - 4\mu = 0,$

$$\Omega(\xi) = \ln\left(-\frac{2\lambda(\xi + E) + 4}{\lambda^2(\xi + E)}\right). \tag{10}$$

Family 5: If $\mu = 0,\ \lambda = 0$ and $\lambda^2 - 4\mu = 0,$

$$\Omega(\xi) = \ln(\xi + E). \tag{11}$$

Step 3: Using the wave transformation, the equation obtained by substituting the required terms in Eqn. (2) is found in the algebraic equation system according to the powers of $\Omega(\xi)$. With the solving of this algebraic equation system, the values of the constants used in the solution function are obtained.

3. Application of Modified Exponential Function Method to Buckley-Leverett Equation

In this section, wave solutions of the Buckley-Leverett equation are obtained through using MEFM. For this, first of all, for Eqn. (1), the wave transformation Eqn. (3) is used to find the nonlinear ordinary differential equation given below,

$$(1-c)u - u^3 - \beta\, k\, u' + \alpha\, c\, k^2\, u'' = 0. \tag{12}$$

Considering the balancing procedure for Eqn. (12), the following equation is obtained regarding the upper limits of the symbols of the sum in Eqn. (5):

$$n = m + 1.$$

According to the equation obtained above, n = 2 for m = 1. In this case, Eqn. (5) and its derivatives terms,

$$\begin{aligned} u(\xi) &= \frac{\psi}{\varphi} = \frac{A_0 + A_1 e^{-\Omega(\xi)} + A_2 e^{-2\Omega(\xi)}}{B_0 + B_1 e^{-\Omega(\xi)}}, \\ u'(\xi) &= \frac{\psi'\varphi - \psi\varphi'}{\varphi^2}, \\ u''(\xi) &= \frac{\psi''\varphi^3 - \varphi^2\psi'\varphi' - (\psi\varphi'' + \psi'\varphi')\varphi^2 + 2(\psi')^2\psi\varphi}{\varphi^4}, \end{aligned} \tag{13}$$

are obtained. By replacing Eqn. (13) in Eqn. (12), the U solution function that provides the nonlinear ordinary differential equation is obtained. It is checked that the solution function found

with the help of Mathematica software provides Eqn. (1). By determining the appropriate parameters, two and three-dimensional graphs of the solution function are obtained with the help of the same program.

CASE 1:

$$A_0 = \frac{1}{2} i \sqrt{-1+c-8ck^2\alpha\mu}\, B_0 - \frac{1}{2}\sqrt{-\left(-1+c\right)B_0^2},$$
$$, A_1 = \frac{-4ck^2\alpha B_0^2 + A_2\left(-i\sqrt{-1+c-8ck^2\alpha\mu}B_0 + \sqrt{-\left(-1+c\right)B_0^2}\right)}{2\sqrt{2}\sqrt{ck}\sqrt{\alpha}B_0}, \quad (14)$$
$$, B_1 = -\frac{A_2}{\sqrt{2}\sqrt{ck}\sqrt{\alpha}}, \beta = \frac{3\sqrt{c}\sqrt{\alpha}\sqrt{-\left(-1+c\right)B_0^2}}{\sqrt{2}\,B_0}, \lambda = -\frac{i\sqrt{-1+c-8ck^2\alpha\mu}}{\sqrt{2}\sqrt{ck}\sqrt{\alpha}}.$$

If the coefficients given above are used, the following solution functions are obtained.

Family 1:

$$U_{1,1}\left(x,t\right) = \frac{1}{2}\frac{\left(-\frac{\sqrt{-\left(-1+c\right)B_0^2}}{B_0} + \left(\begin{array}{l}\zeta\lambda\mu + i\sqrt{-1+c-8ck^2\alpha\mu} \\ \left(4\mu+\left(\lambda^2-4\mu\right)Sech\omega^2\right)- \\ -\zeta\sqrt{\lambda^2-4\mu}\,\mu Tanh\omega\end{array}\right)\right)}{\left(4\mu+\left(\lambda^2-4\mu\right)Sech\omega^2\right)}, \quad (15)$$

where $\omega\left(x,t\right) = \left[\frac{1}{2}\left(EE+\xi\right)\sqrt{\lambda^2-4\mu}\right], \zeta\left(x,t\right) = 4\sqrt{2}\sqrt{ck}\sqrt{\alpha}.$

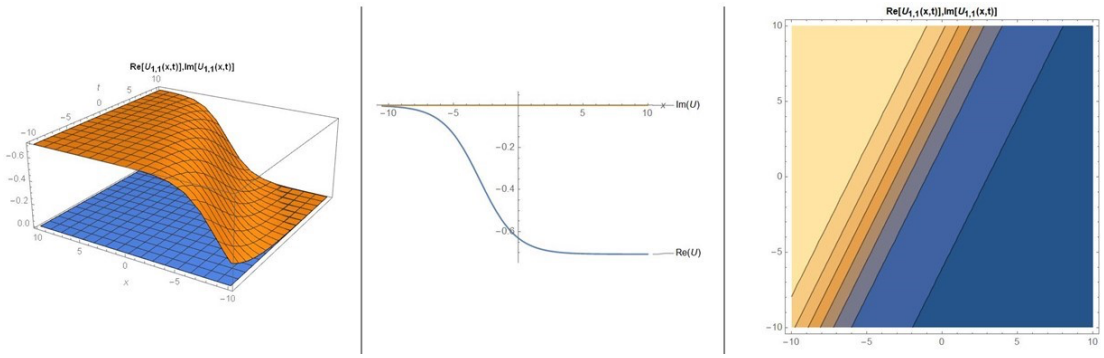

Figure 1: Three-dimensional, contour graphs of real and imaginary parts of Eqn. (15) for values $c = 0, \alpha = 0.1, B_0 = 1, k = 1, \mu = 0.1, \beta = \frac{3}{2\sqrt{2}}, \lambda = 0.948683, EE = 0.75$ and two-dimensional graph $t = 1$

Family 2:

$$U_{1,2}\left(x,t\right)=\left(\frac{1}{2}i\sqrt{-1+c-8ck^2\alpha\mu}+\frac{\frac{\zeta}{4}\mu\left(\lambda+\lambda Cos\left[\kappa\right]+\sqrt{-\lambda^2+4\mu}Sin\left[\kappa\right]\right)}{\lambda^2-2\mu+2\mu Cos\left[\kappa\right]}\right), \tag{16}$$

where $\kappa\left(x,t\right)=\left(EE+\xi\right)\sqrt{-\lambda^2+4\mu}$.

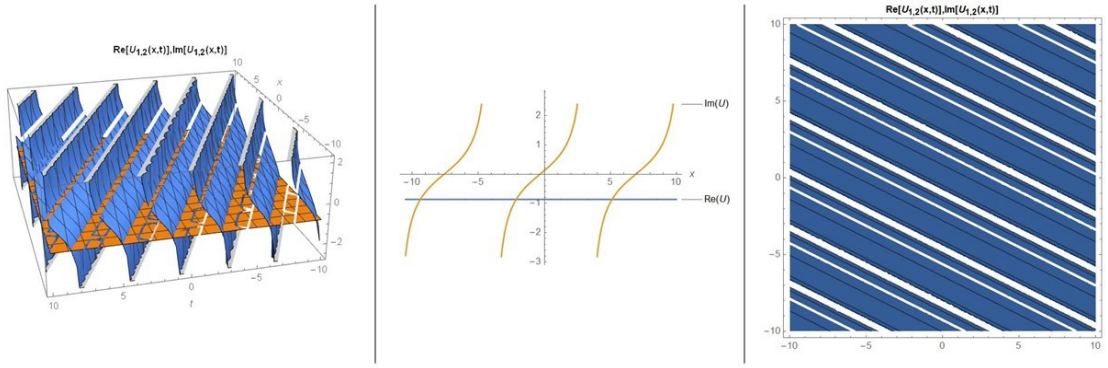

Figure 2: Three-dimensional, contour graphs of real and imaginary parts of Eqn. (16) for values $c=-2,\alpha=1,B_0=3,k=-1,\mu=1,\beta=3i\sqrt{3},\lambda=\frac{\sqrt{13}}{2},EE=0.65$ and two-dimensional graph $t=1$

Family 3:

$$U_{1,3}\left(x,t\right)=\left(\frac{1}{2}i\sqrt{-1+c}-\frac{\zeta\lambda}{4\left(-1+e^{\left(EE+\xi\right)\lambda}\right)}-\frac{\sqrt{-\left(-1+c\right)B_0^2}}{2B_0}\right). \tag{17}$$

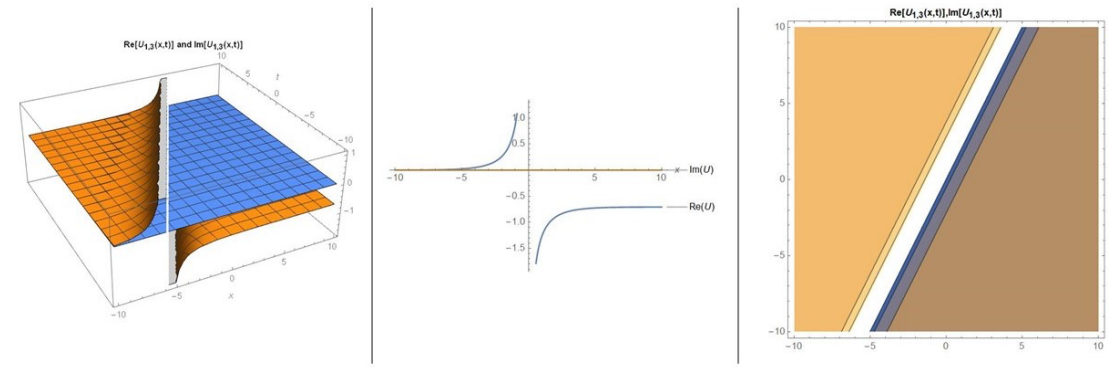

Figure 3: Three-dimensional, contour graphs of real and imaginary parts of Eqn. (17) for values $c=\frac{1}{2},\alpha=1,B_0=3,k=1,\mu=0,\beta=3,\lambda=\frac{1}{\sqrt{2}},EE=0.65$ and two-dimensional graph $t=1$

Family 4:

$$U_{1,4}\left(x,t\right)=\frac{1}{2}\left(\zeta\,\lambda\left(1-\frac{2}{2+EE\,\lambda+\xi\,\lambda}\right)+i\sqrt{-1+c-8ck^{2}\alpha\,\mu}-\frac{\sqrt{-\left(-1+c\right)B_{0}^{2}}}{B_{0}}\right). \tag{18}$$

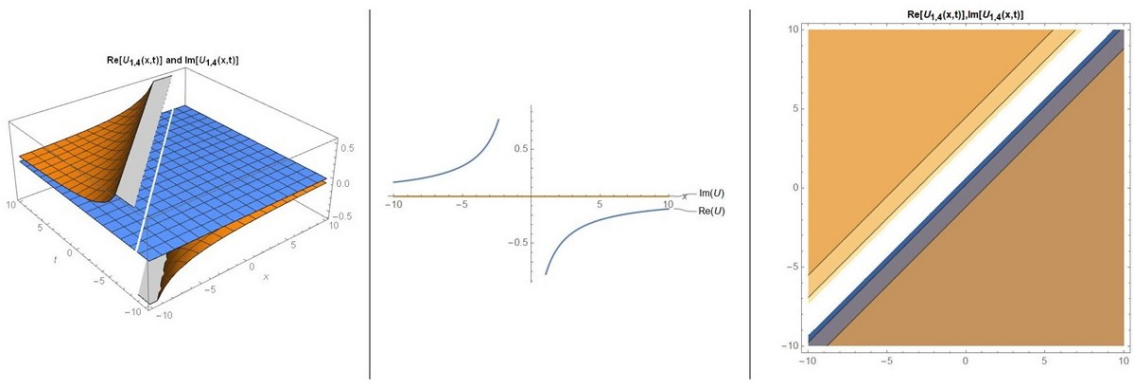

Figure 4: Three-dimensional, contour graphs of real and imaginary parts of Eqn. (18) for values $c=1$, $\alpha=1, B_0=3, k=1, \mu=1, \beta=\frac{3}{2\sqrt{2}}, \lambda=2, EE=0.65$ and two-dimensional graph $t=1$

Family 5:

$$U_{1,5}\left(x,t\right)=\frac{1}{2}\left(i\sqrt{-1+c}-\frac{\zeta}{2\left(EE+\xi\right)}-\frac{\sqrt{-\left(-1+c\right)B_{0}^{2}}}{B_{0}}\right). \tag{19}$$

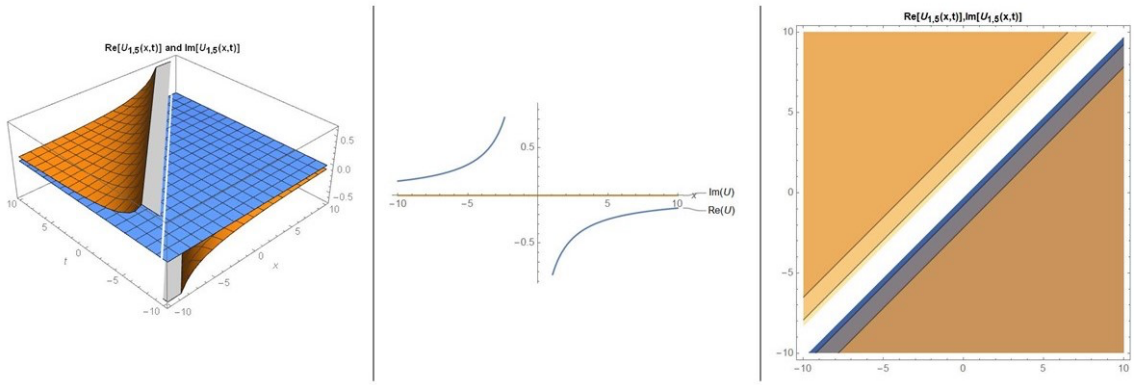

Figure 5: Three-dimensional, contour graphs of real and imaginary parts of Eqn. (19) for values $c=1$, $\alpha=1, B_0=3, k=1, \mu=0, \beta=\frac{3}{2\sqrt{2}}, \lambda=0, EE=0.65$ and two-dimensional graph $t=1$

4. Conclusions

By Bruzón, M. S., et al., The solution function of the Buckley-Leverett equation has been studied byusing Lie theory. They converted the nonlinear partial differential equation into ordinary differential equation format with the help of transformation. Then they obtained the Jacobi Elliptic function as a solution function. When the solution functions obtained in our study are analyzed, it is seen that hyperbolic, trigonometric, and rational solution functions are obtained. In order to understand the physical meanings of the solutions in this study, two and three-dimensional graphics were drawn with contour simulations. Mathematica software program was used to obtain all these numerical operations and to draw graphs. When the algebraic equation system is solved according to MEFM, the analyzed family cases are determined for the coefficients obtained, and the real and imaginary solution functions of the Buckley-Leverett equation are obtained. It has been seen that the method used in this study is a highly effective technique in obtaining analytical solutions of nonlinear partial differential equations.

References

[1] Sun, Y., *New travelling wave solutions for Sine-Gordon equation*, Journal of Applied Mathematics, 2014.

[2] Bulut, H., Akturk, T., Gurefe, Y., *Traveling wave solutions of the (N+ 1)-dimensional sine-cosine-Gordon equation,* American Institute of Physics Conference Proceedings, 1637(1), 145-149, 2014.

[3] Liu, C. S., *Trial equation method and its applications to nonlinear evolution equations*, Acta Physica Sinica., 54(6), 2505-2509, 2005.

[4] Shen, G., Sun, Y., Xiong, Y., *New travelling-wave solutions for Dodd-Bullough equation*, Journal of Applied Mathematics, 2013.

[5] Akturk, T., Bulut, H., Gurefe, Y., *New function method to the (n+1)-dimensional nonlinear problems*, An International Journal of Optimization and Control: Theories & Applications, 7(3), 234-239, 2017.

[6] Pandir, Y., Gurefe, Y., Kadak, U., Misirli, E., *Classification of exact solutions for some nonlinear partial differential equations with generalized evolution*, Abstract and Applied Analysis, 2012, 16, 2012.

[7] Akturk, T., Bulut, H., Gurefe, Y., *An application of the new function method to the Zhiber-Shabat equation*, An International Journal of Optimization and Control: Theories & Applications, 7(3), 271-274, 2017.

[8] Chen, Y., Yan, Z., *New exact solutions of (2+ 1)-dimensional Gardner equation via the new sine-Gordon equation expansion method*, Chaos, Solitons & Fractals, 26(2), 399-406, 2005.

[9] Kudryashov, N.A., *One method for finding exact solutions of nonlinear differential equations*, Communications in Nonlinear Science and Numerical Simulation, 17, 2248-2253, 2012.

[10] Sakar, M.G., Saldır, O., Akgül, A., *A novel technique for fractional Bagley–Torvik equation,* Proceedings of the National Academy of Sciences, India Section A: Physical Sciences, 89(3), 539-545, 2019.

[11] Sakar, M.G., Saldır, O., *Improving variational iteration method with auxiliary parameter for nonlinear time-fractional partial differential equations*, Journal of Optimization Theory and Applications, 174(2), 530-549, 2017.

[12] Ismael, H.F., Bulut, H., Baskonus, H.M., Gao, W., Newly modified method and its application to the coupled Boussinesq equation in ocean engineering with its linear stability analysis, *Communications in Theoretical Physics*, 72(11), 115002, 2020.

[13] Ismael, H.F., Bulut, H., Baskonus, H.M., W-shaped surfaces to the nematic liquid crystals with three nonlinearity laws,. *Soft Computing*, 25(6), 4513-4524, 2021.

[14] Ismael, H.F., Baskonus, H.M., Bulut, H., Abundant novel solutions of the conformable Lakshmanan-Porsezian-Daniel model, *Discrete & Continuous Dynamical Systems-S*, 2020.

[15] Lingyu, M., Liao, X., Chen, Z., Zou, J., Chu, H., Li, R., *Analytical solution of Buckley-Leverett equation for gas flooding including the effect of miscibility with constant-pressure boundary*, Energy Exploration & Exploitation, 37.3: 960-991, 2019.

[16] Bruzón, M.S., Marquez, A.P., Recio, E., Garrido, T.M., de la Rosa, D., *Potential systems of a Buckley–Leverett equation: Lie point symmetries and conservation laws*, Journal of Mathematical Chemistry, 1-10, 2020.

[17] Spayd, K.R., Shearer M., *The Buckley–Leverett equation with dynamic capillary pressure,* SIAM J. Appl. Math., 71, 1088–1108, 2012.

[18] Hassanizadeh, S. M., Gray, W. G., *Mechanics and thermodynamics of multiphase flow in porous media including interphase boundaries,* Advances in water resources, 13.4, 169-186, 1990.

[19] Uddin, S., Alam, N., Hossain, S.M.S., Samiu, H., Akbar, M.A., *Some new exact traveling wave solutions to the (3+ 1)-dimensional Zakharov-Kuznetsov equation and the burgers equations via Exp-Expansion method,* Frontiers of Mathematics and Its Applications, 1.1, 1-8, 2014.